THEORY OF
LAMINAR VISCOUS-INVISCID INTERACTIONS
IN SUPERSONIC FLOW

Thesis by

John Michael Klineberg

In Partial Fulfillment of the Requirements

For the Degree of

Doctor of Philosophy

California Institute of Technology

Pasadena, California

1968

(Submitted May 24, 1968)

ACKNOWLEDGMENTS

I would like to take this opportunity to express my sincere gratitude to Professor Lester Lees for his interest and his continued guidance and support throughout the course of my graduate education.

I would also like to thank Dr. Barry Reeves and Professor Toshi Kubota for the many invaluable contributions and suggestions they have made. My thanks also go to Mrs. Truus Van Harreveld for her assistance in the preparation of many of the figures, and to Miss Kikuko Matsumoto and Mr. Harvey Buss for their help with some of the computer programs. Special appreciation and thanks are also due Mrs. Virginia Conner for her excellent and tireless typing of this manuscript.

I wish to acknowledge with much appreciation the financial support provided me by the Douglas Aircraft Company, Inc., for the years 1961-1963, and by the California Institute of Technology during the remainder of my graduate education. I also appreciate the sponsorship and financial support of the U. S. Air Force Office of Scientific Research provided under Contract AF 49(638)-1298.

With the recognition that this project would have been much more difficult without her encouragement and devotion, I wish to thank my wife, Anne-Marie.

ABSTRACT

This investigation is concerned with those fluid-mechanical problems in which the pressure distribution is determined by the interaction between an external, supersonic inviscid flow and an inner, laminar viscous layer. The boundary-layer approximations are assumed to remain valid throughout the viscous region, and the integral or moment method of Lees and Reeves, extended to include flows with heat transfer, is used in the analysis.

The general features of interacting flows are established, including the important distinctions between subcritical and supercritical viscous layers. The eigensolution representing self-induced boundary-layer flow along a semi-infinite flat plate is determined, and a consistent set of departure conditions is derived for determining solutions to interactions caused by external disturbances. Complete viscous-inviscid interactions are discussed in detail, with emphasis on methods of solution for both subcritical and supercritical flows. The method is also shown to be capable of predicting the laminar flow field in the near wake of blunt bodies.

Results of the present theory are shown to be in good agreement with the measurements of Lewis for boundary-layer separation in adiabatic and non-adiabatic compression corners, and with the near-wake experiments of Dewey and McCarthy for adiabatic flow over a circular cylinder. Extensions of the method to flows with mass injection at the surface and to subsonic interactions are indicated.

TABLE OF CONTENTS

TABLE OF CONTENTS (Cont'd)

TABLE OF CONTENTS (Cont'd)

LIST OF TABLES

LIST OF FIGURES

LIST OF FIGURES (Cont'd)

LIST OF FIGURES (Cont'd)

LIST OF FIGURES (Cont'd)

LIST OF SYMBOLS

a	velocity profile parameter, Eqs. (31) & (B5); also speed of sound
A_1 - A_8	functions defined in Eq. (60)
b	enthalpy profile parameter $\left(\frac{\partial S}{\partial \eta}\right)_{\eta=0}$
B_1 - B_8	functions defined in Eq. (59)
c_v, c_p	specific heats at constant volume and constant pressure
C	$\left(\frac{\mu}{\mu_\infty}\right) \Big/ \left(\frac{T}{T_\infty}\right)$ or $\left(\frac{\mu}{\mu_N}\right) \Big/ \left(\frac{T}{T_N}\right)$
C_o - C_7	coefficients of polynomial representations of profile functions
C_F	$\frac{2\left(\mu \frac{\partial u}{\partial y}\right)_w}{\rho_\infty u_\infty^2}$, skin-friction coefficient
C_H	$\left(k \frac{\partial T}{\partial y}\right)_w \Big/ \left[\rho_\infty u_\infty \left(h_{o_e} - h_{o_w}\right)\right]$, heat-transfer coefficient
d	cylinder diameter
d_1	height of edge of viscous layer above wake axis (Fig. B1a)
D	determinant of system of equations, Eq. (58)
E	$-\frac{1}{\delta_i^*} \int_o^{\delta_i} S \, dY$
f	function defined in Eq. (18); also quantity related to stream function in Falkner-Skan equation
F	$\mathcal{K} + \frac{1+m_e}{m_e} (1-E)$
g	enthalpy ratio $\frac{h_o}{h_{o_e}}$
h	static enthalpy; also function defined in Eq. (39); also leading-edge shock height (Fig. 29).
h_o	total enthalpy

LIST OF SYMBOLS (Cont'd)

$\mathscr{N}$	$\frac{\theta_i}{\delta_i^*}$
I	$\int_o^\delta \rho u^2 \, dy$, flux of momentum
J	$\frac{\theta_i^*}{\delta_i^*}$
k	thermal conductivity
K	$\int_o^\delta u \, dy$; also function defined in Eq. (67)
ℓ	length of Mach wave (Fig. 29a)
m	$\frac{\gamma-1}{2} M^2$
$\dot{m}$	$\int_o^\delta \rho u \, dy$, mass flux
M	Mach number
N_1-N_4	functions defined in Eq. (58)
p	static pressure
P	$\frac{\delta_i^*}{U_e} \left(\frac{\partial U}{\partial Y}\right)_{Y=0}$
P_1-P_4	perturbation functions defined in Eq. (75)
P_r	Prandtl number $\frac{\mu c_p}{k}$
Q	$\delta_i^* \left(\frac{\partial S}{\partial Y}\right)_{Y=0}$
$\overline{Q}$	$\frac{Q}{P_{r_w}}$
R	$\frac{2\delta_i^*}{U_e^2} \int_o^{\delta_i} \left(\frac{\partial U}{\partial Y}\right)^2 dY$
r	cylinder radius

LIST OF SYMBOLS (Cont'd)

$Re_{N,d}$	$\frac{a_N}{\nu_N} M_N d$	Reynolds numbers
Re_x	$\frac{a_\infty}{\nu_\infty} M_\infty x$	
$Re_{\delta_i^*}$	$\frac{a_\infty}{\nu_\infty} M_\infty \delta_i^*$ or $\frac{a_N}{\nu_N} M_N \delta_i^*$	
$Re_{\infty,d}$	$\frac{a_\infty}{\nu_\infty} M_\infty d$	
S	$\left(\frac{h_o}{h_{o_e}} - 1\right)$, total enthalpy function	
T	static temperature	
T(a, b)	$-\int_o^{\eta_{.99}} \frac{U}{U_e} S \, d\eta$	
T^*	$-\frac{1}{\delta_i^*} \int_o^{\delta_i} \frac{U}{U_e} S \, dY$	
u, v	velocity components parallel and normal to surface	
U, V	Stewartson's transformed velocity components	
U^*	$\left(\frac{U}{U_e}\right)_{\psi=0}$, velocity ratio along dividing streamline	
x, y	coordinates parallel and normal to surface	
x_o	beginning of interaction	
X, Y	Stewartson's transformed coordinates	
Z	$\frac{1}{\delta_i^*} \int_o^{\delta_i} \frac{U}{U_e} dY$	
$\alpha(a)$	$\left[\int_o^{\eta_{.99}} (1-U/U_e) d\eta\right]^{-1} = \frac{1}{\eta} \frac{Y}{\delta_i^*}$	
α_w	inclination of local tangent to surface, measured positive for an expansion turn	

LIST OF SYMBOLS (Cont'd)

α_1/β_1	quantity defined in Eq. (102)
β	Falkner-Skan pressure-gradient parameter; also $\frac{a_e}{a_\infty}\frac{p_e}{p_\infty}$ or $\frac{a_e}{a_N}\frac{p_e}{p_N}$
γ	$\frac{c_p}{c_v}$, ratio of specific heats
δ	boundary-layer thickness
δ_u	$\int_o^\delta (1 - \frac{u}{u_e})dy$, velocity thickness
δ_i	transformed boundary-layer thickness
δ^*	$\int_o^\delta \left(1 - \frac{\rho u}{\rho_e u_e}\right)dy$, boundary-layer displacement thickness
δ_i^*	$\int_o^{\delta_i} \left(1 - \frac{U}{U_e}\right)dY$, transformed displacement thickness
δ_r^*	$\left(\frac{a_N}{\nu_N} M_N r\right)\left(\frac{\delta_i^*}{r}\right)^2$
ϵ	perturbation parameter
ζ	function defined in Eq. (102)
η	Falkner-Skan variable; also $\mathcal{N}_1$-$\mathcal{N}_2$
θ	$\int_o^\delta \frac{\rho u}{\rho_e u_e}(1 - \frac{u}{u_e})dy$, boundary-layer momentum thickness
θ_i	$\int_o^{\delta_i} \frac{U}{U_e}(1 - \frac{U}{U_e})dY$, transformed momentum thickness
θ^*	$\int_o^\delta \frac{\rho u}{\rho_e u_e}\left(1 - \frac{u^2}{u_e^2}\right)dy$, mechanical energy thickness
θ_i^*	$\int_o^{\delta_i} \frac{U}{U_e}\left(1 - \frac{U^2}{U_e^2}\right)dY$, transformed mechanical energy thickness
θ^{**}	$\int_o^\delta \frac{\rho u}{\rho_e u_e}\left(\frac{h_o}{h_{o_e}} - 1\right)dy$, boundary-layer energy thickness

LIST OF SYMBOLS (Cont'd)

Θ	local angle between external streamline at $y = \delta$ and the x-axis, $\tan^{-1}\left(\frac{v_e}{u_e}\right)$
μ	viscosity coefficient; also $\frac{M_{e_1}}{M_{e_2}} - 1$
ν	Prandtl-Meyer angle, Eq. (51); also kinematic viscosity $\frac{\mu}{\rho}$
ξ	function defined in Eq. (102)
ρ	gas density
σ	$-\int_0^{\eta_{.99}} S \, d\eta$
τ_k	coefficients for T(a, b), Eq. (49)
$\bar{\chi}$	$\frac{M_\infty^3 \sqrt{C}}{\sqrt{Re_x}}$, hypersonic parameter
ψ	stream function

Subscripts

BL	Blasius point
$\mathfrak{L}$	center-line
CR	critical
e, δ	local external, inviscid
i	transformed, incompressible
LE	leading-edge
N	neck conditions
pp	pressure plateau
r	ratio of quantities upstream and downstream of jump
rsp	rear stagnation point
R, REATT	reattachment point

LIST OF SYMBOLS (Cont'd)

S, SEP	separation point
SI	strong interaction
STAG	stagnation point
TH	throat conditions
w	wall (surface)
WI	weak interaction
o	reference conditions
1	upstream of jump or shock
2	downstream of jump or shock
∞, $\infty-$	free-stream conditions upstream of interaction
$\infty+$	conditions far downstream of interaction

I. INTRODUCTION

In the usual formulation of boundary-layer theory, as proposed by Prandtl,[1] the distribution of static pressure along the surface is determined by the inviscid flow over the body in the absence of a boundary layer. In this sense, the effects produced by the viscous stresses are assumed to result in perturbations on an existing flow field. There are many important problems in fluid mechanics, however, for which the static pressure distribution cannot be specified a priori but is determined by the interaction between the outer, inviscid flow and the inner viscous layer near the surface. One of the most interesting problems of this type is the viscous-inviscid interaction induced by a rise in static pressure in the external supersonic stream. This pressure rise may be generated, for example, by an incident oblique shock, a compression corner, or by causing the flow to turn parallel to the wake axis downstream of the body. The rise in pressure in the external flow is propagated upstream through the subsonic portion of the viscous layer, and often induces boundary-layer separation far upstream of the location of the disturbance. This type of interaction, where there is a strong coupling between the outer inviscid flow and the inner boundary layer, requiring the simultaneous development of both solutions, is the subject of the present theoretical investigation.

The boundary-layer approximations are assumed to remain valid throughout the entire viscous region, although v/u may not be small for separated flows. If the appropriate Reynolds number is sufficiently large, however, rapid streamline curvature can only

occur in regions of low dynamic pressure, such as in the near wake, for example, and $\partial p/\partial y \approx 0$ everywhere. Because of the complexity of this type of viscous-inviscid interaction, an integral or moment method is used in the analysis. A physical description of the flow pattern and a discussion of some of the theoretical considerations are provided in Section II.

The governing differential equations for adiabatic and non-adiabatic flows are developed in Section III, and the nature of the solutions of these equations are discussed in Section IV. Section V contains a description of specific methods of solution for various configurations, while the results of some numerical computations are given in Section VI and in Appendix B. A brief discussion of possible extensions of the present method is provided in Section VII.

II. PRELIMINARY CONSIDERATIONS

II. 1. Flow Description

As an interesting example of the type of viscous-inviscid interaction considered in this investigation, it is instructive to examine the physical features of the interaction between an incident oblique shock wave and a laminar flat-plate boundary layer, shown schematically in Fig. 1. Additional configurations are described in Section IV and in Appendix B.

Because of the presence of the subsonic viscous layer near the wall, the pressure rise across the shock wave approaching the surface is diffused inside the boundary layer, and unless the shock is very weak, separation occurs upstream of the location of impingement. The effect of the incident shock wave decreases continuously in the upstream direction because of viscous dissipation in the boundary layer, and at some point, which can be considered the beginning of the interaction, the pressure rise communicated by the shock becomes negligible. Upstream of this location, the pressure gradient along the plate is induced by the rate of growth of the boundary layer itself and not by the external disturbance.

Because the laminar boundary layer cannot support a sudden rise in pressure, the incident shock wave is reflected as an expansion fan at impingement such that there is no pressure discontinuity along the surface. The thickness of the viscous layer increases ahead of the incident shock and decreases behind the expansion fan, generating convergent compression waves in the inviscid flow field and causing the external flow to turn. The boundary layer downstream of the

impingement point reaches a minimum section, or neck, and eventually approaches a weak interaction region at the new free-stream Mach number. Far from the surface of the body, the two families of compression waves and the expansion fan coalesce to form a shock wave corresponding to reflection from a solid wall in inviscid flow.

This physical description of the laminar boundary-layer/shock-wave interaction remains qualitatively unchanged for highly-cooled flows. The major effect of surface cooling is to increase the fluid density in the viscous layer near the wall, decreasing the boundary-layer thickness. As a result, the upstream distance of propagation of the pressure rise associated with the incident shock wave is considerably reduced. The beginning of the interaction approaches the separation point, which itself is located closer to the point of impingement, and the transition from undisturbed to fully-interacting flow occurs over a shorter distance than in the adiabatic case. This same phenomenon has been observed in turbulent flows, where the subsonic portion of the viscous layer is much smaller than it is in the corresponding laminar interaction.

In the moment method formulation, adiabatic flat-plate flows are subcritical, whereas highly-cooled ($S_w = -0.8$) flat-plate flows are supercritical. As a result, there is a fundamental difference in the analysis of the two situations. This question will be discussed in greater detail in Section IV.

II. 2. Theoretical Considerations

In the solution of many boundary-layer problems, a method utilizing integral relations is often required. The basic advantage

of this approach is that it allows the partial differential equations describing the flow to be integrated across the viscous layer and reduced to ordinary differential equations. In order to do this, however, it is necessary to make certain assumptions about the velocity and total enthalpy profiles, and many of the difficulties previously encountered in the use of integral methods can be traced to poor or inappropriate profile representation. Lees and Reeves[2] have shown that the solutions of the Falkner-Skan[3] equation for similar flow, including the reversed-flow profiles found by Stewartson[4], can be successfully used to represent the flow quantities. This procedure has been followed here for flows with heat transfer, using the Cohen-Reshotko[5] analogs of Stewartson's solutions (Section III. 2).

In addition to the three conservation equations for mass, momentum and energy, it is necessary to use at least one moment of the momentum equation in order to avoid the semi-empirical features inherent in methods such as the Crocco-Lees[6] mixing theory. The use of this additional equation is not unusual, but was first proposed by Sutton[7], and was used by Walz[8], Tani[9], and more recently by Lees and Reeves.[2,10] The energy equation, which was not employed by the authors cited above, assumes an important role for the case of flows with heat transfer, especially for highly-cooled flows. The use of this equation in the analysis provides additional flexibility and permits the introduction of a new independent parameter related to the total enthalpy profiles.

When the moment method was first applied to slightly cooled (or heated) viscous flows along a solid surface, the procedure of

linking the enthalpy and velocity profiles was adopted, and the energy equation was not used. A more general method was later attempted in which the enthalpy flux was regarded as an independent parameter, while all other quantities, including those directly related to the total enthalpy, were associated with the velocity profiles. In this manner the introduction of a second profile parameter was avoided, yet the energy integral equation was satisfied and some of the required flexibility was obtained. This method was not satisfactory because the prescribed relationship between the thermal and velocity layers proved too restrictive, particularly for flows in the presence of a positive pressure gradient.

The only consistent approach to the analysis of flows with heat transfer is to allow the velocity and total enthalpy profiles to be represented independently. At least two parameters are therefore required, one to describe the distribution of velocity through the boundary layer, and the other to describe the distribution of total enthalpy. For a given value of S_w, the most appropriate profile representation can be obtained from the family of Cohen-Reshotko solutions. Using these similar solutions to average all flow quantities across the boundary layer, the governing equations for flows with heat transfer can be reduced to a system of four simultaneous, first-order, non-linear differential equations.

III. THE GOVERNING EQUATIONS

III. 1. Basic Integral Equations

The basic partial differential equations describing a steady, two-dimensional, compressible boundary layer are:

$$(\rho u)_x + (\rho v)_y = 0 \tag{1}$$

$$\rho u u_x + \rho v u_y = - p_x + (\mu u_y)_y \tag{2}$$

$$\rho u h_{o_x} + \rho v h_{o_y} = \left(\frac{\mu}{P_r} h_{o_y}\right)_y - \left[\mu\left(\frac{1}{P_r} - 1\right) u u_y\right]_y \tag{3}$$

A fourth equation for the rate of change of mechanical energy is obtained by multiplying Eq. (2) by the velocity u, i.e.,

$$\rho u^2 u_x + \rho u v u_y = -u p_x + u(\mu u_y)_y \tag{4}$$

Integrating these equations across the viscous layer and assuming h_{o_e} = constant, one obtains:

$$\frac{d\delta^*}{dx} - (\delta - \delta^*)\frac{d\ell n \rho_e u_e}{dx} = \frac{v_e}{u_e} \equiv \tan \Theta \tag{5}$$

$$\frac{d}{dx}(\rho_e u_e^2 \theta) + \delta^* \rho_e u_e \frac{du_e}{dx} = \left(\mu \frac{\partial u}{\partial y}\right)_o \tag{6}$$

$$\frac{d}{dx}(\rho_e u_e^3 \theta^*) + 2(\delta^* - \delta_u)\rho_e u_e^2 \frac{du_e}{dx} = 2\int_o^\delta \mu\left(\frac{\partial u}{\partial y}\right)^2 dy \tag{7}$$

$$\frac{d}{dx}(\rho_e u_e \theta^{**}) = -\left[\frac{\mu}{P_r}\frac{\partial}{\partial y}\left(\frac{h_o}{h_{o_e}}\right)\right]_o \tag{8}$$

where

$$\delta = \int_o^\delta dy \qquad \delta^* = \int_o^\delta \left(1 - \frac{\rho u}{\rho_e u_e}\right) dy$$

$$\theta = \int_o^\delta \frac{\rho u}{\rho_e u_e}\left(1 - \frac{u}{u_e}\right) dy \qquad \theta^* = \int_o^\delta \frac{\rho u}{\rho_e u_e}\left(1 - \frac{u^2}{u_e^2}\right) dy \tag{9}$$

$$\delta_u = \int_o^\delta \left(1 - \frac{u}{u_e}\right) dy \qquad \theta^{**} = \int_o^\delta \frac{\rho u}{\rho_e u_e}\left(\frac{h_o}{h_{o_e}} - 1\right) dy$$

The boundary-layer functions appearing in Eqs. (5)-(8) can be related to equivalent incompressible quantities by assuming a viscosity law of the form:[11]

$$\frac{\mu}{\mu_\infty} = C \frac{T}{T_\infty} \tag{10}$$

and by using the Stewartson transformation [12]

$$dX = C \frac{a_e}{a_\infty} \frac{p_e}{p_\infty} dx \qquad dY = \frac{a_e}{a_\infty} \frac{\rho}{\rho_\infty} dy \tag{11}$$

In this transformation the relation between the transformed and physical velocities is

$$U = \frac{a_\infty}{a_e} u \tag{12}$$

With these assumptions, Eqs. (5)-(8) can be written

$$F \frac{d\delta_i^*}{dx} + \delta_i^* \left[\frac{d\mathcal{H}}{dx} - \frac{1+m_e}{m_e} \frac{dE}{dx}\right] + \delta_i^* f \frac{d\ell n M_e}{dx} = \beta \frac{1+m_e}{m_e(1+m_\infty)} \tan\Theta \tag{13}$$

$$\mathcal{H} \frac{d\delta_i^*}{dx} + \delta_i^* \frac{d\mathcal{H}}{dx} + \delta_i^* (2\mathcal{H}+1-E) \frac{d\ell n M_e}{dx} = \beta C \frac{M_\infty}{M_e} \frac{P}{Re_{\delta_i^*}} \tag{14}$$

$$J \frac{d\delta_i^*}{dx} + \delta_i^* \frac{dJ}{dx} + \delta_i^* (3J-2T^*) \frac{d\ell n M_e}{dx} = \beta C \frac{M_\infty}{M_e} \frac{R}{Re_{\delta_i^*}} \tag{15}$$

$$T^* \frac{d\delta_i^*}{dx} + \delta_i^* \frac{dT^*}{dx} + \delta_i^* T^* \frac{d\ell n M_e}{dx} = \beta C \frac{M_\infty}{M_e} \frac{Q}{Pr_w Re_{\delta_i^*}} \tag{16}$$

where

$$\beta = \frac{a_e}{a_\infty} \frac{p_e}{p_\infty} \qquad m_e = \frac{\gamma-1}{2} M_e^2$$

$$Re_{\delta_i^*} = \frac{a_\infty}{\nu_\infty} M_\infty \delta_i^* \tag{17}$$

and the transformed profile quantities are:

$$\delta_i = \int_o^{\delta_i} dY \qquad \delta_i^* = \int_o^{\delta_i} \left(1 - \frac{U}{U_e}\right) dY \tag{18}$$

$$\theta_i = \int_o^{\delta_i} \frac{U}{U_e}\left(1 - \frac{U}{U_e}\right) dY \qquad \theta_i^* = \int_o^{\delta_i} \frac{U}{U_e}\left(1 - \frac{U^2}{U_e^2}\right) dY$$

$$\mathcal{H} = \frac{\theta_i}{\delta_i^*} \qquad J = \frac{\theta_i^*}{\delta_i^*} \qquad Z = \frac{1}{\delta_i^*} \int_o^{\delta_i} \frac{U}{U_e}\, dY$$

$$R = 2\delta_i^* \int_o^{\delta_i} \left[\frac{\partial}{\partial Y}\left(\frac{U}{U_e}\right)\right]^2 dY \qquad P = \delta_i^* \left[\frac{\partial}{\partial Y}\left(\frac{U}{U_e}\right)\right]_{Y=0}$$

$$Q = \delta_i^* \left(\frac{\partial S}{\partial Y}\right)_{Y=0} \qquad E = \frac{-1}{\delta_i^*} \int_o^{\delta} S\, dY \qquad T^* = \frac{-1}{\delta_i^*} \int_o^{\delta} \frac{U}{U_e}\, S\, dY$$

$$F = \mathcal{H} + \frac{1+m_e}{m_e}(1-E)$$

$$f = \left[2 + \frac{\gamma+1}{\gamma-1}\frac{m_e}{1+m_e}\right]\mathcal{H} + \frac{3\gamma-1}{\gamma-1}(1-E) + \frac{M_e^2 - 1}{m_e(1+m_e)}\, Z$$

The profile quantities depend on both the velocity and total enthalpy distributions through the viscous layer; hence at least two parameters must be used in their description. However, it is not necessary to specify the actual detailed shape of the profiles since only relations among the different boundary-layer functions are required in the integral method. For example, if two parameters a and b are used to denote the velocity and total enthalpy profiles respectively, functional relations of the form $\mathcal{H} = \mathcal{H}(a)$, $J = J(a)$, $E = E(a, b)$, $T^* = T^*(a, b)$ etc. must be determined. One means for obtaining these relations is to assume that they can be approximated by corresponding relations among profile quantities obtained from the similarity solutions of Cohen and Reshotko[5] for both forward and reversed flow. In other words, the functional dependence

$J = J(\mathcal{V};S_w)$, for example, is assumed to be equivalent in non-similar and similar flows, and at a given S_w, all quantities which depend on the velocity profile ($\mathcal{V}$, J, Z, R, P) are determined by the particular value of $\mathcal{V}$ alone. In the same manner, the relations among the various functions of the total enthalpy distribution are assumed identical with those obtained from the similarity solutions. It should be emphasized that this procedure is entirely different from the so-called "method of local similarity" in which the profile shape is related to the local value of the pressure-gradient parameter β. Here there is no such dependence, and the similarity solutions are used only to specify relations among the different functions of the velocity and total enthalpy distributions.

By expressing all required profile quantities in terms of two independent parameters (Sections III. 2-III. 3) the number of unknowns in the system of differential equations, Eqs. (13)-(16), is reduced to five: M_e, δ_i^*, Θ and the two profile parameters. An additional flow relation for the streamline inclination Θ is obtained in Section III. 4.

III. 2. Velocity and Total Enthalpy Profiles

For a perfect fluid, the compressible boundary-layer equations, Eqs. (1)-(3), can be transformed into an equivalent low-speed form by using the Chapman-Rubesin[11] law, Eq. (10), and the Stewartson transformation, Eq. (11). The resulting equations are:

$$\frac{\partial U}{\partial X} + \frac{\partial V}{\partial Y} = 0 \tag{19}$$

$$U\frac{\partial U}{\partial X} + V\frac{\partial U}{\partial Y} = (1+S)U_e\frac{dU_e}{dX} + \nu_\infty\frac{\partial^2 U}{\partial Y^2} \tag{20}$$

$$U \frac{\partial S}{\partial X} + V \frac{\partial S}{\partial Y} = \frac{\nu_\infty}{P_r} \frac{\partial^2 S}{\partial Y^2} - \nu_\infty \left(\frac{1}{P_r} - 1\right) \frac{m_e}{1+m_e} \frac{\partial^2}{\partial Y^2}\left(\frac{U}{U_e}\right) \tag{21}$$

Cohen and Reshotko showed that the compressible flow analog of the Falkner–Skan[3] equation can be generated provided S_w = constant and $P_r = 1$. For these conditions and for a similarity variable of the form:

$$\eta = Y\left[\frac{m+1}{2} \frac{U_e}{\nu_\infty X}\right]^{\frac{1}{2}} \tag{22}$$

the partial differential equations, Eqs. (19)-(21), reduce to a system of ordinary equations:

$$\begin{aligned} f''' + ff'' + \beta(1+S-f'^2) &= 0 \\ S'' + fS' &= 0 \end{aligned} \tag{23}$$

where

$$\begin{aligned} U_e &\sim X^m \\ f' &\equiv \frac{df}{d\eta} = \frac{U}{U_e} \end{aligned} \tag{24}$$

and the pressure-gradient parameter β is defined as

$$\beta = \frac{2m}{m+1} \tag{25}$$

The boundary conditions are:

$$\begin{aligned} f(0) = f'(0) &= 0 \qquad & f'(\infty) &= 1 \\ S(0) &= S_w \qquad & S(\infty) &= 0 \end{aligned} \tag{26}$$

The similarity equations, Eqs. (23), were solved by Cohen and Reshotko for selected values of S_w and β, including a few of the

reversed-flow solutions first found by Stewartson[4] along the lower branch of the Falkner-Skan family. For the purpose of this study, additional solutions were obtained for both adiabatic ($S_w = 0$) and highly-cooled ($S_w = -0.8$) flows for the entire range of the pressure-gradient parameter β. A discussion of the procedures used to perform the numerical integration and some examples of the resulting velocity and total enthalpy profiles are given in Appendix A.

The similarity solutions can be used to determine the profile quantities appearing in Eqs. (13)-(16). For example, since the similarity variable η, Eq. (22), and the Y-coordinate are linearly related, the transformed displacement thickness can be written:

$$\begin{aligned} \delta_i^* &= \int_o^{\delta_i} \left(1 - \frac{U}{U_e}\right) dY \\ &= \frac{Y}{\eta} \int_o^{\eta(\delta_i)} \left(1 - \frac{U}{U_e}\right) d\eta \\ &\equiv \frac{Y}{a\eta} \end{aligned} \tag{27}$$

hence $dY = a\delta_i^* d\eta$

and $\dfrac{\delta_i}{\delta_i^*} = a\eta_{.99}$

where $a = \left[\int_o^{\eta_{.99}} \left(1 - \dfrac{U}{U_e}\right) d\eta\right]^{-1}$ (28)

and $\eta(\delta_i) = (\eta)_{U/U_e = .99} \equiv \eta_{.99}$

i.e., the edge of the boundary layer is arbitrarily taken at the point where the velocity $u = 0.99\, u_e$.

Using the quantity $a = \dfrac{1}{\eta} \dfrac{Y}{\delta_i^*}$ as the scaling parameter, all non-dimensional profile functions can be related to equivalent

similarity expressions. For example:

$$\theta_i \equiv \int_o^{\delta_i} \frac{U}{U_e}\left(1 - \frac{U}{U_e}\right)dY = a\delta_i^* \int_o^{\eta_{.99}} \frac{U}{U_e}\left(1 - \frac{U}{U_e}\right)d\eta \qquad (29)$$

hence

$$\mathcal{H} \equiv \frac{\theta_i}{\delta_i^*} = a\int_o^{\eta_{.99}} \frac{U}{U_e}\left(1 - \frac{U}{U_e}\right)d\eta$$

Similarly,

$$P \equiv \delta_i^*\left[\frac{\partial}{\partial Y}\left(\frac{U}{U_e}\right)\right]_{Y=0} = \frac{1}{a}\left[\frac{d}{d\eta}\left(\frac{U}{U_e}\right)\right]_{\eta=0} = \frac{f''(0)}{a}$$

$$E = \left(\frac{-1}{\delta_i^*}\right)\int_o^{\delta_i} S\,dY = -a\int_o^{\eta_{.99}} S\,d\eta \qquad (30)$$

$$Q = \delta_i^*\left(\frac{\partial S}{\partial Y}\right)_{Y=0} = \frac{1}{a}\left(\frac{dS}{d\eta}\right)_{\eta=0} = \frac{S'(0)}{a}$$

As discussed in Section III. 1, the eight non-dimensional profile quantities must be expressed as functions of at least two independent parameters. These parameters can be selected from any of the quantities appearing in the similarity solutions provided only that they remain single-valued and finite for all profiles. Also, in order to be able to treat problems in adiabatic flow, one of the parameters should be independent of the distribution of total enthalpy. Following the procedure of Lees and Reeves[2], the parameter chosen to specify the velocity distribution is as follows:

Attached velocity profiles ($f''(0) \geq 0$):

$$a(x) = \eta_{.99}\, f''(0) = \left[\frac{\partial(U/U_e)}{\partial(Y/\delta_i)}\right]_{Y=0} \qquad (31a)$$

$$0 \leq a < 4$$

Separated velocity profiles ($f''(0) \leq 0$):

$$a(x) = \frac{(\eta)_{f'=0}}{\eta_{.99}} = \left(\frac{Y}{\delta_i}\right)_{U/U_e = 0} \qquad (31b)$$

$$0 \leq a < 1$$

Although the quantity a(x) satisfies the conditions mentioned above, it is not the best possible parameter because it must be defined differently for attached and separated flows. As a result, derivatives of the profile quantities with respect to a are discontinuous at the separation and reattachment point. Also, since a is an arbitrary parameter not appearing in the differential equations, Eqs. (13)-(16), one more curve-fit that would otherwise be necessary is required (see Section III.3). It is suggested that for future work one of the single-valued integrals appearing in the equations, such as $\mathcal{Y}$ or J, be selected as a more appropriate velocity parameter.

The second parameter was chosen to specify the distribution of total enthalpy as follows:

$$b(x) = S'(0) = \alpha(a)\left[\frac{\partial S}{\partial(Y/\delta_i^*)}\right]_{Y=0} \qquad (32)$$

$$0 \leq b < .5$$

For the case of adiabatic flow in an expansion turn, a difficulty arises from the fact that the integral quantities reach a maximum. As shown by Coles[13], an analytic solution of the similarity equations for $S_w = 0$ can be obtained in the limit $\beta \to \infty$, i.e.,

$$f' = 1 - 3\,\mathrm{sech}^2\left[\sqrt{\frac{\beta}{2}}\,\eta + \tanh^{-1}\sqrt{\frac{2}{3}}\right] \qquad (33)$$

$$\text{hence} \quad a_{max} = \left[\eta_{.99}\, f''(0)\right]_{\beta\to\infty} \simeq 3.92 \quad .$$

When the differential equations are integrated through an adiabatic expansion turn, a(x) exceeds its maximum value, indicating that the profiles become non-similar. This difficulty can be avoided by adopting a new set of profiles for the boundary layer in this region; however, since the integral functions change very slowly in highly-accelerated flows, the easiest procedure is to retain the similarity representation and to assume that all profile quantities remain fixed at their maximum values for $a \geq 3.92$. The parameter a(x) can be allowed to increase, although it has no physical significance in this region and cannot be related to the similar profiles. After the completion of the expansion turn, a(x) begins to decrease, and the similarity solutions can again be used downstream of the location where $a = 3.92$. This difficulty does not arise in non-adiabatic flows because the thermal layer remains finite, even in the limit $\beta \to \infty$, and the similar functions do not reach a maximum. Also, for a given expansion corner, the velocity profiles accelerate less rapidly in highly-cooled than in adiabatic flow, and the parameter a(x) remains relatively small. This is illustrated, for example, by the difference between the two strong-interaction solutions given in Section VI. 1.

III. 3. Curve-Fits of Profile Quantities

The similarity solutions can be used to express all required velocity-dependent quantities as functions of the parameter a, and all enthalpy-dependent quantities are functions of the parameter b. The distributions of a and b as functions of x for any given viscous-inviscid interaction are then determined by the solution of the differential equations with appropriate boundary conditions. These

equations, Eqs. (13)-(16), can be written in terms of the two parameters as follows:

$$F\frac{d\delta_i^*}{dx} + \delta_i^*\left(\frac{\partial F}{\partial a}\frac{da}{dx} + \frac{\partial F}{\partial b}\frac{db}{dx}\right) + \frac{f\delta_i^*}{M_e}\frac{dM_e}{dx} = \beta C\frac{M_\infty}{M_e}\frac{h}{Re_{\delta_i^*}} \tag{34}$$

$$\mathcal{V}\frac{d\delta_i^*}{dx} + \delta_i^*\frac{d\mathcal{V}}{da}\frac{da}{dx} + (2\mathcal{V}+1-E)\frac{\delta_i^*}{M_e}\frac{dM_e}{dx} = \beta C\frac{M_\infty}{M_e}\frac{P}{Re_{\delta_i^*}} \tag{35}$$

$$J\frac{d\delta_i^*}{dx} + \delta_i^*\frac{dJ}{d\mathcal{V}}\frac{d\mathcal{V}}{da}\frac{da}{dx} + (3J-2T^*)\frac{\delta_i^*}{M_e}\frac{dM_e}{dx} = \beta C\frac{M_\infty}{M_e}\frac{R}{Re_{\delta_i^*}} \tag{36}$$

$$T^*\frac{d\delta_i^*}{dx} + \delta_i^*\left(\frac{\partial T^*}{\partial a}\frac{da}{dx} + \frac{\partial T^*}{\partial b}\frac{db}{dx}\right) + T^*\frac{\delta_i^*}{M_e}\frac{dM_e}{dx} = \beta C\frac{M_\infty}{M_e}\frac{\bar{Q}}{Re_{\delta_i^*}} \tag{37}$$

where

$$\frac{\partial F}{\partial a} = \frac{d\mathcal{V}}{da} - \frac{1+m_e}{m_e}\frac{\partial E}{\partial a}\ ;\quad \frac{\partial F}{\partial b} = -\frac{1+m_e}{m_e}\frac{\partial E}{\partial b}\ ;\quad \bar{Q} = \frac{Q}{P_{r_w}} \tag{38}$$

and

$$h = \frac{M_e}{M_\infty}\frac{1+m_e}{m_e(1+m_\infty)}\,Re_{\delta_i^*}\,\frac{\tan\Theta}{C} \tag{39}$$

When a sufficient number of similarity solutions has been obtained and the required profile-related quantities tabulated, the easiest procedure is to express these quantities as polynomial functions of the two parameters using a least-squares curve-fit. The velocity-dependent quantities $\mathcal{V}$, J, Z, R, P and the derivatives $d\mathcal{V}/da$, $dJ/d\mathcal{V}$ are functions of the parameter a only and can be curve-fitted directly. The distributions of these quantities are shown in Figs. 2 - 8 for both an adiabatic ($S_w = 0$) and a highly-cooled ($S_w = -0.8$) surface, and the coefficients of the curve-fits are given in Tables 1 and 2 (i.e. $\mathcal{V} = \sum_{k=0}^{7} C_k\, a^k$). Values of the two derivatives $d\mathcal{V}/da$ and $dJ/d\mathcal{V}$ used to determine the polynomial representations were obtained from the similarity solutions by forming the difference quotient for

adjacent quantities. For example:

$$\frac{d\mathscr{V}}{da}(\bar{a}) = (\mathscr{V}_{i+1}-\mathscr{V}_i)/(a_{i+1}-a_i) \tag{40}$$

where $\bar{a} = (a_i+a_{i+1})/2$

The remaining profile quantities are functions of both the velocity and enthalpy parameters a and b. The difficulty of determining the distributions of these quantities can be simplified to some extent by obtaining the polynomial representation of the function $\alpha = \alpha(a)$, Eq. (28), and by using the integrals:

$$\sigma(b) = -\int_o^{\eta_{.99}} S\, d\eta \tag{41}$$

$$T(a, b) = -\int_o^{\eta_{.99}} \frac{U}{U_e} S\, d\eta \tag{42}$$

such that

$$Q = b/\alpha(a) \tag{43}$$

$$E = \alpha(a)\ \sigma(b) \tag{44}$$

$$T^* = \alpha(a)\ T(a, b) \tag{45}$$

and

$$\frac{\partial E}{\partial a} = \sigma(b)\frac{d\alpha}{da}\ ;\ \frac{\partial E}{\partial b} = \alpha(a)\frac{d\sigma}{db} \tag{46}$$

$$\frac{\partial T^*}{\partial a} = T(a, b)\frac{d\alpha}{da} + \alpha(a)\frac{\partial T}{\partial a}$$

$$\frac{\partial T^*}{\partial b} = \alpha(a)\frac{\partial T}{\partial b} \tag{47}$$

The integral quantity T(a, b), Eq. (42), depends on both parameters and was determined by multiplying every similar velocity profile by every enthalpy profile, point by point, integrating to the value

of $\eta_{.99}$ corresponding to the largest profile. The distribution of T(a, b) was then obtained by using two fifth-order polynomials in the parameter a, for each value of b, to describe the variation in the attached and separated regions respectively. These coefficients were subsequently curve-fitted as functions of b; hence the quantity T(a, b) is given by the expression:

$$T(a, b) = \sum_{k=0}^{5} \tau_k(b)\, a^k \tag{48}$$

where

$$\tau_k(b) = \sum_{\ell=0}^{5} D_{k\ell}\, b^{\ell} \tag{49}$$

The distributions of $\alpha(a)$, $d\alpha/da$, $\sigma(b)$, $d\sigma/db$, $T(a, b)$, $\partial T/\partial a$ and $\partial T/\partial b$ are shown in Figs. 9 - 14 , and the coefficients of the curve-fits of these quantities are given in Tables 2 and 3. It is evident that the polynomial expressions obtained in the manner described provide reasonably accurate representations of the distributions of the required profile functions.

III. 4. The Induced Streamline Inclination Θ

In most viscous-inviscid interactions, the outer flow cannot be specified a priori since it is determined by the normal velocity induced by the growth of the boundary layer. Thus the inclination $\Theta = \tan^{-1} v_e/u_e$ of the inviscid streamline at $y = \delta$ is related to the viscous flow field through the continuity equation, Eqs. (5) or (34). The coupling between the inner and outer flows arises from the fact that the Mach number distribution at the edge of the boundary layer, $M_e(x)$, is related to the induced streamline angle $\Theta(x)$ by the appropriate inviscid solution of the external flow field.

For two-dimensional supersonic inviscid flow, the change in Mach number is determined entirely by the local streamline deflection. In general it is necessary to resort to numerical or graphical methods, such as the method of characteristics, to determine the entire flow field. However, if the flow is irrotational, the Mach number and the streamline inclination can be directly connected through the Prandtl-Meyer relation. Thus for all two-dimensional viscous-inviscid interactions in which the local external flow can be considered isentropic, the following relation between Θ and M_e is a good approximation:

$$\Theta = \alpha_w(x) + \nu(M_{\infty\pm}) - \nu(M_e) \tag{50}$$

where $\alpha_w(x)$ is the inclination of the local tangent to the surface, considered positive for an expansion turn. The Prandtl-Meyer function is defined in the usual manner, i.e.:

$$\nu(M) = \sqrt{\frac{\gamma+1}{\gamma-1}}\,\tan^{-1}\sqrt{\frac{\gamma-1}{\gamma+1}(M^2-1)} - \tan^{-1}\sqrt{M^2-1} \tag{51}$$

The reference condition must be selected such that $M_{\infty\pm}$ is the Mach number which the local external flow either departs from or approaches through and isentropic process. Thus in boundary-layer/shock-wave interactions, for example, the Mach number far upstream, $M_{\infty-}$, is used as the reference point for the flow upstream of the shock impingement location, and the Mach number at downstream infinity, $M_{\infty+}$, is used for the flow downstream of impingement (Section VI.2). For the case of flow around a circular cylinder, the reference point is taken in the wake (Appendix B).

For certain interactions, particularly in hypersonic flow, a direct relation between Θ and the static pressure ratio may be a better, or more convenient, approximation. In these cases, the tangent-wedge relation is useful, i.e.:

$$\Theta = \alpha_w(x) + \frac{(p_e/p_\infty - 1)}{\gamma M_\infty} \left[1 + \frac{\gamma+1}{2\gamma}(p_e/p_\infty - 1)\right]^{-\frac{1}{2}} \tag{52}$$

This relation is obtained by examining the oblique shock equations for small deflections and high Mach number and is therefore valid for non-isentropic flows. However, since the Mach number M_e appears in the differential equations, Eqs. (34)-(37), the external flow must usually be assumed isentropic. This assumption is valid, however, provided that the compression waves generated by the boundary layer coalesce into a shock wave far from the surface and that the effects of vorticity induced by the curvature of the leading-edge shock can be neglected. An approximate method for including some of the effects of the entropy variation produced by the curvature of the leading-edge shock is discussed in Section V.3.

III.5. Final Form of Differential Equations

Once the polynomial representations of the profile quantities have been obtained and either of the relations, Eqs. (50) or (52), for the streamline angle Θ is used, the only dependent variables in the differential equations, Eqs. (34)-(37), are $M_e(x)$, $\delta_1^*(x)$, $a(x)$ and $b(x)$. By regarding the equations as a set of algebraic relations for the four unknown first derivatives and solving simultaneously, the following convenient form for numerical computation is obtained:

$$\frac{\delta_i^*}{M_e}\frac{dM_e}{dx} = \frac{\beta C}{Re_{\delta_i^*}}\frac{M_\infty}{M_e}\left[\frac{N_1(M_e, a, b, h)}{D(M_e, a, b)}\right] \tag{54}$$

$$\frac{d\delta_i^*}{dx} = \frac{\beta C}{Re_{\delta_i^*}}\frac{M_\infty}{M_e}\left[\frac{N_2(M_e, a, b, h)}{D(M_e, a, b)}\right] \tag{55}$$

$$\delta_i^*\frac{da}{dx} = \frac{\beta C}{Re_{\delta_i^*}}\frac{M_\infty}{M_e}\left[\frac{N_3(M_e, a, b, h)}{D(M_e, a, b)}\right] \tag{56}$$

$$\delta_i^*\frac{db}{dx} = \frac{\beta C}{Re_{\delta_i^*}}\frac{M_\infty}{M_e}\left[\frac{N_4(M_e, a, b, h)}{D(M_e, a, b)}\right] \tag{57}$$

where

$$D(M_e, a, b) = B_1\frac{\partial T^*}{\partial b} - B_2\frac{\partial F}{\partial b} \tag{58}$$

$$N_1(M_e, a, b, h) = B_3\frac{\partial T^*}{\partial b} - B_4\frac{\partial F}{\partial b}$$

$$N_2(M_e, a, b, h) = B_5\frac{\partial T^*}{\partial b} - B_6\frac{\partial F}{\partial b}$$

$$N_3(M_e, a, b, h) = B_7\frac{\partial T^*}{\partial b} - B_8\frac{\partial F}{\partial b}$$

$$N_4(M_e, a, b, h) = B_4 f + B_6 F + B_8\frac{\partial F}{\partial a} - B_2 h$$

and

$$B_1 = A_6\frac{\partial F}{\partial a} + (A_3 f - A_8 F)\frac{d\mathcal{V}}{da} \tag{59}$$

$$B_2 = A_6\frac{\partial T^*}{\partial a} + (A_3 - A_8)T^*\frac{d\mathcal{V}}{da}$$

$$B_3 = A_2\frac{\partial F}{\partial a} + (A_3 h - A_4 F)\frac{d\mathcal{V}}{da}$$

$$B_4 = A_2\frac{\partial T^*}{\partial a} + (A_3\bar{Q} - A_4 T^*)\frac{d\mathcal{V}}{da}$$

$$B_5 = A_7\frac{\partial F}{\partial a} + (A_4 f - A_8 h)\frac{d\mathcal{V}}{da}$$

$$B_6 = A_7 \frac{\partial T^*}{\partial a} + (A_4 T^* - A_8 \overline{Q}) \frac{d\chi}{da}$$

$$B_7 = A_6 h - (A_2 f + A_7 F)$$

$$B_8 = A_6 \overline{Q} - (A_2 + A_7) T^*$$

where

$$A_1 = 2\chi + 1 - E \tag{60}$$

$$A_2 = PJ - \chi R$$

$$A_3 = \chi \frac{dJ}{d\chi} - J$$

$$A_4 = P \frac{dJ}{d\chi} - R$$

$$A_5 = 3J - 2T^*$$

$$A_6 = A_1 J - A_5 \chi$$

$$A_7 = A_1 R - A_5 P$$

$$A_8 = A_1 \frac{dJ}{d\chi} - A_5$$

For the adiabatic case, Eqs. (58) reduce to the following:

$$D(M_e, a) = A_6 + A_3 f - A_8 F \tag{61}$$

$$N_1(M_e, a, h) = A_2 + A_3 h - A_4 F$$

$$N_2(M_e, a, h) = A_7 + A_4 f - A_8 h$$

$$N_3(M_e, a, h) = (A_6 h - A_2 f - A_7 F)/(d\chi/da)$$

where $E = T^* = 0$ in Eqs. (60).

IV. NATURE OF SOLUTIONS

IV.1. Subcritical and Supercritical Flows

In Section II.1, a brief allusion was made to the fact that adiabatic flat-plate flows are subcritical, whereas highly-cooled ($S_w = -0.8$) flows are supercritical. In essence, subcritical flows are those which allow the upstream propagation of the effect of an external disturbance, such as the pressure rise associated with an incident shock wave. Supercritical flows, on the other hand, cannot communicate the effect of a disturbance in the upstream direction. Thus subcritical boundary layers will respond to disturbances occurring further downstream, while supercritical boundary layers will not be sensitive to downstream disturbances.

The difference in behavior between the two types of flow is a consequence of the use of an integral method to represent the viscous flow field. Since all physical quantities are averaged across the viscous layer, a boundary layer with a small subsonic region behaves as if it were supersonic in some sense, and there is no mechanism by which it can respond to downstream disturbances. To understand how this situation can arise, it is useful to re-examine the basic equations for compressible boundary-layer flow.

IV.1.1. Analytical Considerations

Following an analysis similar to those of Lees [14] and Lighthill [15], the combined continuity and momentum equations, Eqs. (1)-(2), can be written in the form:

$$\rho u^2 (\tan \Theta)_y + u(u\rho_x + v\rho_y) = p_x - \tau_y \tag{62}$$

where $\tan \Theta = v/u$.

The energy equation, Eq. (3), can be approximated by:

$$(\mu h_{o_y})_y = \rho u(uu_x + vu_y) - \frac{a^2}{\gamma - 1}(u\rho_x + v\rho_y) + \frac{\gamma}{\gamma - 1} up_x \tag{63}$$

where the terms containing the mass flow ρv in the y-direction have been neglected.

Combining these two equations with the equation for mechanical energy, Eq. (4), and integrating across the viscous layer, a relation for the streamline angle at the edge of the boundary layer can be obtained:

$$\tan \Theta_\delta = \frac{1}{\gamma p}\left\{\frac{dp}{dx}\int_o^\delta \frac{1-M^2}{M^2}\, dy - \int_o^\delta \frac{1+(\gamma-1)M^2}{M^2}\tau_y\, dy + \int_o^\delta \frac{\gamma - 1}{u}(\mu h_{o_y})_y\, dy\right\} \tag{64}$$

where $M^2 = u^2/a^2$.

Although the integrands in this equation diverge near $y = 0$, all integrals remain finite since $(p_x - \tau_y) \sim u^2$ and $(\mu h_{o_y})_y \sim u$ near the wall, as is evident from the momentum and energy equations. Defining a small sublayer $S \ll \delta$, Eq. (64) can be written in the form:

$$\tan \Theta_\delta = \varphi + \left(\frac{1}{\gamma p}\frac{dp}{dx}\right)\int_S^\delta \frac{1-M^2}{M^2}\, dy \tag{65}$$

where φ contains those quantities which are not of particular importance in the present simplified analysis.

For supersonic external flow, where $M_e > 1$, the integrand in the integral on the right-hand side of Eq. (65) will be negative above the sonic line, although the integral itself will remain positive so long as the subsonic region of the boundary layer is sufficiently large. When this region becomes small, however, the integral will become negative and the subsonic portion of the boundary layer will be effectively suppressed. In other words, in any integral or moment method, flows in which the distance of the sonic line from the surface is small behave in much the same manner as purely supersonic viscous flows.

One of the consequences of this behavior can be seen for the case where the edge of the boundary layer is a streamline. In this situation $\tan \Theta_\delta = d\delta/dx$, and Eq. (65) shows that if the subsonic portion of the boundary layer is sufficiently large, $d\delta/dp > 0$, whereas if this region is small, $d\delta/dp < 0$. Subcritical flows can be defined as those for which $d\delta/dp > 0$, while supercritical flows are those for which $d\delta/dp < 0$, a distinction first pointed out by Crocco[16] for the case of turbulent boundary layers. Using this definition, subcritical viscous flows are those which interact with the external stream to produce a pressure gradient which is consistent with the deflection of the layer. A thickening subcritical boundary layer, for example, produces a rise in pressure which causes a still greater thickening of the layer. A supercritical boundary layer, on the other hand, cannot generate its own pressure gradient.

Another illustration of the characteristic behavior of subcritical and supercritical flows can be obtained from Eq. (65) by

relating the external streamline angle Θ_δ to the local Mach number M_e through the Prandtl-Meyer relation, i.e.:

$$\frac{M_e^2}{\sqrt{M_e^2-1}} \frac{d\Theta}{dx} = \frac{1}{\gamma p} \frac{dp}{dx} \tag{66}$$

With this relation, Eq. (65) can be integrated to give an expression of the form:

$$\Theta(x) = \Theta_o + C \exp\left[K\left(\frac{x-x_o}{\delta}\right)\right] \tag{67}$$

where

$$K = \left[\frac{M_e^2}{\sqrt{M_e^2-1}} \int_{S/\delta}^{1} \frac{1-M^2}{M^2} d\left(\frac{y}{\delta}\right)\right]^{-1}$$

This equation shows one of the essential differences between the two types of flow. When the quantity K in Eq. (67) is positive, the boundary layer is subcritical and the viscous flow quantities grow exponentially in the downstream direction. If the flow is supercritical, however, K is negative and the boundary layer decays from an initial state to a downstream undisturbed, or Blasius, condition. Thus small perturbations in subcritical flow will be amplified, whereas all perturbations are damped in supercritical flow. Physically, this means that the effect of an external disturbance, such as an incident shock wave, is propagated continuously upstream only so long as the flow is subcritical. An initially supercritical boundary layer can respond to a pressure rise generated downstream only through a sudden transition to a subcritical state, after which the flow proceeds smoothly.

The parameters which affect the location of the sonic line

can be deduced from the equation for the velocity ratio at that point, i.e.:

$$\left(\frac{u}{u_e}\right)_{M=1} = \left[\frac{\gamma-1}{\gamma+1}\,\frac{1+m_e}{m_e}\,(1+S)\right]^{\frac{1}{2}} \tag{68}$$

This relation indicates that the boundary layer may become supercritical as the external Mach number is increased, as the wall is cooled ($S_w \rightarrow -1$) or as the velocity profile is accelerated. Of course, the specific conditions under which subcritical-supercritical transition occurs are determined by the particular choice of velocity and enthalpy profiles and by the equations used to describe the interacting flow field.

IV.2. Subcritical-Supercritical Transition

In the moment method formulation, the simultaneous vanishing of the determinant D and the numerators N, Eqs. (61), describes a locus of singular points at which the derivatives dM_e/dx, da/dx etc. are non-unique. It is this line of singularities of the system of equations which marks the transition between subcritical and supercritical flows.

For adiabatic boundary layers, the locus of points D = 0 is a unique function of M_e and a, as shown in Fig. 15 . In this case, the critical points D = 0 lie in the region $a > a_{BL}$, corresponding to velocity profiles which have been accelerated above the zero pressure-gradient solution, i.e., flow in an expansion turn. Self-induced viscous flow along a flat plate, as well as interactions caused by compressive disturbances, are therefore always subcritical in adiabatic flow, and $D \neq 0$ everywhere in the interaction region.

For non-adiabatic boundary layers, the locus of critical points $D = 0$ is a function of M_e, a and b. In highly-cooled ($S_w = -0.8$) flow, the critical points for $M_e > 2$ lie in the region $a < a_{BL}$, Fig. 15, corresponding to velocity profiles between the separation and flat-plate solutions. Viscous flow along a highly-cooled surface is therefore supercritical unless there is a compressive disturbance which decelerates the flow toward separation. If such a disturbance is present, the boundary layer must undergo a transition from a supercritical to a subcritical state at some location upstream of the disturbance.

Flows which are supercritical in the moment method formulation are actually flows which have a finite, although high, impedance to the upstream propagation of disturbances. Under these conditions, the effect of an external disturbance is felt only a short distance upstream, and the boundary layer at that location changes rapidly from an undisturbed to a fully-interacting state. Although this change takes place over a few boundary layer thicknesses, in the integral formulation the transition from supercritical to subcritical flow must be approximated by a discontinuity, or jump, occurring in the flow quantities at some point upstream of the disturbance. The strength of the jump is obtained by applying the proper conservation relations to the viscous flow, as discussed in Section V.1. Downstream of the jump, the boundary layer is subcritical and the flow proceeds smoothly through the interaction region.

For flows which are initially subcritical and become supercritical at some downstream location because of an expansion turn,

for example, the situation is completely different. Subcritical flows must respond to disturbances occurring further downstream, hence the transition from a subcritical to a supercritical state must be continuous. The requirement for smooth subcritical-supercritical transition is, in fact, one of the boundary conditions for any viscous-inviscid interaction of this type (see Section IV. 3).

In the moment method formulation, the condition for continuous transition between subcritical and supercritical flows is given by the requirement that the numerators N_1, N_2, N_3 and N_4 in Eqs. (57)-(60) vanish when D = 0. It is sufficient, however, for only one of the numerators to vanish at the critical point since the N's are obtained from the same set of equations and thus are not all independent. The relation for the singular point, or throat, can thus be written:

$$h_{TH} = \left\{ \left[\left(A_4 F \frac{d\mathcal{N}}{da} - A_2 \frac{\partial F}{\partial a} \right) \frac{\partial T^*}{\partial b} + B_4 \frac{\partial F}{\partial b} \right] \Big/ \left[A_3 \frac{d\mathcal{N}}{da} \frac{\partial T^*}{\partial b} \right] \right\}_{D=0} \tag{69}$$

where

$$h_{TH} = \left[\frac{M_e}{M_\infty} \frac{1+m_e}{m_e(1+m_\infty)} \, Re_{\delta_i^*} \frac{\tan \Theta}{C} \right]_{N_i = D = 0} \tag{70}$$

For adiabatic flow, Eq. (69) reduces to the simple expression:

$$h_{TH} = \left[(A_4 F - A_2) / A_3 \right]_{D=0} \tag{71}$$

These two relations are shown in Fig. 16 .

One result which can be immediately obtained from these equations is the required sign of the induced streamline angle Θ at the throat. For adiabatic flow, for example, $h_{TH} > 0$, hence the angle Θ must be positive at the critical point to allow the boundary

layer to pass through the singularity. Using the Prandtl-Meyer relation, Eq. (50), this means that transition can only occur along a surface for which

$$a_w(x) > \nu(M_e) - \nu(M_{\infty\pm}) \tag{72}$$

Since the adiabatic boundary layer must be accelerated in order to become supercritical, $M_e > M_{\infty-}$ and the right-hand side of the above inequality is positive. Smooth subcritical-supercritical transition is therefore possible for adiabatic flow in an expansion turn provided the throat is located along the curved portion of the body ($a_w(x) > 0$). An interesting example of this situation is the case of flow around a circular cylinder discussed in Appendix B.

The inequality given in Eq. (72) also indicates a second possibility for smooth transition in adiabatic flow. For the case of a supercritical boundary layer expanding toward a downstream Blasius condition, such that $M_e < M_{\infty+}$, smooth transition from a supercritical to a subcritical state can occur along a flat surface. This situation can arise for flow along an adiabatic flat plate downstream of a blunt leading edge or an expansion corner in which the boundary layer becomes supercritical. This is one example of a class of problems for which continuous supercritical-subcritical transition is possible; in most interactions, as previously discussed, a jump is required to join the two solutions. Smooth transition occurs in this situation because the subcritical portion of the integral curve represents a "relaxing" boundary layer rather than flow upstream of an external disturbance. Since all supercritical flows decay from

an initial state toward the downstream Blasius condition, the two branches of the solution can be smoothly joined at the critical point. The question of relaxing viscous flows will be discussed in greater detail in Section IV. 4.

For highly-cooled boundary layers at moderately supersonic Mach numbers ($M_e > 2$), the induced angle Θ must be negative at the throat. Smooth transition is therefore possible provided

$$a_w(x) < \nu(M_e) - \nu(M_{\infty\pm}) \tag{73}$$

Since non-adiabatic flat-plate flow is initially supercritical, Eq. (73) indicates that continuous supercritical-subcritical transition is not possible on a flat surface upstream of a compressive disturbance ($M_e < M_{\infty-}$). Although the inequality implies that smooth transition might occur in a gradual compression turn ($a_w(x) < 0$), such solutions are unstable and therefore of little physical interest. Thus in highly-cooled flows, any viscous-inviscid interaction caused by a compressive disturbance is initiated by a jump to a subcritical state at some point upstream of the disturbance. The boundary layer remains subcritical through the interaction region and can return to a supercritical state far downstream of the disturbance, where $M_e > M_{\infty+}$ and smooth transition along a flat surface is possible.

From the above discussion, it is evident that the different classes of viscous-inviscid interactions are determined by the subcritical or supercritical character of the flow. By considering specific examples of various types of interactions which occur in supersonic flow, some of the ideas presented in the previous sections

can be clarified.

IV.3. Typical Viscous-Inviscid Interactions

IV.3.1. Completely Subcritical Interactions

An interesting example of subcritical boundary-layer interactions is provided by the case of adiabatic flow in a compression corner. Typical trajectories for the edge Mach number M_e and the velocity profile parameter a for this type of interaction are given in Fig. 17 .

The boundary layer along the forward portion of the flat plate is determined by the leading-edge solution and the subsequent relaxation toward the Blasius condition corresponding to $M_{\infty-}$ (see Section V.3). In this region, the flow is identical with the flow which would have existed along a semi-infinite flat plate in the absence of any external disturbances. At some location x_o upstream of the corner, however, the boundary layer departs from the flat-plate solution. This point can be considered as the beginning of the interaction and is the most upstream location at which the effect of the compression turn is felt. For sufficiently large turns, the boundary layer passes through separation ($a = 0$), into the plateau or constant-pressure region, and through reattachment along the surface of the ramp. Far downstream of the corner the viscous flow approaches the Blasius condition associated with the new reference Mach number $M_{\infty+}$.

This interaction is entirely subcritical, and $D \neq 0$ everywhere in the range of integration. The correct solution curve must satisfy the boundary condition corresponding to Blasius flow at downstream infinity for the particular geometric constraint, i.e., the distribution

of $a_w(x)$, imposed. The location of the beginning of the interaction, x_o, is not known a priori, hence initial conditions for downstream integration cannot be specified and an inverse, or iterative method must be used. The easiest procedure is to select the point x_o far upstream of the interaction and to obtain approximate initial values for the unknown variables from the solution for self-induced flow at that location. The correct set of initial conditions can subsequently be obtained by perturbing the flat-plate solution in some predetermined manner until an integral curve satisfying the downstream boundary condition is obtained. In practice, it turns out that the range of possible values of x_o is restricted for any given configuration because of limitations on the magnitude of the perturbation. This question will be discussed in greater detail in Section V.1.

IV.3.2. Completely Supercritical Interactions

An example of this type of interaction is given by the case of highly-cooled ($S_w = -0.8$) flow through an expansion turn shown in Fig. 18. Since the boundary layer is supercritical, it does not respond to the downstream disturbance caused by the expansion corner. The flow approaching the turn is therefore given by the flat-plate solution, and the integral curve diverges from this solution only at the beginning of the corner where the curvature of the surface $a_w(x) \neq 0$. Downstream of the corner the boundary layer approaches the Blasius condition corresponding to the new free-stream Mach number $M_{\infty+}$. Initial conditions can be obtained at any location upstream of the expansion turn from the eigensolution for self-induced flow, and since integration in the downstream

direction is everywhere stable, the solution for a given configuration can be obtained without iteration.

IV.3.3. Subcritical-Supercritical-Subcritical Interactions

One of the most interesting illustrations of this type of interaction is given by the case of adiabatic flow through an expansion turn. The Mach number and velocity-parameter trajectories for this configuration are shown in Fig. 19 .

As for all interactions occurring along a surface having a sharp leading edge, the upstream portion of the flow field is given by the semi-infinite flat-plate solution. The boundary layer begins to diverge from this solution at the point x_o upstream of the corner, continues to accelerate as it enters the turn and becomes supercritical along the curved portion of the body. The supercritical flow expands until the completion of the turn, after which it begins to decelerate, passes through a second throat into the subcritical region, and relaxes toward the downstream Blasius condition.

As in the case of completely subcritical interactions, the location x_o is not known a priori and an iterative method must be used to obtain the proper integral curve. For this configuration, of course, the perturbation of the solution for self-induced flow at x_o must be in the direction of an accelerating boundary layer. There is one fundamental and important difference between the two types of interactions, however. For all subcritical flows which become supercritical at some point, the downstream boundary condition is given by the requirement for smooth transition at the throat. The correct initial conditions at x_o are therefore those which give the

trajectory for which $N_i = 0$ when $D = 0$ and hence allow the integral curve to pass continuously through the singularity. Since supercritical flows relax toward the Blasius condition, the boundary layer downstream of the corner will pass smoothly back into the subcritical region and approach the flat-plate solution.

This interaction is entirely analogous to the case of flow through a converging-diverging nozzle followed by a supersonic diffuser. The throat of the nozzle plays the same role as the first singular point in the moment method analysis, and the solution is uniquely determined by the requirement for smooth transition from a subcritical to a supercritical state at this station. The throat of the diffuser is equivalent to the second singular point in the interaction, and the flow passes smoothly through this location under normal conditions. However, if the pressure downstream of the diffuser is high, corresponding to a compressive disturbance in the flow field following the expansion corner, there will be a shock, or jump, to a subcritical state at some point upstream of the second throat. The location of the jump and subsequent flow are determined by the downstream boundary conditions, while the integral path in the region upstream of the jump remains uniquely determined by the requirement for smooth subcritical-supercritical transition. This type of viscous-inviscid interaction will be examined in considerably greater detail in succeeding sections.

IV.3.4. Supercritical-Subcritical-Supercritical Interactions

The problem of non-adiabatic ($S_w = -0.8$) flow in a compression corner provides an interesting example of this kind of interaction

(Fig. 20). Since the flow upstream of the corner is supercritical, a jump is required to initiate the interaction solution. The jump may be located either on the flat surface or along the curved portion of the body, depending on the total angle and the radius of curvature of the turn. The complete solution is determined by the requirement for smooth subcritical-supercritical transition downstream of the corner. This solution can be obtained by iterating for the jump location which generates the integral path passing through the throat; the procedure is therefore an inverse one as for the case of initially subcritical interactions. For supercritical boundary layers, however, the perturbation of the solution for self-induced flow is given by the jump relations (Section V.1), which uniquely determine the flow immediately downstream of a jump for given upstream conditions. The locus of possible initial states for a particular supercritical-subcritical interaction is therefore obtained by applying the jump relations to the eigensolution representing flat-plate flow. The correct jump location is the one associated with the trajectory which passes smoothly through the throat.

IV.3.5. Subcritical-Supercritical Interactions

For certain configurations, it is possible to have a flow field which is subcritical near the leading edge of the body and supercritical everywhere else. One example of this type of interaction is given by the case of highly-cooled flow over a blunt-nosed body, as shown in Fig. 21. In the vicinity of the stagnation point $M_e < 1$, hence the boundary layer is always subcritical in this region. The velocity-profile parameter decreases in the downstream direction,

but the edge Mach number M_e increases and the viscous layer becomes supercritical at some point along the surface. Transition can occur on either the curved or flat portions of the body, depending on the free-stream Mach number and the shape of the nose. As for all subcritical-supercritical interactions, the complete solution is determined by the requirement for smooth transition at the throat.

IV.3.6. Supercritical-Subcritical Interactions

This type of interaction occurs for moderately-cooled boundary layers ($-.8 < S_w < 0$) where the locus of critical points $D = 0$ lies between the value of the parameter **a** corresponding to the Blasius solution and the one corresponding to either the strong-interaction or the stagnation-point profiles. An example of this situation is given for the case of flow along a semi-infinite flat plate shown in Fig. 22 . There are no external disturbances in this problem, hence the boundary layer is everywhere relaxing toward the downstream Blasius condition. Smooth supercritical-subcritical transition therefore occurs, exactly as in the case of adiabatic flow following an expansion turn.

If there is a compressive disturbance at some location along the plate, however, an interesting interaction results. For weak disturbances located sufficiently far downstream of the leading edge, the effect of the disturbance will not propagate upstream into the supercritical region. The interaction due to the disturbance is therefore completely subcritical, and the method of solution is identical with the one described for subcritical flows in Section IV.3.1. As the disturbance is increased in strength or moved forward along

the plate, however, the location of the beginning of the interaction x_o moves upstream toward the region of supercritical flow. At some point a completely subcritical interaction is no longer possible, and a jump must occur in the supercritical flow field near the leading edge. The correct jump location is the one which gives the integral curve satisfying the downstream boundary condition of undisturbed flow. Interactions along a moderately-cooled flat plate can thus be initiated either smoothly or discontinuously, depending on the strength and location of the disturbance.

The various classes of viscous-inviscid interactions described above can be combined to form more complicated situations, such as the case of flow over a circular cylinder discussed in Appendix B. Solutions for most interactions in supersonic flow are, in fact, obtained by using the procedures outlined here. Before entering into a detailed description of the actual methods required to obtain specific solutions, however, it is useful to examine some of the general features of interacting flows from a different point of view.

IV.4. Solutions in the Phase Space

An understanding of some of the aspects of viscous-inviscid interactions can be obtained from an analysis of the behavior of integral curves in the $Re_{\delta_i^*}$-a-M_e phase space. Solutions for adiabatic interactions along flat surfaces can be examined in this manner, since for these problems the angle Θ depends only on the edge Mach number M_e for given free-stream conditions. The phase-space representation is of course not complete for adiabatic flows along curved surfaces, where Θ is a function of x, nor for non-adiabatic

flows, which must be described by the additional parameter b. An examination of the relatively simple case of adiabatic flat-plate flow does provide, however, several important insights into more complicated situations.

In the phase space, the critical points D = 0 define a cylindrical surface parallel to the $Re_{\delta_i^*}$-axis dividing the domain into subcritical and supercritical regions. At a given reference Mach number, the singular points N_i = D = 0, Eq. (71), describe a line on this surface for each value of $a_w(x)$. For the special case of flat-plate flow ($a_w(x) = 0$), the locus of singularities represents the intersection of the critical surface with the surface containing the Blasius point at downstream infinity. This second surface has been called the "relaxation surface" by Tyson[17] who demonstrated numerically that all integral paths which relax to the Blasius condition lie in this surface. Also, an analysis by Kubota[18] of solutions in the neighborhood of the singular point at downstream infinity shows that these solutions all belong to a one-parameter family (Section V.2) and as a result must be in a well-defined surface. By using the proper form of the moment equations (Section VI.1), the relaxation surface can be extended to include the leading-edge singularity, hence the complete eigensolution for undisturbed viscous flow over a semi-infinite flat plate lies in the surface. With this consideration, the geometry of the phase space for adiabatic flow appears as shown in Fig. 23 .

The existence of the relaxation surface is very important in the analysis of viscous-inviscid interactions. Only those integral

paths which lie in the relaxation surface can decay toward the downstream Blasius condition, while all other solutions diverge away from the surface. The diverging solutions, or departure integrals, correspond to flow upstream of some disturbance, whereas solutions in the relaxation surface represent flow downstream of a disturbance. In the supercritical portion of the phase space, on the other hand, all integral paths converge toward the singular line, hence there are no departure integrals. These flows can respond to a downstream disturbance only through a jump from the solution in the supercritical region to the corresponding subcritical departure integral. In the absence of external disturbances, however, the solution curves pass continuously into the relaxation surface on the subcritical side. The locus of singularities $N_i = D = 0$ is therefore a line of nodal points for all supercritical-subcritical trajectories, and at every singular point there is one exceptional nodal path which remains in the relaxation surface. All other integral paths leave the relaxation surface in response to the upstream propagation of the effect of an external disturbance.

Some of the above ideas can be clarified by considering the case of adiabatic flow through an expansion turn, previously discussed in Section IV.3.3. The phase-space trajectory for this interaction is shown in Fig. 24 . The integral curve originates at the leading edge along the eigensolution corresponding to undisturbed flat-plate flow at the free-stream Mach number M_{∞_-}. At some point (the location x_o in Fig. 19), the influence of the corner is felt, and the solution leaves the relaxation surface along a

departure integral. As the flow enters the expansion turn, the integral curve passes into the supercritical region through the line of singularities corresponding to the value of $a_w(x)$ at the throat. The phase-space representation of the interaction is of course not unique for this portion of this flow-field since $\Theta = \Theta(x)$. After the completion of the turn, however, the phase-space representation is again complete, but the relaxation surface must be taken as the one corresponding to the downstream Mach number $M_{\infty+}$. The integral curve in this region decays toward the singular line, passes smoothly through the second throat and remains in the relaxation surface as it approaches the Blasius point.

If there is a subsequent disturbance far downstream of the second singular point, such as a compression corner or an incident shock wave, the solution curve leaves the relaxation surface along a departure integral and a new interaction begins. If the disturbance is located close to the expansion turn, however, the beginning of the new interaction may not occur downstream of the second throat and a jump will be required to join the supercritical flow with the interacting subcritical boundary layer upstream of the disturbance. A similar situation can occur if the surface of the body continues to turn such that the viscous flow separates and enters the subcritical near-wake region. An analogous interaction is given by the case of flow over a circular cylinder discussed in Appendix B.

The analysis of viscous-inviscid interactions in the phase space indicates an important procedure for obtaining solutions to many interaction problems. Since all departure integrals diverge

away from the relaxation surface in the downstream direction, any infinitesimal perturbation of a solution lying in the surface will generate a departure integral. As a result, it is difficult to obtain an integral curve remaining in the relaxation surface, particularly if the trajectory lies in the vicinity of the line of singularities. Integration upstream away from the Blasius solution is stable, however, since the departure integral passing through any point in the phase space can be traced back to its origin on the relaxation surface by integrating in the upstream direction. Thus for the case of adiabatic flow through an expansion turn, for example, the portion of the solution downstream of the second throat must be obtained by integrating away from the Blasius point corresponding to the final free-stream Mach number. The complete integral curve is determined by matching the upstream and downstream branches of the solution at the second singular point. The method of iterating for the correct trajectory in the relaxation surface will be described in Section V.3.

For highly-cooled ($S_w = -0.8$) flows, the Blasius point lies in the supercritical portion of the phase space. The relaxation surface therefore contains those integral curves which converge toward the line of singularities, since these are the only trajectories which can relax to a downstream Blasius condition. All solutions in the supercritical region decay toward the Blasius point, hence there are no departure integrals in this portion of the phase space. Supercritical-subcritical transition on a highly-cooled flat plate therefore always takes place through a discontinuity, or jump, in

the flow quantities. The location of the jump is determined by the condition that the subcritical branch of the solution downstream of the disturbance must lie in the relaxation surface corresponding to $M_{\infty+}$ and subsequently pass through the critical surface at the singular line. For non-adiabatic flows in smooth compression turns ($a_w(x) < 0$), the supercritical boundary layer can be decelerated by the curvature of the surface and the jump may be very weak and occur close to the critical surface. A jump of finite strength is always required to satisfy the boundary condition at the throat, however.

From the above discussion, it is evident that the eigensolution representing undisturbed flat-plate flow monotonically approaches the critical surface with increased cooling. The determinant D of the system of equations thus tends toward zero, and as a result all flow quantities change with increasing rapidity in the vicinity of an external disturbance. If the surface is cooled below a certain level, the flat-plate solution becomes supercritical and the change in the quantities becomes discontinuous, i.e., a jump is required to initiate the interaction. As the wall temperature is decreased even more, the beginning of the interaction occurs closer to the location of the disturbance, and the strength of the jump increases. There is therefore a continuous decrease in the overall length of any viscous-inviscid interaction as the surface is cooled and the boundary layer changes from a subcritical to a highly supercritical state.

V. METHODS OF SOLUTION

V. 1. Departure Conditions

Once the eigensolution representing undisturbed flat-plate flow has been determined for given free-stream conditions (see Section VI. 1), the integral curve far upstream of any viscous-inviscid interaction is known. This solution must subsequently be used to obtain the trajectory in the vicinity of the external disturbance by applying the appropriate departure conditions to the self-induced flow at the beginning of the interaction.

V. 1. 1. Subcritical Flows

As shown in the previous section, a small perturbation of any of the integral paths lying in the relaxation surface generates a departure solution on integration in the downstream direction. If the initial point in the relaxation surface lies along the trajectory passing through the leading-edge singularity, the departure integrals form a single-parameter family of solutions which can be described, for example, by the extent of departure from any fixed point in the surface. This family contains those integral paths usually referred to as "free-interaction" solutions (see Lewis[19]). The parameter describing the departure distance can be determined by linearizing the equations about any point along the eigensolution representing undisturbed flat-plate flow.

Kubota[20] has performed this linearization for adiabatic flow in the vicinity of the Blasius solution, using the hypersonic form of the moment equations (see Section VI. 1). The method of analysis used is completely general, however, and the results are valid for all

initial points except those in the immediate neighborhood of the leading edge, where the surface derivatives are of the same order of magnitude as the departure derivatives. The required perturbations for adiabatic and slightly-cooled subcritical flows are of the form:

$$M_e = M_{e_o}(1+P_1\epsilon) \tag{74}$$

$$\delta_i^* = \delta_{i_o}^*(1+P_2\epsilon)$$

$$a = a_o(1+P_3\epsilon)$$

$$b = b_o(1+P_4\epsilon)$$

where

$$P_1 = \left[\mathcal{V}\frac{dJ}{d\mathcal{V}} - J\right] \tag{75}$$

$$P_2 = \left[3J - 2T^* - (2\mathcal{V}+1-E)\frac{dJ}{d\mathcal{V}}\right]$$

$$P_3 = \left[(2\mathcal{V}+1-E)J - (3J-2T^*)\mathcal{V}\right] / \left[\frac{d\mathcal{V}}{da}\right]$$

$$P_4 = \left[(P_1+P_2)T^* + P_3\frac{\partial T^*}{\partial a}\right] / \left[\frac{\partial T^*}{\partial b}\right]$$

The effect of the perturbation quantity ϵ on the static pressure ratio upstream of a disturbance in adiabatic flow is shown in Fig. 25. The integral path $\epsilon = 0$ does not correspond exactly to the unperturbed eigensolution because the weak-interaction expansion places the initial point slightly off the relaxation surface. In general, however, $\epsilon < 0$ generates the family of solutions going toward separation, while $\epsilon > 0$ gives trajectories corresponding to flow upstream of an expansion corner. As can be seen from Fig. 25, the length scale for accelerating boundary layers is much shorter than the scale for separating flows.

Also shown in Fig. 25 is the predicted pressure distribution upstream of a disturbance using the initial conditions suggested by Lees and Reeves[2], i.e., $a = a_{BL}$ and $dM_e/dx = 0$ at the beginning of the interaction. The difference between the two methods is magnified when only free-interaction solutions are considered, and for a given external disturbance, the Lees-Reeves method predicts a slightly less extensive region of upstream influence than does the present procedure. The two methods become identical as $Re_x \to \infty$.

Because of the requirement that $\epsilon \ll 1$ for the linearization of the equations to be accurate, the Reynolds number at the beginning of the interaction must be iterated at a fixed value of ϵ until the approximately correct trajectory is obtained. The quantity ϵ can then be varied until the exact solution is determined. The perturbation procedure described here is useful for determining the correct departure integral for flows in smooth compression or expansion turns, where only a very weak perturbation of the flat-plate solution is required at the beginning of the interaction, and for all subcritical viscous-inviscid interactions which are initiated in the vicinity of the leading edge.

V.1.2. Supercritical Flows

For highly-cooled flat-plate flows, the boundary layer is supercritical and therefore does not respond to disturbances occurring further downstream. There are no departure solutions in the sense of the previous section since supercritical flows are characterized by negative, rather than positive, exponential behavior. As indicated in Section IV, the transition from supercritical to subcritical flow must occur over a few boundary-layer thicknesses. Since this rapid

change in flow quantities cannot be analyzed within the framework of the integral method, the transition is regarded as discontinuous, and sudden jumps in the fluxes of mass, momentum and mechanical energy are allowed.

The flow upstream of a non-adiabatic jump is characterized by four quantities, M_e, δ_i^*, a and b; hence four conditions are required to uniquely determine the flow downstream of the jump. Three of these relations are derived from the known conservation laws for mass, momentum, and total enthalpy. In general, the fourth quantity, the mechanical energy, is not a conservative quantity, but in the limit of Δx_1 and Δx_2 both $\to 0$ (Fig. 26), the volume dissipation vanishes and approximate jump conditions for this quantity can also be written.

By referring to Fig. 26, one sees that as Δx_1 and $\Delta x_2 \to 0$ the effects of skin friction and heat transfer vanish, as well as the volume dissipation. Also the effect of the streamline inclination at the edge of the boundary layer does not appear in the continuity equation. With these observations the three jump conditions derived from the conservation laws are as follows:

MASS

$$\dot{m}_2 - \dot{m}_1 = (\rho_e u_e)_1 (\delta_2 - \delta_1) \tag{76}$$

MOMENTUM

$$I_2 - I_1 = (\rho_e u_e^2)_1 (\delta_2 - \delta_1) - \delta_2 (p_2 - p_1) \tag{77}$$

TOTAL ENTHALPY

$$(M_e \delta_i^* T^*)_2 - (M_e \delta_i^* T^*)_1 = 0 \tag{78}$$

where

$$\dot{m} = \int_o^\delta \rho u dy = \rho_\infty a_\infty M_e \delta_i^* Z \tag{79}$$

$$I = \int_o^\delta \rho u^2 dy = \rho_\infty a_\infty u_e M_e \delta_i^* (Z-\mathcal{K}) \tag{80}$$

and

$$\delta = \frac{a_\infty \rho_\infty}{a_e \rho_e} \delta_i^* (m_e F + Z) \tag{81}$$

where

$$F = \mathcal{K} + \frac{1+m_e}{m_e} (1-E)$$

The fourth jump condition, for mechanical energy or moment of momentum, is derived from the differential equation for continuous flow by passing to the limit of a finite change in flow quantities occurring over a very short distance. By integrating the mechanical energy equation across the boundary layer one obtains

$$\frac{\partial}{\partial x}\left[\int_o^\delta \left(\frac{\rho u^3}{2}\right) dy\right] - \left(\frac{\rho u^3}{2}\right)_{y=\delta} \frac{d\delta}{dx} + (\rho v)_\delta \left(\frac{u_\delta^2}{2}\right) = -\left(\frac{dp}{dx}\right)\int_o^\delta u dy - \int_o^\delta \mu \left(\frac{\partial u}{\partial y}\right)^2 dy \tag{82}$$

In a supercritical-subcritical jump $\frac{d\delta}{dx}$, $\frac{dp}{dx}$ and the rate of change of mechanical energy flux all $\to \infty$, while the dissipation term and the term $(\rho v)_\delta \left(\frac{u_\delta^2}{2}\right)$ arising from the streamline inclination remain finite and can therefore be neglected in comparison to the other terms. Eq. (82) thus takes a form quite similar to the integrated momentum equation, except that δ is replaced by $\int_o^\delta u dy = K$. Formally multiplying Eq. (82) by $\Delta x = \Delta x_1 + \Delta x_2$ and taking the limit as $\Delta x \to 0$, the following jump condition is obtained:

MECHANICAL ENERGY (MOMENT OF MOMENTUM)

$$G_2 - G_1 = (\rho_e u_e^3)_1 (\delta_2 - \delta_1) - 2K_2(p_2 - p_1) \tag{83}$$

where

$$G = \int_o^\delta \rho u^3 dy = \rho_\infty a_\infty u_e^2 M_e \delta_i^* (Z - J) \tag{84}$$

and

$$K = \int_o^\delta u dy = \frac{\rho_\infty}{\rho_e} a_\infty M_e \delta_i^* [(1+m_e)(Z - T^*) - m_e(Z - J)] \tag{85}$$

An average value of $K = \overline{K}$ should have been used in Eq. (83), although the quantity K_2 was adopted here by analogy with the momentum equation, Eq. (77). The difference between K_2 and $\overline{K}$ is very small in any case.

Substituting the expressions for $\dot{m}$, I, G, K and δ into Eqs. (76)-(78) and Eq. (83) the relation:

$$\frac{M_r \delta_r^*}{\rho_r u_r} = \frac{m_{e_1} F_1}{m_{e_2} F_2 + (1 - \rho_r u_r) Z_2} \tag{86}$$

is obtained from the continuity equation, Eq. (82). The subscript r denotes the ratio of quantities upstream and downstream of the jump, i.e.,

$$M_r = \frac{M_{e_2}}{M_{e_1}} \qquad \delta_r^* = \frac{\delta_{i_2}^*}{\delta_{i_1}^*} \qquad \rho_r u_r = \frac{\rho_{e_2} u_{e_2}}{\rho_{e_1} u_{e_1}} \tag{87}$$

Utilizing this relation, Eq. (86), in the jump equations for momentum, mechanical energy and total enthalpy, the following three expressions are obtained:

$$m_{e_2} F_2 \left[\frac{\mathcal{K}_1}{m_{e_1} F_1} - \frac{\mathcal{K}_2}{m_{e_2} F_2}\right] + \frac{1}{\gamma M_{e_1}^2}\left(\frac{p_2}{p_1} - 1\right)\left[m_{e_2} F_2 + Z_2\right]$$

$$- (1-\rho_r u_r^2)(Z_2 - \mathcal{K}_2) + (1-\rho_r u_r)\left(1 + \frac{\mathcal{K}_1}{m_{e_1} F_1}\right) Z_2 = 0 \qquad (88)$$

$$m_{e_2} F_2 \left[\frac{J_1}{m_{e_1} F_1} - \frac{J_2}{m_{e_2} F_2}\right] + \frac{2u_r}{\gamma M_{e_1}^2}\left(\frac{p_2}{p_1} - 1\right)\left[m_{e_2} J_2 + Z_2\right.$$

$$\left. - (1+m_{e_2}) T_2^*\right] - (1-\rho_r u_r^3)(Z_2 - J_2)$$

$$+ (1-\rho_r u_r)\left(1 + \frac{J_1}{m_{e_1} F_1}\right) Z_2 = 0 \qquad (89)$$

$$m_{e_2} F_2 \left[\frac{T_1^*}{m_{e_1} F_1} - \frac{T_2^*}{m_{e_2} F_2}\right] + (1-\rho_r u_r)\left(T_2^* + \frac{T_1^*}{m_{e_1} F_1} Z_2\right) = 0 \qquad (90)$$

The pressure and density ratios can be determined from the change in Mach number M_e by means of the oblique shock relations, hence the above equations can be solved for a_2, b_2 and M_{e_2} for any given upstream conditions. The method for obtaining the solution is to assume $M_{e_2} = 0.95\, M_{e_1}$, $b_2 = 0.20$ and to determine a_2 from Eq. (88) by iteration. The assumed value of M_{e_2} must then be adjusted until the second equation, Eq. (89), is also satisfied. The procedure is then repeated with a new value for b_2 until a solution to the system of three equations has been found. Since the first two relations are relatively insensitive to the choice of b_2, this method of iteration is very effective, and a complete calculation usually takes less than 0.5 second on a high-speed computer. Some typical jumps from the Blasius and strong-interaction solutions for highly-cooled ($S_w = -0.8$) flow are shown in Fig. 27.

The relative change in Mach number M_e across laminar supercritical-subcritical jumps is always small, and the free-stream quantities appearing in the equations can be connected to the velocity difference by approximate relations such as those used in small disturbance theory. In the limiting case of an infinitesimal jump, the velocity difference $(1 - u_{e_2}/u_{e_1}) \to 0$, and, using the continuity relation, Eq. (86), the jump equations for momentum and mechanical energy, Eqs. (88)-(89), take the form:

$$(M_e \delta_i^* \mathcal{H})_2 - (M_e \delta_i^* \mathcal{H})_1 \to - \frac{\Delta u_e}{u_e}\left[(1+m_e)(\mathcal{H}+1-E) M_e \delta_i^*\right]_2 \qquad (97)$$

$$(M_e \delta_i^* J)_2 - (M_e \delta_i^* J)_1 \to -2 \frac{\Delta u_e}{u_e}\left[(1+m_e)(J-T^*) M_e \delta_i^*\right]_2 \qquad (98)$$

Rewriting the two basic differential equations for continuous flow, Eqs. (35) and (36), in the form

$$\left[M_e \mathcal{H} \frac{d\delta_i^*}{dx} + M_e \delta_i^* \frac{d\mathcal{H}}{dx} + \mathcal{H} \delta_i^* \frac{dM_e}{dx}\right] + (\mathcal{H}+1-E)\, \delta_i^* \frac{dM_e}{dx} = (RHS) M_e \qquad (99)$$

and

$$\left[M_e J \frac{d\delta_i^*}{dx} + M_e \delta_i^* \frac{dJ}{dx} + \delta_i^* J \frac{dM_e}{dx}\right] + 2(J-T^*)\, \delta_i^* \frac{dM_e}{dx} = (RHS) M_e \qquad (100)$$

and making use of the relation $\frac{dM_e}{M_e} = (1+m_e) \frac{du_e}{u_e}$, it is evident that the last two equations are identical to the two corresponding jump equations in the limit $\Delta x \to 0$ with the RHS $\to 0$. It can also be shown that the continuity relation, Eq. (86), for an infinitesimal jump reduces to the equation for continuous flow, Eq. (34), in the same limit. In other words, the equations for an infinitesimal jump correspond to the relations obtained from Eqs. (34)-(37) by multiplying by Δx and passing to the limit $\Delta x \to 0$.

Since the equations for an infinitesimal jump correspond exactly to the homogeneous form of the continuous flow equations, non-trivial solutions exist only when the determinant of the matrix vanishes, i.e., when $D = 0$. An infinitesimal jump can therefore occur only at the critical point. The analogy to a normal shock wave of infinitesimal strength in a nozzle is complete; such a standing shock occurs only at the throat.

Another interesting point of resemblance between the jump relations and an ordinary gasdynamic shock wave is the occurrence of hypersonic freezing. When $M_{e_1} \to \infty$, the strength of the jump approaches a constant and a_2 and b_2 become unique functions of the upstream values. This phenomenon is evident in Fig. 27.

For all jump conditions investigated, the boundary-layer thickness decreases across the jump, and mass flux is lost to the inviscid flow. The physical displacement thickness increases slightly, however, which is consistent with a compression occurring over a downstream distance of one or two boundary-layer thicknesses. In all cases the strength of the jump, as measured by the reduction in Mach number, is very small. Even for $M_{e_1} = 10$, a jump from the strong interaction solution produces a relative change in M_e of less than 6%, corresponding to a static pressure ratio of 1.48. Changes in the shape parameters a and b, on the other hand, are considerable, although the minimum a_2 is always far from separation.

The subcritical flow downstream of the jump generates a pressure gradient along the surface which produces separation and the beginning of a region of reversed flow. The departure integrals,

consisting of the jump and the interacting boundary layer upstream of the disturbance, form a one-parameter family of solutions for initial states corresponding to flat-plate flow. Thus as a given disturbance moves toward the leading edge, the boundary layer upstream of the jump becomes more supercritical, the strength of the jump increases and the separation point approaches the jump location. For supercritical as well as subcritical flows, the correct departure integral is always determined by the downstream boundary condition appropriate to the specific viscous-inviscid interaction considered.

V.2. Solutions in the Relaxation Surface

In the preceding section, methods for obtaining the departure integrals representing flow upstream of an external disturbance were described. For supercritical flows, the correct jump location is determined by the requirement for smooth transition downstream of the disturbance, while for subcritical boundary layers, the correct departure path is the one generating the trajectory downstream of the disturbance which lies in the relaxation surface corresponding to $M_{\infty+}$. For flows approaching the Blasius condition from the separated region, solutions which lie in the relaxation surface can be obtained by numerically suppressing the departure integrals appearing in the downstream integration (see Section VI.2). This procedure cannot be used for accelerated boundary layers because integral paths in the vicinity of the line of singularities depart too rapidly from the relaxation surface for the trajectory remaining in the surface to be determined. Thus the downstream portion of the solution must be obtained by integrating in the upstream direction away from the Blasius point.

In this manner the integration is stable and all integral paths remain in the relaxation surface. The downstream branch of the solution can be joined to the upstream portion at some intermediate location, such as the second throat in the interaction due to an expansion turn, for example. To join the two solutions, however, it is necessary to iterate for the correct integral path in the relaxation surface. A consistent iteration procedure can be developed by making use of an analysis by Kubota[18] of the singular point at downstream infinity.

Kubota showed that for adiabatic flow in the neighborhood of the Blasius point, all solutions are of the form:

$$\begin{aligned} \zeta &= \left[-\frac{A_1}{\xi} + \cdots \right] + C_1 \xi^{\sigma} \left[1 + \frac{\varphi_1}{\xi} + \cdots \right] \\ h &= \left[\frac{A_2}{\xi} + \cdots \right] - C_1 \frac{a_1}{\beta_1} \xi^{\sigma} \left[1 + \frac{\varphi_2}{\xi} + \cdots \right] \end{aligned} \tag{101}$$

where

$$\begin{aligned} \zeta &= \left(1 - \frac{M_e}{M_\infty} \right) \xi - \left[(1+\nu) \frac{P}{\nu} \right]_{BL} \\ \xi &= \frac{4}{(\gamma-1)^2} \frac{Re_{\delta_i^*}}{M_\infty^3 C} \\ h &= \nu - \nu_{BL} \end{aligned} \tag{102}$$

$$\frac{a_1}{\beta_1} = \left[\frac{d}{d\nu} \left(\frac{P \frac{dJ}{d\nu} - R}{J - \nu \frac{dJ}{d\nu}} - P \right) \right]_{BL}^{-1}$$

The first group of terms on the right-hand side of Eqs. (101) represent the weak-interaction expansions, hence these equations can be rewritten in the form:

$$\zeta - \zeta_{WI} \equiv \left[\left(\frac{M_e}{M_\infty}\right)_{WI} - \left(\frac{M_e}{M_\infty}\right)\right]\xi = C_1 \xi^\sigma + \cdots$$
$$h - h_{WI} \equiv \mathcal{H} - \mathcal{H}_{WI} = C_1 \frac{a_1}{\beta_1} \xi^\sigma + \cdots \tag{103}$$

Combining these two expressions, the following useful relation is obtained:

$$\mathcal{H} - \mathcal{H}_{WI} = \frac{a_1}{\beta_1}\left[\frac{M_e}{M_\infty} - \left(\frac{M_e}{M_\infty}\right)_{WI}\right]\xi + \cdots \tag{104}$$

Solutions in the relaxation surface can therefore be determined by selecting initial values for integration in the upstream direction such that:

$$\begin{aligned} M_e &= M_{e_{WI}} + \Delta M_e \\ Re_{\delta_i^*} &= (Re_{\delta_i^*})_{WI} \\ a &= a_{WI} + \Delta a \end{aligned} \tag{105}$$

where

$$\begin{aligned} \Delta a &= \frac{4}{(\gamma-1)^2}\left[\frac{\frac{dP}{da}\frac{dJ}{d\mathcal{H}} - \frac{dR}{da}}{J - \mathcal{H}\frac{dJ}{d\mathcal{H}}} - \frac{dP}{da}\right]^{-1}_{BL}\left(\frac{Re_{\delta_i^*}}{M_\infty^3 C}\right)_{WI}\left(\frac{\Delta M_e}{M_\infty}\right) \\ &\approx -5.63\left(\frac{Re_{\delta_i^*}}{M_\infty^3 C}\right)_{WI}\left(\frac{\Delta M_e}{M_\infty}\right) \end{aligned} \tag{106}$$

From the analysis, it is evident that in adiabatic flow, all integral paths which relax to the Blasius point at downstream infinity belong to a one-parameter family described by the value of M_e at a given $Re_{\delta_i^*}$, for example. The derived relations also prove that weak-interaction coupling with the outer flow is not significant in the

immediate neighborhood of the Blasius solution, and $\frac{dM_e}{da} \to 0$ as $Re_{\delta_i^*} \to \infty$.

It is not possible to integrate the equations toward the leading edge in the physical space because the weak-interaction solution is obtained in the asymptotic limit $\bar{\chi} \to 0$ (see Section VI. 1) and the initial value of the Reynolds number Re_x is therefore not determined within a small constant. In the phase space, the equations to be integrated are:

$$\begin{aligned} \frac{dM_e}{dRe_{\delta_i^*}} &= \frac{M_e N_1}{Re_{\delta_i^*} N_2} \\ \frac{da}{dRe_{\delta_i^*}} &= \frac{N_3}{Re_{\delta_i^*} N_2} \end{aligned} \tag{107}$$

The solution can be transformed into physical coordinates by means of the integral:

$$\int_{Re_{x_o}}^{Re_x} dRe_x = \frac{1}{C} \int_{(Re_{\delta_i^*})_{WI}}^{Re_{\delta_i^*}} \frac{M_e}{M_\infty} \frac{D}{\beta N_3} Re_{\delta_i^*} \, dRe_{\delta_i^*} \tag{108}$$

where the value of Re_{x_o} is not known a priori. Initial conditions for Eqs. (107) are obtained from the weak-interaction expansion and are iterated according to Eqs. (105)-(106) until the integral path which joins the upstream branch of the solution is obtained. From the value of Re_x at the joining point, the downstream solution can be located in the physical space. Some of the trajectories in the relaxation surface determined by this iteration procedure are shown in Fig. 28.

V.3. The Effect of Finite Length

For many interactions, it may not be possible to assume that the body extends far enough downstream for the effect of the trailing edge to be neglected. In supercritical flow, if the trailing edge is located downstream of the throat, the solution is independent of the length of the body. For the subcritical case, however, the effect of finite length may propagate upstream into the interaction region. There is always a rapid expansion of the flow field at the trailing edge, hence the boundary layer must become supercritical and $D \to 0$ at this location. The beginning of the interaction and the magnitude of the perturbation ϵ must therefore be determined such that $D = 0$ at the given location of the trailing edge. This boundary condition is often easier to satisfy than the condition of Blasius flow far downstream of the interaction and also represents a more realistic physical situation. The solution for flow over a body of finite length can be obtained by downstream integration using the parameter a as the independent variable. The correct solution is the one for which $dx/da = 0$ at the specified location of the trailing edge.

For the case of adiabatic flow in a smooth compression turn, Ko and Kubota[21] demonstrated that when the trailing edge is sufficiently far downstream of the reattachment point, the influence on the overall interaction is small. As the length of the ramp is decreased, however, the effect of the trailing edge lowers the entire pressure level and reduces the extent of the separated flow region. For a large variation in the length of the models examined, the agreement between theory and experiment was extremely good, even in the immediate vicinity

of the trailing edge.

V.4. Non-Isentropic Effects

As previously discussed, in order to avoid the difficulty of calculating the inviscid flow field for every interaction, the external flow at the edge of the boundary layer is usually taken to be isentropic. In certain situations this assumption cannot be completely justified, and it may be necessary to combine the boundary-layer equations with a characteristics net to determine the entropy level of each streamline as it crosses the edge of the viscous layer. This is a complicated problem in itself, and since the primary interest of the present study is in the general nature of interaction phenomena, a detailed coupling of the viscous and inviscid flow fields is not attempted. It is often useful to include some of the variable-entropy effects in an approximate manner, however. In particular, the entropy variation caused by the curvature of the leading-edge shock has a strong influence on the development of the boundary layer and should be considered in many interactions (see Lees[22]). By means of an iterative procedure, some of the effects of this shock-wave heating can be included in the computation.

If the shape of the leading-edge shock wave is determined from Schlieren or flow measurements, the calculation is greatly simplified. If the shock shape is not known a priori, however, it is still possible to obtain an approximate representation of the rotational flow field by first performing the interaction calculation assuming isentropic external conditions. In the vicinity of the leading edge, the shock shape $h(x)$ can then be obtained from the similarity solution of Stewartson[23]

for the inviscid rotational flow, or by using hypersonic small-disturbance theory. For a flat plate, these results can be written in the form:

$$h(x) = \frac{h_o}{\delta_o}\,\delta^*(x) = \left(\frac{h_o}{\delta_o}\right)\delta_o\, x^{3/4} \tag{109}$$

where $\dfrac{h_o}{\delta_o} = 1.692$ for $\gamma = 1.4$ (Kubota*)

$= 2.110$ for $\gamma = 1.67$ (Mirels[24])

The first-order coefficient δ_o can be obtained from the strong-interaction solution for the physical displacement thickness derived in Section VI. 1.

In the region far downstream of the leading edge, the assumption can be made that the flow conditions between the boundary layer and the shock wave are constant along Mach waves. Referring to Fig. 29a, the relation derived from the mass flow balance is

$$\rho_\infty u_\infty h(x_2) = \left[\rho_e u_e(\delta-\delta^*)\right]_{x_1} + \left(\rho_e a_e\right)_{x_1} \ell \tag{110}$$

where $\ell = (h_2-\delta)(\sin\mu)^{-1} = M_{e_1}[h(x_2)-\delta(x_1)]$

hence $$h(x_2) = \delta^*(x_1)\left[1 - \frac{\rho_\infty u_\infty}{\rho_{e_1} u_{e_1}}\right]^{-1} \tag{111}$$

and $$x_2 = x_1 + [h(x_2) - \delta(x_1)]\sqrt{M_{e_1}^2-1}$$

By combining the results of Eqs. (109) and (111) and joining the solutions in the two regions, a valid representation of the leading-edge shock shape can be obtained.

---

* Private communication.

Referring to Fig. 29b, the mass flow in the boundary layer at at a given station x_1 can be related to the free-stream mass flow through the leading-edge shock, i. e.

$$\rho_\infty u_\infty h(x_0) = [\rho_e u_e(\delta-\delta^*)]_{x_1} \tag{112}$$

By means of this relation it is possible to locate the streamline at the shock which crosses the edge of the viscous layer at the selected station x_1. Since the flow behind the shock expands isentropically along streamlines, the distribution of $M_e(x)$ at the boundary-layer edge can be obtained. In other words, the shock curvature $\theta_s(x) = \frac{dh}{dx}$ is calculated from the known shape h(x), and the static pressure ratio $\frac{p_2}{p_\infty}(x)$ and the Mach number $M_2(x)$ downstream of the shock are obtained from the oblique shock relations. The Mach number at the edge of the viscous layer is then given by the isentropic expression:

$$M_e^2(x_1) = \frac{2}{\gamma-1}\left\{\left[1+\frac{\gamma-1}{2}M_2^2(x_0)\right]\left[\frac{\frac{p_2}{p_\infty}(x_0)}{\frac{p_{e_1}}{p_\infty}(x_1)}\right]^{\frac{\gamma-1}{\gamma}} - 1\right\} \tag{113}$$

where the relation between x_0 and x_1 is determined from Eq. (112). By dropping the continuity equation, Eq. (34), and using the calculated variation of $M_e(x)$, the remaining boundary-layer equations can be solved again with new edge conditions, and a second mass flow balance made. This procedure can then be repeated until convergence is obtained. For flow over a blunt leading edge, the problem is complicated by the subsonic region in the vicinity of the stagnation

point and the first-order isentropic solution cannot be obtained. For these configurations, the distribution of $M_e(x)$ must be taken from a relevant experiment up to the location on the body at which the inviscid flow is supersonic. Dropping the continuity equation, Eq. (34), the remaining boundary-layer equations can be integrated around the body to this location and the full set of equations used for the subsequent downstream integration. An example of this procedure is given in Appendix B for the case of flow around a circular cylinder.

VI. NUMERICAL RESULTS

VI. 1. Flow Over a Semi-Infinite Flat Plate

For all sharp-nosed bodies in the absence of external disturbances, the flow field can be divided asymptotically into two regions, the strong and weak interaction zones. The strong interaction zone is characterized by the fact that $(M_\infty \, d\delta^*/dx) >> 1$, hence this region is close to the sharp leading edge. The weak interaction zone is located far downstream where $(M_\infty \, d\delta^*/dx) << 1$ and the effects produced by the self-induced pressure gradient are essentially perturbations on an existing uniform flow. Because of the singular nature of the solutions in these two regions, asymptotic expansions for the flow variables can be obtained for the interactions in both limits. The two expansions can subsequently be joined by integrating the differential equations in the intermediate region by the methods previously discussed.

VI. 1. 1. The Strong Interaction Region

In the moment method formulation, the leading edge is characterized by the simultaneous vanishing of $Re_{\delta_i^*}$, N_3 and N_4 such that the velocity and total enthalpy profiles become similar. As shown by Lees[25], the behavior of the viscous flow in the strong interaction region can be obtained by a coordinate expansion in large $\bar{\chi}$, where $\bar{\chi} = M_\infty^3 \sqrt{C} / \sqrt{Re_x}$. In order for the boundary-layer equations to be applicable, however, the limit $\bar{\chi} \to \infty$ implies that M_∞ must become very large. The integral equations also show that this is the only appropriate limit, and the asymptotic expansion near the leading edge can be obtained only for the hypersonic form of the equations,

i.e., Eqs. (34)-(37) in the limit

$$\frac{\gamma-1}{2} M_e^2 \gg 1 \quad \text{and} \quad \frac{\gamma-1}{2} M_\infty^2 \gg 1$$

Assuming isentropic external flow and using the tangent-wedge relation, Eq. (52), the hypersonic moment equations in the strong interaction region can be written:

$$\overline{F} \frac{d\Delta}{dX} + \Delta\left(\frac{\partial \overline{F}}{\partial a}\frac{da}{dX} + \frac{\partial \overline{F}}{\partial b}\frac{db}{dX}\right) - \frac{3\gamma-1}{2\gamma}\frac{\overline{F}\Delta}{p}\frac{dp}{dX} = \frac{1}{X}\left[\frac{4\widetilde{\Theta}p}{\gamma(\gamma-1)}^{\frac{3\gamma-1}{2\gamma}} - \frac{3\overline{F}\Delta}{2}\right] \tag{114}$$

$$\chi \frac{d\Delta}{dX} + \Delta \frac{d\chi}{da}\frac{da}{dX} - \frac{\gamma-1}{2\gamma}\frac{(2\chi+1-E)}{p}\Delta\frac{dp}{dX} = \frac{1}{X}\left[\frac{2Pp}{\Delta}^{\frac{2\gamma-1}{\gamma}} - \frac{\chi+(\gamma-1)(2\chi+1-E)}{2\gamma}\Delta\right]$$

$$J \frac{d\Delta}{dX} + \Delta \frac{dJ}{d\chi}\frac{d\chi}{dX} - \frac{\gamma-1}{2\gamma}\frac{(3J-2T^*)}{p}\Delta\frac{dp}{dX} = \frac{1}{X}\left[\frac{2Rp}{\Delta}^{\frac{2\gamma-1}{\gamma}} - \frac{J+(\gamma-1)(3J-2T^*)}{2\gamma}\Delta\right]$$

$$T^* \frac{d\Delta}{dX} + \Delta\left(\frac{\partial T^*}{\partial a}\frac{da}{dX} + \frac{\partial T^*}{\partial b}\frac{da}{dX}\right) - \frac{\gamma-1}{2\gamma}\frac{T^*}{p}\Delta\frac{dp}{dX} = \frac{1}{X}\left[\frac{2\overline{Q}p}{\Delta}^{\frac{2\gamma-1}{\gamma}} - \frac{T^*\Delta}{2}\right]$$

where

$$\begin{aligned}
\overline{F} &= \chi+1-E \\
X &= \frac{1}{\overline{\chi}} = \frac{\sqrt{Re_x}}{M_\infty^3\sqrt{C}} \\
\Delta &= \frac{Re_{\delta_i^*}}{M_\infty^3 C}\overline{\chi}^{\frac{1}{2\gamma}} \\
p &= \frac{P_e}{P_\infty}\frac{1}{\overline{\chi}} \\
\widetilde{\Theta} &= \gamma M_\infty \sqrt{X}\,\Theta = (p-X)\left[X + \frac{\gamma+1}{2\gamma}(p-X)\right]^{-\frac{1}{2}}
\end{aligned} \tag{115}$$

Assuming algebraic coordinate expansions for the dependent variables of the form:

$$\phi = p_0(1+p_1X + p_2X^2 + ---) \tag{116}$$

$$\Delta = \delta_0(1+\delta_1X + \delta_2X^2 + ---)$$

$$a = a_0 + a_1X + a_2X^2 + ---$$

$$b = b_0 + b_1X + b_2X^2 + ---$$

and substituting these expressions into Eqs. (114), it is possible to obtain the coefficients of the expansions from the resulting system of algebraic equations.

For $\gamma = 1.4$, the results of the expansions for adiabatic ($S_w = 0$) flow are:

$$\left(\frac{p_e}{p_\infty}\right)_{SI} = 0.50912\,\bar{\chi}\,[1.0+1.51542\,/\,\bar{\chi} + 0.25274/\bar{\chi}^2 + ---] \tag{117}$$

$$\left(\frac{Re_{\delta_i^*}}{M_\infty^3 C}\right)_{SI} = 1.19437\bar{\chi}^{-\frac{1}{2\gamma}}[1.0+0.94786/\bar{\chi} - 0.19876/\bar{\chi}^2 + ---]$$

$$a_{SI} = 2.28785 - 1.10976/\bar{\chi} + 2.13581/\bar{\chi}^2 + ---$$

while for non-adiabatic ($S_w = -0.8$) flow :

$$\left(\frac{p_e}{p_\infty}\right)_{SI} = 0.21628\,\bar{\chi}\,[1.0 + 3.40242/\bar{\chi} + 2.00303/\bar{\chi}^2 + ---] \tag{118}$$

$$\left(\frac{Re_{\delta_i^*}}{M_\infty^3 C}\right)_{SI} = 0.79594\bar{\chi}^{-\frac{1}{2\gamma}}[1.0 + 1.73140/\bar{\chi} - 0.23521/\bar{\chi}^2 + ---]$$

$$a_{SI} = 1.90245 - 1.12390/\bar{\chi} + 3.09669/\bar{\chi}^2 + ---$$

$$b_{SI} = 0.39880 - 0.14903/\bar{\chi} + 0.46129/\bar{\chi}^2 + ---$$

From these relations it is possible to obtain all required boundary-layer functions in the strong-interaction region, i.e., for adiabatic flow:

$$\left(M_\infty \frac{\delta^*}{x}\right)_{SI} = 0.73400\,\bar{\chi}^{\frac{1}{2}}\,[1.0-0.82208/\bar{\chi} + 0.77712/\bar{\chi}^2 + --] \qquad (119)$$

$$\left(C_F\sqrt{\frac{Re_x}{C}}\right)_{SI} = 0.54352\,\bar{\chi}^{\frac{1}{2}}[1.0+0.51672/\bar{\chi} - 0.07013/\bar{\chi}^2 + --\,]$$

and for the highly-cooled ($S_w = -0.8$) flow:

$$\left(M_\infty \frac{\delta^*}{x}\right)_{SI} = 0.47840\,\bar{\chi}^{\frac{1}{2}}\,[1.0-1.98462/\bar{\chi} + 4.31997/\bar{\chi}^2 + ---] \qquad (120)$$

$$\left(C_F\sqrt{\frac{Re_x}{C}}\right)_{SI} = 0.27261\,\bar{\chi}^{\frac{1}{2}}[1.0+1.82059/\bar{\chi} - 0.14139/\bar{\chi}^2 + ---]$$

$$\left(C_H\sqrt{\frac{Re_x}{C}}\right)_{SI} = 0.11484\,\bar{\chi}^{\frac{1}{2}}[1.0+2.30072/\bar{\chi} - 0.13827/\bar{\chi}^2 + ---]$$

The first-order terms in the expansions agree well with the exact values obtained for similar flow in the vicinity of a sharp leading edge, indicating that the curve-fits of the profile quantities are quite accurate. The similarity solution in the strong interaction region corresponds to the profile for which $\beta = \frac{\gamma-1}{\gamma}$ (Lees[26]), i.e., $a = 2.275$ for $S_w = 0$ and $a = 1.897$, $b = 0.395$ for $S_w = -0.8$ (see Tables A5 and A10).

VI. 1. 2. The Weak Interaction Region

The Blasius solution is characterized by the condition that N_3 and N_4 vanish as $Re_{\delta_i^*} \to \infty$. The behavior of the viscous flow in the vicinity of this point can be obtained by a coordinate expansion in small $\bar{\chi}$, hence the boundary-layer assumption remains valid for all

Mach numbers and the supersonic moment equations can be used. A convenient form of these equations, Eqs. (34)-(37), for flow in the weak interaction region is:

$$F\frac{d\Delta}{d\bar{\chi}} + \Delta\left(\frac{\partial F}{\partial a}\frac{da}{d\bar{\chi}} + \frac{\partial F}{\partial b}\frac{db}{d\bar{\chi}}\right) + \frac{f\Delta}{M_e}\frac{dM_e}{d\bar{\chi}} = \frac{1}{\bar{\chi}}\left[F\Delta - 2\left(\frac{1+m_\infty}{1+m_e}\right)^{\frac{\gamma+1}{2(\gamma-1)}}\frac{M_\infty^3 \tan\Theta}{m_e\bar{\chi}}\right]$$

$$\mathcal{N}\frac{d\Delta}{d\bar{\chi}} + \Delta\frac{d\mathcal{N}}{da}\frac{da}{d\bar{\chi}} + \frac{(2\mathcal{N}+1-E)}{M_e}\Delta\frac{dM_e}{d\bar{\chi}} = \frac{1}{\bar{\chi}}\left[\mathcal{N}\Delta - 2\left(\frac{1+m_\infty}{1+m_e}\right)^{\frac{3\gamma-1}{2(\gamma-1)}}\frac{M_\infty P}{M_e\Delta}\right] \tag{121}$$

$$J\frac{d\Delta}{d\bar{\chi}} + \Delta\frac{dJ}{d\mathcal{N}}\frac{d\mathcal{N}}{da}\frac{da}{d\bar{\chi}} + \frac{(3J-2T^*)}{M_e}\Delta\frac{dM_e}{d\bar{\chi}} = \frac{1}{\bar{\chi}}\left[J\Delta - 2\left(\frac{1+m_\infty}{1+m_e}\right)^{\frac{3\gamma-1}{2(\gamma-1)}}\frac{M_\infty R}{M_e\Delta}\right]$$

$$T^*\frac{d\Delta}{d\bar{\chi}} + \Delta\left(\frac{\partial T^*}{\partial a}\frac{da}{d\bar{\chi}} + \frac{\partial T^*}{\partial b}\frac{db}{d\bar{\chi}}\right] + \frac{T^*\Delta}{M_e}\frac{dM_e}{d\bar{\chi}} = \frac{1}{\bar{\chi}}\left[T^*\Delta - 2\left(\frac{1+m_\infty}{1+m_e}\right)^{\frac{3\gamma-1}{2(\gamma-1)}}\frac{M_\infty \bar{Q}}{M_e\Delta}\right]$$

where

$$\Delta = \frac{Re_{\delta_i^*}}{M_\infty^3 C} \qquad \bar{\chi} = \frac{\delta_i^*}{x}\sqrt{\frac{Re_x}{C}} \tag{122}$$

and

$$\tan\Theta \approx \Theta = \nu(M_\infty) - \nu(M_e) = \int_{M_e}^{M_\infty} \frac{\sqrt{M^2-1}}{1+\frac{\gamma-1}{2}M^2}\frac{dM}{M}$$

The coordinate expansions must be of the form:

$$\begin{aligned} M_{e_{WI}} &= M_\infty\,(1+m_1\bar{\chi} + m_2\bar{\chi}^2 + \text{---}) \\ \Delta_{WI} &= \delta_0(1+\delta_1\bar{\chi} + \varepsilon_2\bar{\chi}^2 \ell n\,\bar{\chi} + \delta_2\bar{\chi}^2 + \text{---}) \\ a_{WI} &= a_0 + a_1\bar{\chi} + a_2\bar{\chi}^2 + \text{---} \\ b_{WI} &= b_0 + b_1\bar{\chi} + b_2\bar{\chi}^2 + \text{---} \end{aligned} \tag{123}$$

The logarithmic term in the expression for Δ must be included since the coefficient δ_2 does not appear when the expansions are substituted into the equations. The value of δ_2 can be obtained from the other coefficients by noting from Eq. (55) that:

$$\frac{d\delta_i^*}{dx} \sim \frac{1}{Re_{\delta_i^*}}$$

Hence there must be an expansion of the form:

$$\frac{dRe_x}{dRe_{\delta_i^*}} = a_0 Re_{\delta_i^*} + a_1 + \frac{a_2}{Re_{\delta_i^*}} + \cdots \tag{124}$$

i.e. $$Re_x = \frac{a_0}{2} Re_{\delta_i^*}^2 + a_1 Re_{\delta_i^*} a_2 \ell n\, Re_{\delta_i^*} + \cdots$$

or $$\frac{1}{\bar{\chi}^2} = \tilde{a}_0 \left(\frac{\Delta}{\bar{\chi}}\right)^2 + \tilde{a}_1 \left(\frac{\Delta}{\bar{\chi}}\right) + \tilde{a}_2 \ell n \left(\frac{\Delta}{\bar{\chi}}\right) + \cdots$$

but $$\frac{\Delta}{\bar{\chi}} = \frac{\delta_0}{\bar{\chi}} \left(1 + \delta_1 \bar{\chi} + \varepsilon_2 \bar{\chi}^2 \ell n \bar{\chi} + \delta_2 \bar{\chi}^2 + \cdots\right)$$

Expanding and equating coefficients, the required relation for δ_2 is obtained:

$$\delta_2 = \frac{1}{2} \delta_1^2 - \varepsilon_2 \ell n\, \delta_0 \tag{125}$$

The result of the coordinate expansion for the other coefficients can be written in the following form:

$$m_1 = \frac{-(\gamma-1)(1+m_\infty)}{4M_\infty \sqrt{M_\infty^2 - 1}} \left[m_{11} + \frac{1+m_\infty}{m_\infty} m_{12}\right] \tag{126}$$

$$m_2 = \left[\frac{\sqrt{M_\infty^2 - 1}}{M_\infty^3} m_{21}\right] m_1 + \left[\frac{m_\infty}{1+m_\infty} - \frac{1}{2(M_\infty^2 - 1)}\right] m_1^2$$

$$\delta_1 = (d_{11} - K_1)m_1$$

$$\epsilon_2 = (d_{21} + K_1 d_{22} + K_2)m_1^2 + (K_1 - d_{22})m_2$$

$$a_1 = a_{11} m_1$$

$$a_2 = (a_{21} + K_1 a_{22})m_1^2 + (a_{11} - a_{22})m_2$$

$$b_1 = b_{11} m_1$$

$$b_2 = (b_{21} + K_1 b_{22})m_1^2 + (b_{11} - b_{22})m_2$$

where

$$K_1 = \frac{3\gamma-1}{\gamma-1} \frac{m_\infty}{1+m_\infty}$$

$$K_2 = \frac{3\gamma-1}{2(\gamma-1)} \frac{m_\infty}{1+m_\infty} \left[1 - \frac{5\gamma-3}{\gamma-1} \frac{m_\infty}{1+m_\infty}\right]$$

For adiabatic flow:

$$\delta_0 = 1.73287 \quad a_0 = 1.63310 \tag{127}$$

$$m_{11} = 0.66235 \quad m_{12} = 1.72387 \quad m_{21} = 1.61411$$

$$d_{11} = 2.11079 \quad d_{21} = -6.07980 \quad d_{22} = 3.73839$$

$$a_{11} = -3.63008 \quad a_{21} = -8.59653 \quad a_{22} = 4.15375$$

and for highly-cooled ($S_w = -0.8$) flow:

$$\delta_0 = 1.72403 \quad a_0 = 1.63284 \quad b_0 = 0.37953 \tag{128}$$

$$m_{11} = 0.66210 \quad m_{12} = 0.34260 \quad m_{21} = 1.61275$$

$$d_{11} = 1.02236 \quad d_{21} = -3.14874 \quad d_{22} = 2.44135$$

$$a_{11} = -1.33576 \quad a_{21} = -3.81059 \quad a_{22} = 1.57323$$

$$b_{11} = 0.12736 \quad b_{21} = -4.90174 \quad b_{22} = 2.87405$$

The expansion for the pressure ratio is of the form:

$$\left(\frac{p_e}{p_\infty}\right)_{WI} = 1.0 + p_1 \bar{\chi} + p_2 \bar{\chi}^2 + \text{---} \tag{129}$$

where

$$p_1 = \frac{-2\gamma}{\gamma-1} \frac{m_\infty}{1+m_\infty} m_1$$

$$p_2 = \frac{-2\gamma}{\gamma-1} \frac{m_\infty}{1+m_\infty}\left[m_2 + \left(\frac{1}{2} - \frac{2\gamma-1}{\gamma-1} \frac{m_\infty}{1+m_\infty}\right)m_1^2\right]$$

The effect of free-stream Mach number on the adiabatic weak-interaction pressure distribution is shown in Fig. 30.

For hypersonic flow, i.e., $\frac{\gamma-1}{2} M_\infty^2 \gg 1$, the Mach number does not appear in the coefficients and the expansions become independent of M_∞. Thus in the limit $M_\infty \to \infty$, these relations become, for adiabatic flow:

$$\left(\frac{M_e}{M_\infty}\right)_{WI} = 1.0 - 0.04790 \bar{\chi} + 0.00229 \bar{\chi}^2 + \text{---} \tag{130}$$

$$\left(\frac{\delta_i^*}{x}\sqrt{\frac{Re_x}{C}}\right)_{WI} = 1.72387(1.0+0.28106 \bar{\chi} - 0.01802 \bar{\chi}^2 \ell n \bar{\chi} + 0.04931 \bar{\chi}^2 + \text{--})$$

$$a_{WI} = 1.63310 + 0.17324 \bar{\chi} + 0.03838 \bar{\chi}^2 + \text{---}$$

hence:

$$\left(\frac{p_e}{p_\infty}\right)_{WI} = 1.0 + 0.33407 \bar{\chi} + 0.04783 \bar{\chi}^2 + \text{---}$$

$$\left(M_\infty \frac{\delta^*}{x}\right)_{WI} = 0.47724 \bar{\chi}(1.0 - 0.09290 \bar{\chi} - 0.01802 \bar{\chi}^2 \ell n \bar{\chi} + 0.02470 \bar{\chi}^2 + \text{--})$$

$$\left(C_F \sqrt{\frac{Re_x}{C}}\right)_{WI} = 0.66235(1.0+0.17193 \bar{\chi} - 0.01802 \bar{\chi}^2 \ell n \bar{\chi} + 0.00114 \bar{\chi}^2 + \text{--})$$

and for non-adiabatic ($S_w = -0.8$) flow:

$$\left(\frac{M_e}{M_\infty}\right)_{WI} = 1.0 - 0.02009\bar{\chi} + 0.00040\bar{\chi}^2 + \text{---} \tag{131}$$

$$\left(\frac{\delta_i^*}{x}\sqrt{\frac{Re_x}{C}}\right)_{WI} = 1.72403(1.0+0.14021\bar{\chi} - 0.00568\bar{\chi}^2 ln\bar{\chi} + 0.00938\bar{\chi}^2 + \text{--})$$

$$a_{WI} = 1.63284 + 0.02684\bar{\chi} + 0.00237\bar{\chi}^2 + \text{---}$$

$$b_{WI} = 0.37953 - 0.00256\bar{\chi} + \text{---}$$

hence:

$$\left(\frac{p_e}{p_\infty}\right)_{WI} = 1.0 + 0.14066\bar{\chi} + 0.00848\bar{\chi}^2 + \text{---}$$

$$\left(M_\infty \frac{\delta^*}{x}\right)_{WI} = 0.20094\bar{\chi}\,[1.0-0.04487\bar{\chi} - 0.00568\bar{\chi}^2 ln\bar{\chi} + 0.00069\bar{\chi}^2 + \text{--}]$$

$$\left(C_F\sqrt{\frac{Re_x}{C}}\right)_{WI} = 0.66210\,[1.0+0.03049\bar{\chi} - 0.00568\bar{\chi}^2 ln\bar{\chi} - 0.00039\bar{\chi}^2 + \text{--}]$$

$$\left(C_H\sqrt{\frac{Re_x}{C}}\right)_{WI} = 0.33122\,[1.0+0.\bar{\chi} - 0.00568\bar{\chi}^2 ln\bar{\chi} - 0.00280\bar{\chi}^2 + \text{--}]$$

In these relations, the asymptotic expansion for the enthalpy parameter b has been terminated at the first term. The reason for this procedure will be explained in the following section.

VI. 1. 3. The Complete Interaction

As previously discussed, in the adiabatic case the eigensolution for self-induced flow lies in the subcritical portion of the phase space. Integration in the downstream direction is therefore inherently unstable, and the integral path originating at the leading edge can be obtained only by integrating upstream, away from the Blasius point. Using the

iteration procedure described in Section V. 2, the correct trajectory is matched to the strong-interaction expansion to determine the initial value of Re_x, and from this the solution in the physical space can be obtained. The results of this iteration are shown in Figs. 31-34. It is evident that except for $a(\bar{\chi})$, the two second-order asymptotic series provide a good representation of the eigensolution for self-induced viscous flow over most of the region.

For highly-cooled ($S_w = -0.8$) flat-plate flows, integration in the downstream direction is stable and the solution in the intermediate region can be obtained directly. Using initial conditions given by the strong-interaction expansion, Eqs. (118), the set of differential equations can be integrated away from the leading edge in the physical space. The results of this integration are shown in Figs. 35-40. The asymptotic relations are in good agreement with the integral solution provided only the first two terms of the weak-interaction expansion for the enthalpy parameter b are used (Fig. 37). This type of behavior is typical of asymptotic series, and since none of the coefficients of the expansions for the remaining variables depends on the second-order term b_2, this term can be neglected. The linear, or first-order, weak-interaction expansion for the enthalpy parameter was used to obtain the physical boundary-layer functions shown in Figs. 38-40. By implication, the truncated series should also be used for computations at finite Mach number.

As previously indicated, because of viscous dissipation the effect of any external disturbance can be considered to propagate only a finite distance upstream of the location of the disturbance. The

pressure gradient forward of that point is determined primarily by the growth of the viscous layer itself and is not influenced by the external disturbance. Thus the interaction caused by an incident shock wave or a change in the slope of the surface, for example, must be obtained by first determining the flow field which would have existed in the absence of these disturbances. The results discussed in this section, therefore, not only give a solution to the classical problem of hypersonic viscous flow on a semi-infinite flat plate, but also provide a method for obtaining the locus of approximate initial states for other viscous-inviscid interactions. Interactions caused by external disturbances can subsequently be obtained from this eigensolution by applying the correct departure conditions (Section V.1) to the viscous flow at a location where the effects of the disturbance are small. The solution for the interaction caused by an incident shock wave in adiabatic and highly-cooled ($S_w = -0.8$) flow is described in the following section.

VI.2. Interactions Generated by Incident Shock Waves

The interaction between a laminar boundary layer and an incident shock wave was shown schematically in Fig. 1, and some of the more important physical features of the resulting flow were described in Section II.1. The primary difficulty encountered in the analysis of this type of interaction is the requirement for a simplified model of the flow field in the vicinity of the shock-impingement location. Assuming that the shock wave is thin, however, the incident wave and the boundary layer can be considered to intersect at only one location. If discontinuities in the viscous layer are not permitted,

then the velocity profiles, the enthalpy profiles and the transformed displacement thickness must be continuous at this point. Also, since the incident shock is reflected as an expansion fan, the static pressure ratio should remain continuous. The conditions at the shock impingement point can therefore be written:

$$\begin{aligned} p_{e_2} &= p_{e_1} & a_2 &= a_1 \\ \delta_i^*{}_2 &= \delta_i^*{}_1 & b_2 &= b_1 \end{aligned} \tag{132}$$

where the subscript 2 denotes conditions immediately downstream of impingement and the subscript 1 those just upstream. With these assumptions, the local Mach number M_e is discontinuous because of the change in stagnation pressure across the incident shock, and hence the physical boundary-layer and displacement thicknesses also exhibit small discontinuities at this location. Of course, the conditions at the shock impingement point given by Eqs. (132) are not the only ones possible, and a different model of the flow field could have been adopted. In the Lees-Reeves[2] formulation, for example, the local Mach number rather than the static pressure ratio was assumed to be continuous. Except for very strong incident shocks, however, both assumptions give essentially the same results for the overall boundary-layer/shock-wave interaction.

The induced streamline angle Θ downstream of impingement must be related to the free-stream Mach number at downstream infinity, i.e.,

$$\Theta_2 = \nu(M_{e_2}) - \nu(M_{\infty_+}) \tag{133}$$

where M_{e_2} is calculated from the static pressure at impingement and from the entropy change across the incident wave. The Mach number at downstream infinity, M_{∞_+}, is obtained by assuming that, far from the impingement point, reflection of the incident shock from the viscous layer is indistinguishable from reflection from a solid boundary. Thus M_{∞_+} is taken to be the Mach number behind the reflected shock wave which turns the inviscid flow back to a direction parallel to the surface. In calculating M_{∞_+}, the total pressure ratio across both shocks is considered, whereas only the entropy change across the incident shock is included in the interaction computation. As a result, the final static pressure ratio obtained from integration in the downstream direction is always higher than the corresponding inviscid pressure ratio, while the Mach numbers are identical. This type of discrepancy is to be expected, however, since the complicated flow field produced by the reflected compression waves and by the entropy variation across streamlines passing through different portions of the shock system cannot be included in the analysis without considerable difficulty (Section V.4). Here again it is possible to adopt several different models of the flow, and a reasonable assumption, for example, would be to take M_{∞_+} as the Mach number downstream of an isentropic compression which turns the inviscid flow parallel to the surface. In this manner the change in stagnation pressure ratio across the reflected shock would not appear in the computation. Of course, the two methods are almost identical unless the incident shock is very strong.

Solutions for boundary-layer interactions caused by incident

shock waves can be used to obtain corresponding solutions for interactions in sharp compression corners. As indicated by Reeves[27], the two flow fields are similar provided that $Re_{x_{corner}} = Re_{x_{shock}}$ and that the total pressure ratio $p_{\infty+}/p_{\infty-}$ is identical. Experimental results for flows in sharp compression turns have been used for comparison with the theoretical computations of boundary-layer/shock-wave interactions given in this section.

In most interactions caused by incident shock waves, both the location of impingement and the strength of the shock are specified a priori. As a result, a number of inverse solutions must be constructed in order to duplicate desired conditions. For adiabatic or slightly-cooled subcritical flows, the Reynolds number Re_x denoting the beginning of the interaction must be selected far upstream of the point of incidence. A departure integral leaving the eigensolution for undisturbed flow and proceeding toward separation can be obtained by applying a small negative value of the perturbation parameter ϵ to the viscous flow at that location (see Fig. 25). Integration of the equations is continued smoothly through separation to the point of shock impingement, where new initial conditions for the integral path downstream of the incident shock are determined through Eqs. (132)-(133). If the subsequent trajectory does not approach the downstream boundary conditions, the assumed value for Re_{x_o} must be modified and the entire procedure repeated. When the approximately correct integral curve has been obtained, iteration of the perturbation ϵ can be used to determine the exact solution. As a general rule, $0 < |\epsilon| < |\epsilon_{max}|$ where ϵ_{max} is the value of the perturbation parameter which gives $dM_e/dx=0$

at the beginning of the interaction.

The results of a typical computation for adiabatic flow are shown in Fig. 41. The two solutions represent interactions beginning in the weak-interaction zone for both a finite ($D \to 0$ at the trailing edge) and a semi-infinite (N_1, $N_3 \to 0$ as $Re_x \to \infty$) flat plate. It is evident that a small change in the value of ϵ can provide very different integral curves because of the high non-linearity of the equations in the subcritical region. The procedure used to determine the solution corresponding to Blasius flow at infinity is to iterate for the perturbation parameter ϵ until two adjacent trajectories which leave the relaxation surface in different directions downstream of reattachment are obtained. For example, one integral curve will depart toward the critical point ($D = 0$), and the other toward separation ($a = 0$). By linearly interpolating between these two curves at a point where the difference in values is relatively small, new initial conditions can be determined to continue the integration in the downstream direction. This procedure can be repeated at successive locations until the complete solution is obtained.

For non-adiabatic supercritical flows, the interaction due to an incident shock wave must be initiated by a jump to a subcritical state at some point upstream of the location of impingement. The correct jump location is determined by the requirement for smooth subcritical-supercritical transition downstream of reattachment. The method of solution is very similar to the one used for subcritical flows except that there is only one iteration parameter, the Reynolds number Re_{x_0} denoting the beginning of the interaction and the location of the jump.

The results of a typical computation for highly-cooled ($S_w = -0.8$) flow at the same free-stream conditions as the previous adiabatic interaction are shown in Fig. 42. Since the throat is a true saddle-point singularity for the system of differential equations, it is not possible in practice to obtain an integral curve passing continuously from the subcritical to the supercritical region. The procedure required is to first iterate for the correct jump location Re_{x_0} and then to linearly interpolate between adjacent trajectories downstream of reattachment to continue the integration toward the throat. It may often also be necessary to slightly vary either the strength of the incident shock or the point of impingement in order to extend the integral curve in the downstream direction. When the location of the throat has been determined as precisely as possible, the solution in the subcritical region can be graphically extrapolated through the singularity into the supercritical region. Downstream of this point the equations are stable and the integration proceeds smoothly toward the Blasius condition at infinity.

VI. 2. 1. Comparison with Experiment

Figs. 43-46 show comparisons of the present theory with several experimental pressure distributions in sharp compression corners obtained by Lewis[19]. In all cases the agreement is quite good, particularly since the experimental value of the free-stream pressure p_{∞}- represents an approximate quantity.* If the effect of even a very small flow inclination on the surface pressures is included, i.e., if the plate is assumed to be at an angle of attack

* Lewis, private communication

$\alpha = -\frac{1}{2}^{\circ}$, the small systematic discrepancies between theory and experiment disappear and the agreement is extremely good (Fig. 43).

VI. 2. 2. The Effect of Surface Cooling

The effect of a highly-cooled surface can be seen from a comparison of the previous figures and from Figs. 47-48, where the Reynolds number Re_{δ^*}, based on the physical displacement thickness, and the skin-friction coefficient C_F are shown. The most dramatic effect of cooling is the marked decrease in the overall length of the interaction. For example, if the region of influence of the incident shock is considered to extend downstream to the point where $M_e = M_{\infty+}$, the length of the interaction in highly-cooled ($S_w = -0.8$) flow is reduced to 40% of the length of the corresponding interaction in adiabatic flow. From Fig. 47, however, one can see that at a given location, the ratio of displacement thicknesses is also approximately 2:5. Thus the propagation of the effect of an external disturbance, in both adiabatic and non-adiabatic flows, scales closely with the displacement thickness. Another effect of surface cooling is to increase the value of the skin-friction coefficient C_F in the interaction region, as shown in Fig. 48.

VI. 2. 3. The Effect of Unit Reynolds Number

Some of the effects of free-stream Reynolds number for fixed incident shock strength and location of impingement are shown in Figs. 49-51 for both adiabatic and highly-cooled ($S_w = -0.8$) flows. In all cases, the upstream propagation of the effect of the external disturbance increases as the unit Reynolds number is increased. Also shown is the decrease in the heat-transfer coefficient C_H with increasing $\frac{Re}{in.}$.

VI. 2. 4. The Effect of Disturbance Strength

Fig. 52 shows the pressure distributions for two interactions occurring close to the plate leading edge in highly-cooled ($S_w = -0.8$) flow. The computations correspond to ramp angles of 22.5° and 27.5° at a free-stream Mach number $M_{\infty -} = 16.0$. These conditions are similar to those investigaged by Miller, Hijman and Childs,[28] although a direct comparison between theory and experiment is not possible unless the non-isentropic effects caused by the curvature of the leading-edge shock wave are included in the calculations. It is evident, however, that the moment method is capable of predicting the more important features of the flow field, even for interactions which occur in the immediate vicinity of the leading edge.

VII. CONCLUDING REMARKS

The present formulation of the moment or integral method for the analysis of laminar viscous-inviscid interactions contains four major assumptions: (1) the boundary-layer approximations are assumed to remain valid throughout the viscous flow region; (2) two single-parameter families of similarity solutions are assumed to be adequate to describe the velocity and total enthalpy profiles; (3) under certain conditions, a set of jump relations is assumed to correctly approximate the rapid, but continuous, change in flow quantities upstream of a disturbance, and (4) the external, inviscid flow at the boundary-layer edge is usually assumed to be isentropic, although the effects of entropy variation can be included in the computations by an iterative procedure if necessary.

The validity of these approximations depends on the specific interaction considered, and in certain situations some of these assumptions are not justified. For example, for the case of separating flow in a sharp expansion corner, it may be necessary to adopt a family of velocity profiles containing an inflection point near the surface and to include the effects of the normal pressure gradient in the analysis. For most interactions, however, a more complicated approach is not warranted, and one of the major advantages of the moment method is its relative simplicity and ease of application to a wide variety of problems. As previously indicated, the moment method described in this investigation is fully capable of predicting the more important physical features of a large class of laminar viscous-inviscid interactions in supersonic flow.

VIII. PROBLEMS FOR FUTURE INVESTIGATION

VIII.1. Flows with Variable S_w

Extensions of the present study to interactions along surfaces for which the distribution of S_w is specified or for which the heat-transfer rate is given are not as complicated as might be expected. In particular, as is evident from Figs. 2-8, the only velocity-profile parameter which depends strongly on the value of S_w is the quantity P(a) in the separated flow region. Also, as shown by Savage[29], the normalized total-temperature distributions for attached flow can be represented quite well by one universal curve, and Rae[30] has obtained the family of lower-branch solutions of the Cohen-Reshotko equations for $S_w = -0.95$ and has indicated that a correlation of the profiles is possible in this region, at least for $S_w \leq -0.8$. Thus by obtaining a number of additional similarity solutions for various values of S_w by the method described in Appendix A, a generalized representation of the profile functions given in Tables 1-3 for all S_w should be relatively easy to determine. In this manner the computations will not be restricted to interactions along constant-enthalpy surfaces.

VIII.2. Interactions with Surface Mass Addition

For the case of boundary layers with mass injection (or suction), the procedure is very similar to the one described for flows with heat transfer. A two-parameter family of similarity solutions can be obtained, using the parameters a(x) and $f(0) = f_w$ to describe the profiles. For $f_w \geq 2$, the asymptotic solutions of Kubota and Fernandez[31] can be used to determine the profile functions. Similar solutions are difficult to obtain for separated boundary layers with strong blowing,

however, and it may be necessary to devise a more appropriate iteration scheme than the one described in Appendix A. For certain interactions, the linearized solutions for small f_w discussed by Strahle[32] may prove useful.

VIII. 3. Interactions in Subsonic Flow

The integral continuity, momentum and mechanical energy equations for incompressible flow can be obtained from Eqs. (34)-(36) by taking the limit as $M_e \to 0$. A system of three equations for four unknowns, δ^*, a, U_e and Θ results; hence an inviscid flow relation between Θ and U_e is required, as in the supersonic case. In subsonic flow, however, the edge velocity U_e is not determined by the local streamline inclination, but depends on the distribution of Θ throughout the entire flow field. Using thin airfoil theory, as suggested by Green[33], the required relation between Θ and U_e can be written:

$$\tan\Theta = \frac{1}{\pi}\int_{-\infty}^{\infty} \frac{(x-\xi)\left[1 - \frac{U_e}{U_\infty}(\xi, 0)\right]}{(x-\xi)^2 + \delta^2}\, d\xi \qquad (134)$$

The continuity equation, Eq. (34), thus becomes an integro-differential equation, and solutions can be obtained only by an iterative procedure. One possible method of iteration is to assume a distribution of $\tan\Theta(x)$, solve the full set of equations, determine a new distribution of $\tan\Theta(x)$ from Eq. (134), and repeat the procedure until convergence is obtained. This method has been discussed by Alber[34] for the case of flow in an incompressible wake.

TABLE 1. COEFFICIENTS OF POLYNOMIAL FUNCTIONS FOR $S_w = 0$

FCT.	C_0	C_1	C_2	C_3	C_4	C_5	C_6	C_7
				ATTACHED PROFILES				
$\mathcal{K}$	.24711	.11056	-.02122	.00435	-.00097	.000099		
J	.37372	.16969	-.02336	.00572	-.00175	.000191		
Z	1.03539	.48373	-.01502	.02610	-.00370			
R	1.25782	-.55550	.31964	-.09077	.01398	-.000935		
P		.48745	-.09927	.00960	-.00031			
$d\mathcal{K}/da$	.11056	-.04245	.01304	-.00389	.00050			
$dJ/d\mathcal{K}$	1.50031	.28105	-.04287	.00262				
				SEPARATED PROFILES				
$\mathcal{K}$	.24711	-.25057	-.43012	.1430	-.4267	-10.8587	38.7425	-31.209
J	.37372	-.42859	.33036	-5.1517	10.5964	-5.8174		
Z	1.03539	-1.02605	-1.12405	-1.1456	3.3434			
R	1.25782	1.09008	7.01736	-33.8762	196.7688	-371.9762	244.3095	
P		-1.19450	-.70990	-7.1253	20.8568	-100.2729	310.2394	-263.587
$d\mathcal{K}/da$	-.25057	-.86024	.42888	-1.7068	-54.2937	232.4553	-218.4644	
$dJ/d\mathcal{K}$	1.50031	-.84045	3.32376	-13.8668	5.4767	30.1770		

TABLE 2. COEFFICIENTS OF POLYNOMIAL FUNCTIONS FOR $S_w = -0.8$

FCT.	C_0	C_1	C_2	C_3	C_4	C_5	C_6
			ATTACHED PROFILES				
χ	.21360	.14559	-.02557	-.00186	.001535	-.000166	
J	.31943	.21814	-.02530	-.00236	.000699		
Z	.85886	.57514	-.07002	.11862	-.043803	.004701	
R	1.46008	-.97913	.66413	-.22727	.040415	-.002924	
P		.53307	-.13418	.00786	.004420	-.000652	
$d\chi/da$	.14559	-.05113	-.00559	.00614	-.000828		
$dJ/d\chi$	1.47875	.30409	-.04296				
a	.34201	.27176	-.17846	.22393	-.077497	.008345	
da/da	.27176	-.35692	.67179	-.30999	.041725		
			SEPARATED PROFILES				
χ	.21360	-.06348	-1.82056	10.5576	-37.0821	57.6139	-31.3578
J	.31943	-.19173	-.86790	3.4359	-15.7682	28.6497	-16.5293
Z	.85886	-.55378	-.28422	-6.2356	12.5892	-6.4777	
R	1.46008	-.39010	28.23864	-174.5137	579.1440	-831.3955	449.0166
P		-.67296	1.87130	-18.2666	32.7836	-13.0597	
$d\chi/da$	-.14158	-.73754	-.63091	6.2296	-66.1475	190.6747	-148.9183
$dJ/d\chi$	1.47875	-1.08822	6.76658	-27.6252	34.3417		
a	.34201	-.16153	-.66107	.1122	.4768		
da/da	-.16153	-1.32214	.33669	1.9073			

TABLE 3. COEFFICIENTS OF POLYNOMIAL FUNCTIONS FOR $S_w = -0.8$

FCT.	C_0	C_1	C_2	C_3	C_4	C_5
			ALL PROFILES			
τ_o	3.83752	-50.4572	298.3153	-931.740	1484.142	-946.400
σ	6.58297	-65.9303	388.3395	-1281.151	2169.799	-1462.240
$d\sigma/db$†	-67.73754	822.7200	-3964.621	6877.003		
$d\sigma/db$‡	-26.00272	156.8862	-364.054	303.164		
			ATTACHED PROFILES			
τ_1	1.40078	-5.4123	-5.0795	72.853	-159.677	114.788
τ_2	-0.61326	3.1527	5.2273	-72.156	178.176	-142.029
τ_3	0.27055	-1.4014	-0.7717	27.041	-76.321	66.368
τ_4	-0.07926	0.3459	0.0244	-5.457	16.185	-14.452
τ_5	0.00886	-0.0293	-0.0827	0.993	-2.676	2.312
			SEPARATED PROFILES			
τ_1	-2.40293	2.6544	106.704	-599.404	1245.35	-922.51
τ_2	9.90203	148.1774	-2296.430	10542.237	-20643.13	14902.15
τ_3	-64.89342	-732.9078	11501.861	-51438.209	98239.36	-69432.32
τ_4	85.64821	1753.8714	-22042.646	91942.596	-168678.92	115980.25
τ_5	-37.67211	-946.2056	10221.085	-38487.998	64640.07	-41071.43

† $b \leq 0.2$ ‡ $b \geq 0.2$

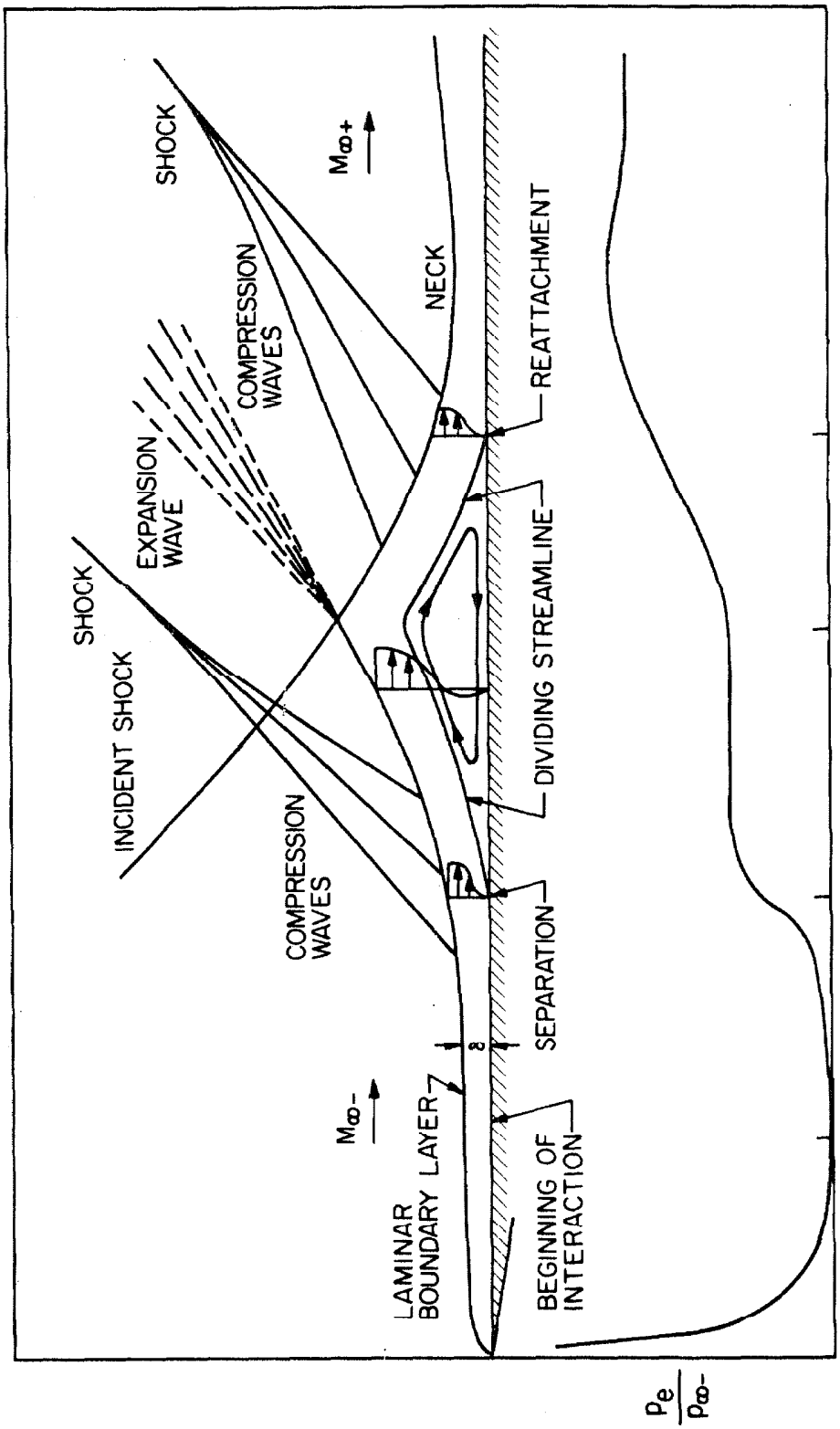

FIG. 1 SCHEMATIC REPRESENTATION OF LAMINAR BOUNDARY-LAYER/SHOCK-WAVE INTERACTION

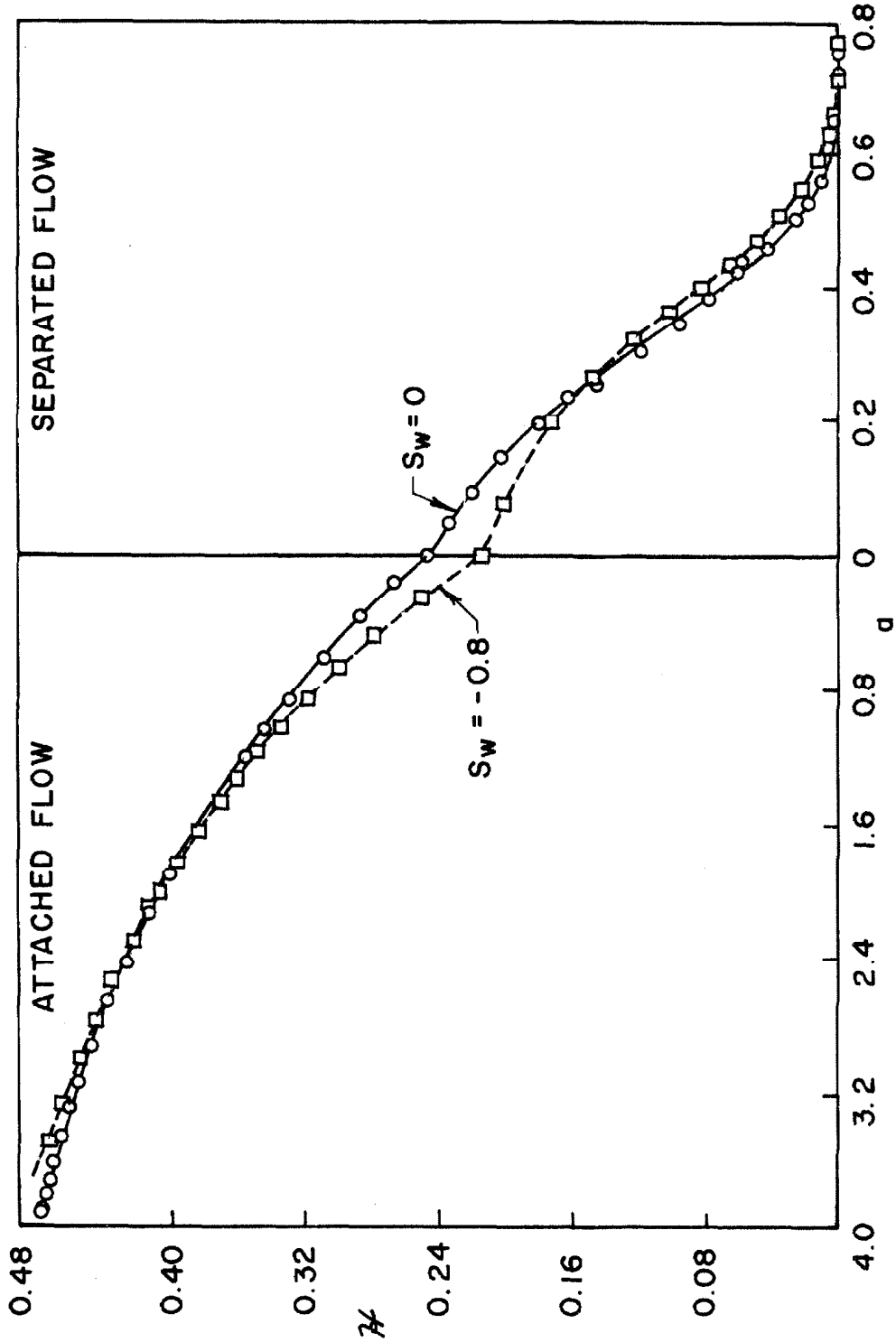

FIG. 2 THEORETICAL $\mathcal{H}$ DISTRIBUTIONS FOR FLOWS NEAR A SOLID SURFACE

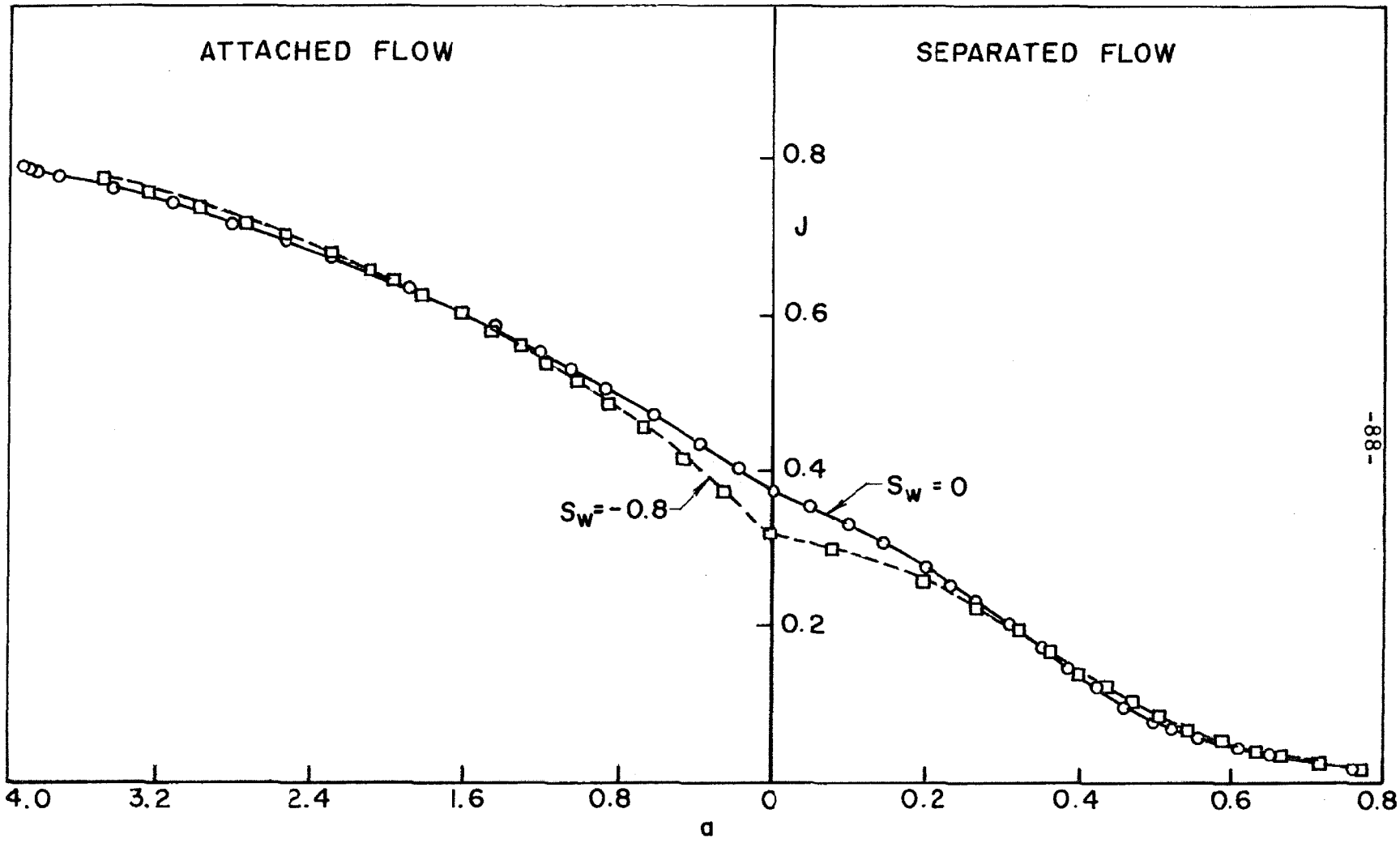

FIG. 3 THEORETICAL J DISTRIBUTIONS FOR FLOWS NEAR A SOLID SURFACE

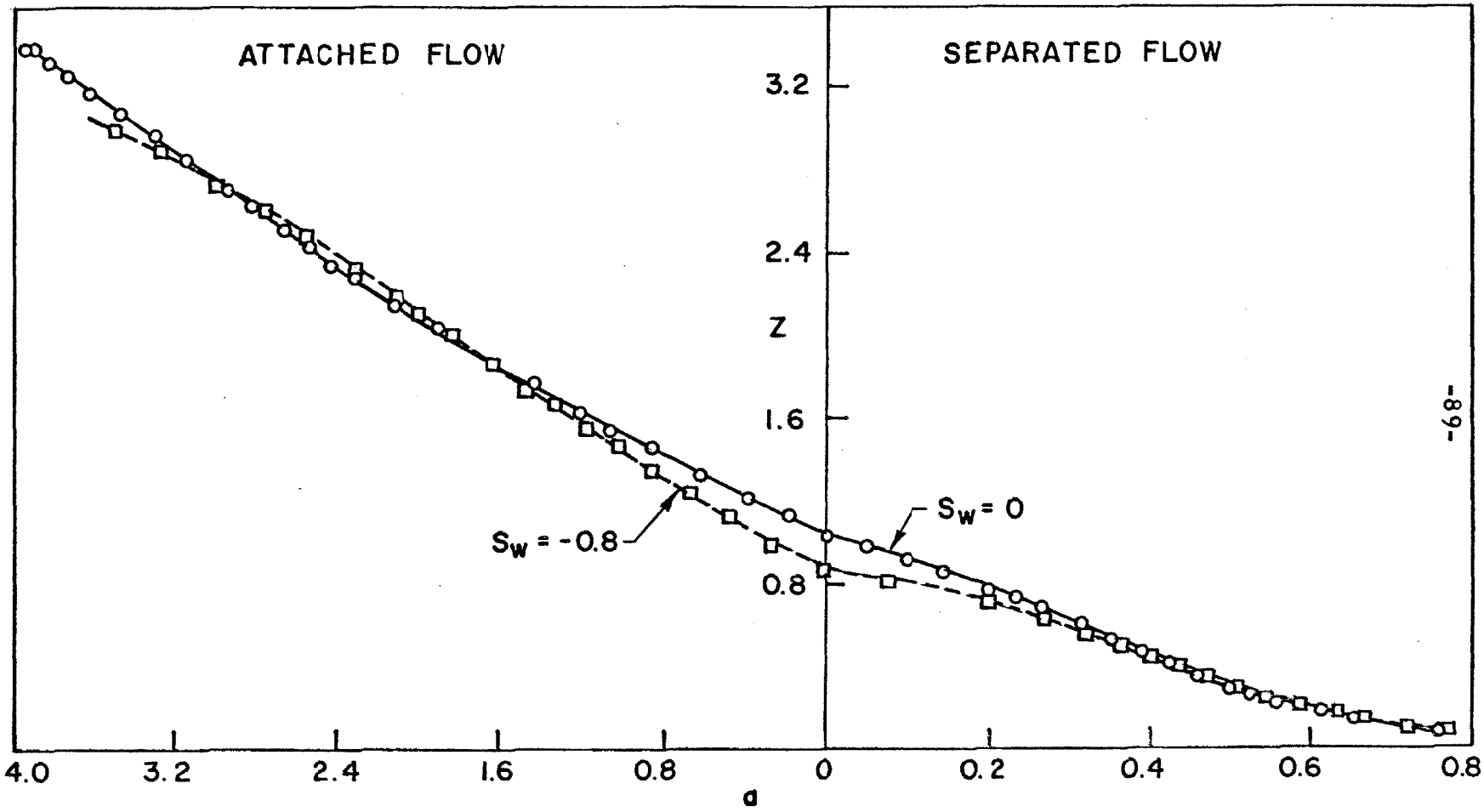

FIG. 4 THEORETICAL Z DISTRIBUTIONS FOR FLOWS NEAR A SOLID SURFACE

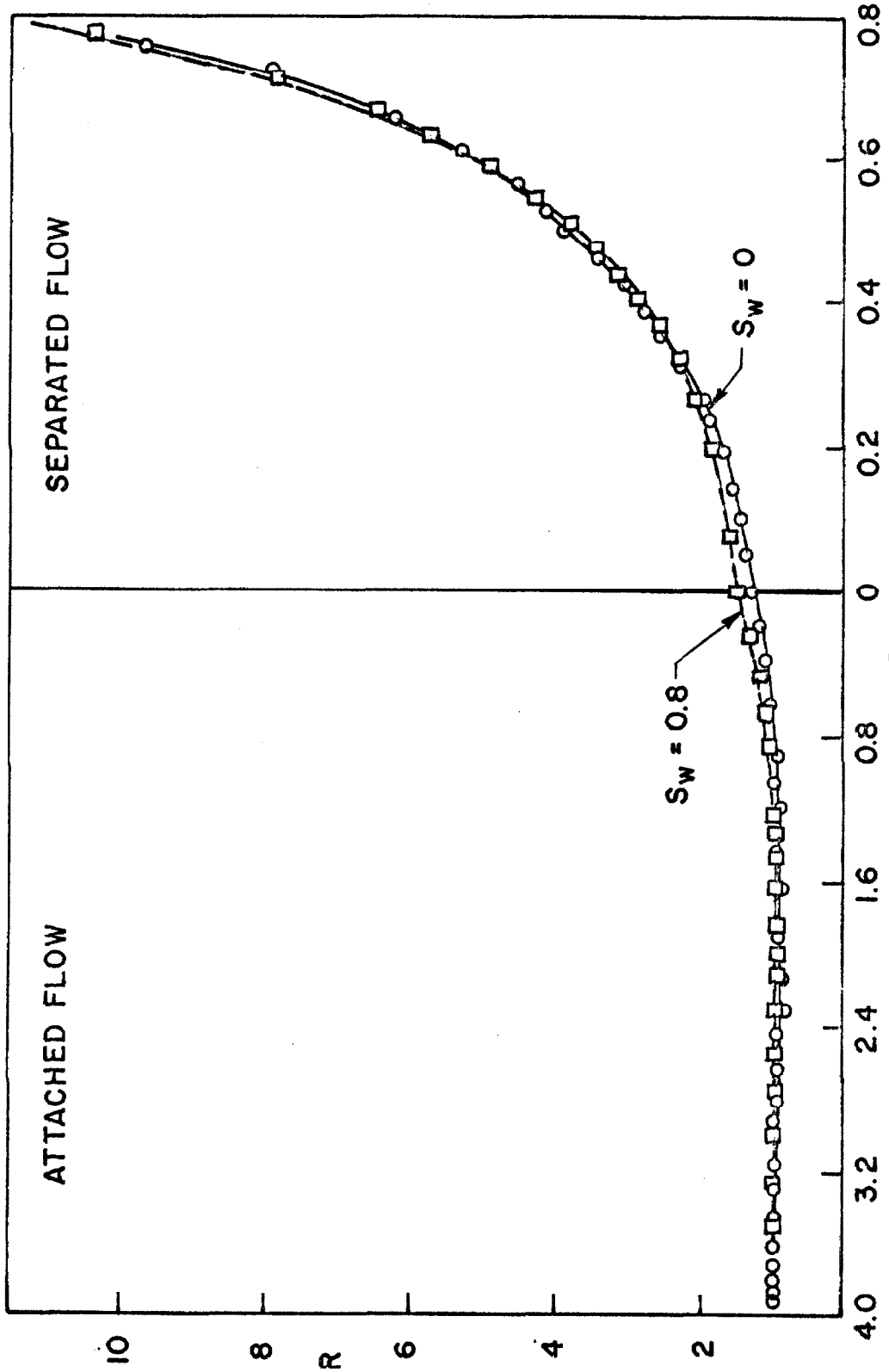

FIG. 5 THEORETICAL R DISTRIBUTIONS FOR FLOWS NEAR A SOLID SURFACE

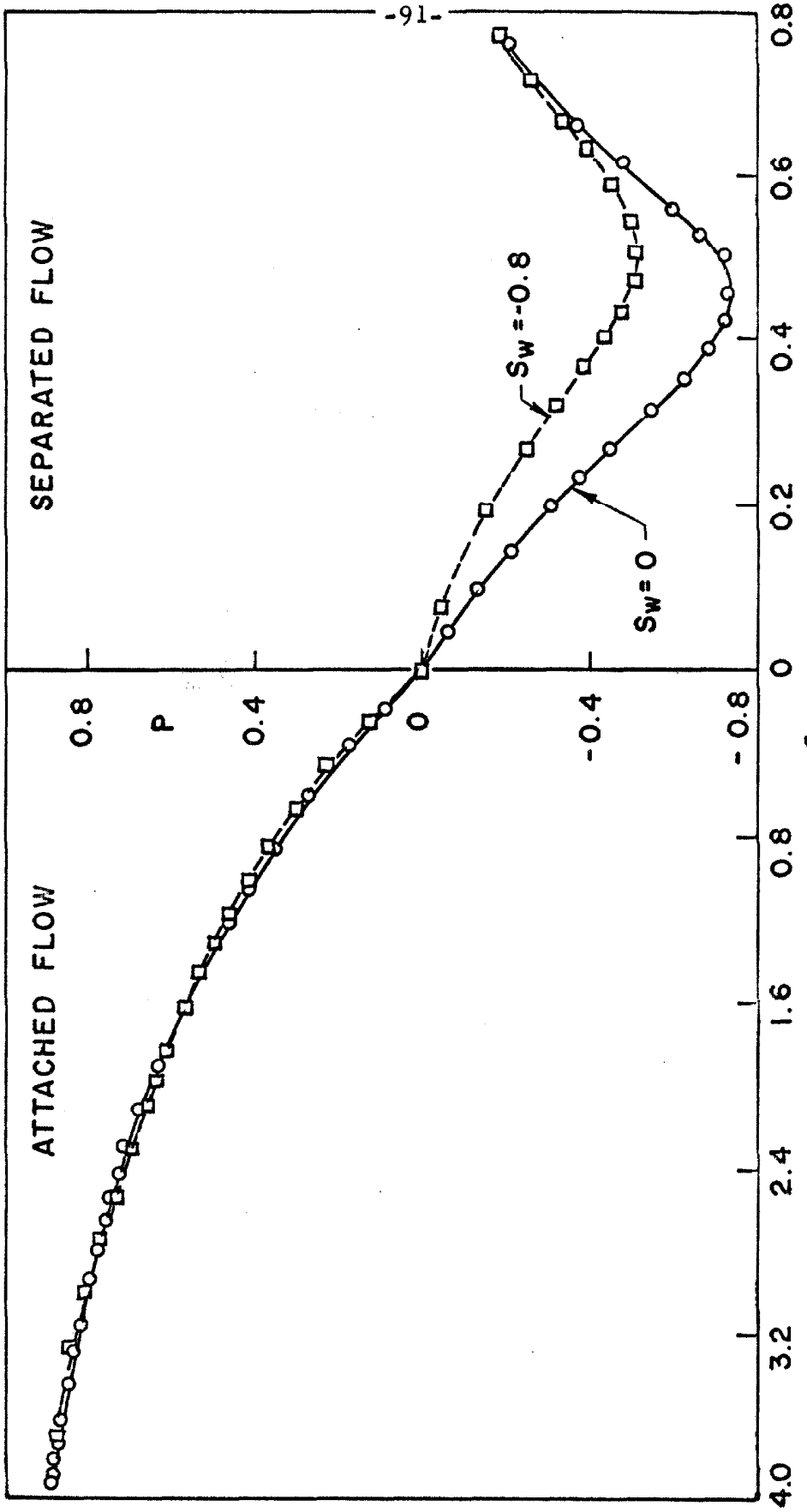

FIG. 6 THEORETICAL P DISTRIBUTIONS FOR FLOWS NEAR A SOLID SURFACE

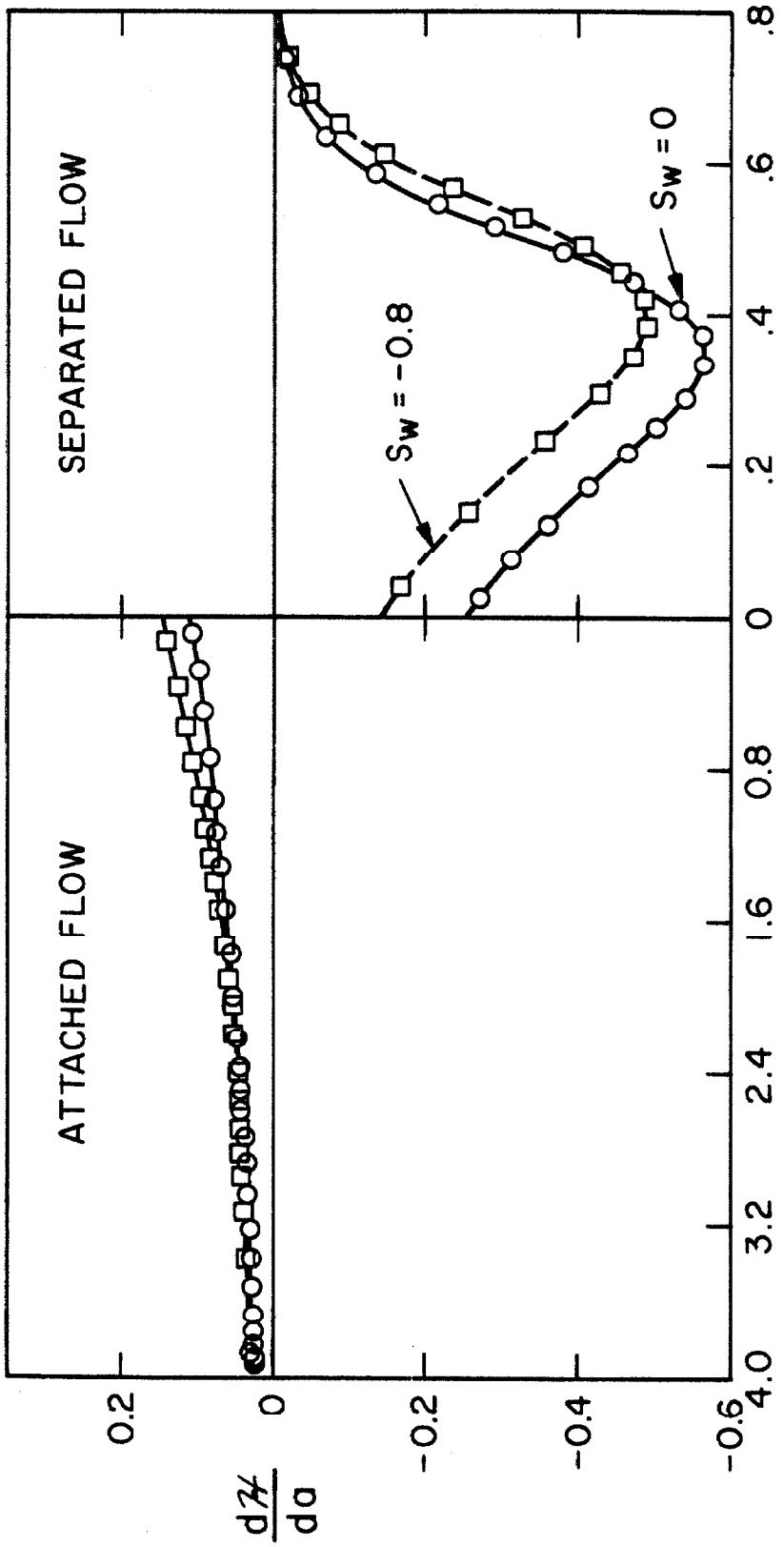

FIG. 7 THEORETICAL $d\psi/da$ DISTRIBUTIONS FOR FLOWS NEAR A SOLID SURFACE.

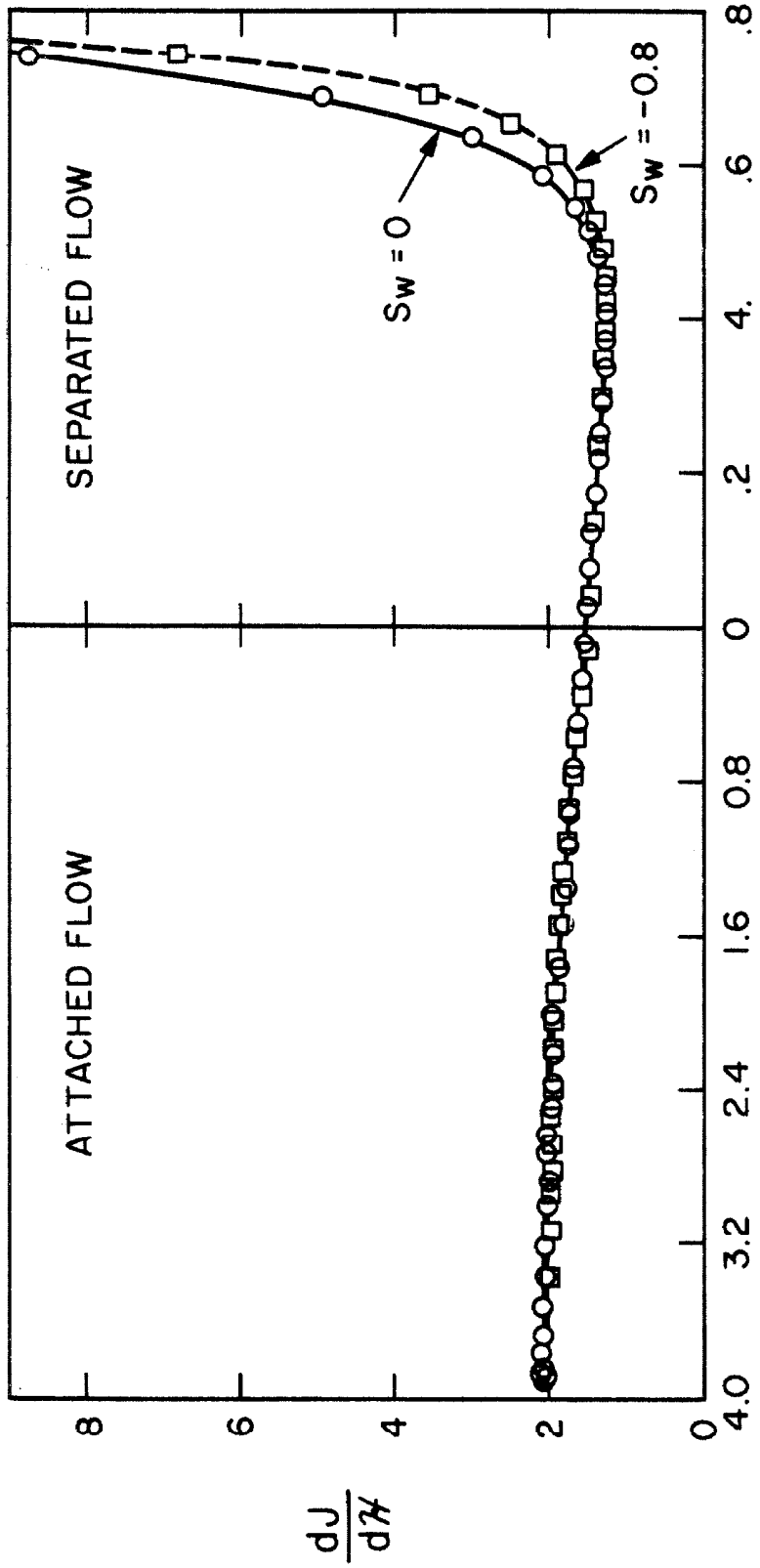

FIG. 8 THEORETICAL $dJ/d\mathcal{H}$ DISTRIBUTIONS FOR FLOWS NEAR A SOLID SURFACE

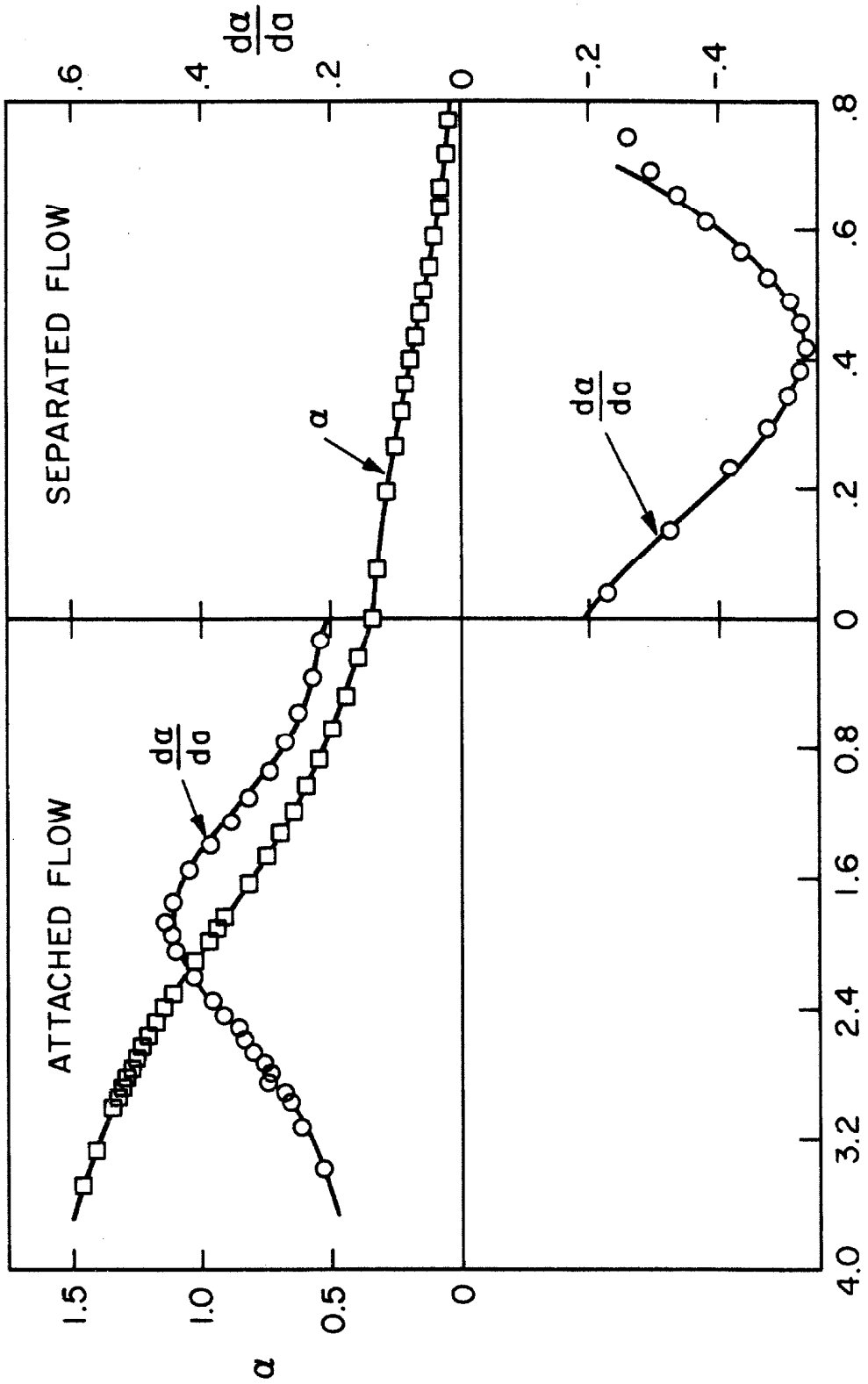

FIG. 9 THEORETICAL α AND $d\alpha/d\alpha$ DISTRIBUTIONS FOR FLOWS NEAR A SOLID SURFACE.

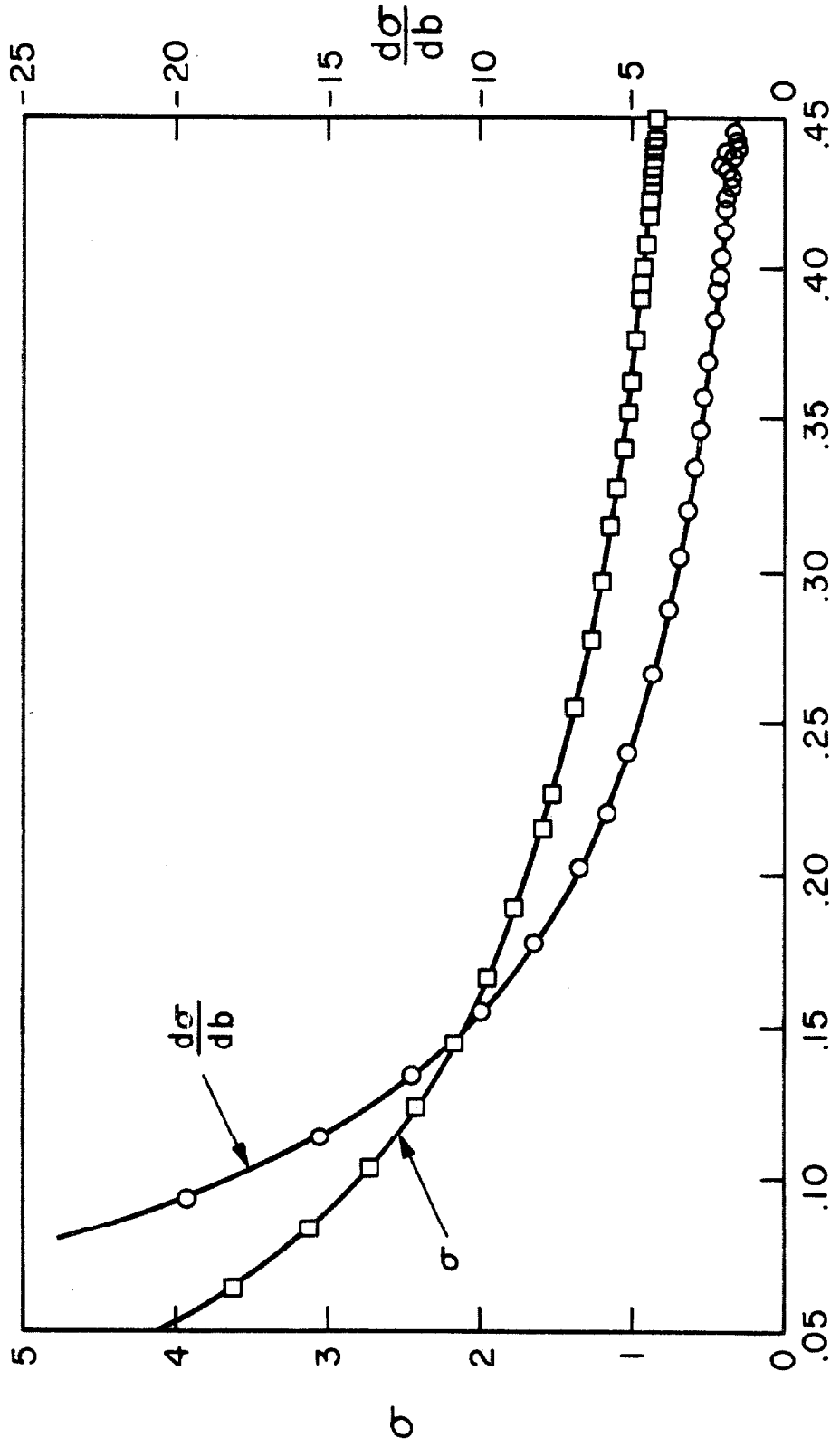

FIG. 10 THEORETICAL σ AND $d\sigma/db$ DISTRIBUTIONS FOR FLOWS NEAR A SOLID SURFACE.

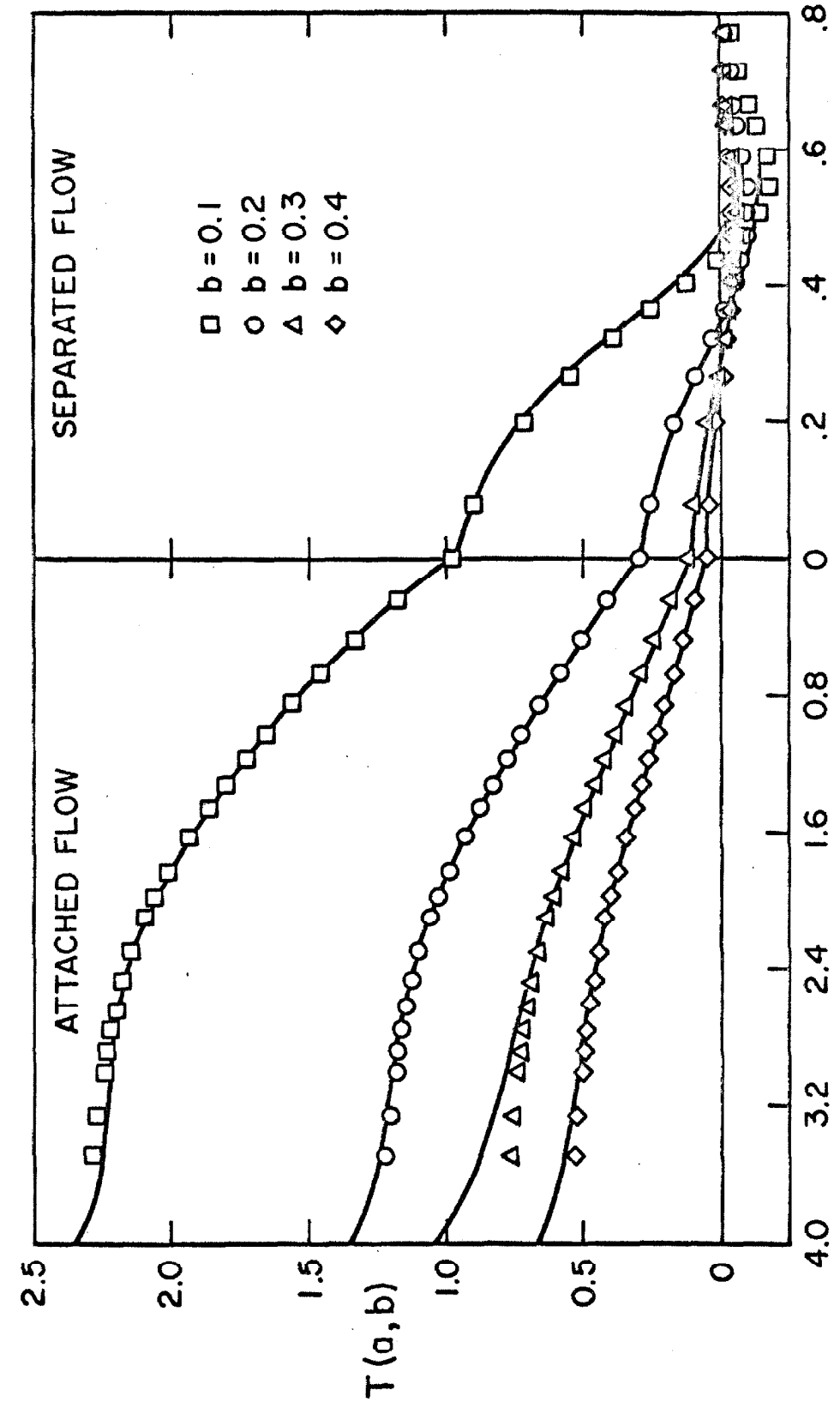

FIG. II THEORETICAL T DISTRIBUTIONS FOR FLOWS NEAR A SOLID SURFACE.

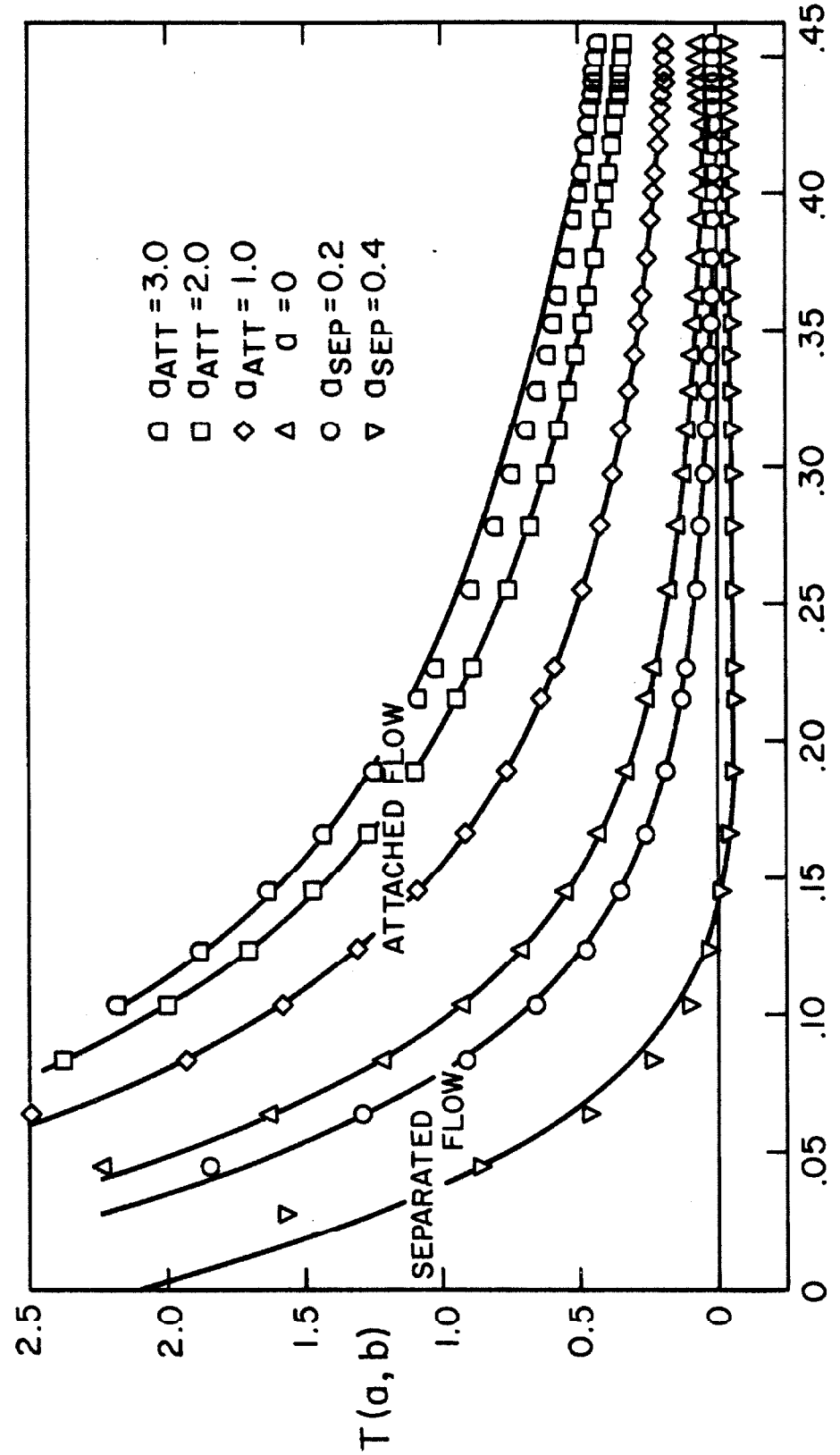

FIG. 12 THEORETICAL T DISTRIBUTIONS FOR FLOWS NEAR A SOLID SURFACE.

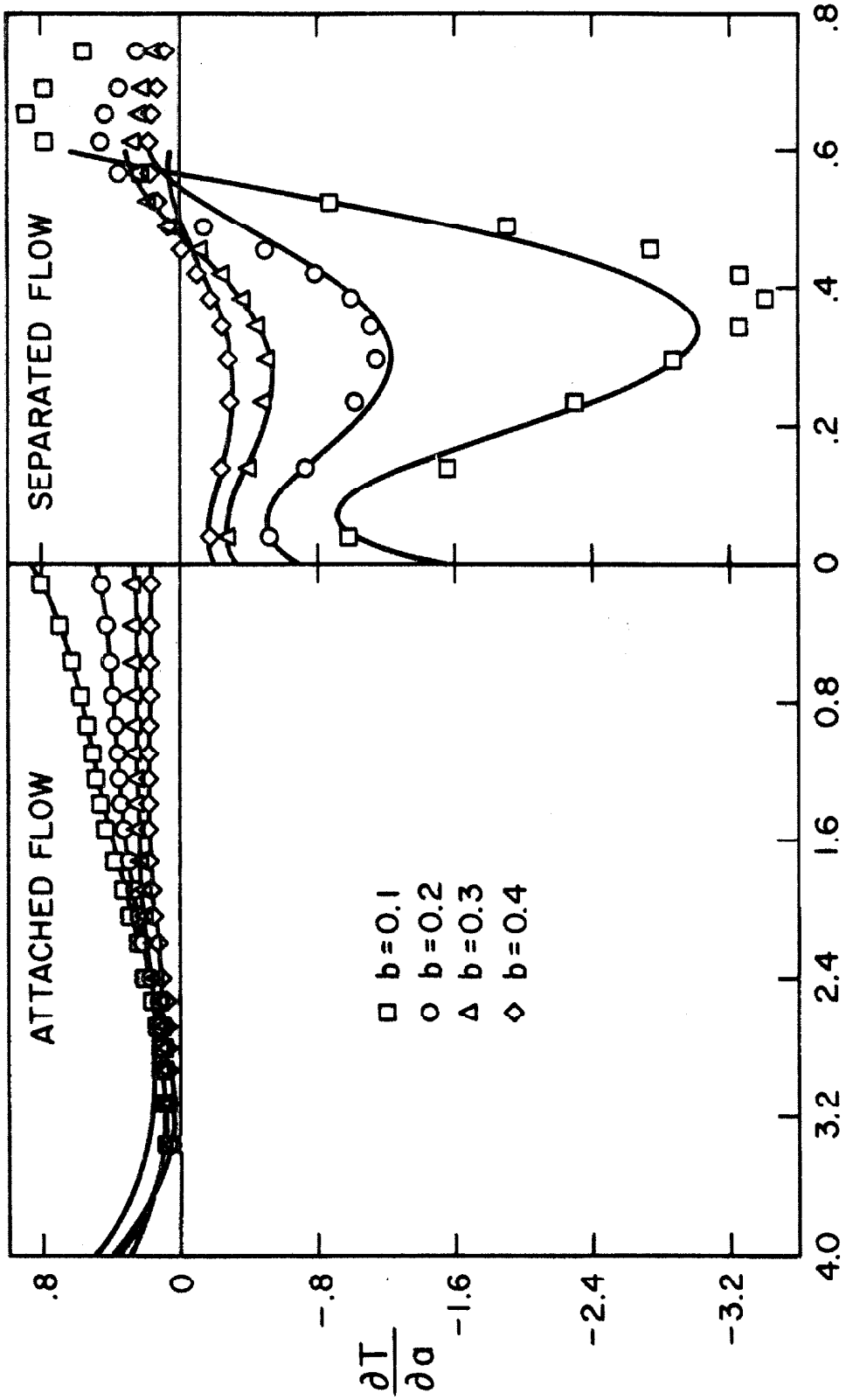

FIG. 13 THEORETICAL $\partial T/\partial a$ DISTRIBUTIONS FOR FLOWS NEAR A SOLID SURFACE.

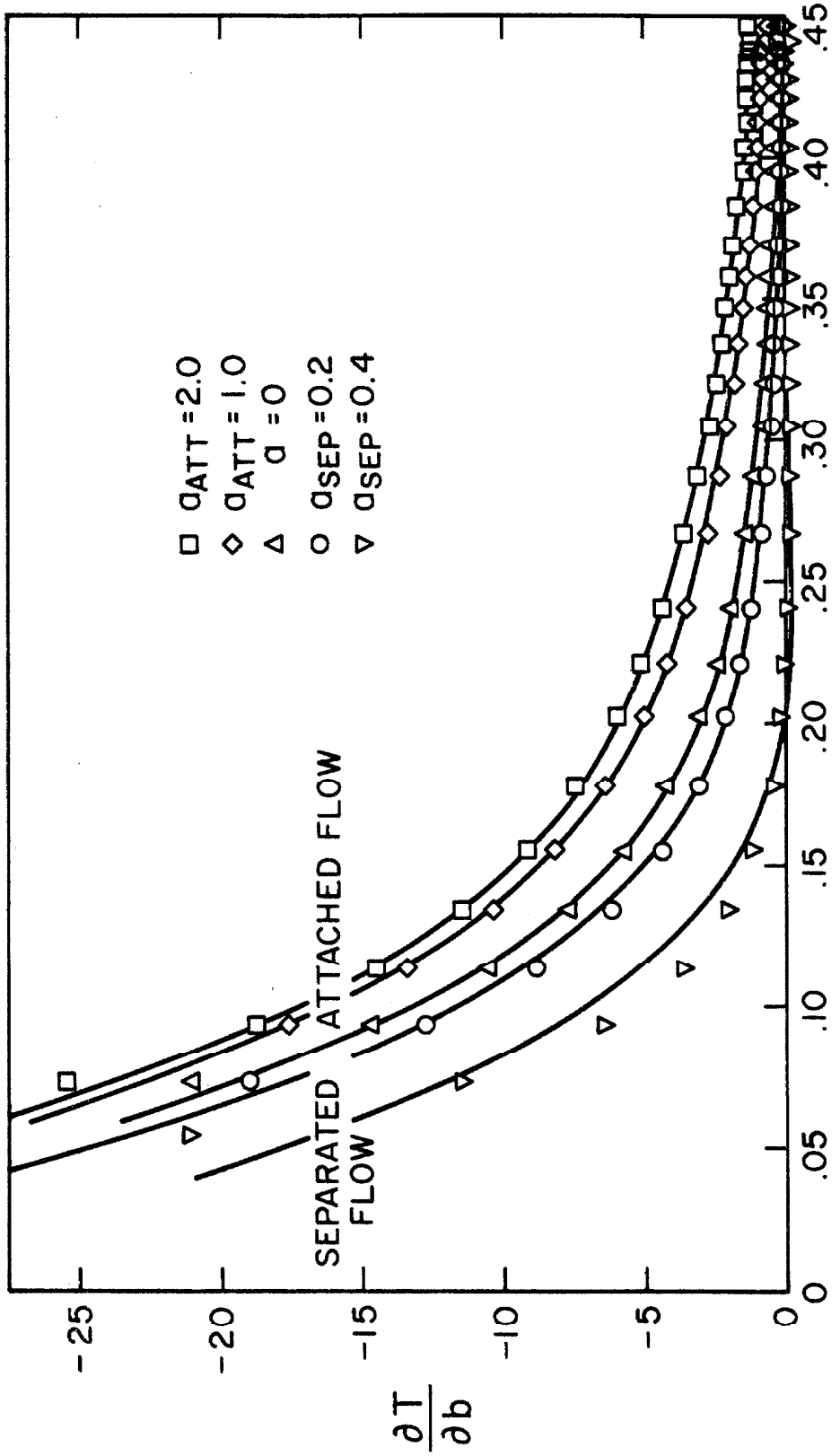

FIG. 14 THEORETICAL $\partial T/\partial b$ DISTRIBUTIONS FOR FLOWS NEAR A SOLID SURFACE.

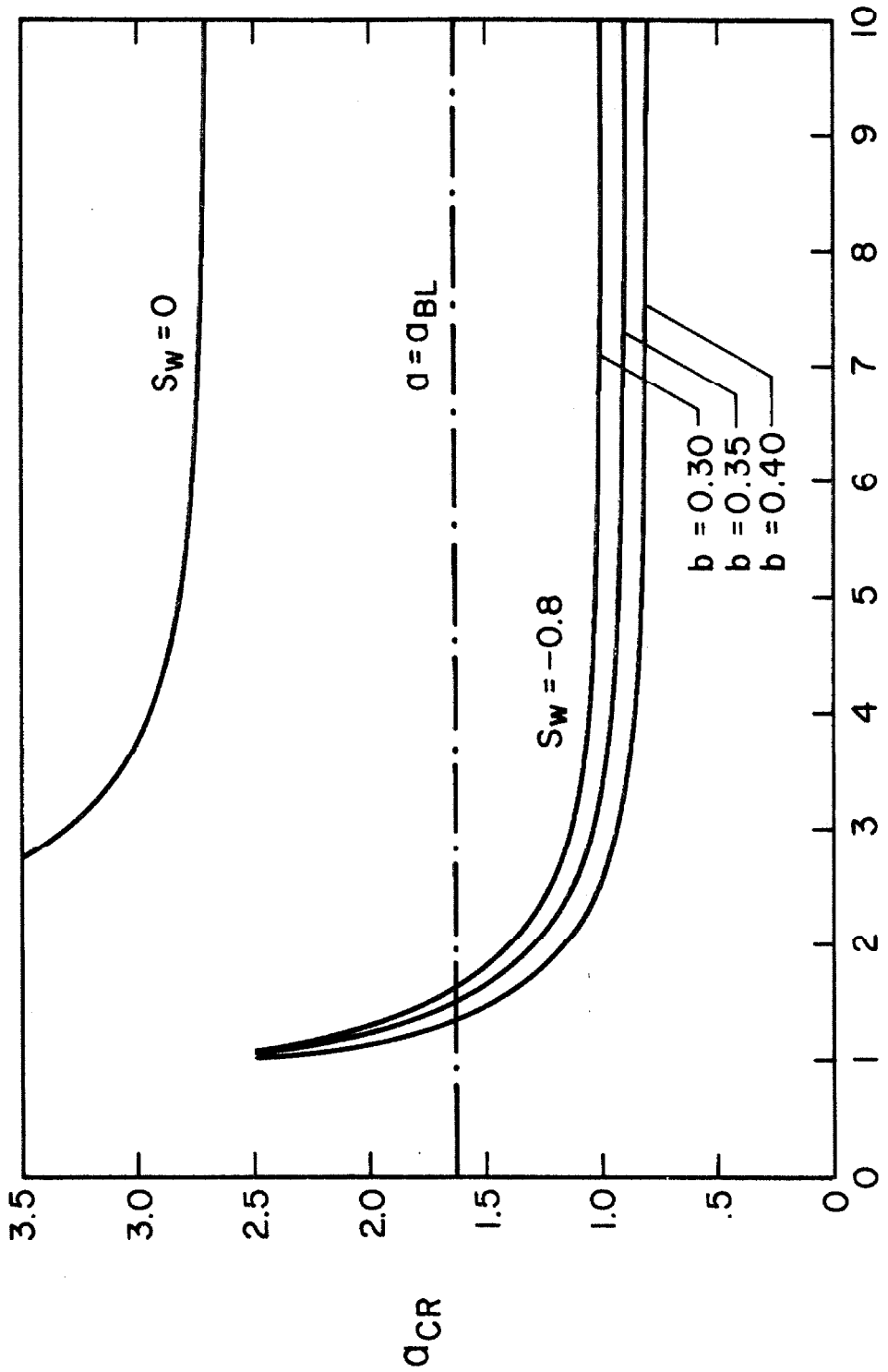

FIG. 15 LOCUS OF CRITICAL POINTS FOR $S_w = 0$ AND $S_w = -0.8$

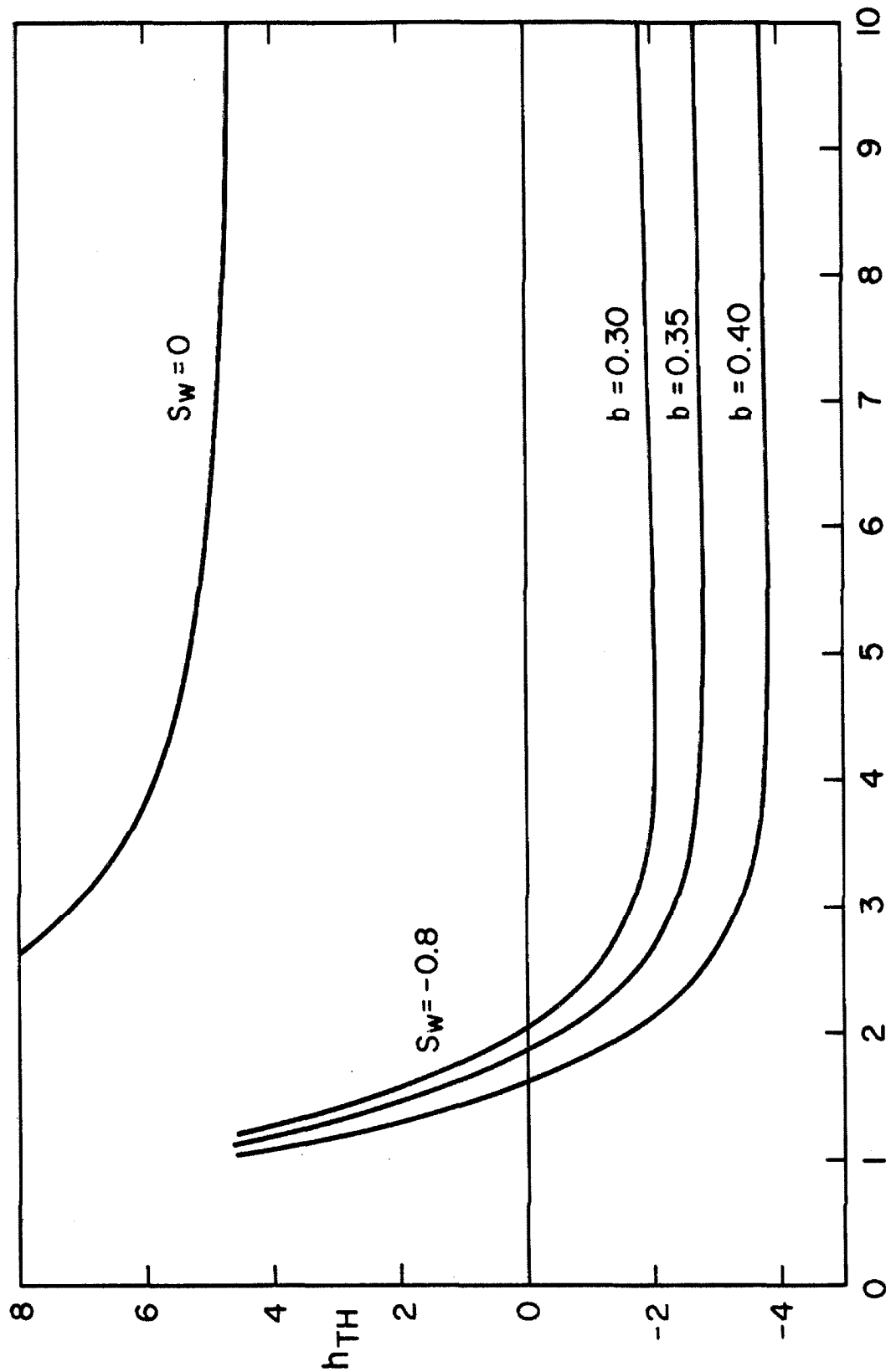

FIG. 16 VARIATION OF h_{THROAT} WITH M_e FOR $S_w=0$ AND $S_w=-0.8$

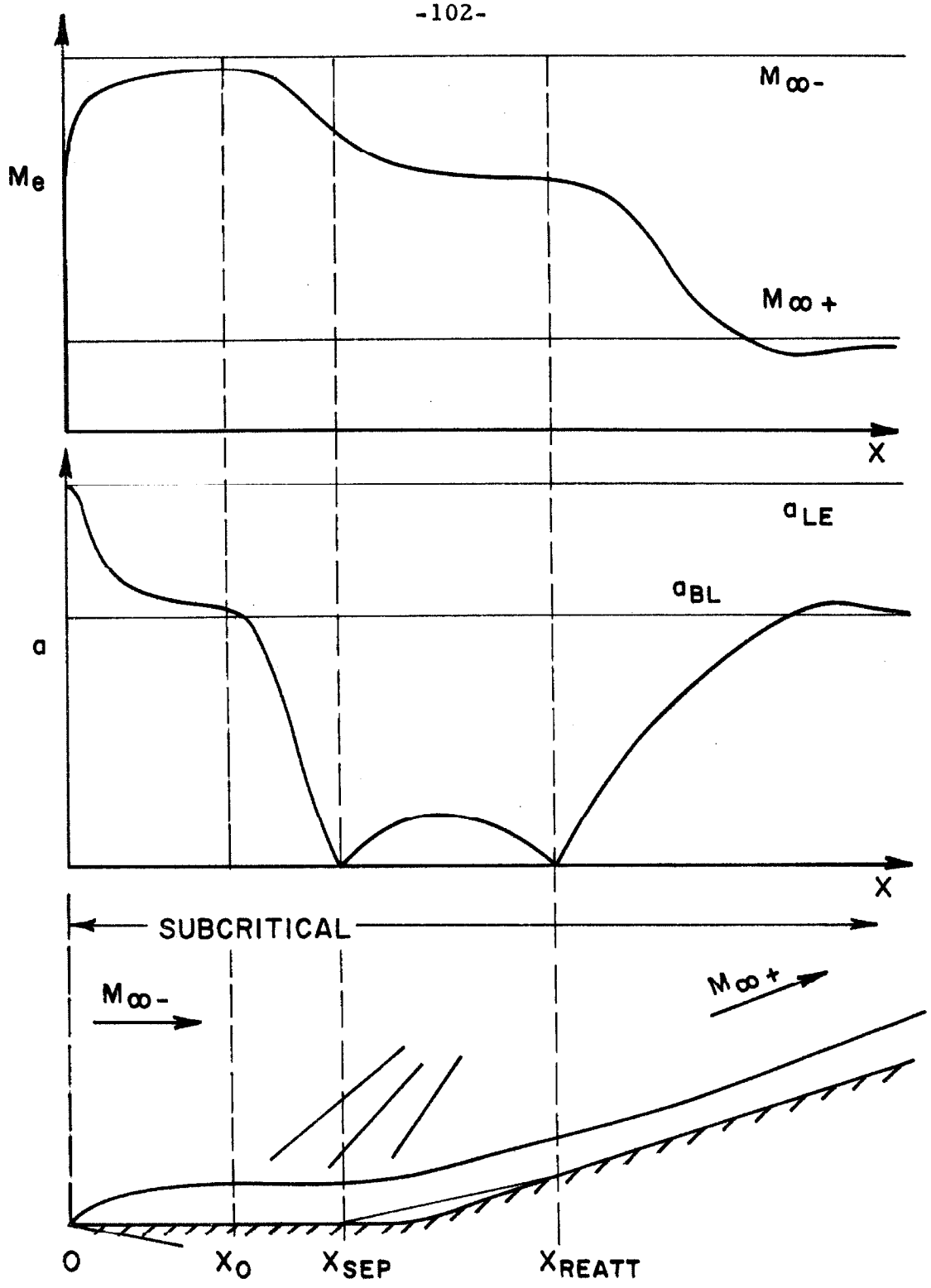

FIG. 17 TYPICAL SUBCRITICAL VISCOUS - INVISCID INTERACTION ($S_w = 0$)

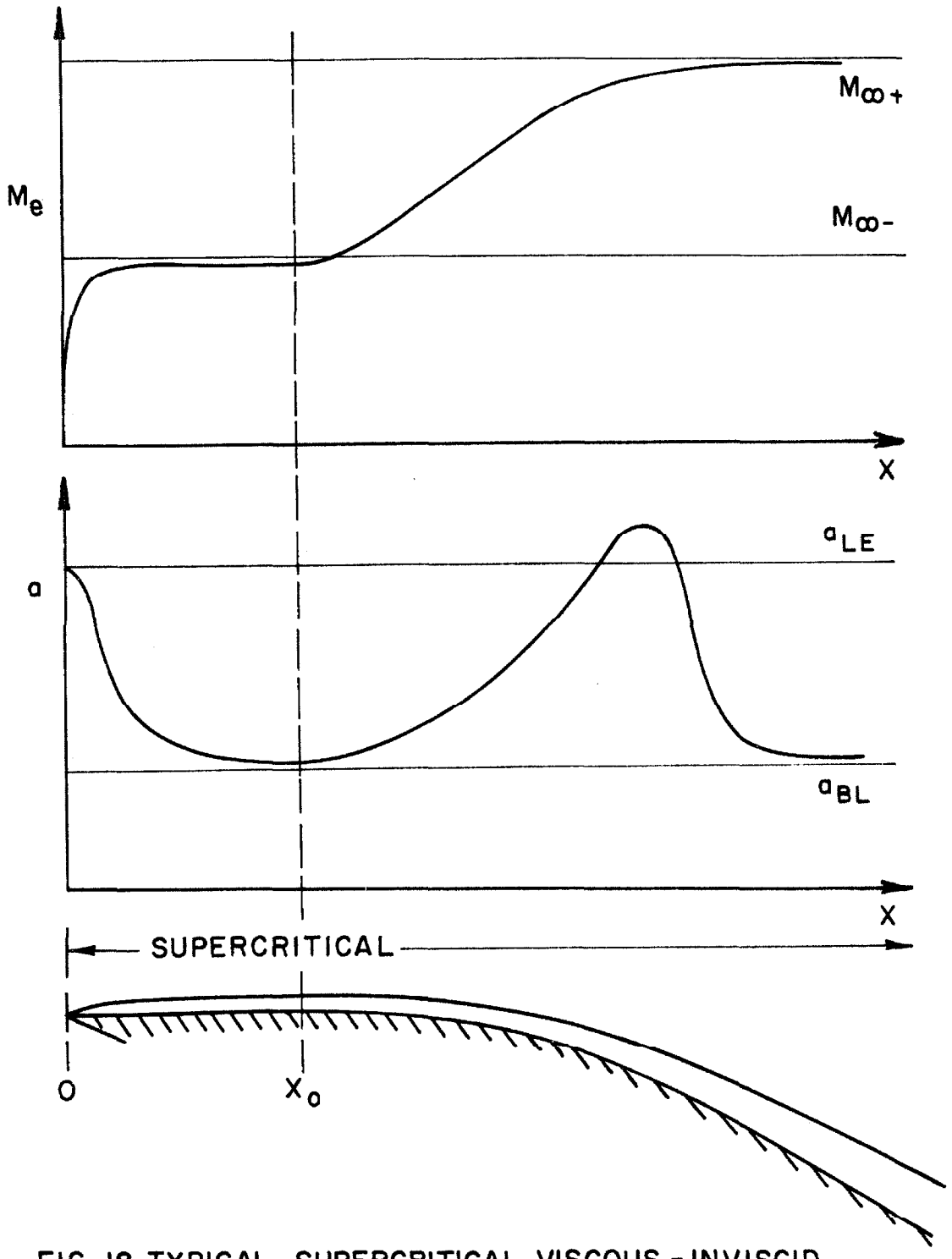

FIG. 18 TYPICAL SUPERCRITICAL VISCOUS - INVISCID INTERACTION ($S_w = -0.8$)

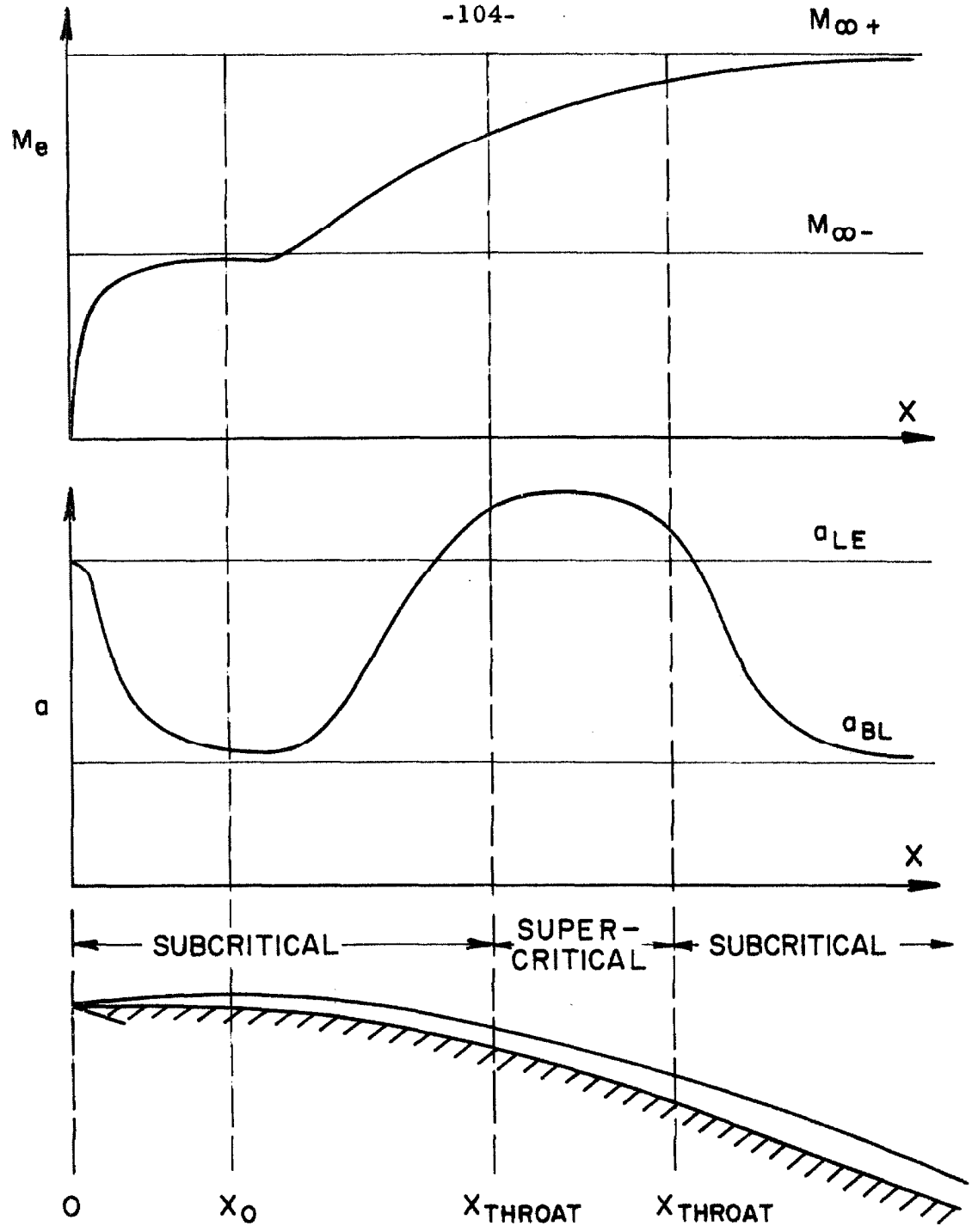

FIG. 19 SUBCRITICAL-SUPERCRITICAL-SUBCRITICAL INTERACTION ($S_w = 0$)

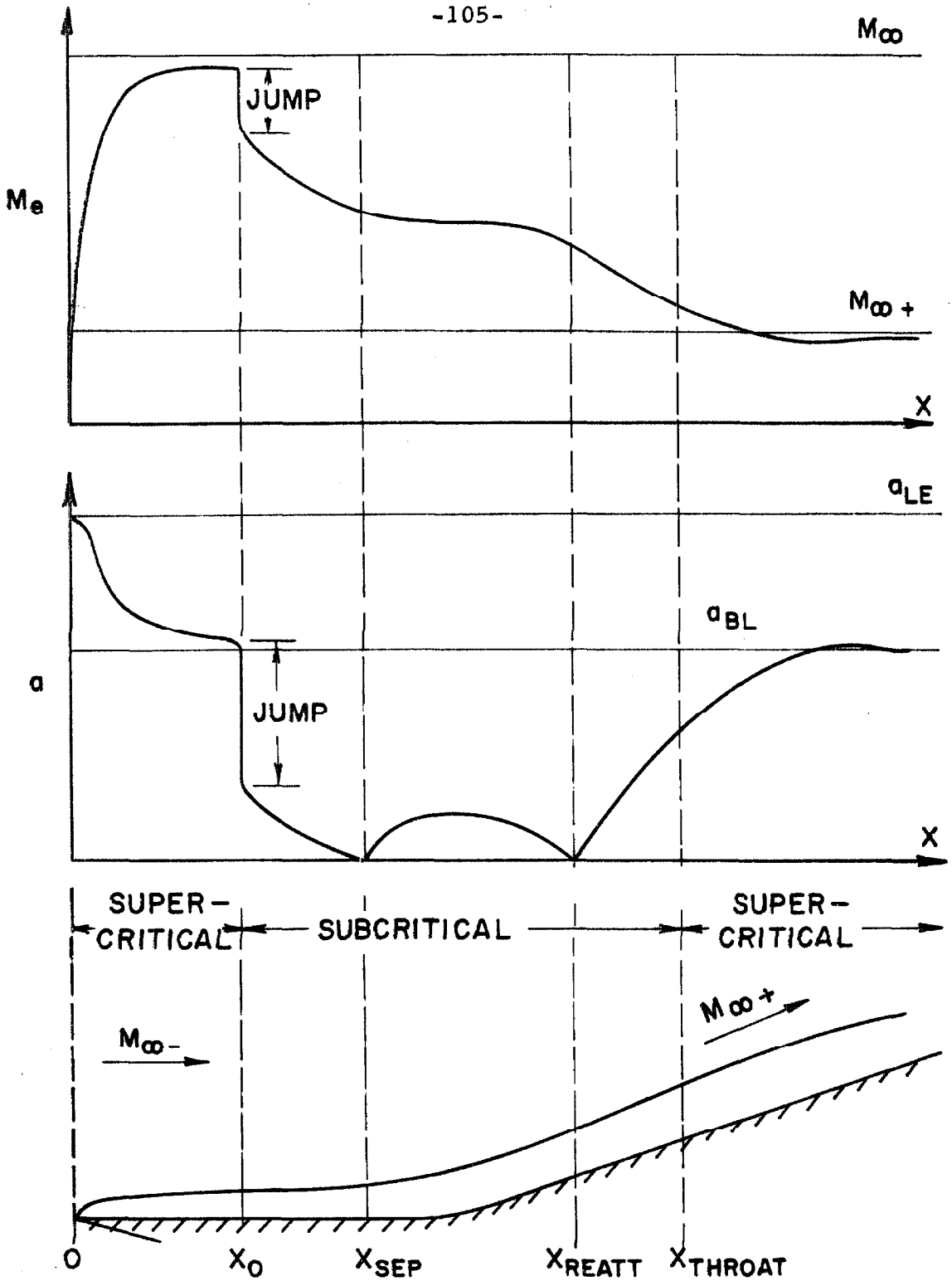

FIG.20 SUPERCRITICAL-SUBCRITICAL-SUPERCRITICAL INTERACTION ($S_w = -0.8$)

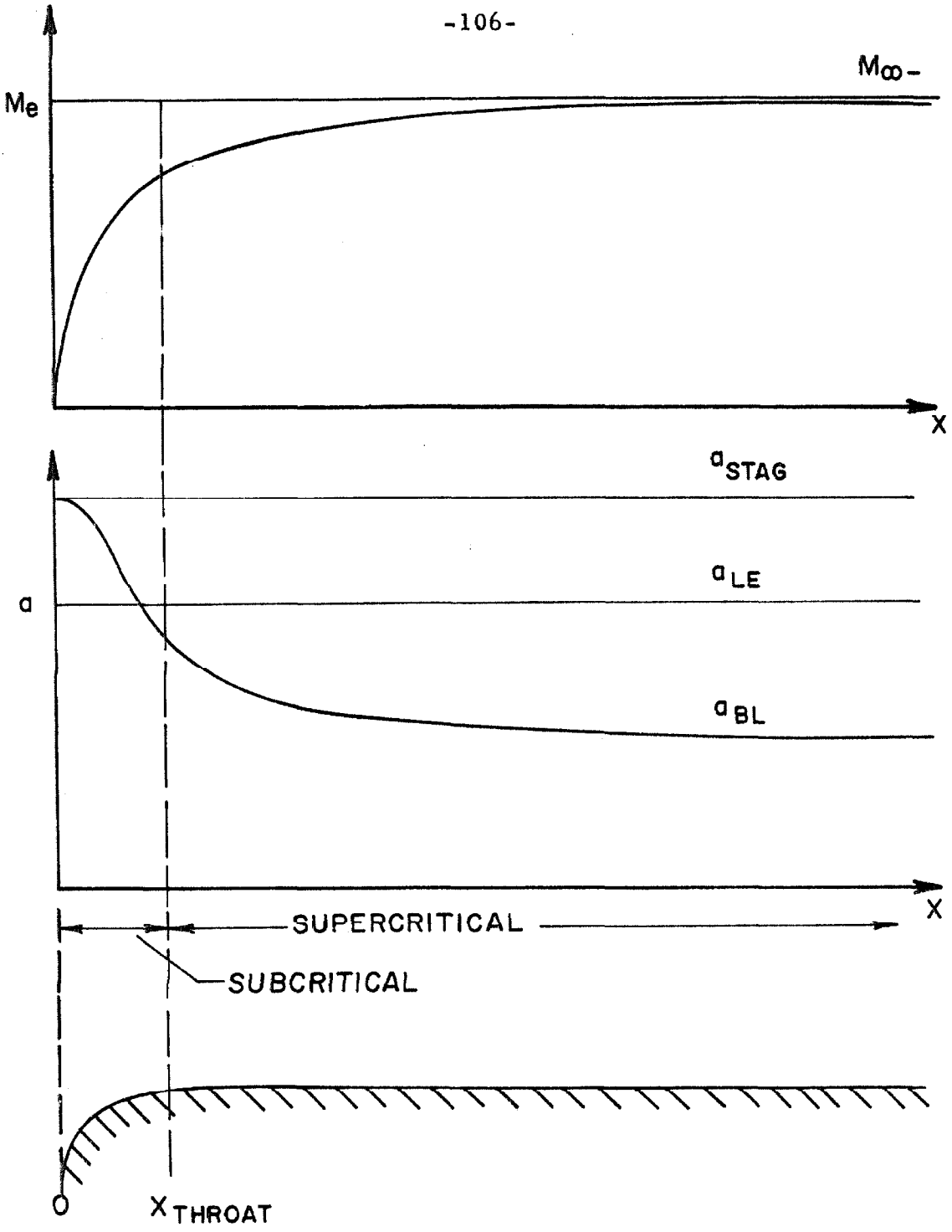

FIG. 21 TYPICAL SUBCRITICAL - SUPERCRITICAL INTERACTION ($S_w = -0.8$)

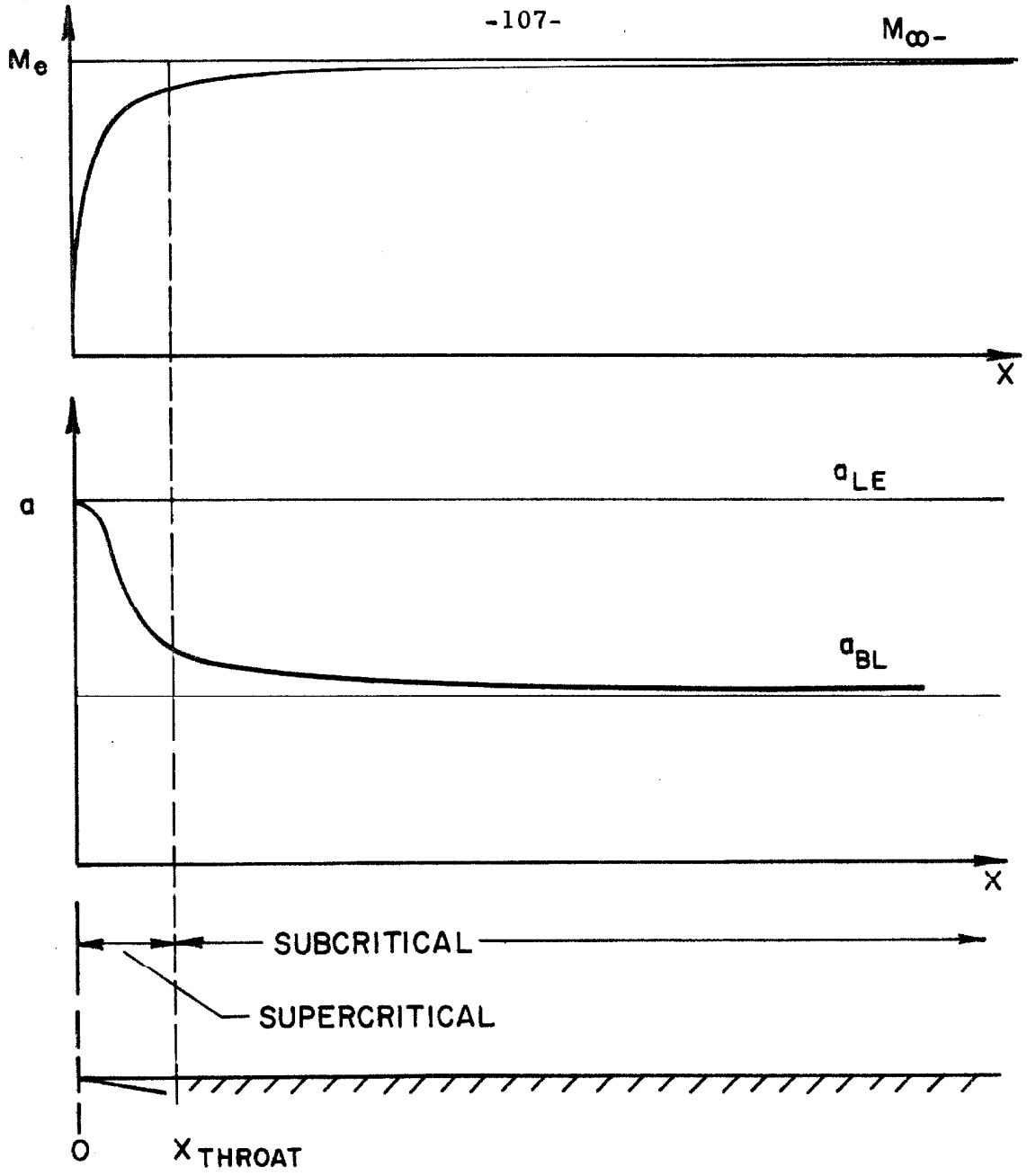

FIG. 22 TYPICAL SUPERCRITICAL – SUBCRITICAL INTERACTION
$(-0.8 < S_w < 0)$

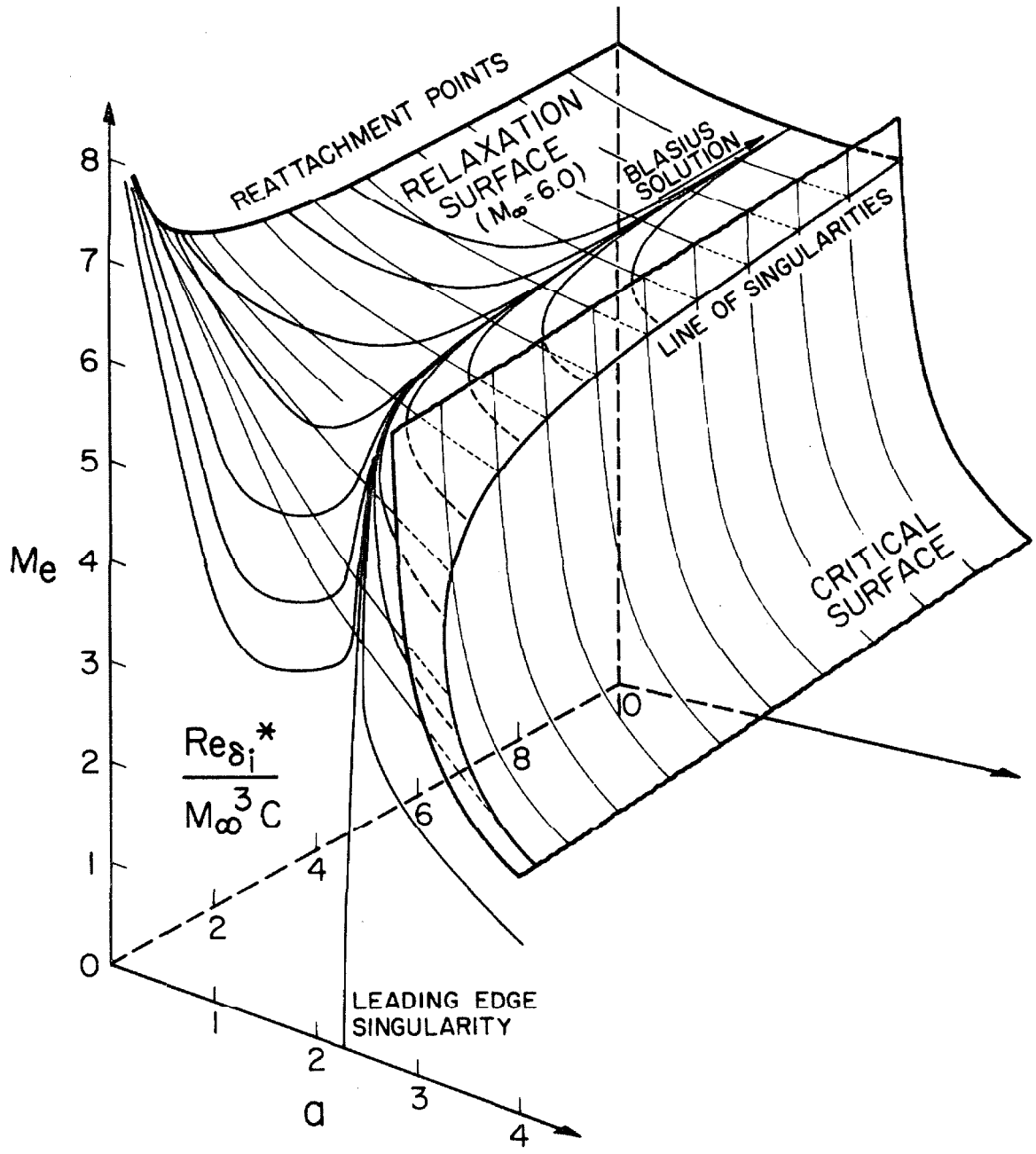

FIG. 23 PHASE-SPACE GEOMETRY FOR ADIABATIC FLOW

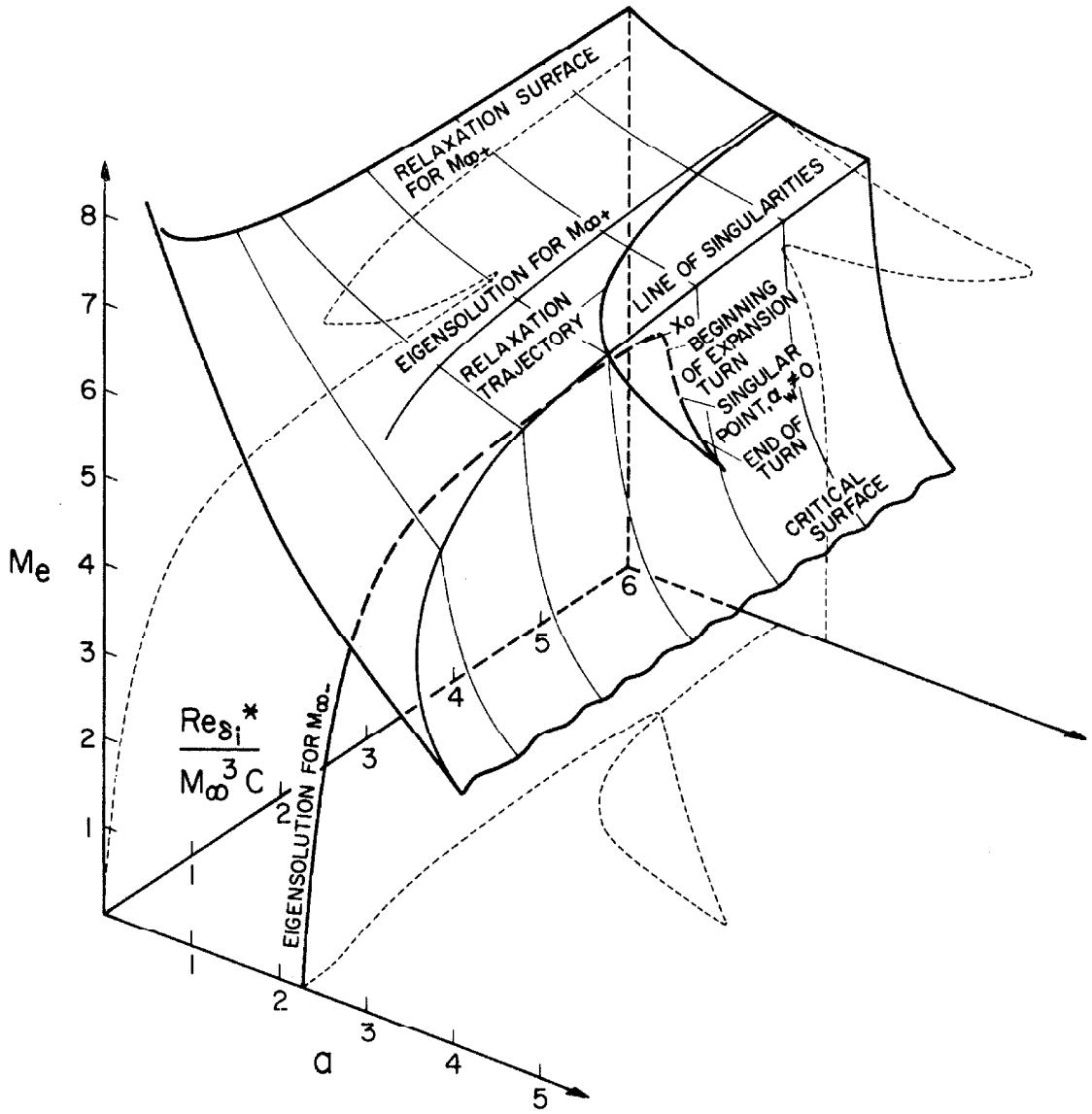

FIG. 24 PHASE-SPACE REPRESENTATION FOR ADIABATIC FLOW THROUGH AN EXPANSION TURN

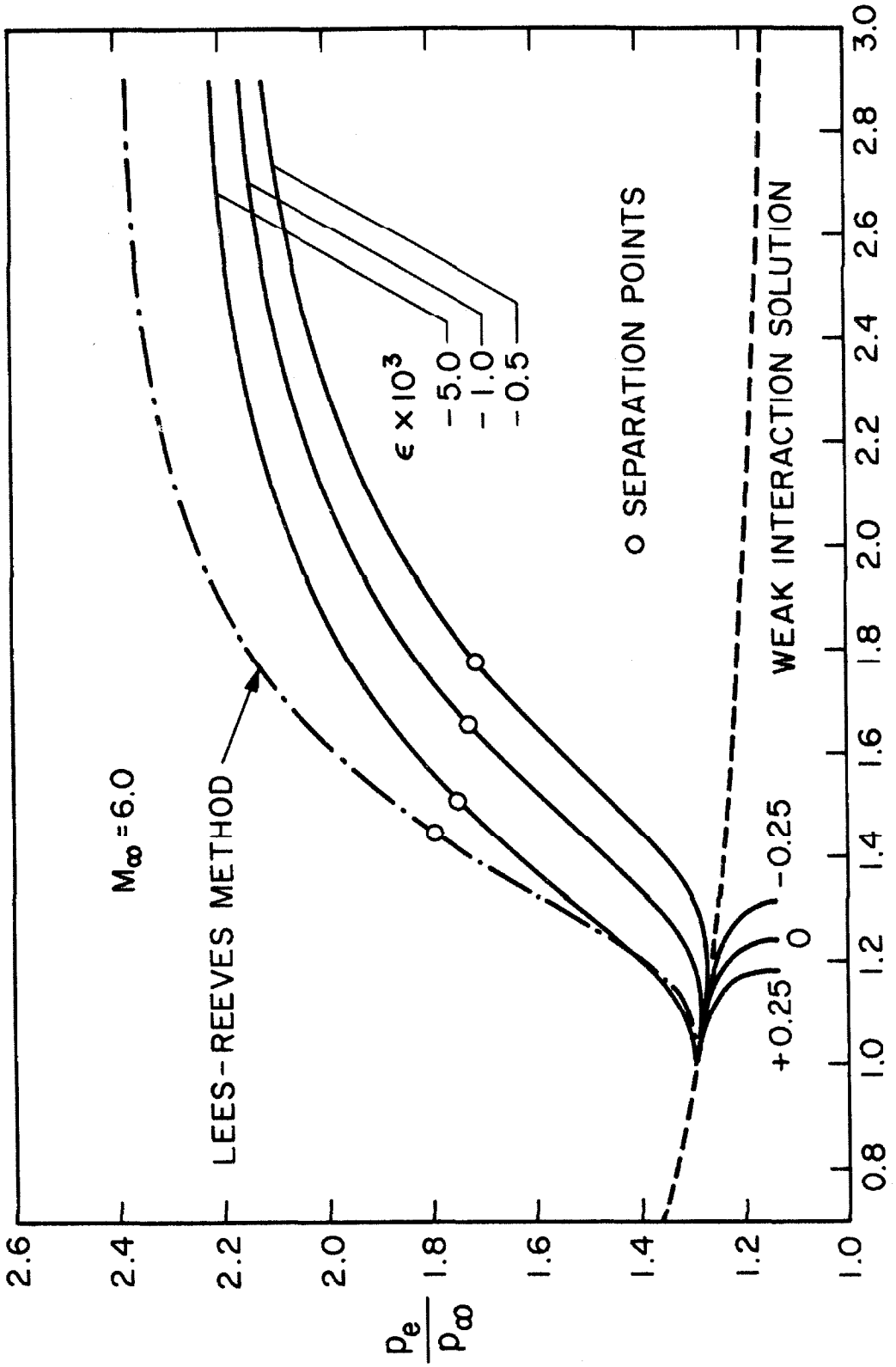

FIG. 25 EFFECT OF ϵ ON ADIABATIC FREE INTERACTION

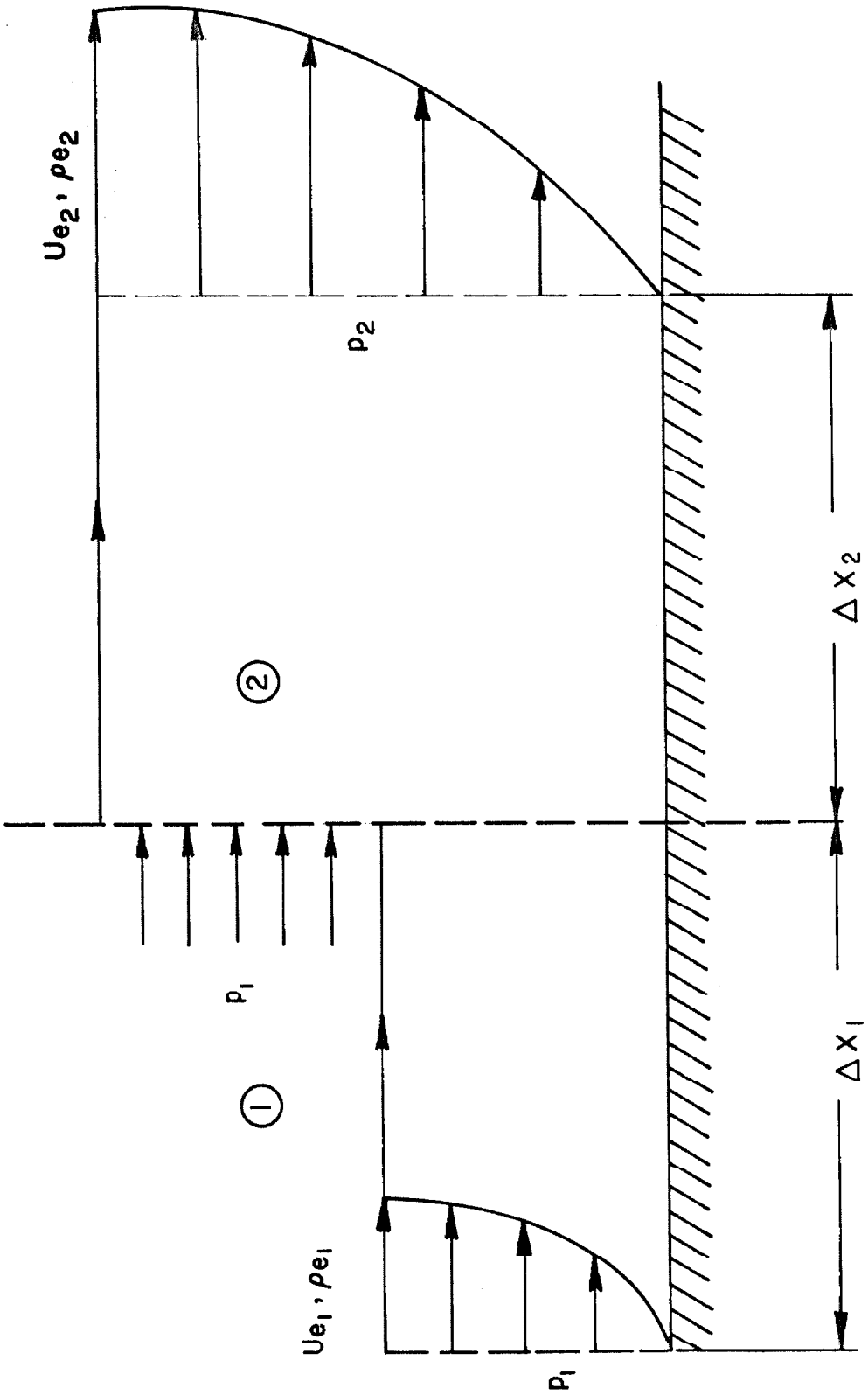

FIG.26 MODEL FOR SUPERCRITICAL-SUBCRITICAL JUMP

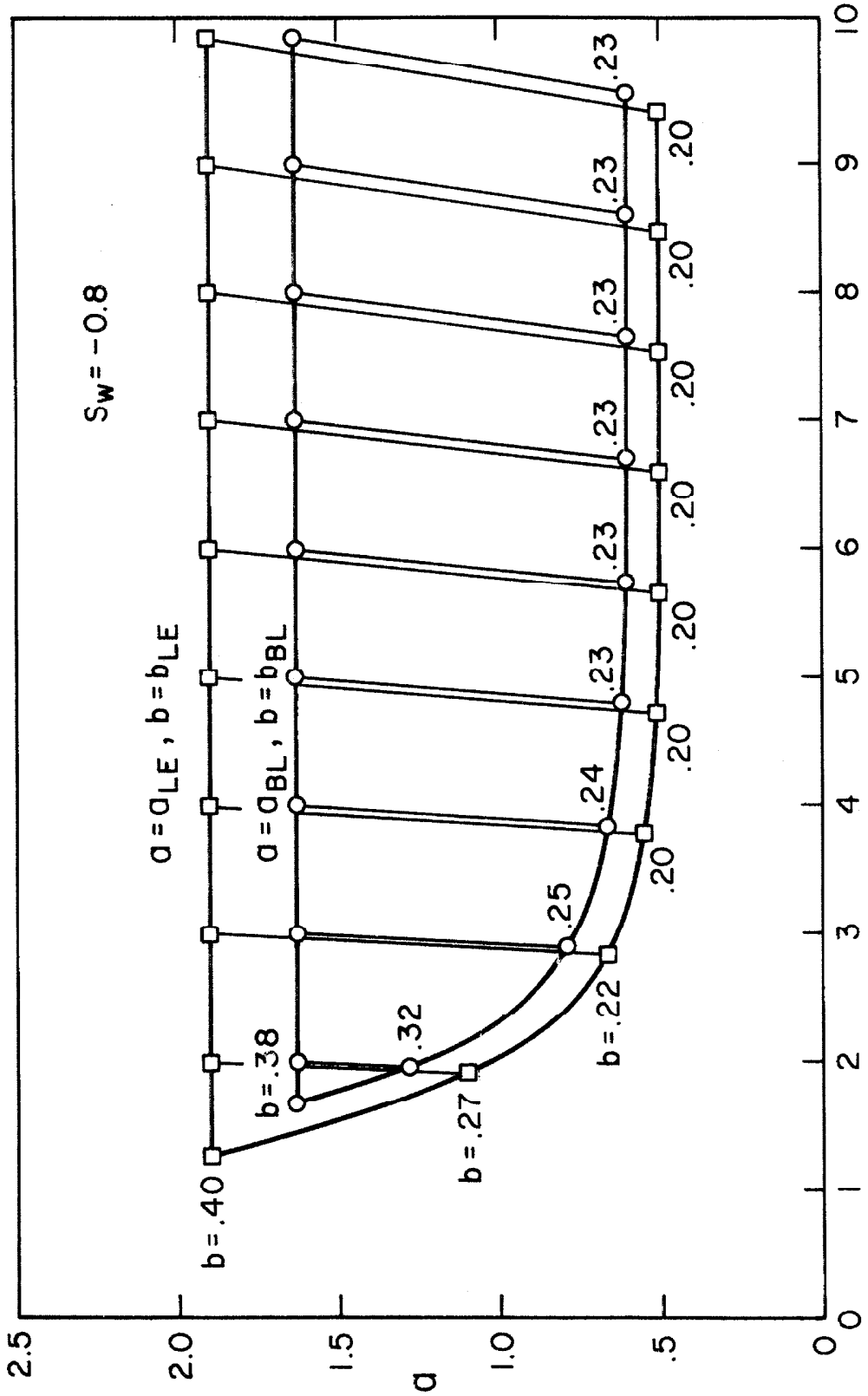

FIG.27 LOCUS OF JUMPS FROM BLASIUS AND LEADING-EDGE SOLUTIONS

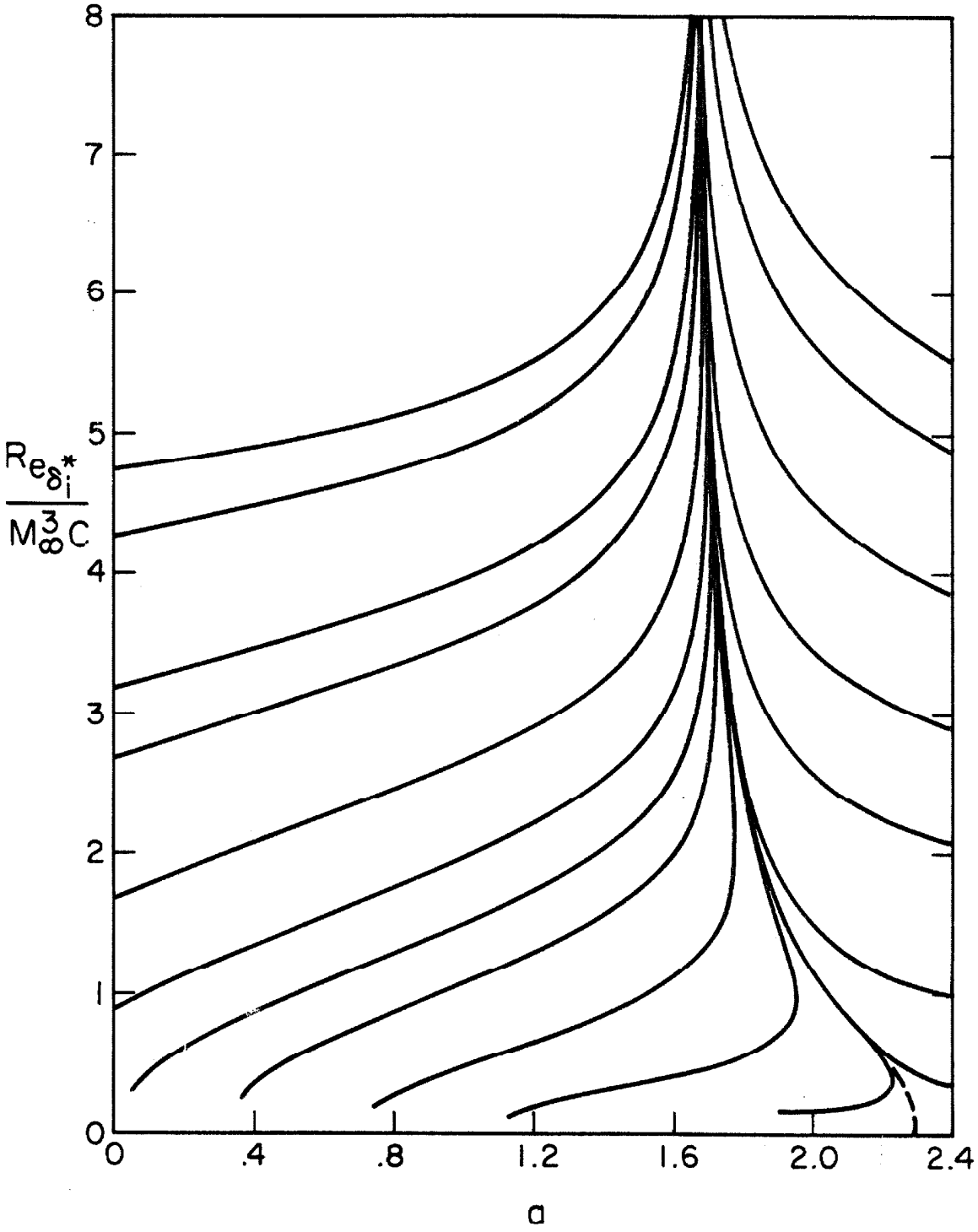

FIG. 28 RELAXATION SURFACE TRAJECTORIES

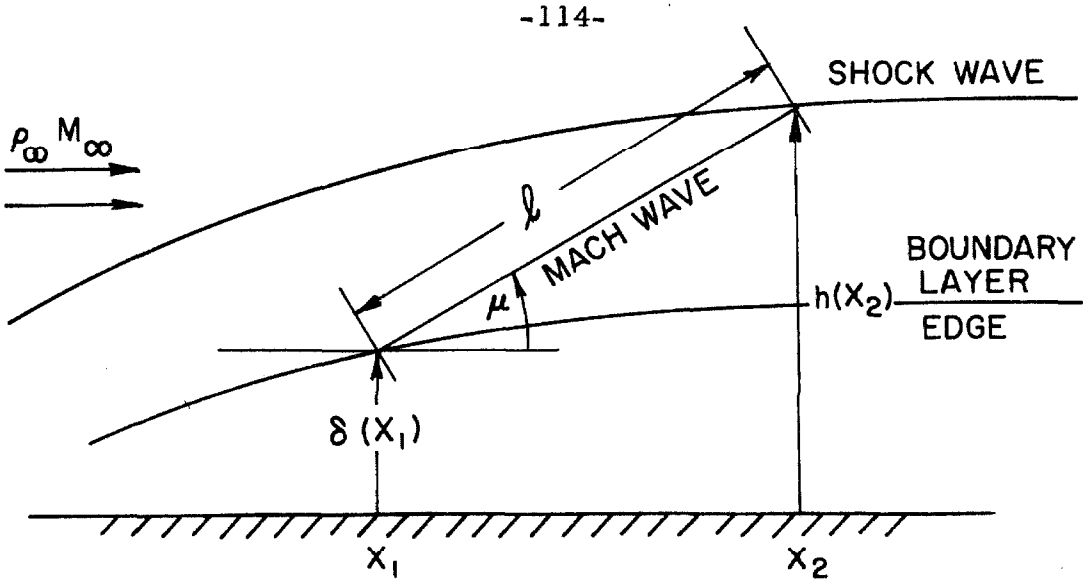

FIG. 29 a MODEL FOR SHOCK – SHAPE DETERMINATION

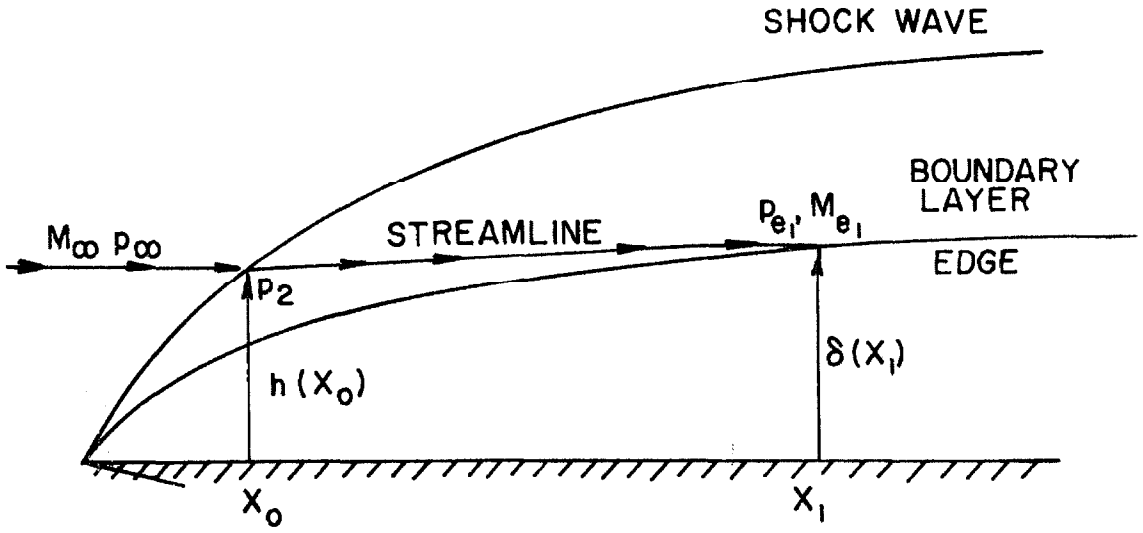

FIG. 29 b MODEL FOR MASS – FLOW BALANCE

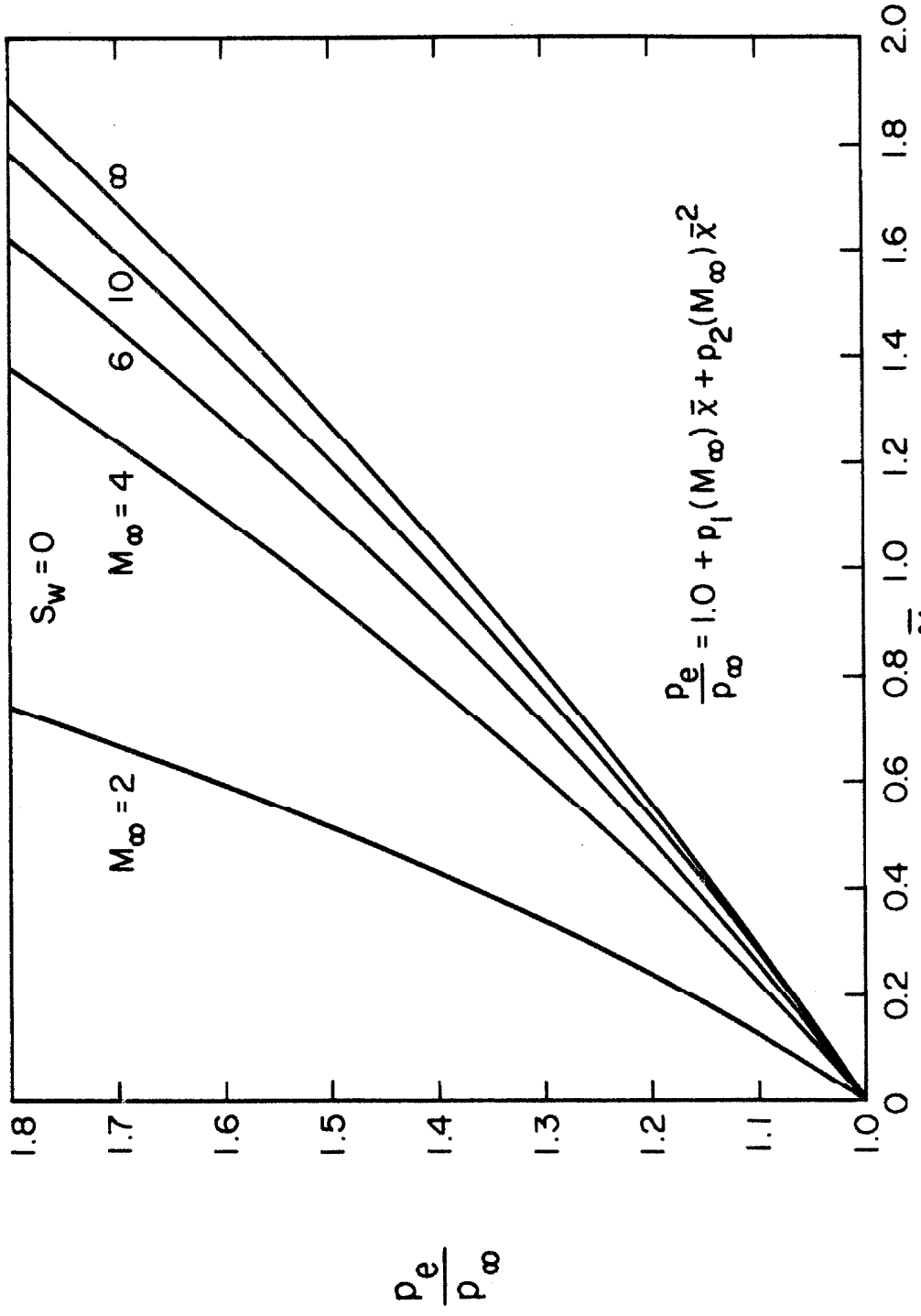

FIG. 30 EFFECT OF MACH NUMBER ON ADIABATIC WEAK-INTERACTION PRESSURE DISTRIBUTION.

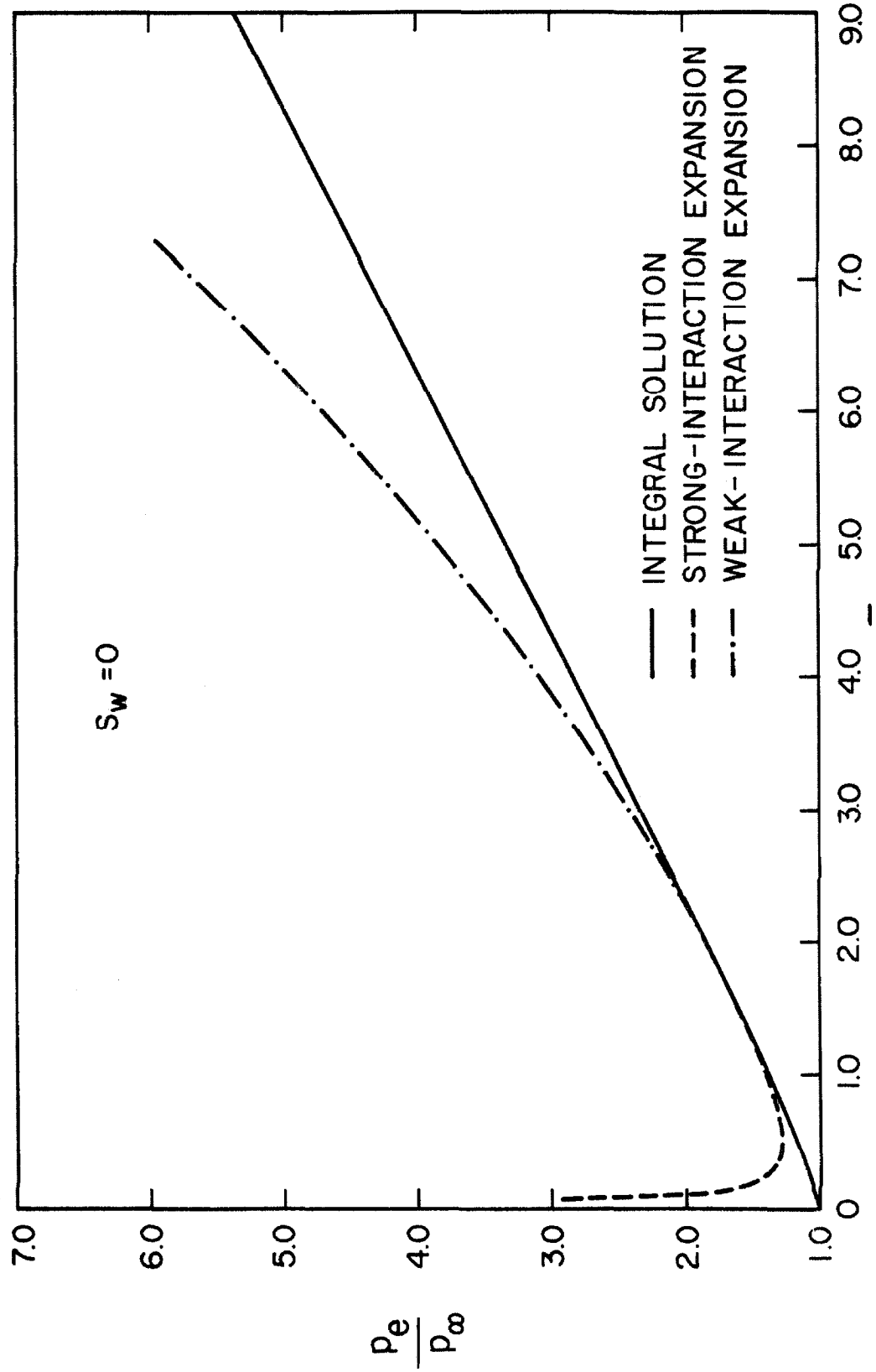

FIG. 31 HYPERSONIC FLAT-PLATE PRESSURE DISTRIBUTION FOR ADIABATIC FLOW.

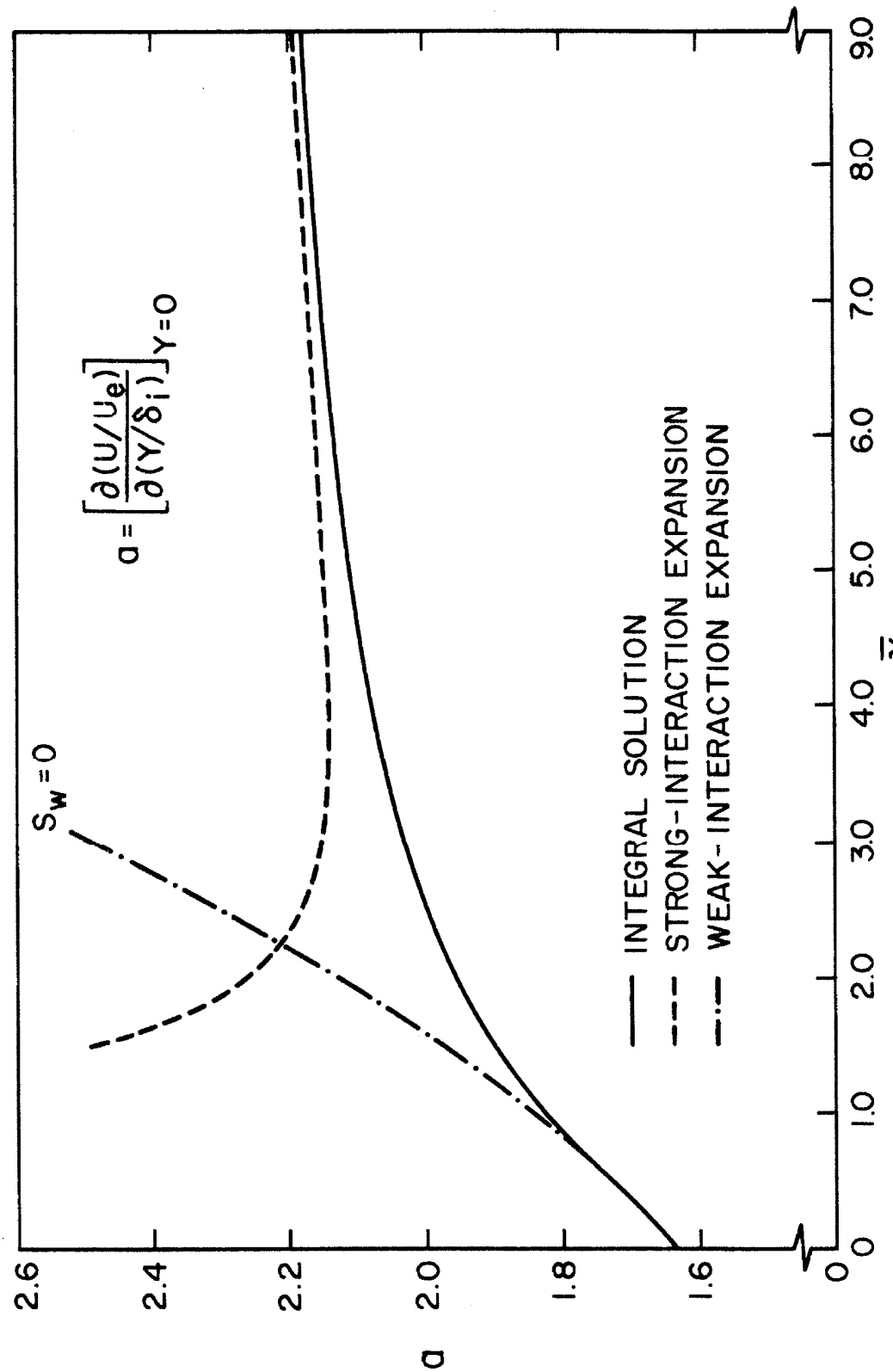

FIG. 32 HYPERSONIC FLAT-PLATE DISTRIBUTION OF a FOR ADIABATIC FLOW.

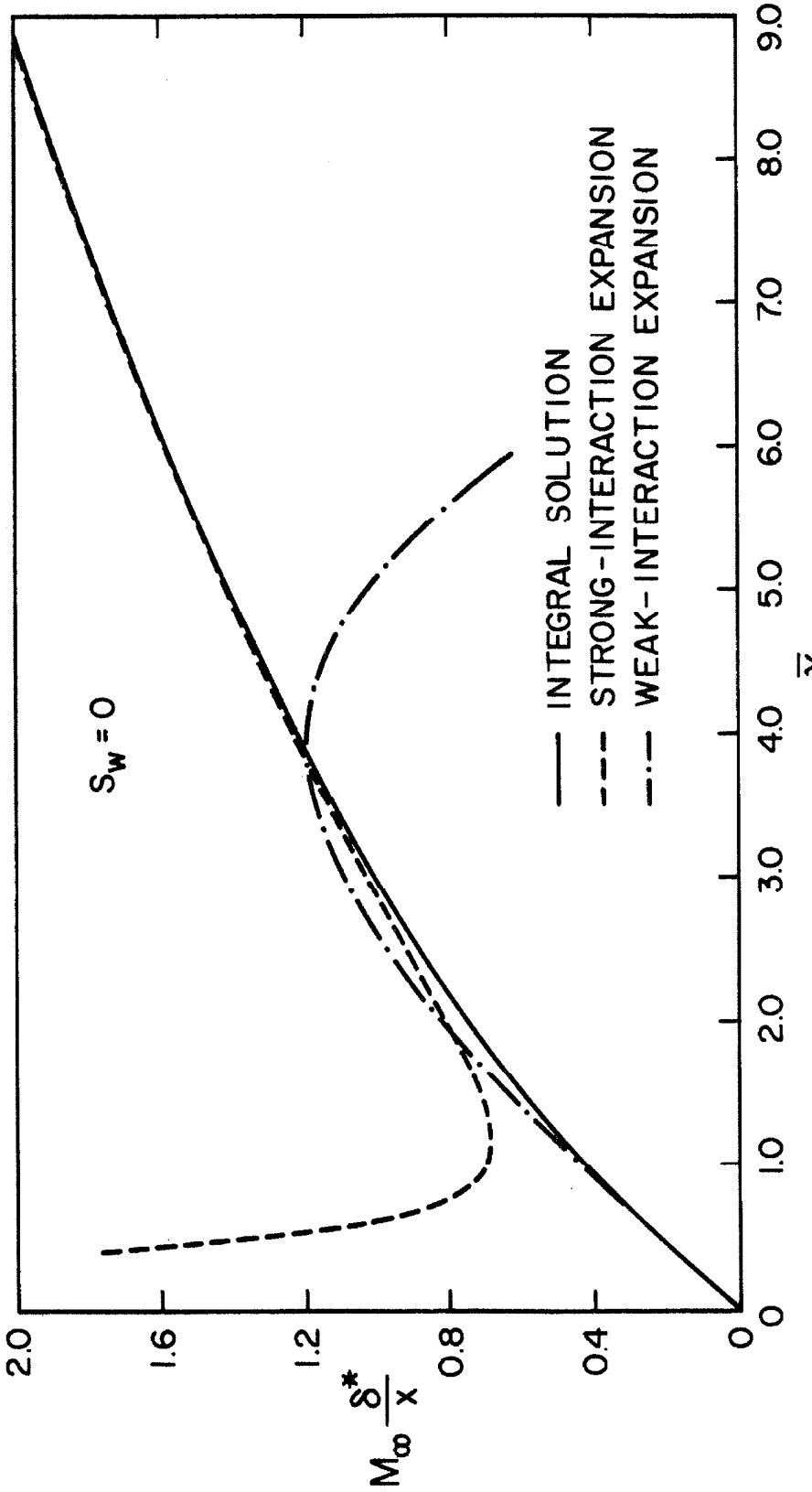

FIG. 33 HYPERSONIC FLAT-PLATE DISPLACEMENT-THICKNESS DISTRIBUTION FOR ADIABATIC FLOW.

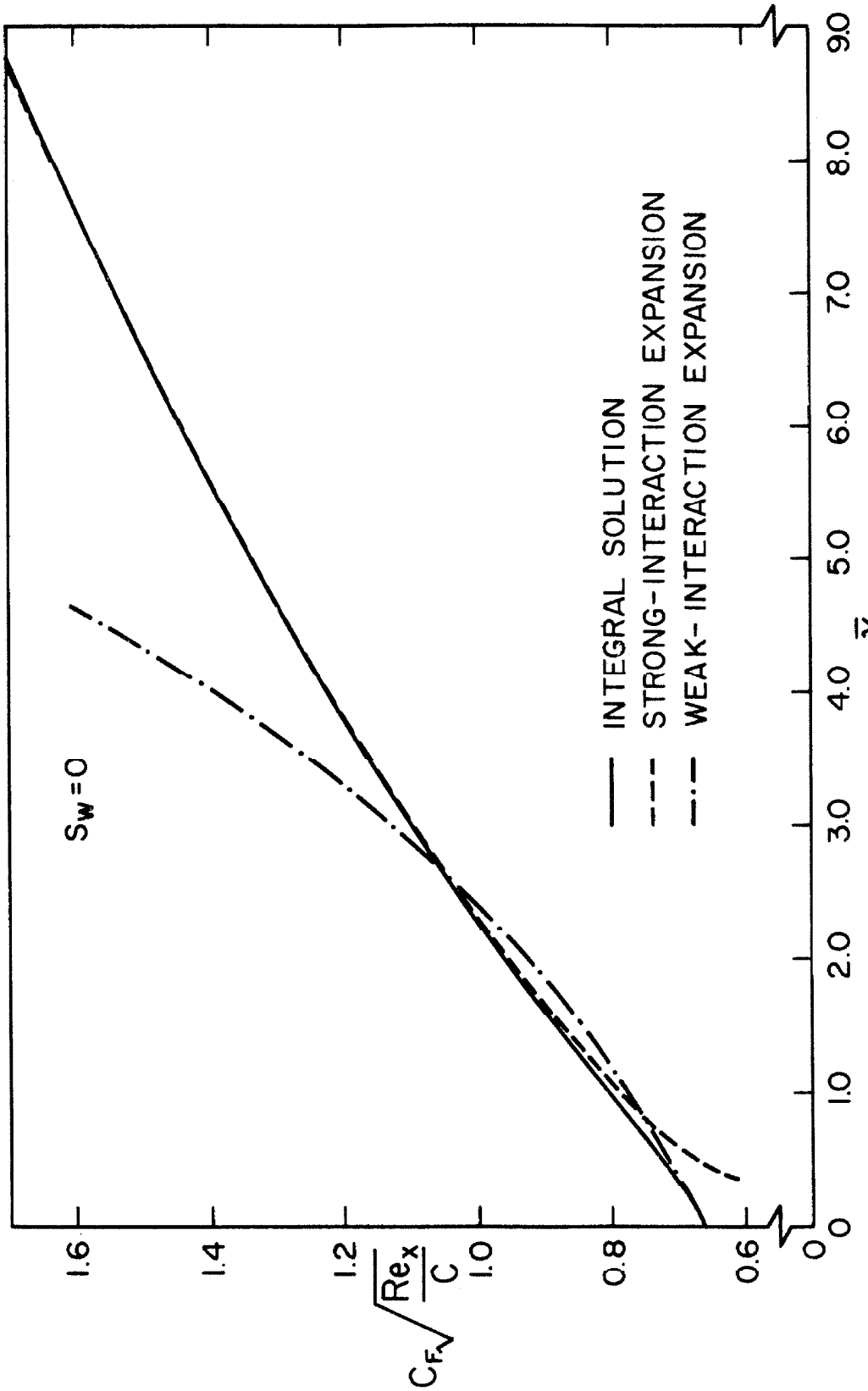

FIG. 34 HYPERSONIC FLAT-PLATE SKIN-FRICTION DISTRIBUTION FOR ADIABATIC FLOW.

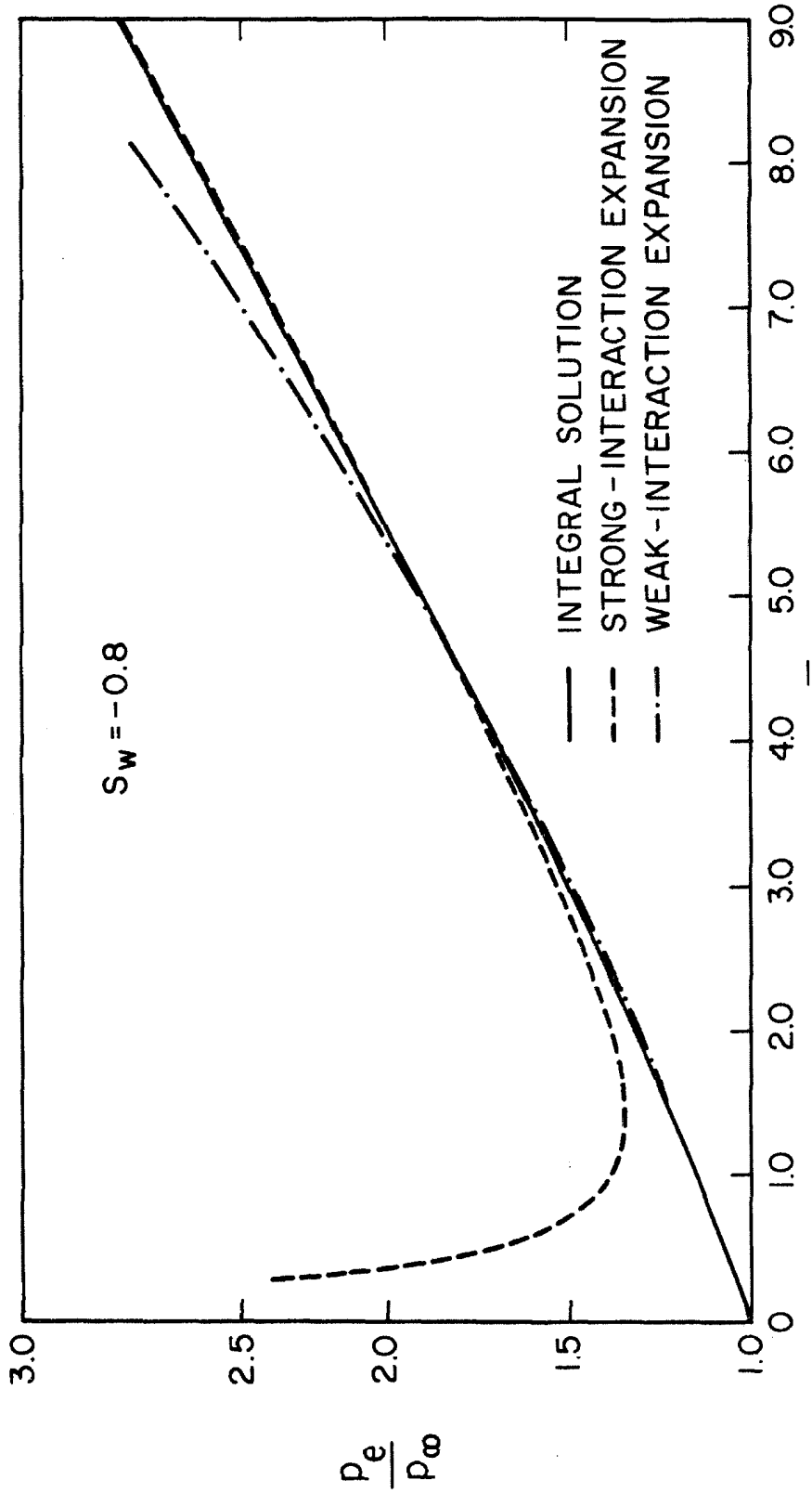

FIG. 35 HYPERSONIC FLAT-PLATE PRESSURE DISTRIBUTION FOR NON-ADIABATIC FLOW.

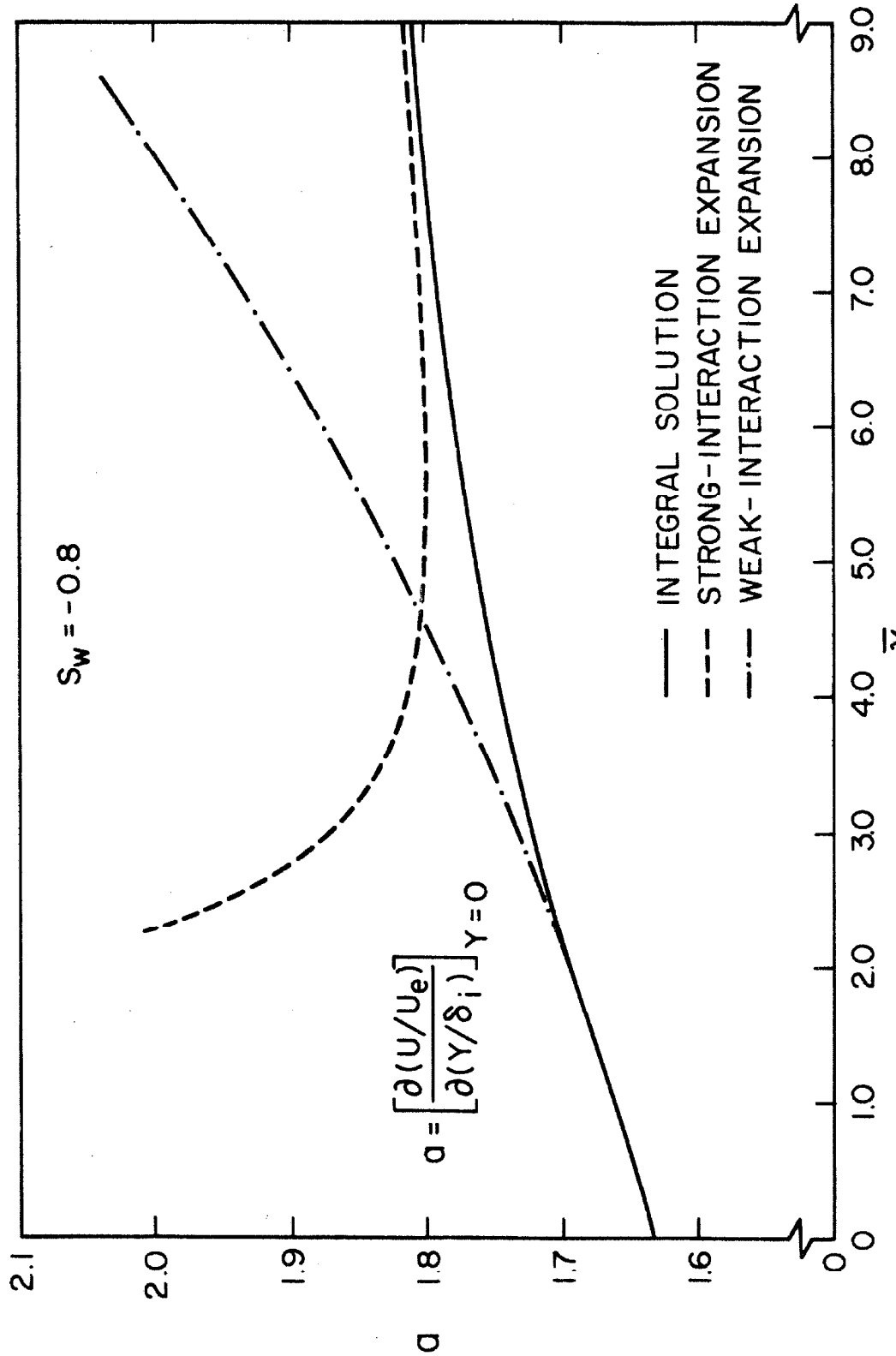

FIG. 36 HYPERSONIC FLAT-PLATE DISTRIBUTION OF a FOR NON-ADIABATIC FLOW.

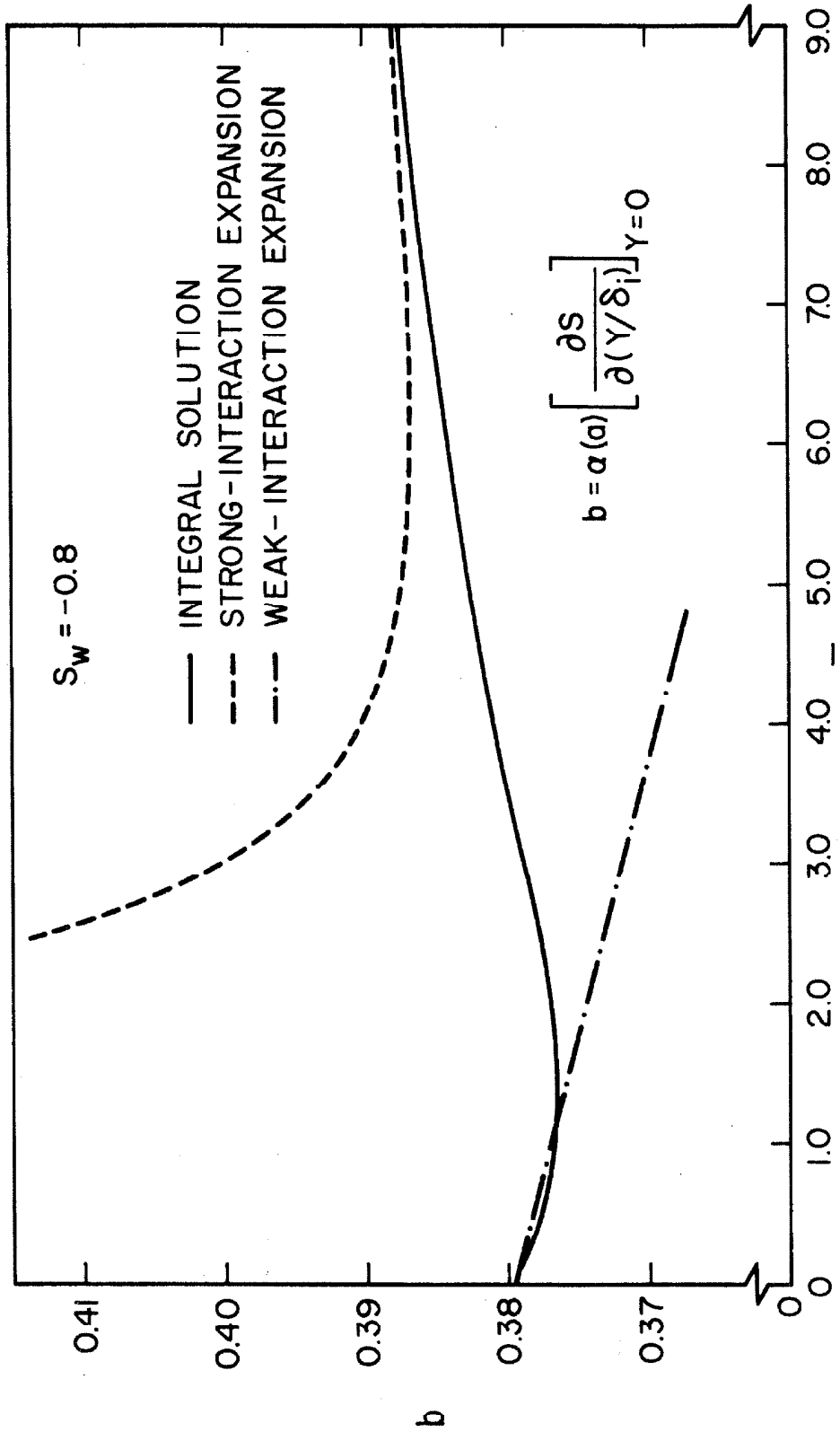

FIG. 37 HYPERSONIC FLAT-PLATE DISTRIBUTION OF b FOR NON-ADIABATIC FLOW.

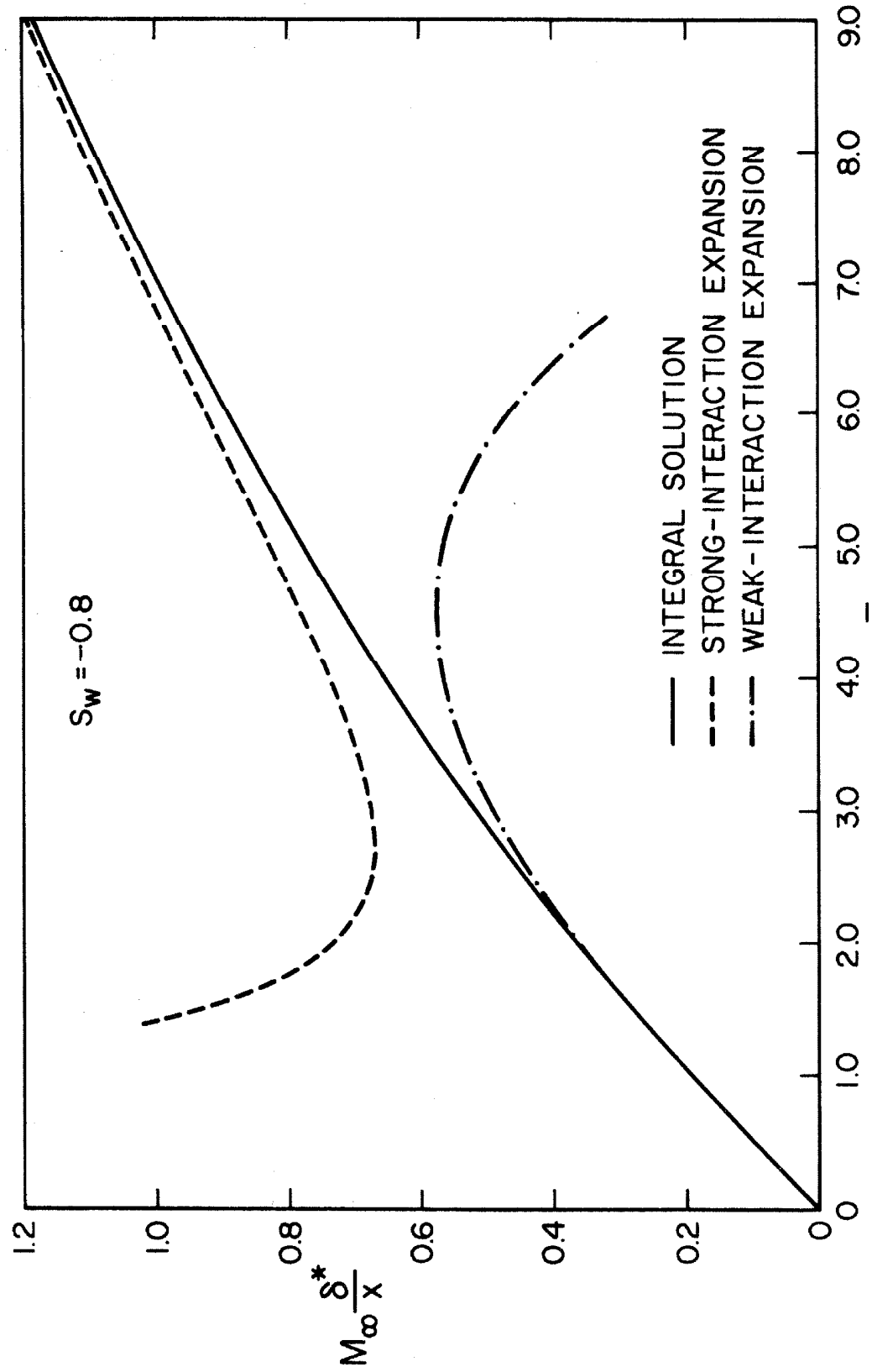

FIG. 38 HYPERSONIC FLAT-PLATE DISPLACEMENT-THICKNESS DISTRIBUTION FOR NON-ADIABATIC FLOW.

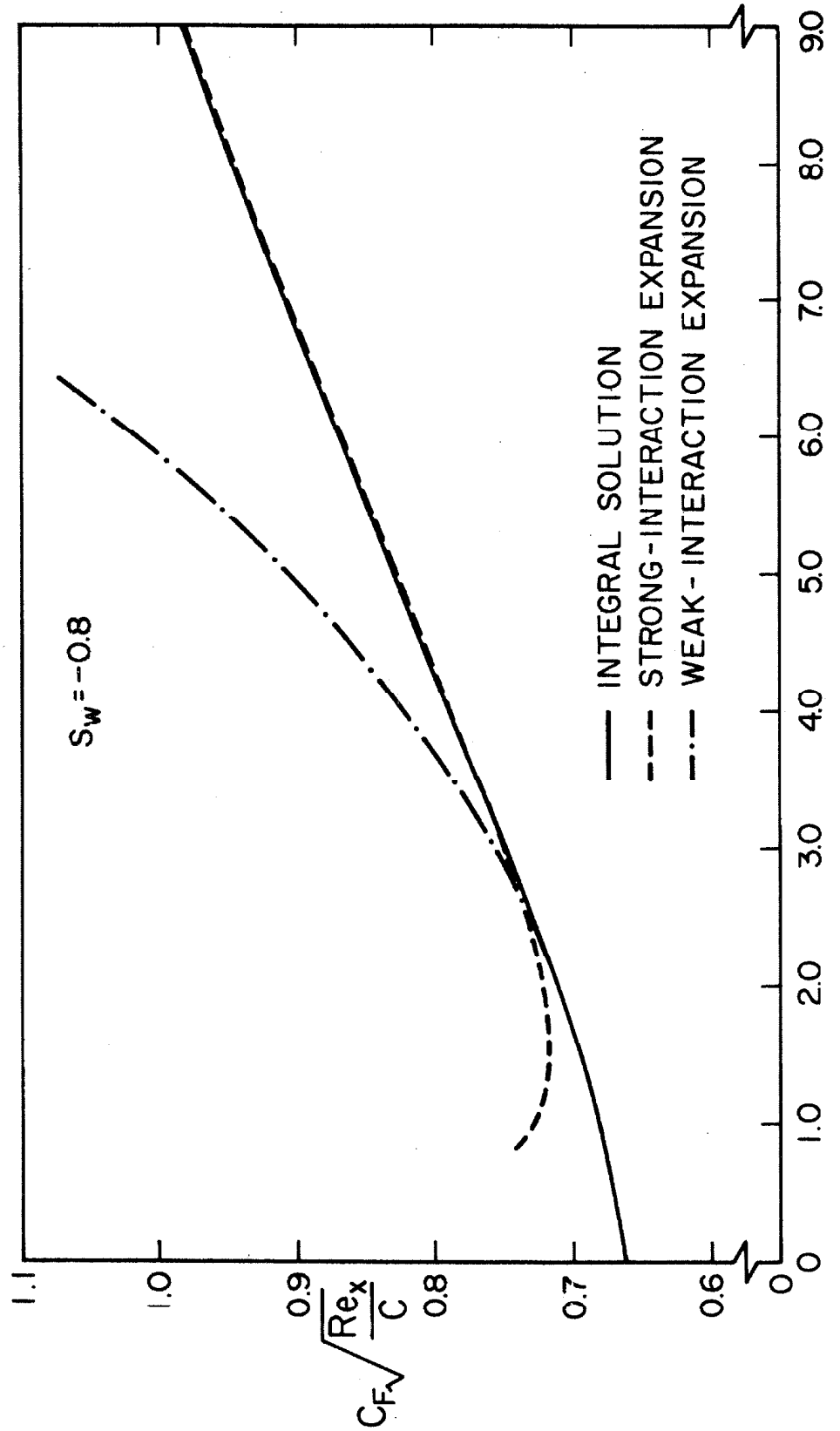

FIG. 39 HYPERSONIC FLAT-PLATE SKIN-FRICTION DISTRIBUTION FOR NON-ADIABATIC FLOW.

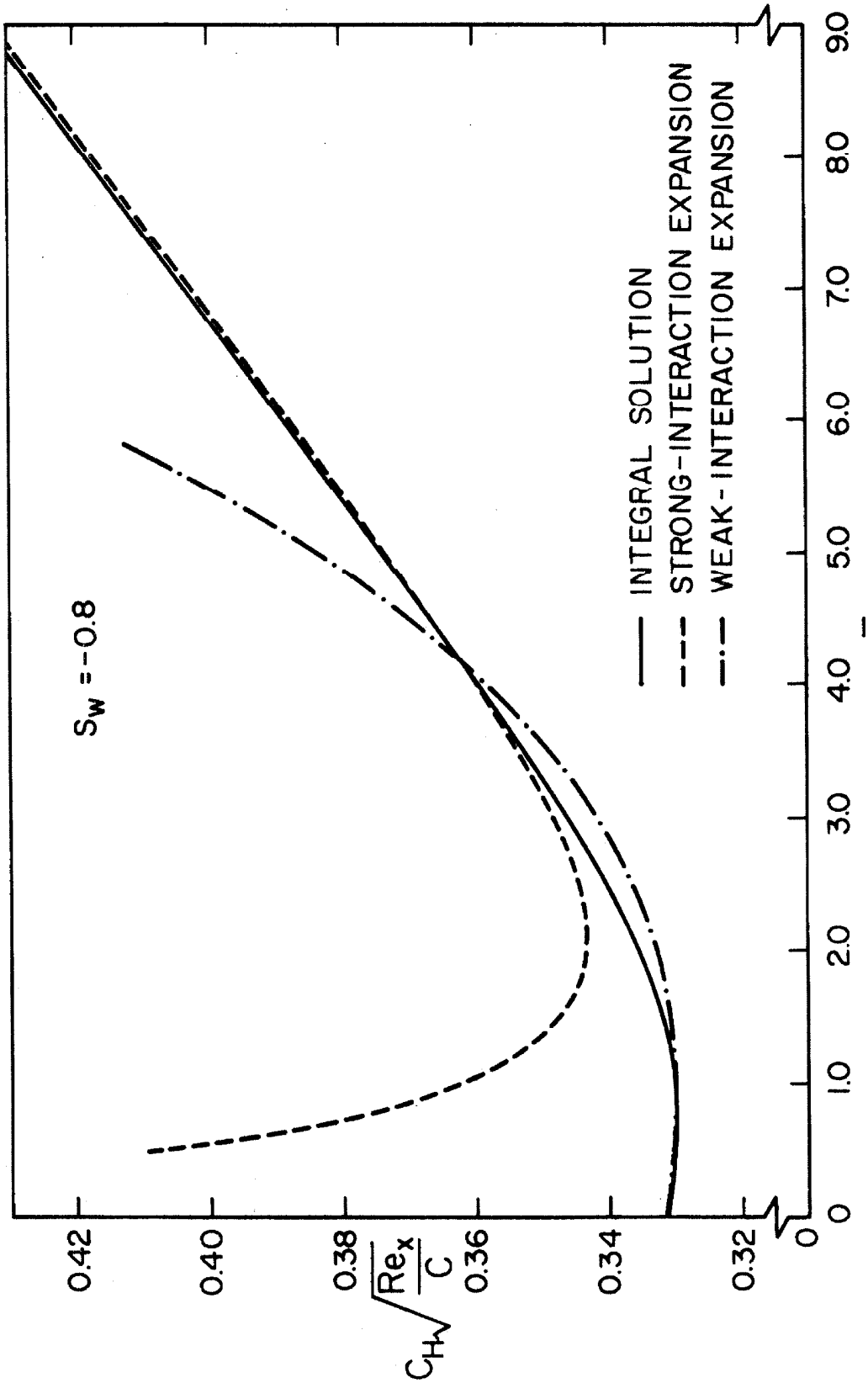

FIG. 40 HYPERSONIC FLAT-PLATE HEAT-TRANSFER DISTRIBUTION FOR NON-ADIABATIC FLOW.

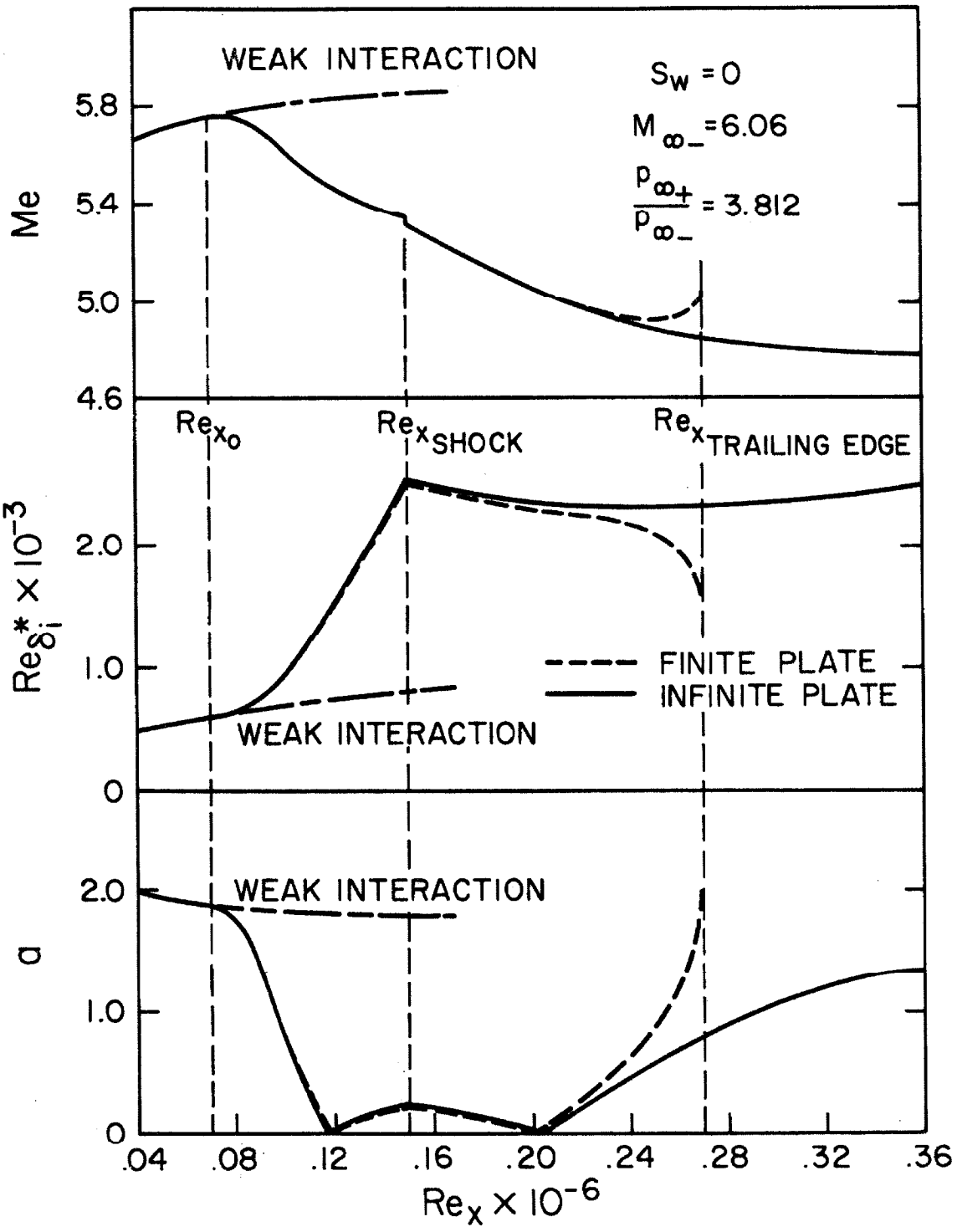

FIG. 41 TRAJECTORIES FOR ADIABATIC BOUNDARY-LAYER/ SHOCK-WAVE INTERACTION (M_e, $Re^*_{\delta_i}$ AND a)

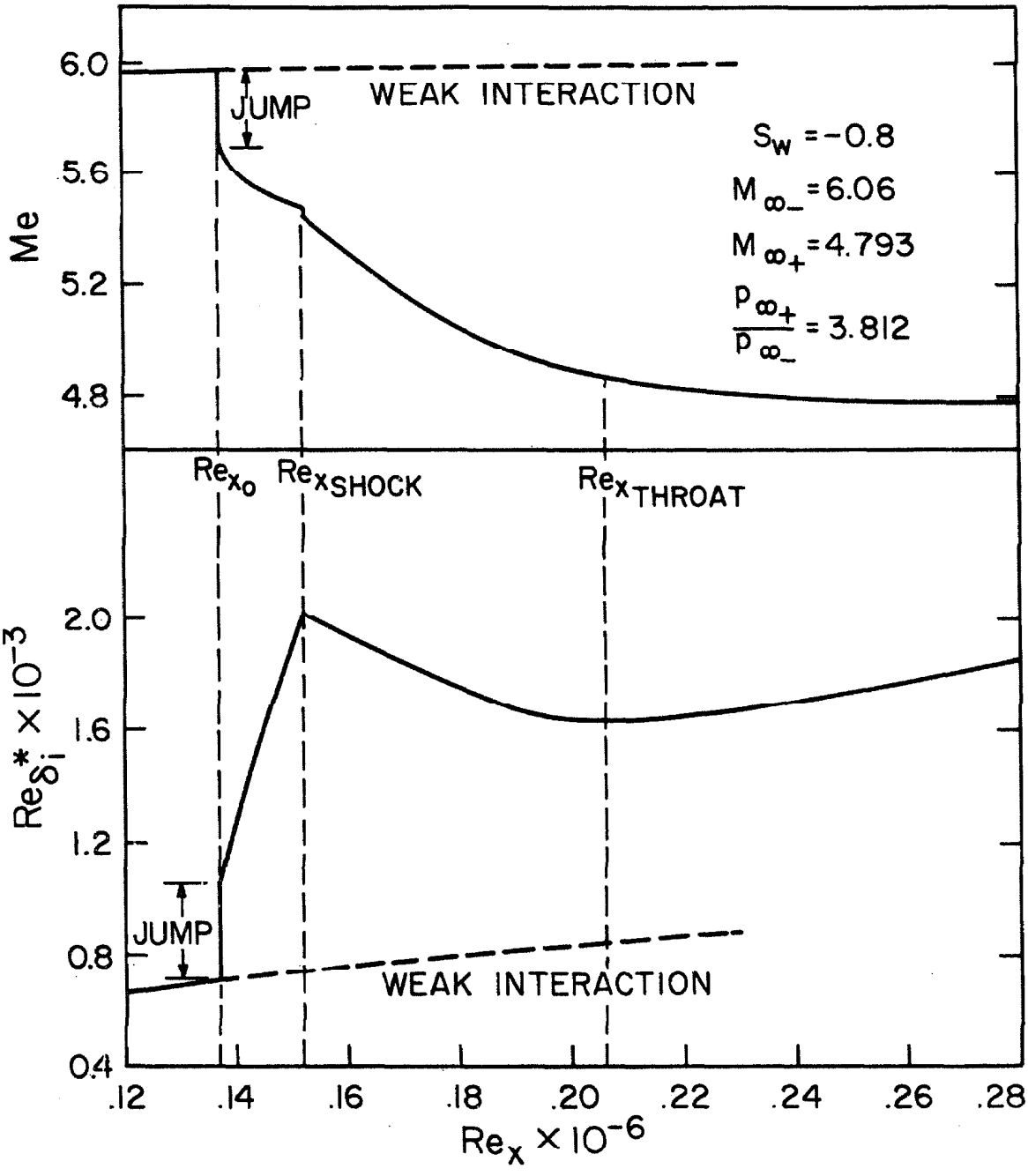

FIG. 42a TRAJECTORIES FOR NON-ADIABATIC BOUNDARY-LAYER/SHOCK-WAVE INTERACTION (M_e AND $Re^*_{\delta_i}$)

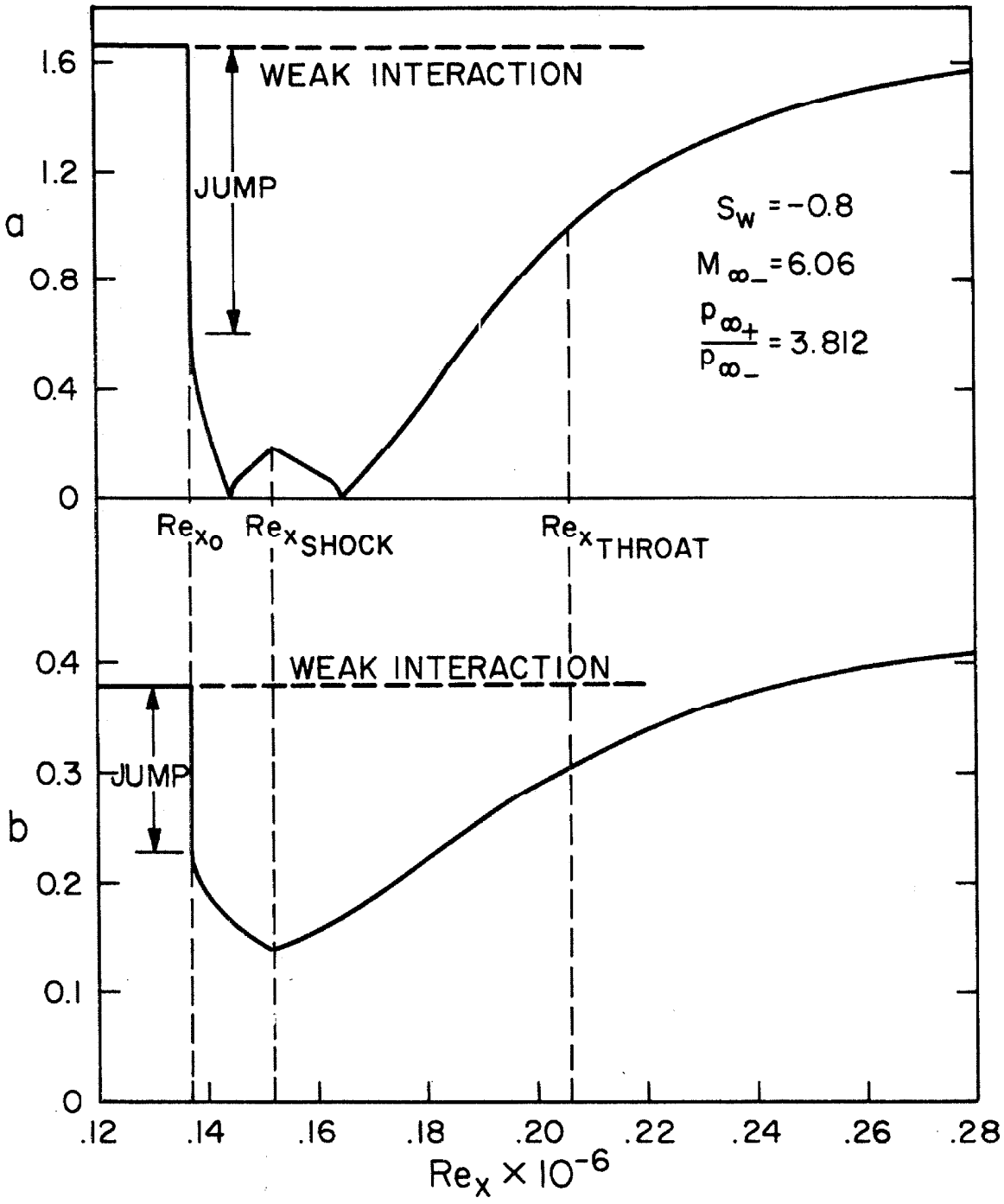

FIG. 42b TRAJECTORIES FOR NON-ADIABATIC BOUNDARY-LAYER/SHOCK-WAVE INTERACTION (a AND b)

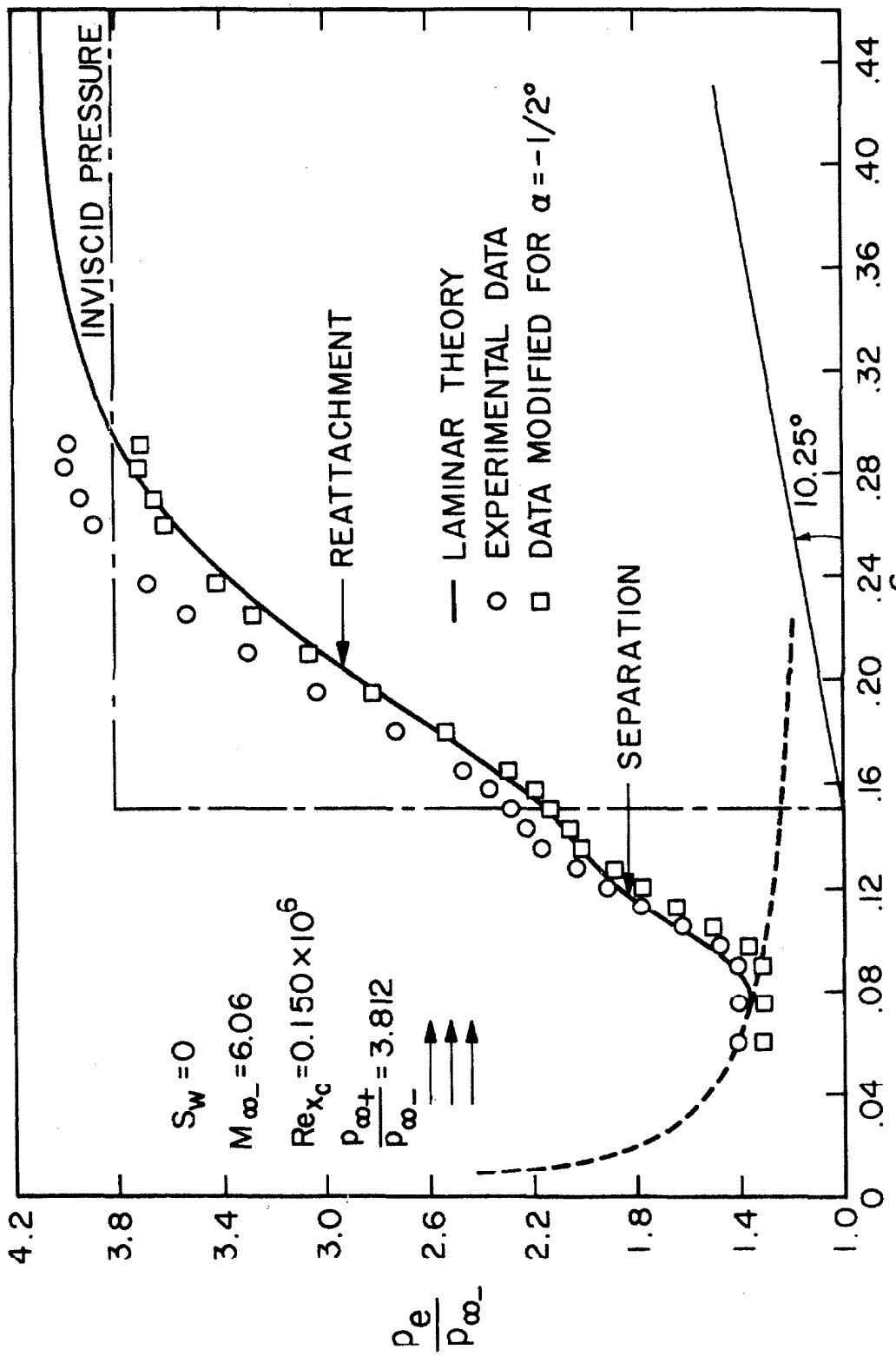

FIG. 43 EXPERIMENTAL AND THEORETICAL PRESSURE DISTRIBUTIONS FOR ADIABATIC FLOW.

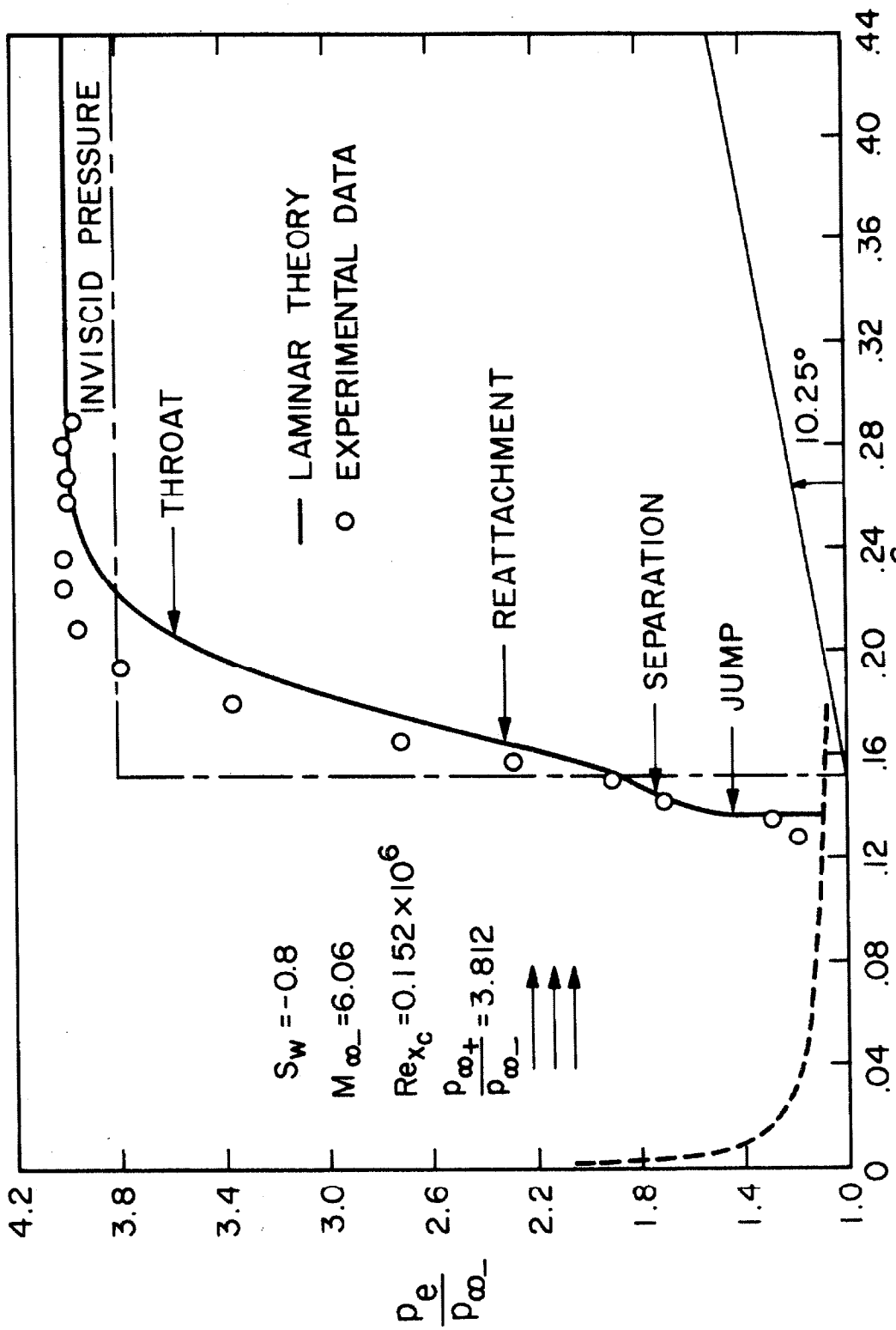

FIG. 44 EXPERIMENTAL AND THEORETICAL PRESSURE DISTRIBUTIONS FOR NON-ADIABATIC FLOW.

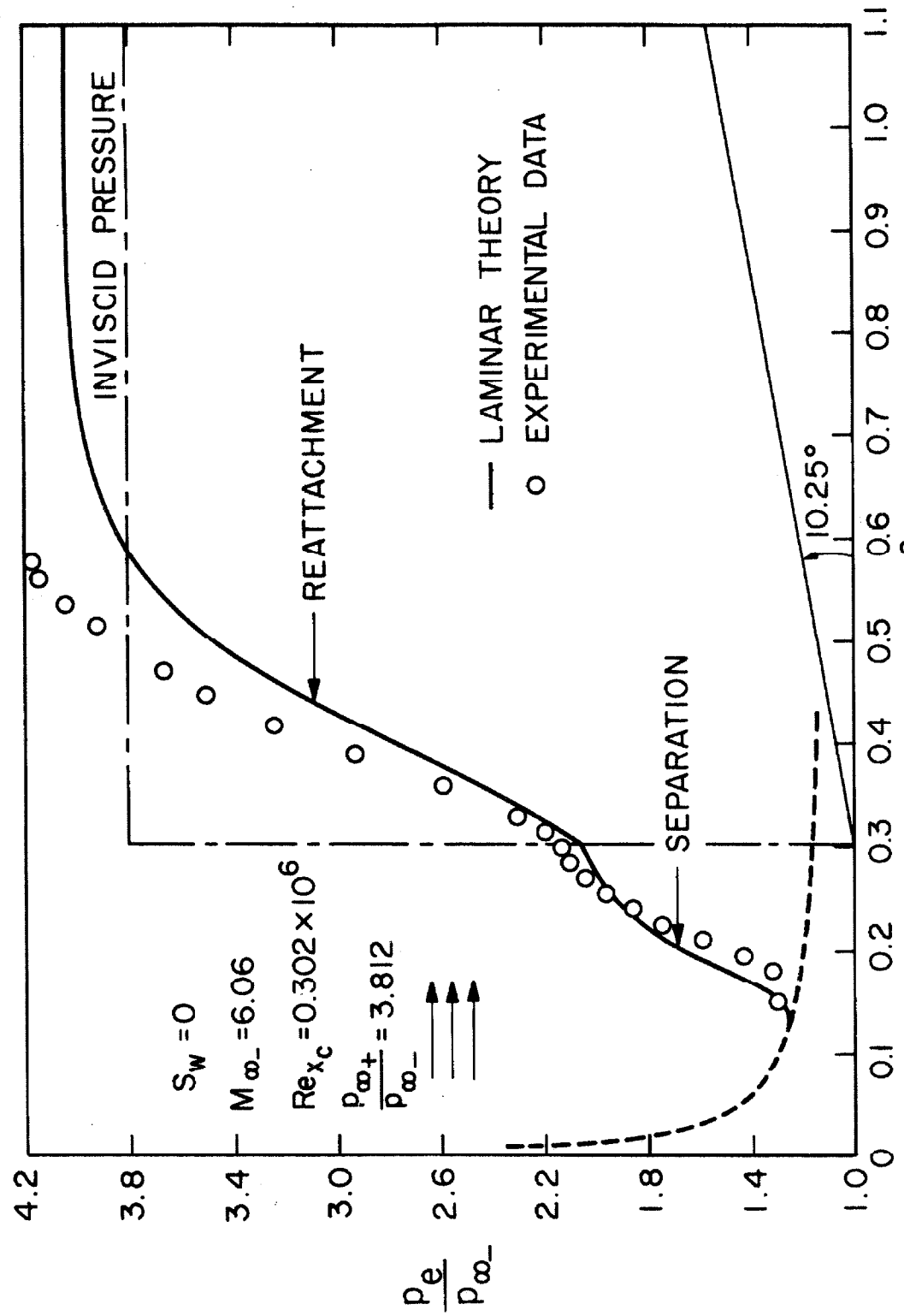

FIG. 45 EXPERIMENTAL AND THEORETICAL PRESSURE DISTRIBUTIONS FOR ADIABATIC FLOW.

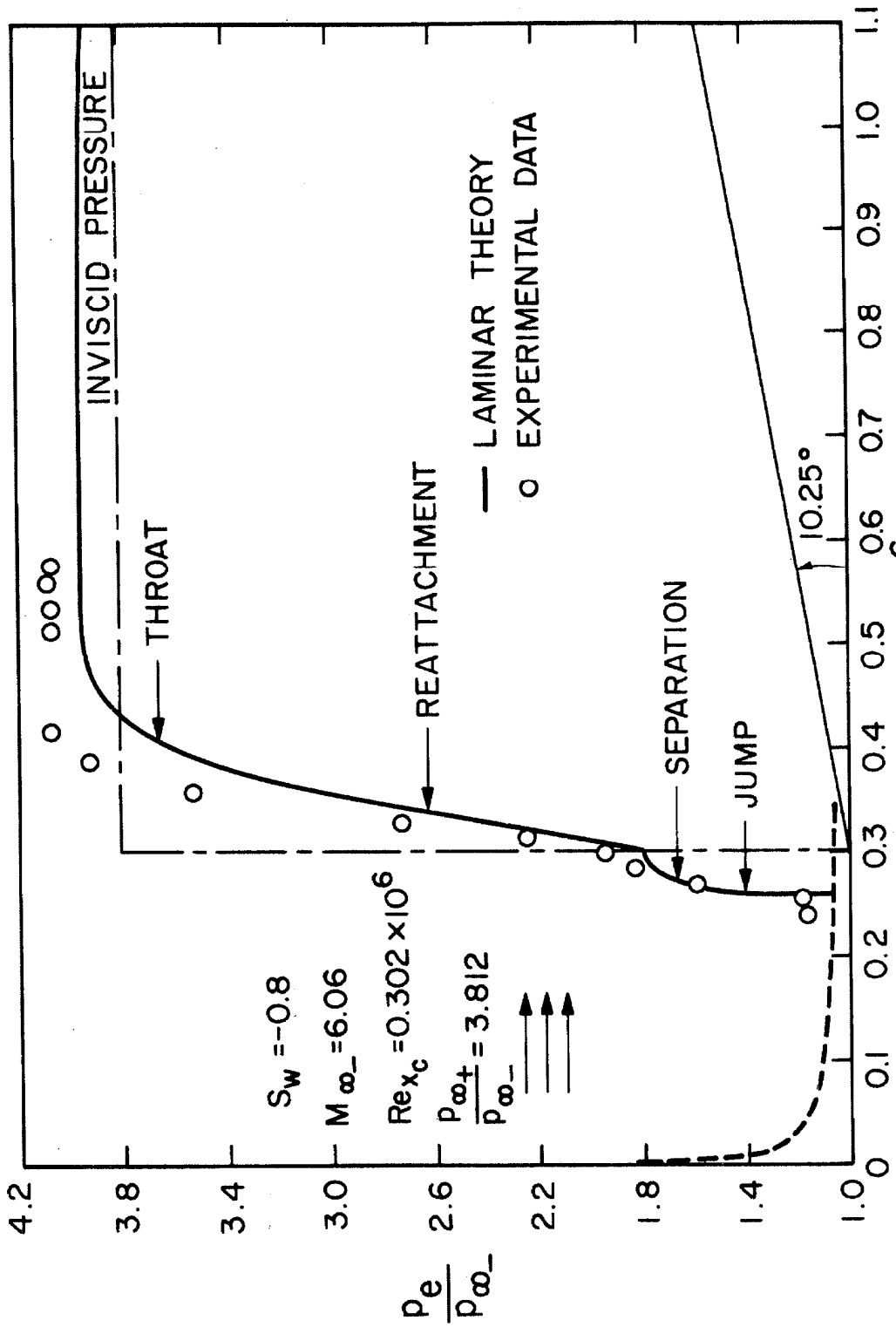

FIG. 46 EXPERIMENTAL AND THEORETICAL PRESSURE DISTRIBUTIONS FOR NON-ADIABATIC FLOW.

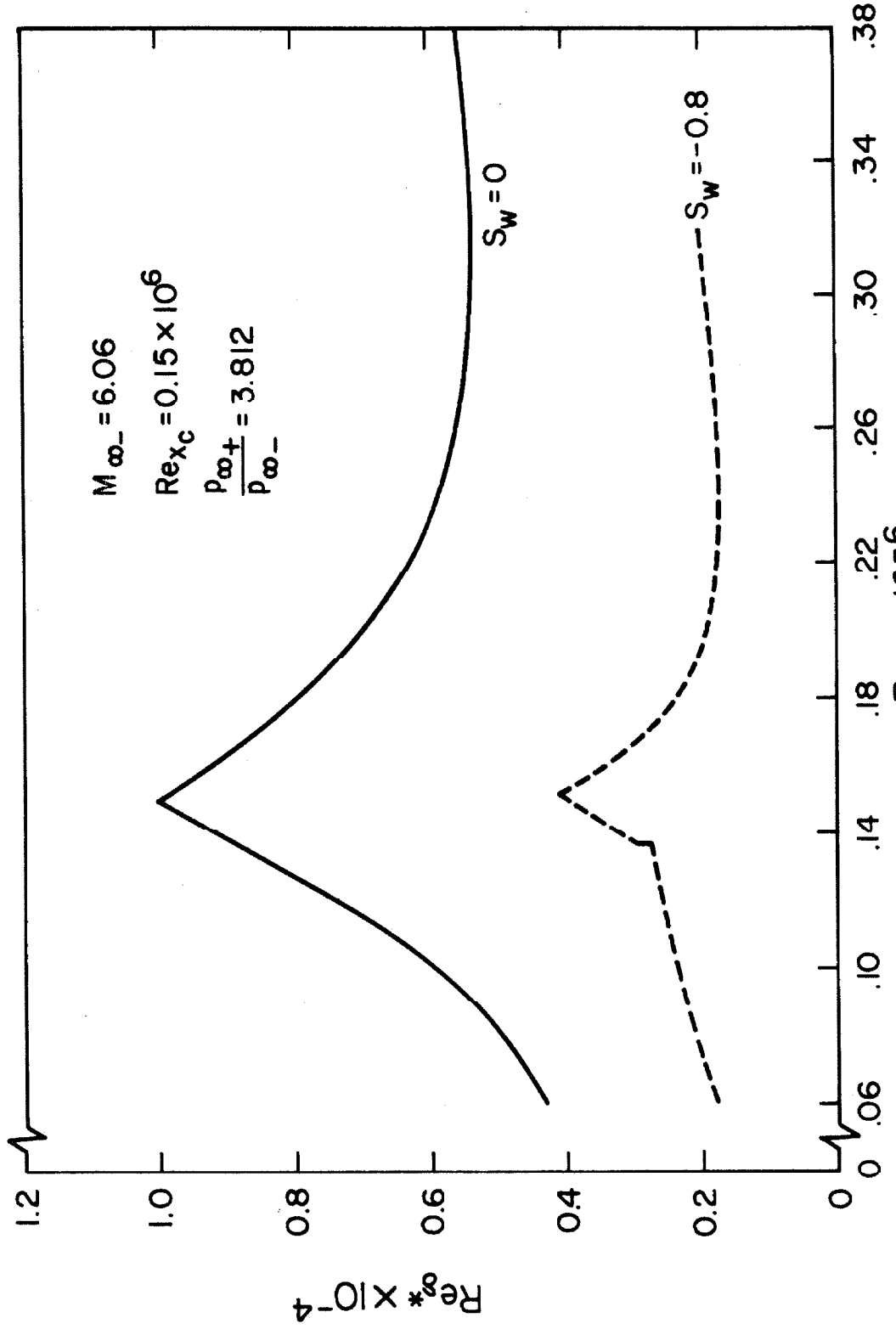

FIG. 47 EFFECT OF SURFACE COOLING ON BOUNDARY-LAYER/SHOCK-WAVE INTERACTIONS (DISPLACEMENT-THICKNESS DISTRIBUTIONS)

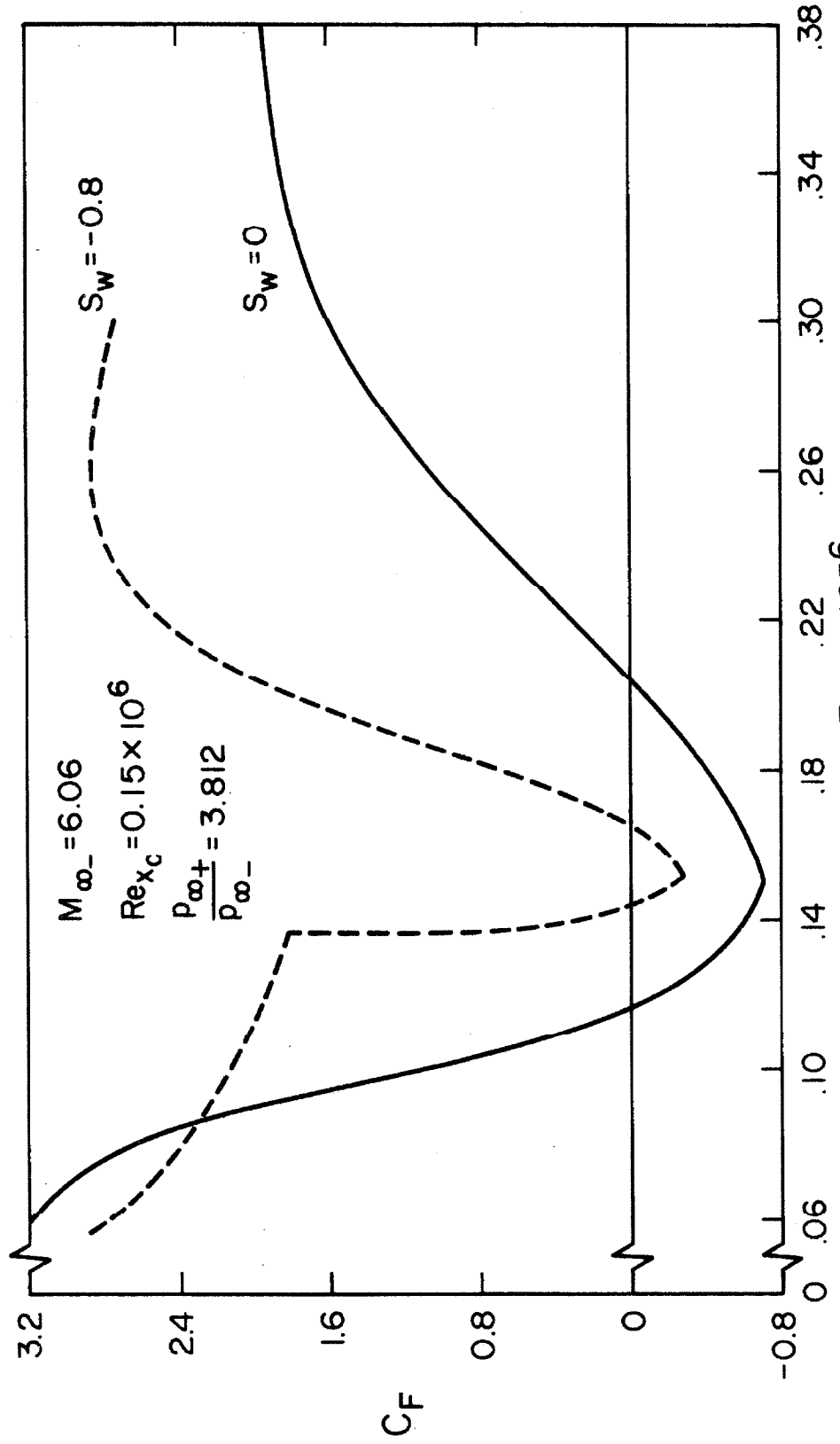

FIG. 48 EFFECT OF SURFACE COOLING ON BOUNDARY-LAYER/SHOCK-WAVE INTERACTIONS (SKIN-FRICTION DISTRIBUTIONS)

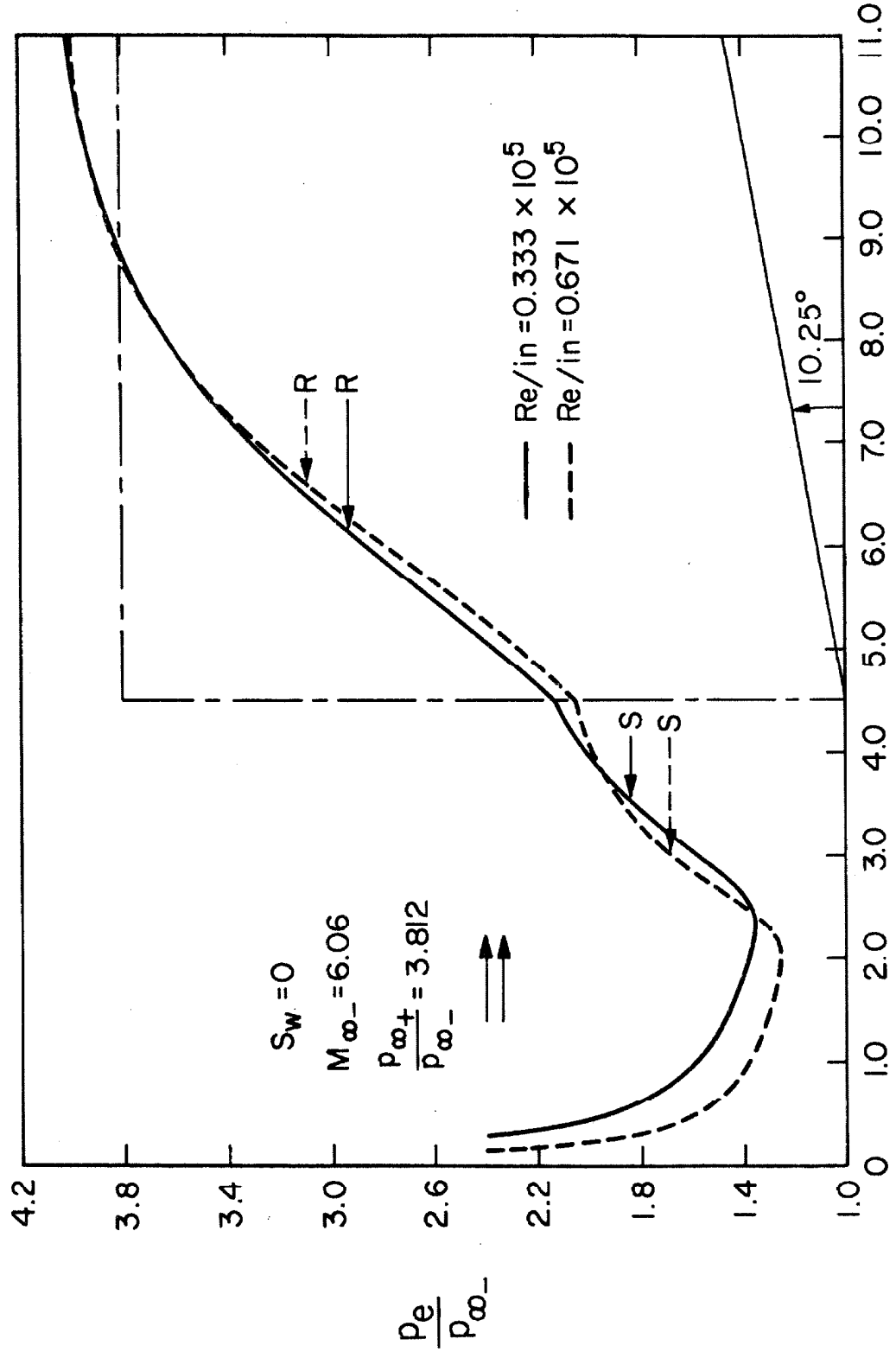

FIG. 49 EFFECT OF UNIT REYNOLDS NUMBER FOR ADIABATIC FLOW (PRESSURE DISTRIBUTIONS)

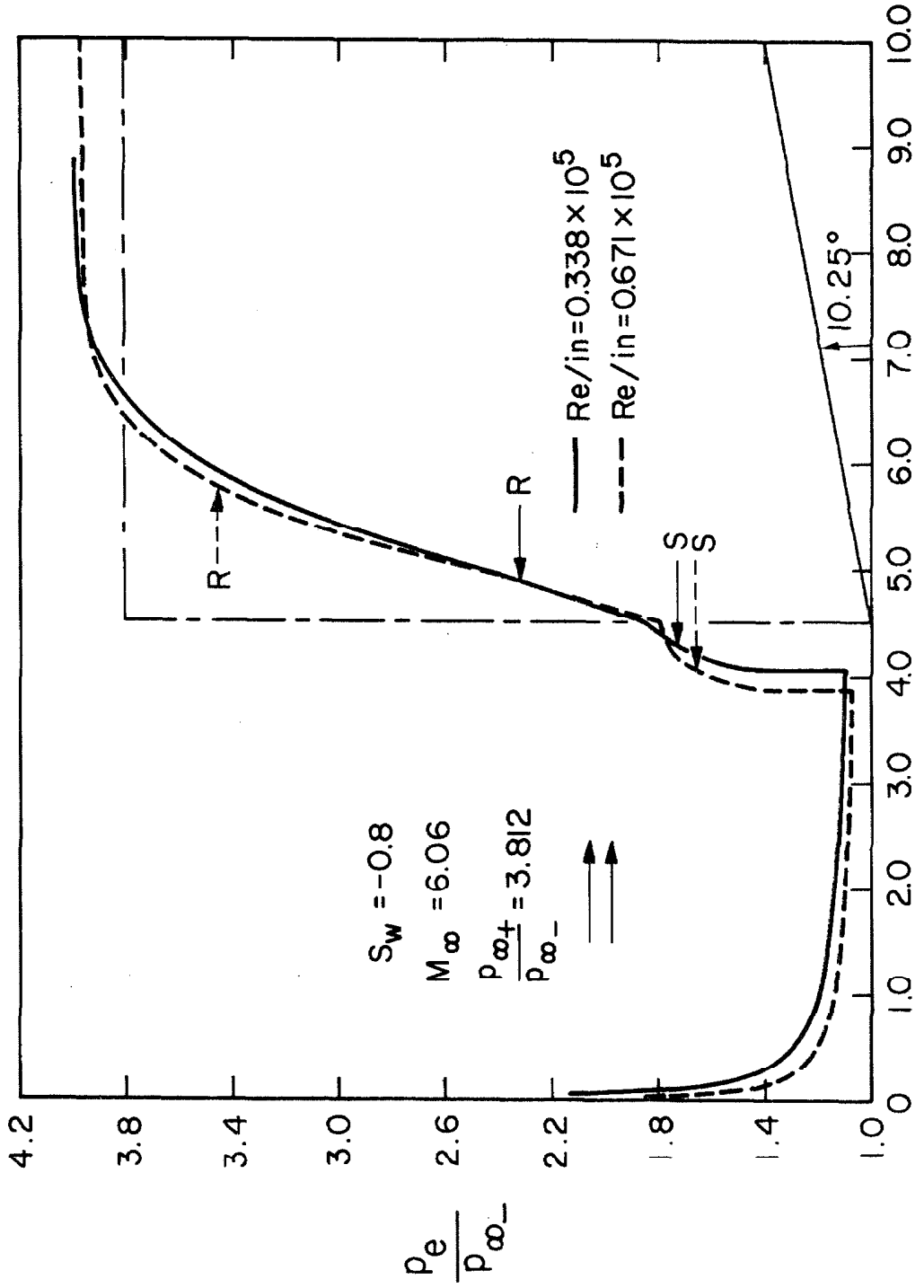

FIG. 50 EFFECT OF UNIT REYNOLDS NUMBER FOR NON-ADIABATIC FLOW (PRESSURE DISTRIBUTIONS)

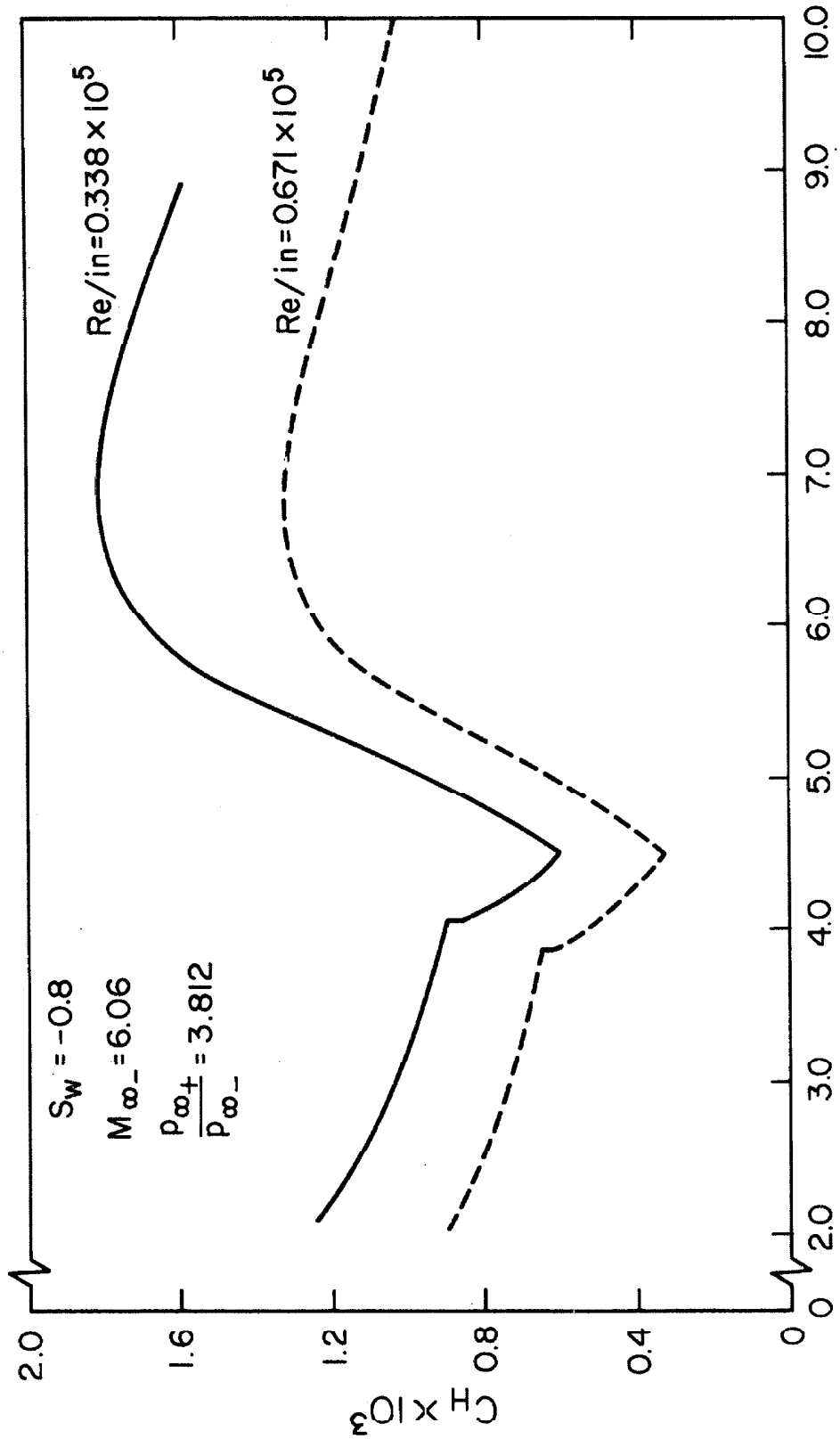

FIG. 51 EFFECT OF UNIT REYNOLDS NUMBER FOR NON-ADIABATIC FLOW (HEAT-TRANSFER DISTRIBUTIONS)

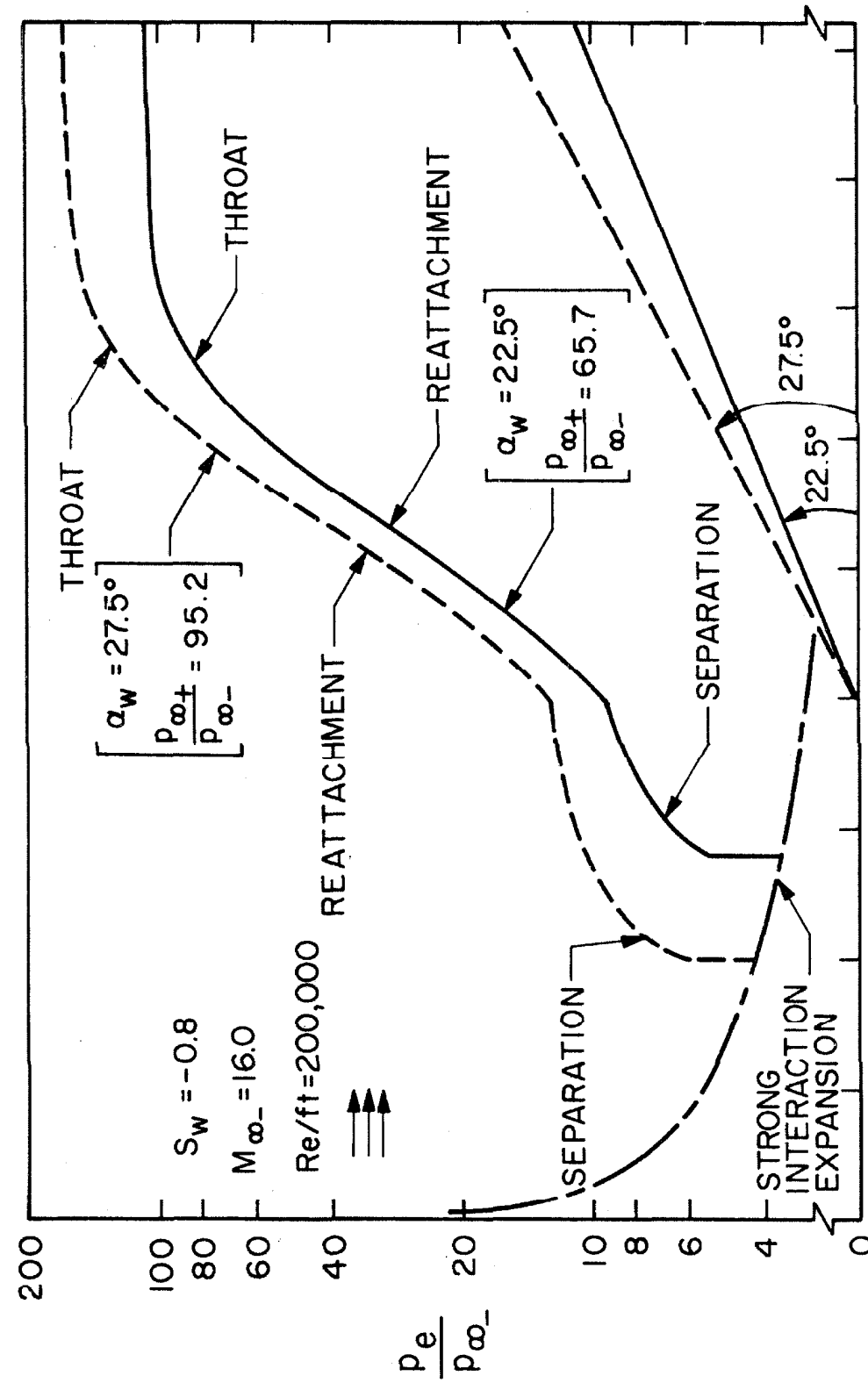

FIG. 52 EFFECT OF STRENGTH OF DISTURBANCE IN NON-ADIABATIC FLOW (PRESSURE DISTRIBUTIONS)

APPENDIX A

THE SOLUTION OF THE COHEN-RESHOTKO EQUATIONS*

A. 1. Differential Equations and Boundary Conditions

The compressible flow analog of the Falkner-Skan equation for Prandtl number $P_r = 1$ and constant wall enthalpy ratio $\frac{h_{o_w}}{h_{o_e}} = g_w$ is given by the system of ordinary equations:

$$\begin{aligned} f_{\eta\eta\eta} + ff_{\eta\eta} + \beta(g - f_\eta^2) &= 0 \\ g_{\eta\eta} + fg_\eta &= 0 \end{aligned} \tag{A1}$$

subject to the boundary conditions

$$f(0) = f_\eta(0) = 0$$

$$\lim_{\eta\to\infty} f_\eta = 1$$

and

$$g(0) = g_w$$

$$\lim_{\eta\to\infty} g = 1$$

A. 2. Numerical Analysis

The basic equations, Eqs. (A1), can be transformed into a system of first-order differential equations:

$$\begin{aligned} f_\eta &= u \\ u_\eta &= v \\ v_\eta &= -fv + \beta(u^2 - g) \\ g_\eta &= w \\ w_\eta &= -fw \end{aligned} \tag{A3}$$

---

* The author is indebted to Mr. Harvey Buss, now Staff Scientist, Avco Corp., Wilmington, Mass., for his invaluable assistance in the solution of this problem.

The problem of solving Eqs. (A1) with boundary conditions given by Eqs. (A2) can thus be regarded as the initial-value problem of determining the quantities $v(0) = f_{\eta\eta}(0)$ and $w(0) = g_{\eta}(0)$ such that $u(\eta)$ and $g(\eta) \to 1$ as $\eta \to \infty$.

Denoting the values of u and g as $\eta \to \infty$ as u_∞ and g_∞, respectively, these quantities can be regarded as functions of the initial values $v(0) = v_o$ and $w(0) = w_o$. A solution of the following set of equations is therefore required:

$$\begin{aligned} u_\infty(v_o, w_o) - 1 &= 0 \\ g_\infty(v_o, w_o) - 1 &= 0 \end{aligned} \tag{A4}$$

In general, these relations will not be satisfied by an arbitrary choice of initial values, and it will be necessary to modify v_o and w_o to obtain the solution. If the changes δv_o and δw_o in these quantities are small, the new values of u_∞ and g_∞ are given by the first-order approximations:

$$u_\infty(v_o+\delta v_o,\ w_o+\delta w_o) = u_\infty(v_o, w_o) + \delta v_o \frac{\partial u_\infty}{\partial v_o} + \delta w_o \frac{\partial u_\infty}{\partial w_o}$$

$$g_\infty(v_o+\delta v_o, w_o+\delta w_o) = g_\infty(v_o, w_o) + \delta v_o \frac{\partial g_\infty}{\partial v_o} + \delta w_o \frac{\partial g_\infty}{\partial w_o}$$

If these quantities are to satisfy Eqs. (A4), the changes in the initial values δv_o and δw_o must be selected such that:

$$\begin{aligned} \frac{\partial u_\infty}{\partial u_o} \delta v_o + \frac{\partial u_\infty}{\partial w_o} \delta w_o &= 1 - u_\infty(v_o, w_o) \\ \frac{\partial g_\infty}{\partial v_o} \delta v_o + \frac{\partial g_\infty}{\partial w_o} \delta w_o &= 1 - g_\infty(v_o, w_o) \end{aligned} \tag{A5}$$

The partial derivatives appearing in these expressions can be obtained by differentiating the system of first-order equations given in Eq. (A3), i.e.:

$$\left.\begin{aligned}
\left(\frac{\partial f}{\partial v_o}\right)_\eta &= \frac{\partial u}{\partial v_o} \\
\left(\frac{\partial u}{\partial v_o}\right)_\eta &= \frac{\partial v}{\partial v_o} \\
\left(\frac{\partial v}{\partial v_o}\right)_\eta &= -f\frac{\partial v}{\partial v_o} - v\frac{\partial f}{\partial v_o} + \beta\left(2u\frac{\partial u}{\partial v_o} - \frac{\partial g}{\partial v_o}\right) \\
\left(\frac{\partial g}{\partial v_o}\right)_\eta &= \frac{\partial w}{\partial v_o} \\
\left(\frac{\partial w}{\partial v_o}\right)_\eta &= -f\frac{\partial w}{\partial v_o} - w\frac{\partial f}{\partial v_o}
\end{aligned}\right\} \qquad \text{(A6)}$$

and

$$\left.\begin{aligned}
\left(\frac{\partial f}{\partial w_o}\right)_\eta &= \frac{\partial u}{\partial w_o} \\
\left(\frac{\partial u}{\partial w_o}\right)_\eta &= \frac{\partial v}{\partial w_o} \\
\left(\frac{\partial v}{\partial w_o}\right)_\eta &= -f\frac{\partial v}{\partial w_o} - v\frac{\partial f}{\partial w_o} + \beta\left(2u\frac{\partial u}{\partial w_o} - \frac{\partial g}{\partial w_o}\right) \\
\left(\frac{\partial g}{\partial w_o}\right)_\eta &= \frac{\partial w}{\partial w_o} \\
\left(\frac{\partial w}{\partial w_o}\right)_\eta &= -f\frac{\partial w}{\partial w_o} - w\frac{\partial f}{\partial w_o}
\end{aligned}\right\} \qquad \text{(A7)}$$

To evaluate the required partial derivatives as $\eta \to \infty$ it is necessary to integrate this system of equations from $\eta = 0$, where the initial values are known, to a point $\eta = \eta_\infty$, where $\eta_\infty >> 1$. The initial conditions

for these equations at $\eta = 0$ are:

$$\frac{\partial u}{\partial v_o} = \frac{\partial f}{\partial v_o} = \frac{\partial g}{\partial v_o} = \frac{\partial w}{\partial v_o} = \frac{\partial u}{\partial w_o} = \frac{\partial v}{\partial w_o} = \frac{\partial g}{\partial w_o} = \frac{\partial f}{\partial w_o} = 0$$

$$\frac{\partial v}{\partial v_o} = \frac{\partial w}{\partial w_o} = 1$$

In certain situations, the value $f_{\eta\eta}(0) = v_o$ may be specified and the pressure-gradient parameter β not known. The analysis is identical to the one described above with β substituted for v_o in Eqs. (A4)-(A5) and with Eqs. (A6) replaced by:

$$\left.\begin{aligned}
\left(\frac{\partial f}{\partial \beta}\right)_\eta &= \frac{\partial u}{\partial \beta} \\
\left(\frac{\partial u}{\partial \beta}\right)_\eta &= \frac{\partial v}{\partial \beta} \\
\left(\frac{\partial v}{\partial \beta}\right)_\eta &= -f\frac{\partial v}{\partial \beta} - v\frac{\partial f}{\partial \beta} + (u^2 - g) + \beta\left(2u\frac{\partial u}{\partial \beta} - \frac{\partial g}{\partial \beta}\right) \\
\left(\frac{\partial g}{\partial \beta}\right)_\eta &= \frac{\partial w}{\partial \beta} \\
\left(\frac{\partial w}{\partial \beta}\right)_\eta &= -f\frac{\partial w}{\partial \beta} - w\frac{\partial f}{\partial \beta}
\end{aligned}\right\} \qquad \text{(A8)}$$

where the initial conditions at $\eta = 0$ are

$$\frac{\partial u}{\partial \beta} = \frac{\partial v}{\partial \beta} = \frac{\partial f}{\partial \beta} = \frac{\partial g}{\partial \beta} = \frac{\partial w}{\partial \beta} = 0$$

The 10 equations for the partial derivatives, Eqs. (A6)-(A7) or Eqs. (A7)-(A8), can be integrated simultaneously with the basic differential equations, Eqs. (A3), to the location $\eta = \eta_\infty$. The solution of Eqs. (A5) then provides new initial values for the subsequent iteration, i.e.,

$$(v_o)_{i+1} = (v_o)_i + \delta v_o \qquad \text{or} \qquad \beta_{i+1} = \beta_i + \delta\beta$$

and $$(w_o)_{i+1} = (w_o)_i + \delta w_o$$

A.3. Numerical Procedure

A.3.1. Specification of η_∞

Since it is not possible to satisfy the boundary conditions numerically (Eqs. (A2)) as $\eta \to \infty$, the edge of the boundary layer η_∞ must be specified in advance to terminate the forward integration. If the value of η_∞ is too small, then $f_{\eta\eta}(\eta_\infty) \neq 0$ and η_∞ will be increased automatically until the condition $f_{\eta\eta}(\eta_\infty) < \epsilon$ is satisfied (see Section A.3.2). This procedure provides an effective means for avoiding the oscillations often encountered when the boundary-layer edge is allowed to vary during the iteration process.

A.3.2. Termination of Integration

The integration is terminated if the following two conditions are satisfied

$$[1-f'(\eta_\infty)]^2 + [1-g(\eta_\infty)]^2 < 10^{-8}$$

$$[f''(\eta_\infty)]^2 + [g'(\eta_\infty)]^2 < 10^{-7}$$

A.3.3. Correction Limitation

In certain cases, the initial guesses for v_o and w_o will be such that the iteration method described above will be inapplicable, and the new values of v_o and w_o will give u_∞ and g_∞ to lower accuracy than the previous solution. In these situations, the original correction is halved and the integration repeated until more accurate values of

u_∞ and g_∞ are obtained. For this reason, the norm $[(1-u_\infty)^2+(1-g_\infty)^2]$ is computed, and this quantity is required to decrease monotonically during the iteration process.

A.3.4. Program Inputs

The inputs required for the program are as follows:

BETA assumed or specified β (see Fig. A1)

FNNO assumed or specified $f_{\eta\eta}(0)$ (see Fig. A1)

GNO assumed $g_\eta(0)$ (see Fig. A2)

DETA integration step size ($\approx .01\ \eta_\infty$)

ETAMAX initial value of η_∞ (see Figs. A3-A5)

DETAM increment for changing η_∞ ($\approx .1\ \eta_\infty$)

GWALL specified $g_w = g(0)$

KIT iteration parameter, 1 or 2, i.e., KIT = 1 iteration for $f_{\eta\eta}(0)$; KIT = 2 iteration for β

A.3.5. Fortran Listing

A Fortran listing of the program used to solve the Cohen-Reshotko equations (Eqs. A1) is given in Table A1.

A.3.6. Program Outputs

The program gives the solution vectors η, f, f_η, $f_{\eta\eta}$, g and g_η as well as the profile functions a, $\mathcal{N}$, J, Z etc. used in the moment method, as shown in Tables A2-A11.

TABLE AI - FORTRAN LISTING

```
C     SOLUTION OF THE FALKNER - SKAN EQUATIONS

      DIMENSION F(500), FN(500), FNN(500), G(500), GN(500),
     1 ET1(500)
      COMMON DELSTR, THETA, THESTR, H, XJ, Z, TSTAR, R, P,
     1 SW, A, USTAR, DELTA, SIGMA, E, SSTAR
    5 READ (5,1) BETA, FNNO, GNO, DETA, ETAMAX, DETAM,
     1 GWALL, KIT
    1 FORMAT(7F10.0,I1)

C     BETA = PRESSURE GRADIENT PARAMETER
C     FNNO = SHEAR AT WALL
C     GNO = ENTHALPY GRADIENT AT WALL
C     DETA = INTEGRATION STEP SIZE
C     ETAMAX = LOCATION OF BOUNDARY-LAYER EDGE
C     DETAM = CHANGE IN ETAMAX FOR ITERATION
C     GWALL = ENTHALPY RATIO AT WALL
C     KIT = 1, ITERATE FOR FNNO
C     KIT = 2, ITERATE FOR BETA

      CALL METH1(F,FN,FNN,G,GN,BETA,FNNO,GWALL,GNO,ETAMAX,
     1 DETA,DETAM,KIT,ICON,L)
      GO TO (10,5), ICON

C     ICON = 1, NORMAL RETURN
C     ICON = 2, ERROR RETURN

   10 LM1=L-1
      ETA=0.
      DO 20 I=1,LM1
      ET1(I)=ETA
   20 ETA=ETA+DETA
      CALL INTGRL(LM1,ET1,F,FN,FNN,G,GWALL)
      SW=GWALL-1.
      WRITE(6,501) BETA, SW
  501 FORMAT(1H1 20X 7HBETA = F10.5, 5X5HSW = F10.4//)
      WRITE(6,502)
  502 FORMAT(8X3HETA 10X1HF 11X2HFN 9X3HFNN 8X1HG 11X2HGN//)

C     ONE - PAGE  PRINTOUT

      IF(LM1.GE.0)KOUT=1
      IF(LM1.GE.52)KOUT=2
      IF(LM1.GE.104)KOUT=4
      IF(LM1.GE.208)KOUT=5
      IF(LM1.GE.260)KOUT = 8
      IF(LM1.GE.416)KOUT = 10
      IF(LM1.GE.520)KOUT = 20
```

TABLE AI (CONT.)

```
      LM2=LM1-1
      DO 45 I=1,LM2,KOUT
   45 WRITE(6,503)ET1(I),F(I),FN(I),FNN(I),G(I),GN(I)
      WRITE(6,503)ET1(LM1),F(LM1),FN(LM1),FNN(LM1),G(LM1),
     1 GN(LM1)
  503 FORMAT( 1X7F12.5 )

C     PROFILE FUNCTIONS FOR CONVERGED SOLUTION

      WRITE (6,504)
  504 FORMAT( /27X18HINTEGRAL FUNCTIONS /)
      WRITE (6,505) DELTA,A,TSTAR,DELSTR,H,R,THETA,XJ,P,
     1  THESTR,Z,USTAR,SIGMA,E,SSTAR
  505 FORMAT(/5X10H DELTA  = F10.5,8X5HA   = F10.5,9X5HT* =
     1 F10.5,/5X10H DELTA* = F10.5,8X5HH   = F10.5,9X5HR  =
     2 F10.5,/5X10H THETA  = F10.5,8X5HJ   = F10.5,9X5HP  =
     3 F10.5,/5X10H THETA* = F10.5,8X5HZ   = F10.5,9X5HU* =
     4 F10.5,/5X10H SIGMA  = F10.5,8X5HE   = F10.5,9X5HS* =
     5 F10.5 /// )
      GO TO 5
      END
```

TABLE AI (CONT.)

```
      SUBROUTINE METH1 (F,FN,FNN,G,GN,BETA,FNNO,GWALL,GNO,
     1 ETAMAX,DETA,DETAM,KIT,ICON,L)

C     SIMULTANEOUS SOLUTION OF THE MOMENTUM AND ENERGY EQNS

      DIMENSION F(200),FN(200),FNN(200),G(200),GN(200),
     1 Y(20),D(20),Q(20)
      GO TO (10,20), KIT
   10 WRITE (6,2)
    2 FORMAT(28H1 ITERATION ON SHEAR AT WALL)
      GO TO 30
   20 WRITE (6,4)
    4 FORMAT(19H1 ITERATION ON BETA)
   30 M = 0
      L = 1
      NORM = 1
      KNORM = 1
      KCONT = 0
      KCON = 0
      NEWT = 1

C     M = 0 INITIALIZES THE FORWARD INTEGRATION
C     L = AN INDEX USED TO STORE THE FINAL SOLUTION
C     NORM = 1 INDICATES A NORM HAS NOT BEEN COMPUTED
C     NORM = 2 INDICATES A NORM HAS BEEN COMPUTED
C     KNORM = 1 INDICATES THE INTEGRATION WAS TERMINATED AT
C     THE LOCATION ETA = ETAMAX
C     KNORM = 2 INDICATES THE INTEGRATION WAS TERMINATED
C     BECAUSE FN WAS GREATER THAN 1.5 OR LESS THAN -1.0 AT
C     A POINT WHERE ETA WAS LESS THAN ETAMAX.  IF A NORM
C     HAS BEEN COMPUTED, THE CORRECTIONS GIVEN BY THE LAST
C     ITERATION ARE HALVED.  IF NORM = 1, A CORRECTION IS
C     BASED ON AN ETA LESS THAN ETAMAX
C     KCONT = THE NUMBER OF ITERATIONS, NOT EXCEEDING 50
C     NEWT = 1 INDICATES THE SOLUTION HAS NOT BEEN FOUND
C     NEWT = 2 INDICATES THE EQUATIONS HAVE CONVERGED

   40 K = 2
      ETA = 0.
      DO 42 I = 1, 15
   42 Y(I) = 0.
      Y(3) = FNNC
      Y(4) = GWALL
      Y(5) = GNO
      GO TO (43,44), KIT
   43 Y(8) = 1.
   44 Y(15) = 1.
   50 D(1) = Y(2)
      D(2) = Y(3)
      D(3) = -Y(1) * Y(3) + BETA * (Y(2)**2-Y(4))
```

TABLE AI (CONT.)

```
      D(4) = Y(5)
      D(5) = -Y(1) * Y(5)
      D(6) = Y(7)
      D(7) = Y(8)
      GO TO (51,52), KIT
   51 D(8) = -Y(1)*Y(8)-Y(3)*Y(6) + BETA*(2.*Y(2)*Y(7)-Y(9))
      GO TO 53
   52 D(8) = -Y(1)*Y(8)-Y(3)*Y(6)+Y(2)**2-Y(4)+BETA*(2.*Y(2)
     1 *Y(7)-Y(9))
   53 D(9) = Y(10)
      D(10) = -Y(1)*Y(10)-Y(5)*Y(6)
      D(11) = Y(12)
      D(12) = Y(13)
      D(13) = -Y(1)*Y(13)-Y(3)*Y(11)+BETA*(2.*Y(2)*Y(12)-
     1 Y(14))
      D(14) = Y(15)
      D(15) = -Y(1)*Y(15)-Y(5)*Y(11)
      GO TO (60,70), K
   60 K = MRKSUB (15,Y,D,Q,ETA,DETA,M)
      GO TO 50
   70 IF(ETA.GE.ETAMAX) GO TO 100
      IF(Y(2).GE.1.5) GO TO 90
      IF((Y(2) + 1.).LE.0.) GO TO 90
      GO TO (60,65), NEWT
   65 F(L) = Y(1)
      FN(L) = Y(2)
      FNN(L) = Y(3)
      G(L) = Y(4)
      GN(L) = Y(5)
      L = L + 1
      GO TO 60
   90 KNORM = 2
  100 GO TO (120,180),NEWT
  120 F1 = 1.-Y(2)
      F2 = 1.-Y(4)
      ENORM = F1**2 + F2**2
      GO TO (105,110), NORM
  105 GO TO (112,108), KNORM
  112 NORM = 2
      ENORMS = ENORM
      GO TO 108
  110 GO TO (119,115), KNORM
  119 IF(ENORM.GE.ENORMS) GO TO 115
      ENORMS = ENORM
  108 DET = Y(7) * Y(14) - Y(9) * Y(12)
      CORFOB = (F1*Y(14)-F2*Y(12)) / DET
      CORG = (Y(7)*F2-Y(9)*F1) / DET
      GO TO (121,122), KIT
  121 CONTINUE
      IF(FNNC .GE. 0.0) GO TO 220
```

TABLE AI (CONT.)

```
  222 IF(FNNO + CORFOB) 220,221,221
  221 CORFOB = 0.5*CORFOB
      CORG = 0.5 * CORG
      GO TO 222
  220 FNNO = FNNO + CORFOB
      GO TO 123
  122 BETA = BETA + CORFOB
  123 GNO = GNO + CORG
      GO TO (130,132), KNORM
  132 KNORM = 1
      GO TO 140
  115 CORFOB = .5 * CORFOB
      CORG = .5 * CORG
      GO TO (116,117), KIT
  116 FNNO = FNNO - CORFOB
      GO TO 118
  117 BETA = BETA - CORFOB
  118 GNO = GNO - CORG
      GO TO 140
  130 IF(ENORM.LE.1.E-08) GO TO 150
  140 WRITE(6,6) Y(2),Y(4),Y(3),Y(5),Y(7),Y(9),Y(12),Y(14),
     1 DET,CORFOB,CORG,ETA
    6 FORMAT (1X4F15.6)
      KNORM = 1
      IF(KCONT.GT.50) GO TO 142
      KCONT = KCONT + 1
      GO TO 40
  142 WRITE(6,8)
    8 FORMAT(39H EXCEEDED 50 ITERATIONS FOR BETA OR FNN )
  149 ICON = 2
      RETURN
  150 IF((Y(3)**2+Y(5)**2).LE.1.E-07) GO TO 160
      IF(KCON.GT.5) GO TO 165
      KCON = KCON + 1
      ETAMAX = ETAMAX + DETAM
      WRITE(6,7)
    7 FORMAT(41HOEQUATIONS CONVERGED BUT ETAMAX TOO SMALL)
      NORM = 1
      GO TO 40
  165 WRITE(6,3)
    3 FORMAT(37H CANNOT LOCATE EDGE OF BOUNDARY LAYER )
      GO TO 149
  160 NEWT = 2
      WRITE(6,11)
   11 FORMAT(21HC EQUATIONS CONVERGED )
      ICON = 1
      GO TO 40
  180 RETURN
       ENC
```

TABLE AI (CONT.)

```
      FUNCTION MRKSUB (N,Y,F,Q,X,H,M)
C     RUNGE-KUTTA INTEGRATION ROUTINE
      DIMENSION Y(20),F(20),Q(20)
      M=M+1
      GO TO (1,4,5,3,7),M
    1 DO 2 I=1,N
    2 Q(I)=0.
      A=.5
      GO TO 9
    3 A=1.7071068
    4 X=X+.5*H
    5 DO 6 I=1,N
      Y(I)=Y(I)+A*(F(I)*H-Q(I))
    6 Q(I)=2.0*A*F(I)*H+(1.0-3.0*A)*Q(I)
      A=.29289322
      GO TO 9
    7 DO 8 I=1,N
    8 Y(I)=Y(I)+.16666667*F(I)*H-.33333333*Q(I)
      M=0
      MRKSUB=2
      GO TO 10
    9 MRKSUB=1
   10 RETURN
      END
```

TABLE AI (CONT.)

```
      SUBROUTINE INTGRL(N,ET,F,F1,F2,G,GW)
C     TRAPEZOIDAL INTEGRATION ROUTINE FOR CONVERGED SOLUTION
      DIMENSION ET(200), F(200), F1(200), F2(200), G(200)
      COMMON DELSTR, THETA, THESTR, H, XJ, Z, TSTAR, R, P,
     1 SW, A, USTAR, DELTA, SIGMA, E, SSTAR
      SW = GW-1.0
      II = N
      DO 10 I = 1, N
      IF(F1(II) .LE. .99) GO TO 15
      II = II - 1
   10 CONTINUE
   15 CONTINUE
      IF (II .EQ.N) GO TO 50
      DIF = (.99 - F1(II)) / (F1(II+1) - F1(II))
      ET99 = DIF * (ET(II+1) - ET(II)) + ET(II)
      F99 = DIF * (F(II+1) - F(II)) + F(II)
      F992 = DIF * (F2(II+1) - F2(II)) + F2(II)
      G99 = DIF * (G(II+1) - G(II)) + G(II)
      DELTA = ET99
      IF(F2(1) .LT. 0.) GO TO 60
      A = DELTA*F2(1)
      USTAR = 0.0
      SSTAR = 1.0
   30 CONTINUE
      DETA = ET(2) - ET(1)
      DELSTR = .5 * (1.00 - F1(1))
      THETA = .5 * (F1(1) - F1(1)**2)
      THESTR = .5 * (F1(1) - F1(1)**3)
      SIGMA = .5 * (1.00 - G(1))
      Z = .5 * F1(1)
      TSTAR = .5 * (F1(1) - F1(1) * G(1))
      R = F2(1) **2
      III = II - 1
      DO 40 I = 2, III
      DELSTR = DELSTR + 1.00 - F1(I)
      THETA = F1(I) - F1(I) **2 + THETA
      THESTR = F1(I) - F1(I) **3 + THESTR
      SIGMA = SIGMA + 1.00 - G(I)
      Z = Z + F1(I)
      TSTAR = F1(I) - F1(I) * G(I) + TSTAR
      R = F2(I)**2*2.0 + R
   40 CONTINUE
      DETAF = ET99 - ET(II)
      DELSTR = (DELSTR + .5*(1.0-F1(II)) ) * DETA + .5 *
     1 (1.0-F1(II) + 1.0-.99) * DETAF
      THETA = (THETA + .5*(F1(II)-F1(II)**2) )*DETA + .5 *
     1 (F1(II)-F1(II)**2 + .99-.9801) * DETAF
```

TABLE AI (CONT.)

```
      THESTR =  (THESTR + .5*(F1(II)-F1(II)**3) ) * DETA +
     1 .5 * (F1(II)-F1(II)**3 + .99-.970299) * DETAF
      SIGMA = (SIGMA + .5*(1.0-G(II)) ) * DETA + .5 *
     1 (1.0 - G(II) + 1.0 - G99) * DETAF
      H = THETA / DELSTR
      XJ = THESTR / DELSTR
      E = SIGMA / DELSTR
      Z = ((Z+.5*F1(II))*DETA+.5*(F1(II)+.99)*DETAF)/DELSTR
      TSTAR = ((TSTAR+.5*(F1(II)-F1(II)*G(II)))*DETA + .5*
     1 (F1(II)-F1(II)*G(II)+.99-.99*G99)*DETAF)/(-DELSTR*SW)
      R = DELSTR * ((R + F2(II)**2) * DETA + (F2(II)**2
     1 +F992*F992) * DETAF )
      P = DELSTR * F2(1)
      RETURN
   60 CONTINUE
      FNO = F1(1)
      DO 65 I = 2,II
      IF(F1(I).GE.0.) GO TO 70
   65 CONTINUE
   70 CONTINUE
      IF(I.EQ.II) GO TO 50
      ETO = F1(I-1)/(F1(I-1)-F1(I))*(ET(I)-ET(I-1))+ET(I-1)
      A = ETO/DELTA
      FC = F(1)
      FNC = F1(I)
      DO 75 I = 2,II
      IF(F(I).GE.0.) GO TO 80
   75 CONTINUE
   80 CONTINUE
      IF ( I.EQ.II) GO TO 50
      USTAR = F(I-1)/(F(I-1)-F(I))*(F1(I)-F1(I-1)) + F1(I-1)
      SSTAR = (F(I-1)/(F(I-1)-F(I))*(G(I)-G(I-1)) + G(I-1) -
     1 1.0 ) / SW
      GO TO 30
   50 WRITE (6,500) II, ET(II), F1(II)
  500 FORMAT (/24H SOLUTION NOT FAR ENOUGH  I5,2E20.8)
      RETURN
       END
```

BETA = -0.00100 SW = 0.

ETA	F	FN	FNN	G	GN
0.	0.	0.	-0.00861	1.00000	0.
0.80000	-0.00267	-0.00657	-0.00782	1.00000	0.
1.60000	-0.01034	-0.01251	-0.00705	1.00000	0.
2.40000	-0.02254	-0.01787	-0.00634	1.00000	0.
3.20000	-0.03879	-0.02267	-0.00568	1.00000	0.
4.00000	-0.05868	-0.02698	-0.00509	1.00000	0.
4.80000	-0.08183	-0.03084	-0.00456	1.00000	0.
5.60000	-0.10791	-0.03429	-0.00409	1.00000	0.
6.40000	-0.13660	-0.03739	-0.00367	1.00000	0.
7.20000	-0.16765	-0.04017	-0.00329	1.00000	0.
8.00000	-0.20080	-0.04267	-0.00295	1.00000	0.
8.80000	-0.23585	-0.04490	-0.00264	1.00000	0.
9.60000	-0.27258	-0.04689	-0.00235	1.00000	0.
10.40000	-0.31081	-0.04866	-0.00206	1.00000	0.
11.20000	-0.35037	-0.05019	-0.00177	1.00000	0.
12.00000	-0.39105	-0.05148	-0.00145	1.00000	0.
12.80000	-0.43265	-0.05249	-0.00106	1.00000	0.
13.60000	-0.47494	-0.05315	-0.00057	1.00000	0.
14.40000	-0.51757	-0.05334	0.00014	1.00000	0.
15.20000	-0.56009	-0.05283	0.00122	1.00000	0.
16.00000	-0.60180	-0.05121	0.00296	1.00000	0.
16.80000	-0.64155	-0.04778	0.00590	1.00000	0.
17.60000	-0.67741	-0.04119	0.01105	1.00000	0.
18.39999	-0.70599	-0.02901	0.02031	1.00000	0.
19.19999	-0.72117	-0.00672	0.03706	1.00000	0.
19.99999	-0.71194	0.03377	0.06697	1.00000	0.
20.79999	-0.65875	0.10592	0.11738	1.00000	0.
21.59999	-0.52914	0.22796	0.19099	1.00000	0.
22.39999	-0.27703	0.41261	0.26713	1.00000	0.
23.19999	0.14297	0.64004	0.28588	1.00000	-0.
23.99999	0.74015	0.84172	0.20327	1.00000	-0.
24.79999	1.46542	0.95541	0.08472	1.00000	-0.
25.59999	2.24810	0.99258	0.01924	1.00000	-0.
26.39999	3.04572	0.99930	0.00232	1.00000	-0.
27.19999	3.84553	0.99996	0.00015	1.00000	-0.
27.99999	4.64553	1.00000	0.00001	1.00000	-0.

INTEGRAL FUNCTIONS

DELTA =	23.49294	A =	0.75975	T* =	-0.
DELTA* =	23.35087	H =	0.00048	R =	9.66991
THETA =	0.01124	J =	0.01748	P =	-0.20107
THETA* =	0.40817	Z =	0.09173	U* =	0.57144
SIGMA =	0.	E =	0.	S* =	0.

TABLE A2-SIMILAR SOLUTIONS FOR $\beta = -0.001$, $S_w = 0$

BETA = -0.19886 SW = 0.

ETA	F	FN	FNN	G	GN
0.	0.	0.	0.	1.00000	0.
0.20000	0.00027	0.00398	0.03977	1.00000	0.
0.40000	0.00212	0.01591	0.07952	1.00000	0.
0.60000	0.00716	0.03578	0.11918	1.00000	0.
0.80000	0.01696	0.06356	0.15852	1.00000	0.
1.00000	0.03310	0.09914	0.19715	1.00000	0.
1.20000	0.05712	0.14233	0.23441	1.00000	0.
1.40000	0.09052	0.19275	0.26937	1.00000	0.
1.60000	0.13467	0.24984	0.30079	1.00000	0.
1.80000	0.19084	0.31274	0.32722	1.00000	0.
2.00000	0.26008	0.38029	0.34703	1.00000	0.
2.20000	0.34317	0.45100	0.35866	1.00000	0.
2.40000	0.44057	0.52312	0.36080	1.00000	0.
2.60000	0.55237	0.59464	0.35272	1.00000	0.
2.80000	0.67825	0.66352	0.33445	1.00000	0.
3.00000	0.81748	0.72781	0.30699	1.00000	0.
3.20000	0.96896	0.78583	0.27225	1.00000	0.
3.40000	1.13131	0.83640	0.23286	1.00000	0.
3.60000	1.30297	0.87886	0.19178	1.00000	0.
3.80000	1.48231	0.91319	0.15191	1.00000	0.
4.00000	1.66774	0.93987	0.11560	1.00000	0.
4.20000	1.85781	0.95978	0.08446	1.00000	0.
4.40000	2.05127	0.97404	0.05921	1.00000	0.
4.60000	2.24713	0.98385	0.03982	1.00000	0.
4.80000	2.44455	0.99032	0.02569	1.00000	0.
5.00000	2.64310	0.99442	0.01590	1.00000	0.
5.20000	2.84225	0.99691	0.00944	1.00000	0.
5.40000	3.04179	0.99835	0.00537	1.00000	0.
5.60000	3.24155	0.99916	0.00293	1.00000	0.
5.80000	3.44143	0.99960	0.00154	1.00000	0.
6.00000	3.64137	0.99982	0.00077	1.00000	0.
6.20000	3.84135	0.99993	0.00037	1.00000	0.
6.40000	4.04134	0.99998	0.00017	1.00000	0.
6.50000	4.14134	0.99999	0.00011	1.00000	0.

INTEGRAL FUNCTIONS

DELTA =	4.78811	A =	0.	T* =	-0.
DELTA* =	2.35529	H =	0.24709	R =	1.25776
THETA =	0.58198	J =	0.37367	P =	0.
THETA* =	0.88011	Z =	1.03292	U* =	0.
SIGMA =	0.	E =	0.	S* =	1.00000

TABLE A3 - SIMILAR SOLUTIONS FOR $f''(0) = 0$, $S_w = 0$

BETA = 0. Sw = 0.

ETA	F	FN	FNN	G	GN
0.	0.	0.	0.46964	1.00000	0.
0.10000	0.00235	0.04696	0.46960	1.00000	0.
0.20000	0.00939	0.09391	0.46934	1.00000	0.
0.30000	0.02113	0.14082	0.46865	1.00000	0.
0.40000	0.03755	0.18762	0.46729	1.00000	0.
0.50000	0.05865	0.23425	0.46507	1.00000	0.
0.60000	0.08439	0.28060	0.46177	1.00000	0.
0.70000	0.11475	0.32656	0.45721	1.00000	0.
0.80000	0.14969	0.37199	0.45123	1.00000	0.
0.90000	0.18913	0.41675	0.44366	1.00000	0.
1.00000	0.23301	0.46067	0.43441	1.00000	0.
1.10000	0.28123	0.50357	0.42340	1.00000	0.
1.20000	0.33368	0.54529	0.41059	1.00000	0.
1.30000	0.39024	0.58563	0.39601	1.00000	0.
1.40000	0.45076	0.62443	0.37972	1.00000	0.
1.50000	0.51507	0.66152	0.36183	1.00000	0.
1.60000	0.58300	0.69675	0.34251	1.00000	0.
1.70000	0.65436	0.72998	0.32197	1.00000	0.
1.80000	0.72893	0.76111	0.30046	1.00000	0.
1.90000	0.80651	0.79005	0.27826	1.00000	0.
2.00000	0.88686	0.81675	0.25568	1.00000	0.
2.10000	0.96978	0.84119	0.23302	1.00000	0.
2.20000	1.05503	0.86336	0.21058	1.00000	0.
2.30000	1.14238	0.88332	0.18868	1.00000	0.
2.40000	1.23162	0.90112	0.16756	1.00000	0.
2.50000	1.32253	0.91687	0.14747	1.00000	0.
2.60000	1.41493	0.93066	0.12861	1.00000	0.
2.70000	1.50861	0.94263	0.11112	1.00000	0.
2.80000	1.60340	0.95293	0.09511	1.00000	0.
2.90000	1.69914	0.96171	0.08063	1.00000	0.
3.00000	1.79569	0.96911	0.06771	1.00000	0.
3.10000	1.89292	0.97530	0.05630	1.00000	0.
3.20000	1.99072	0.98042	0.04637	1.00000	0.
3.30000	2.08898	0.98462	0.03781	1.00000	0.
3.40000	2.18761	0.98803	0.03053	1.00000	0.
3.50000	2.28656	0.99076	0.02441	1.00000	0.
3.60000	2.38575	0.99294	0.01933	1.00000	0.
3.70000	2.48513	0.99466	0.01515	1.00000	0.
3.80000	2.58467	0.99600	0.01176	1.00000	0.
3.90000	2.68432	0.99703	0.00903	1.00000	0.
4.00000	2.78407	0.99782	0.00687	1.00000	0.
4.10000	2.88388	0.99842	0.00518	1.00000	0.
4.20000	2.98374	0.99887	0.00386	1.00000	0.
4.30000	3.08365	0.99920	0.00285	1.00000	0.
4.40000	3.18358	0.99945	0.00208	1.00000	0.
4.50000	3.28354	0.99963	0.00151	1.00000	0.
4.60000	3.38351	0.99976	0.00108	1.00000	0.
4.70000	3.48349	0.99985	0.00077	1.00000	0.
4.80000	3.58347	0.99991	0.00054	1.00000	0.
4.90000	3.68347	0.99996	0.00037	1.00000	0.
5.00000	3.78346	0.99999	0.00026	1.00000	0.

INTEGRAL FUNCTIONS

DELTA =	3.47046	A =	1.62986	T* =	-0.
DELTA* =	1.21325	H =	0.38406	R =	0.89575
THETA =	0.46596	J =	0.60280	P =	0.56979
THETA* =	0.73135	Z =	1.86047	U* =	0.
SIGMA =	0.	E =	0.	S* =	1.00000

TABLE A4-SIMILAR SOLUTIONS FOR $\beta = 0$, $S_w = 0$

BETA = 0.28571 SW = 0.

ETA	F	FN	FNN	G	GN
0.	0.	0.	0.76276	1.00000	0.
0.10000	0.00377	0.07485	0.73415	1.00000	0.
0.20000	0.01487	0.14682	0.70532	1.00000	0.
0.30000	0.03303	0.21590	0.67609	1.00000	0.
0.40000	0.05795	0.28202	0.64634	1.00000	0.
0.50000	0.08934	0.34514	0.61598	1.00000	0.
0.60000	0.12688	0.40520	0.58499	1.00000	0.
0.70000	0.17027	0.46212	0.55339	1.00000	0.
0.80000	0.21920	0.51586	0.52124	1.00000	0.
0.90000	0.27334	0.56635	0.48865	1.00000	0.
1.00000	0.33236	0.61358	0.45577	1.00000	0.
1.10000	0.39594	0.65750	0.42279	1.00000	0.
1.20000	0.46375	0.69814	0.38992	1.00000	0.
1.30000	0.53546	0.73550	0.35741	1.00000	0.
1.40000	0.61074	0.76964	0.32550	1.00000	0.
1.50000	0.68928	0.80063	0.29444	1.00000	0.
1.60000	0.77077	0.82856	0.26447	1.00000	0.
1.70000	0.85490	0.85357	0.23583	1.00000	0.
1.80000	0.94139	0.87578	0.20870	1.00000	0.
1.90000	1.02997	0.89536	0.18327	1.00000	0.
2.00000	1.12038	0.91250	0.15966	1.00000	0.
2.10000	1.21239	0.92736	0.13796	1.00000	0.
2.20000	1.30578	0.94015	0.11821	1.00000	0.
2.30000	1.40036	0.95107	0.10044	1.00000	0.
2.40000	1.49594	0.96031	0.08461	1.00000	0.
2.50000	1.59237	0.96805	0.07066	1.00000	0.
2.60000	1.68951	0.97450	0.05848	1.00000	0.
2.70000	1.78723	0.97981	0.04798	1.00000	0.
2.80000	1.88543	0.98414	0.03900	1.00000	0.
2.90000	1.98403	0.98765	0.03142	1.00000	0.
3.00000	2.08294	0.99047	0.02508	1.00000	0.
3.10000	2.18210	0.99270	0.01984	1.00000	0.
3.20000	2.28147	0.99447	0.01555	1.00000	0.
3.30000	2.38098	0.99584	0.01207	1.00000	0.
3.40000	2.48062	0.99690	0.00928	1.00000	0.
3.50000	2.58036	0.99772	0.00708	1.00000	0.
3.60000	2.68016	0.99833	0.00534	1.00000	0.
3.70000	2.78002	0.99880	0.00399	1.00000	0.
3.80000	2.87992	0.99914	0.00296	1.00000	0.
3.90000	2.97984	0.99940	0.00217	1.00000	0.
4.00000	3.07979	0.99958	0.00158	1.00000	0.
4.10000	3.17976	0.99972	0.00114	1.00000	0.
4.20000	3.27974	0.99982	0.00081	1.00000	0.
4.30000	3.37972	0.99989	0.00058	1.00000	0.
4.40000	3.47971	0.99993	0.00040	1.00000	0.
4.50000	3.57971	0.99997	0.00028	1.00000	0.
4.60000	3.67970	0.99999	0.00020	1.00000	0.

INTEGRAL FUNCTIONS

DELTA =	2.58241	A =	2.27486	T* =	-0.
DELTA* =	0.91704	H =	0.41990	R =	0.89661
THETA =	0.38507	J =	0.67076	P =	0.69948
THETA* =	0.61511	Z =	2.25222	U* =	0.
SIGMA =	0.	E =	0.	S* =	1.00000

TABLE A5- SIMILAR SOLUTIONS FOR $\beta = \frac{\gamma-1}{\gamma}$, $S_W = 0$

BETA = 5.00000 SW = 0.

ETA	F	FN	FNN	G	GN
0.	0.	0.	2.61578	1.00000	0.
0.10000	0.01225	0.23681	2.12469	1.00000	0.
0.20000	0.04578	0.42642	1.67734	1.00000	0.
0.30000	0.09615	0.57446	1.29491	1.00000	0.
0.40000	0.15952	0.68773	0.98202	1.00000	0.
0.50000	0.23276	0.77303	0.73405	1.00000	0.
0.60000	0.31339	0.83641	0.54214	1.00000	0.
0.70000	0.39949	0.88299	0.39634	1.00000	0.
0.80000	0.48957	0.91690	0.28718	1.00000	0.
0.90000	0.58255	0.94137	0.20642	1.00000	0.
1.00000	0.67762	0.95890	0.14729	1.00000	0.
1.10000	0.77417	0.97137	0.10437	1.00000	0.
1.20000	0.87177	0.98018	0.07348	1.00000	0.
1.30000	0.97011	0.98636	0.05139	1.00000	0.
1.40000	1.06898	0.99067	0.03572	1.00000	0.
1.50000	1.16820	0.99366	0.02468	1.00000	0.
1.60000	1.26768	0.99572	0.01694	1.00000	0.
1.70000	1.36732	0.99712	0.01156	1.00000	0.
1.80000	1.46709	0.99808	0.00784	1.00000	0.
1.90000	1.56693	0.99873	0.00529	1.00000	0.
2.00000	1.66683	0.99917	0.00355	1.00000	0.
2.10000	1.76676	0.99946	0.00237	1.00000	0.
2.20000	1.86671	0.99965	0.00158	1.00000	0.
2.30000	1.96669	0.99978	0.00105	1.00000	0.
2.40000	2.06667	0.99987	0.00071	1.00000	0.
2.50000	2.16666	0.99993	0.00048	1.00000	0.
2.60000	2.26665	0.99997	0.00034	1.00000	0.
2.70000	2.36665	1.00000	0.00026	1.00000	0.

INTEGRAL FUNCTIONS

DELTA =	1.38208	A =	3.61523	T* =	-0.
DELTA* =	0.33098	H =	0.46985	R =	0.94934
THETA =	0.15551	J =	0.77163	P =	0.86578
THETA* =	0.25540	Z =	3.17569	U* =	0.
SIGMA =	0.	E =	0.	S* =	1.00000

TABLE A6 – SIMILAR SOLUTIONS FOR β = 5.0, S_w = 0

BETA = -0.00400 SW = -0.8000

ETA	F	FN	FNN	G	GN
0.	0.	0.	-0.00730	0.20000	0.00004
1.00000	-0.00352	-0.00690	-0.00651	0.20004	0.00004
2.00000	-0.01354	-0.01302	-0.00575	0.20009	0.00004
3.00000	-0.02932	-0.01843	-0.00507	0.20013	0.00004
4.00000	-0.05018	-0.02318	-0.00445	0.20018	0.00005
5.00000	-0.07550	-0.02736	-0.00392	0.20022	0.00005
6.00000	-0.10474	-0.03104	-0.00345	0.20027	0.00005
7.00000	-0.13743	-0.03428	-0.00304	0.20033	0.00006
8.00000	-0.17317	-0.03714	-0.00269	0.20040	0.00007
9.00000	-0.21159	-0.03967	-0.00238	0.20047	0.00009
10.00000	-0.25240	-0.04190	-0.00210	0.20057	0.00011
11.00000	-0.29530	-0.04387	-0.00184	0.20070	0.00014
12.00000	-0.34005	-0.04558	-0.00159	0.20086	0.00020
13.00000	-0.38638	-0.04704	-0.00132	0.20110	0.00028
14.00000	-0.43403	-0.04820	-0.00100	0.20144	0.00042
15.00000	-0.48267	-0.04900	-0.00057	0.20198	0.00067
16.00000	-0.53185	-0.04926	0.00010	0.20285	0.00111
17.00000	-0.58090	-0.04864	0.00126	0.20433	0.00194
18.00000	-0.62861	-0.04642	0.00342	0.20699	0.00356
19.00000	-0.67273	-0.04110	0.00773	0.21199	0.00682
20.00000	-0.70873	-0.02944	0.01668	0.22179	0.01363
21.00000	-0.72724	-0.00446	0.03562	0.24172	0.02799
22.00000	-0.70847	0.04851	0.07485	0.28283	0.05764
23.00000	-0.61196	0.15668	0.14789	0.36554	0.11255
24.00000	-0.36503	0.35392	0.24690	0.51499	0.18647
25.00000	0.12410	0.63134	0.28661	0.72391	0.21531
26.00000	0.88606	0.87386	0.17720	0.90575	0.13261
27.00000	1.82363	0.97910	0.04625	0.98441	0.03452
28.00000	2.81581	0.99853	0.00458	0.99890	0.00341
29.00000	3.81538	0.99996	0.00017	0.99996	0.00013
29.75000	4.56537	1.00000	0.00001	0.99999	0.00001

INTEGRAL FUNCTIONS

DELTA =	27.32740	A =	0.77262	T* =	-0.00013
DELTA* =	25.18101	H =	0.00050	R =	10.36634
THETA =	0.01268	J =	0.01621	P =	-0.18375
THETA* =	0.40821	Z =	0.08524	U* =	0.57108
SIGMA =	19.32256	E =	0.76735	S* =	0.40174

TABLE A7 – SIMILAR SOLUTIONS FOR $\beta = -0.004$, $S_w = -0.8$

BETA = -0.30867 SW = -0.8000

ETA	F	FN	FNN	G	GN
0.	0.	0.	0.	0.20000	0.22602
0.20000	0.00009	0.00133	0.01374	0.24520	0.22602
0.40000	0.00073	0.00568	0.03027	0.29041	0.22600
0.60000	0.00260	0.01362	0.04958	0.33560	0.22593
0.80000	0.00646	0.02570	0.07161	0.38077	0.22574
1.00000	0.01319	0.04244	0.09628	0.42588	0.22531
1.20000	0.02378	0.06437	0.12338	0.47087	0.22449
1.40000	0.03931	0.09193	0.15259	0.51564	0.22310
1.60000	0.06095	0.12551	0.18339	0.56005	0.22090
1.80000	0.08993	0.16535	0.21502	0.60393	0.21762
2.00000	0.12751	0.21151	0.24645	0.64701	0.21297
2.20000	0.17495	0.26382	0.27632	0.68900	0.20666
2.40000	0.23342	0.32182	0.30300	0.72955	0.19843
2.60000	0.30400	0.38469	0.32468	0.76823	0.18809
2.80000	0.38755	0.45124	0.33949	0.80464	0.17556
3.00000	0.48464	0.51992	0.34577	0.83832	0.16093
3.20000	0.59553	0.58889	0.34231	0.86889	0.14449
3.40000	0.72008	0.65616	0.32869	0.89602	0.12671
3.60000	0.85775	0.71973	0.30545	0.91952	0.10823
3.80000	1.00761	0.77780	0.27414	0.93932	0.08983
4.00000	1.16841	0.82900	0.23716	0.95551	0.07228
4.20000	1.33869	0.87248	0.19744	0.96834	0.05626
4.40000	1.51687	0.90800	0.15797	0.97815	0.04229
4.60000	1.70138	0.93586	0.12133	0.98541	0.03065
4.80000	1.89076	0.95685	0.08940	0.99057	0.02141
5.00000	2.08373	0.97200	0.06316	0.99412	0.01439
5.20000	2.27925	0.98250	0.04278	0.99646	0.00930
5.40000	2.47650	0.98947	0.02777	0.99794	0.00578
5.60000	2.67487	0.99391	0.01728	0.99885	0.00345
5.80000	2.87394	0.99662	0.01030	0.99938	0.00198
6.00000	3.07344	0.99820	0.00589	0.99968	0.00109
6.20000	3.27318	0.99909	0.00323	0.99984	0.00058
6.40000	3.47305	0.99957	0.00169	0.99993	0.00030
6.60000	3.67299	0.99981	0.00085	0.99997	0.00014
6.80000	3.87297	0.99993	0.00041	0.99999	0.00007
7.00000	4.07296	0.99999	0.00019	1.00000	0.00003

INTEGRAL FUNCTIONS

DELTA =	5.42009	A =	0.	T* =	0.09636
DELTA* =	2.92370	H =	0.21356	R =	1.45993
THETA =	0.62438	J =	0.31934	P =	0.
THETA* =	0.93364	Z =	0.85385	U* =	0.
SIGMA =	1.52008	E =	0.51991	S* =	1.00000

TABLE A8 - SIMILAR SOLUTIONS FOR $f''(0) = 0$, $S_w = -0.8$

BETA = 0. SW = -C.8000

ETA	F	FN	FNN	G	GN
0.	C.	0.	0.46964	0.20000	0.37571
0.10000	0.00235	C.04696	0.46960	0.23757	0.37568
0.20000	0.00939	0.09391	0.46934	0.27513	0.37548
0.30000	0.02113	0.14082	0.46865	0.31265	0.37492
0.40000	0.03755	0.18762	0.46729	0.35010	0.37383
0.50000	0.05865	0.23425	0.46507	0.38740	0.37205
0.60000	0.08439	0.28060	0.46177	0.42448	0.36942
0.70000	0.11475	0.32656	0.45721	0.46125	0.36577
0.80000	0.14969	0.37199	0.45123	0.49759	0.36098
0.90000	0.18913	0.41675	0.44366	0.53340	0.35493
1.00000	0.23301	0.46067	0.43441	0.56854	0.34753
1.10000	0.28123	0.50357	0.42340	0.60286	0.33872
1.20000	0.33368	0.54529	0.41059	0.63623	0.32848
1.30000	0.39024	0.58563	0.39601	0.66851	0.31681
1.40000	0.45076	0.62443	0.37972	0.69955	0.30377
1.50000	0.51507	0.66152	0.36183	0.72922	0.28946
1.60000	0.58300	0.69675	0.34251	0.75740	0.27401
1.70000	0.65436	0.72998	0.32197	0.78399	0.25757
1.80000	0.72893	0.76111	0.30046	0.80889	0.24037
1.90000	0.80651	0.79005	0.27826	0.83204	0.22261
2.00000	0.88686	0.81675	0.25568	0.85340	0.20454
2.10000	0.96978	0.84119	0.23302	0.87295	0.18641
2.20000	1.05503	0.86336	0.21058	0.89069	0.16847
2.30000	1.14238	0.88332	0.18868	0.90666	0.15094
2.40000	1.23162	0.90112	0.16756	0.92090	0.13405
2.50000	1.32253	0.91687	0.14747	0.93349	0.11798
2.60000	1.41493	0.93066	0.12861	0.94453	0.10289
2.70000	1.50861	0.94263	0.11112	0.95411	0.08890
2.80000	1.60340	0.95293	0.09511	0.96235	0.07609
2.90000	1.69914	0.96171	0.08063	0.96937	0.06451
3.00000	1.79569	0.96911	0.06771	0.97529	0.05416
3.10000	1.89292	0.97530	0.05630	0.98024	0.04504
3.20000	1.99072	0.98042	0.04637	0.98434	0.03709
3.30000	2.08898	0.98462	0.03781	0.98770	0.03025
3.40000	2.18761	0.98803	0.03053	0.99042	0.02443
3.50000	2.28656	0.99076	0.02441	0.99261	0.01953
3.60000	2.38575	0.99294	0.01933	0.99435	0.01546
3.70000	2.48513	0.99466	0.01515	0.99573	0.01212
3.80000	2.58467	0.99600	0.01176	0.99680	0.00941
3.90000	2.68432	0.99703	0.00903	0.99763	0.00723
4.00000	2.78407	0.99782	0.00687	0.99826	0.00550
4.10000	2.88388	0.99842	0.00518	0.99874	0.00414
4.20000	2.98374	0.99887	0.00386	0.99910	0.00309
4.30000	3.08365	0.99920	0.00285	0.99936	0.00228
4.40000	3.18358	0.99945	0.00208	0.99956	0.00167
4.50000	3.28354	0.99963	0.00151	0.99970	0.00121
4.60000	3.38351	0.99976	0.00108	0.99980	0.00086
4.70000	3.48349	0.99985	0.00077	0.99988	0.00061
4.80000	3.58347	0.99991	0.00054	0.99993	0.00043
4.90000	3.68347	0.99996	0.00037	0.99997	0.00030
5.00000	3.78346	0.99999	0.00026	0.99999	0.00021

INTEGRAL FUNCTIONS

DELTA =	3.47046	A =	1.62986	T* =	0.38406
DELTA* =	1.21325	H =	0.38406	R =	0.89575
THETA =	C.46596	J =	C.60280	P =	0.56979
THETA* =	0.73135	Z =	1.86C47	U* =	0.
SIGMA =	C.57060	E =	0.80000	S* =	1.00000

TABLE A9 - SIMILAR SOLUTIONS FOR $\beta = 0$, $S_w = -0.8$

BETA = 0.28571 SW = -0.8000

ETA	F	FN	FNN	G	GN
0.	0.	0.	0.58830	0.20000	0.39460
0.10000	0.00293	0.05852	0.58199	0.23946	0.39456
0.20000	0.01168	0.11636	0.57442	0.27890	0.39429
0.30000	0.02618	0.17336	0.56545	0.31830	0.39357
0.40000	0.04632	0.22940	0.55496	0.35760	0.39216
0.50000	0.07202	0.28430	0.54285	0.39671	0.38987
0.60000	0.10314	0.33791	0.52907	0.43553	0.38648
0.70000	0.13955	0.39006	0.51357	0.47396	0.38184
0.80000	0.18110	0.44057	0.49635	0.51185	0.37578
0.90000	0.22760	0.48927	0.47745	0.54907	0.36820
1.00000	0.27888	0.53600	0.45695	0.58544	0.35900
1.10000	0.33473	0.58061	0.43498	0.62081	0.34817
1.20000	0.39493	0.62295	0.41168	0.65502	0.33571
1.30000	0.45924	0.66291	0.38728	0.68790	0.32168
1.40000	0.52743	0.70038	0.36200	0.71931	0.30621
1.50000	0.59923	0.73529	0.33611	0.74910	0.28944
1.60000	0.67440	0.76759	0.30991	0.77716	0.27159
1.70000	0.75267	0.79727	0.28367	0.80339	0.25289
1.80000	0.83377	0.82434	0.25772	0.82772	0.23361
1.90000	0.91745	0.84883	0.23232	0.85010	0.21403
2.00000	1.00345	0.87083	0.20777	0.87052	0.19444
2.10000	1.09153	0.89042	0.18429	0.88900	0.17510
2.20000	1.18146	0.90773	0.16211	0.90556	0.15629
2.30000	1.27301	0.92289	0.14138	0.92028	0.13824
2.40000	1.36597	0.93606	0.12223	0.93324	0.12116
2.50000	1.46016	0.94739	0.10474	0.94455	0.10519
2.60000	1.55539	0.95706	0.08896	0.95432	0.09047
2.70000	1.65152	0.96524	0.07487	0.96269	0.07707
2.80000	1.74840	0.97209	0.06244	0.96978	0.06502
2.90000	1.84590	0.97778	0.05159	0.97574	0.05432
3.00000	1.94392	0.98246	0.04223	0.98069	0.04495
3.10000	2.04237	0.98628	0.03425	0.98477	0.03683
3.20000	2.14115	0.98935	0.02751	0.98809	0.02987
3.30000	2.24021	0.99181	0.02189	0.99078	0.02400
3.40000	2.33950	0.99376	0.01725	0.99292	0.01909
3.50000	2.43895	0.99529	0.01347	0.99462	0.01503
3.60000	2.53854	0.99648	0.01042	0.99596	0.01172
3.70000	2.63824	0.99740	0.00798	0.99699	0.00905
3.80000	2.73802	0.99810	0.00605	0.99778	0.00691
3.90000	2.83785	0.99862	0.00454	0.99839	0.00523
4.00000	2.93774	0.99902	0.00338	0.99884	0.00392
4.10000	3.03765	0.99931	0.00249	0.99918	0.00291
4.20000	3.13759	0.99952	0.00182	0.99943	0.00213
4.30000	3.23755	0.99968	0.00131	0.99961	0.00155
4.40000	3.33753	0.99979	0.00094	0.99975	0.00112
4.50000	3.43751	0.99987	0.00067	0.99984	0.00080
4.60000	3.53750	0.99992	0.00047	0.99991	0.00056
4.70000	3.63749	0.99996	0.00033	0.99995	0.00039
4.80000	3.73749	0.99999	0.00023	0.99999	0.00027

INTEGRAL FUNCTIONS

DELTA =	3.22485	A =	1.89717	T* =	0.46072
DELTA* =	1.05922	H =	0.40107	R =	0.89250
THETA =	0.42482	J =	0.63504	P =	0.62314
THETA* =	0.67265	Z =	2.04455	U* =	0.
SIGMA =	0.92781	E =	0.87594	S* =	1.00000

TABLE A10 - SIMILAR SOLUTIONS FOR $\beta = \frac{\gamma-1}{\gamma}$, $S_w = -0.8$

BETA = 5.00000 SW = -0.8000

ETA	F	FN	FNN	G	GN
0.	0.	0.	1.28167	0.20000	0.45462
0.10000	0.00623	0.12285	1.17262	0.24546	0.45452
0.20000	0.02418	0.23420	1.05359	0.29089	0.45388
0.30000	0.05267	0.33355	0.93409	0.33620	0.45217
0.40000	0.09050	0.42121	0.82042	0.38127	0.44898
0.50000	0.13655	0.49795	0.71623	0.42593	0.44394
0.60000	0.18977	0.56483	0.62317	0.46999	0.43678
0.70000	0.24922	0.62297	0.54154	0.51321	0.42732
0.80000	0.31411	0.67350	0.47077	0.55537	0.41547
0.90000	0.38371	0.71745	0.40980	0.59623	0.40124
1.00000	0.45741	0.75575	0.35740	0.63554	0.38472
1.10000	0.53469	0.78918	0.31230	0.67310	0.36612
1.20000	0.61510	0.81841	0.27333	0.70870	0.34567
1.30000	0.69825	0.84401	0.23945	0.74218	0.32371
1.40000	0.78380	0.86644	0.20980	0.77341	0.30059
1.50000	0.87145	0.88609	0.18367	0.80228	0.27672
1.60000	0.96094	0.90327	0.16050	0.82874	0.25250
1.70000	1.05203	0.91827	0.13986	0.85278	0.22832
1.80000	1.14453	0.93132	0.12142	0.87442	0.20458
1.90000	1.23824	0.94262	0.10493	0.89372	0.18160
2.00000	1.33300	0.95236	0.09019	0.91078	0.15970
2.10000	1.42866	0.96071	0.07706	0.92570	0.13910
2.20000	1.52510	0.96782	0.06540	0.93864	0.12000
2.30000	1.62219	0.97384	0.05511	0.94976	0.10253
2.40000	1.71983	0.97889	0.04609	0.95921	0.08675
2.50000	1.81794	0.98309	0.03823	0.96716	0.07269
2.60000	1.91643	0.98657	0.03146	0.97380	0.06031
2.70000	2.01523	0.98942	0.02566	0.97928	0.04954
2.80000	2.11429	0.99173	0.02075	0.98376	0.04030
2.90000	2.21356	0.99359	0.01662	0.98739	0.03246
3.00000	2.31300	0.99508	0.01320	0.99029	0.02589
3.10000	2.41257	0.99625	0.01037	0.99260	0.02044
3.20000	2.51224	0.99717	0.00808	0.99441	0.01598
3.30000	2.61195	0.99788	0.00622	0.99583	0.01237
3.40000	2.71181	0.99843	0.00475	0.99691	0.00948
3.50000	2.81167	0.99884	0.00358	0.99774	0.00719
3.60000	2.91157	0.99915	0.00266	0.99837	0.00540
3.70000	3.01150	0.99938	0.00195	0.99883	0.00402
3.80000	3.11145	0.99955	0.00140	0.99918	0.00296
3.90000	3.21141	0.99966	0.00098	0.99943	0.00216
4.00000	3.31138	0.99974	0.00065	0.99962	0.00156
4.10000	3.41136	0.99980	0.00041	0.99975	0.00111
4.20000	3.51134	0.99983	0.00021	0.99984	0.00079
4.30000	3.61132	0.99984	0.00006	0.99991	0.00055
4.40000	3.71130	0.99984	-0.00006	0.99996	0.00038
4.50000	3.81129	0.99983	-0.00017	0.99999	0.00026

INTEGRAL FUNCTIONS

DELTA =	2.72396	A =	3.49121	T* =	0.81552
DELTA* =	0.68528	H =	0.47294	R =	0.95290
THETA =	0.32410	J =	0.77629	P =	0.87830
THETA* =	0.53197	Z =	2.97498	U* =	0.
SIGMA =	0.81882	E =	1.19487	S* =	1.00000

TABLE AII - SIMILAR SOLUTIONS FOR $\beta = 5.0$, $S_w = -0.8$

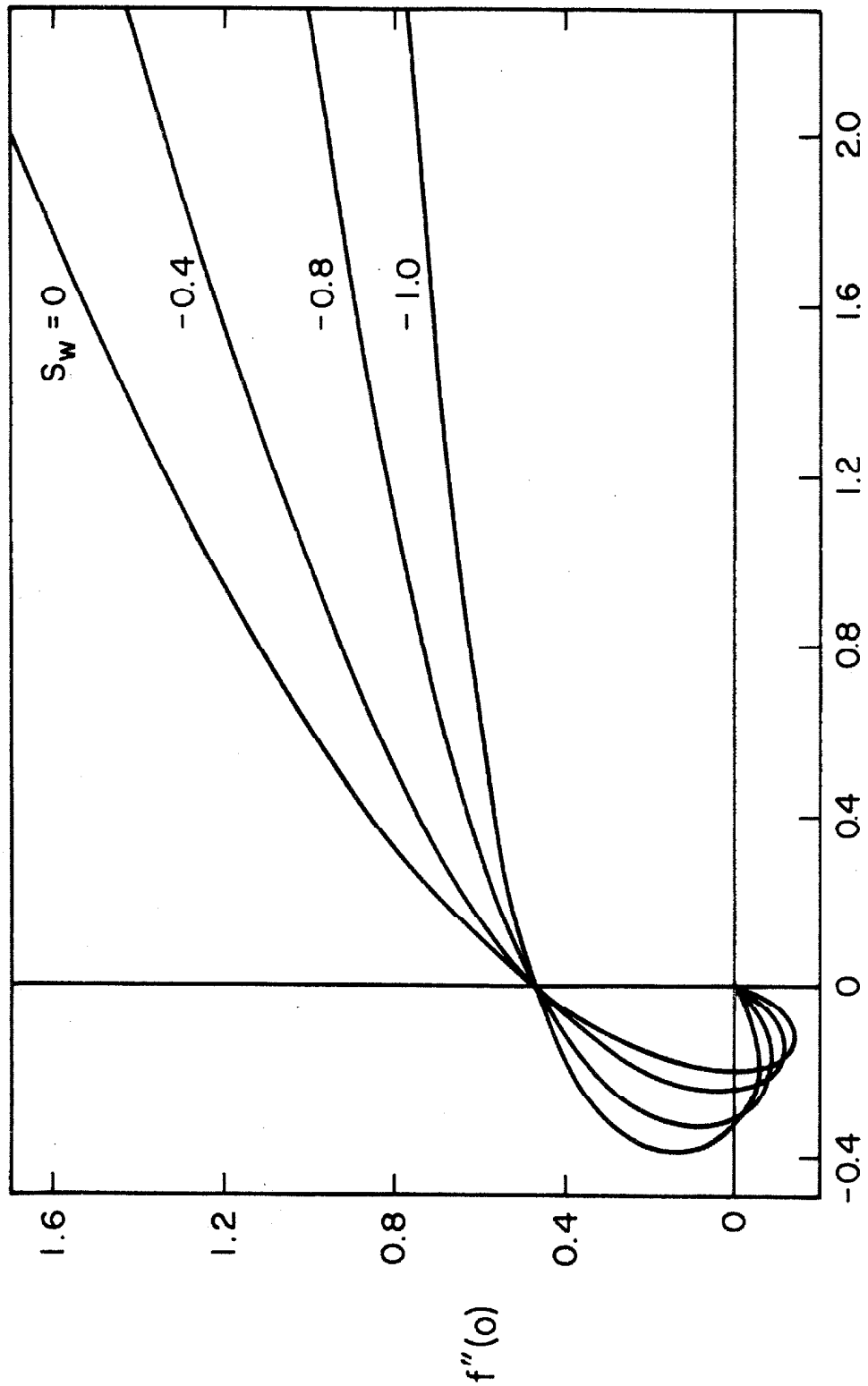

FIG. A1 DISTRIBUTION OF SHEAR FUNCTION AT WALL

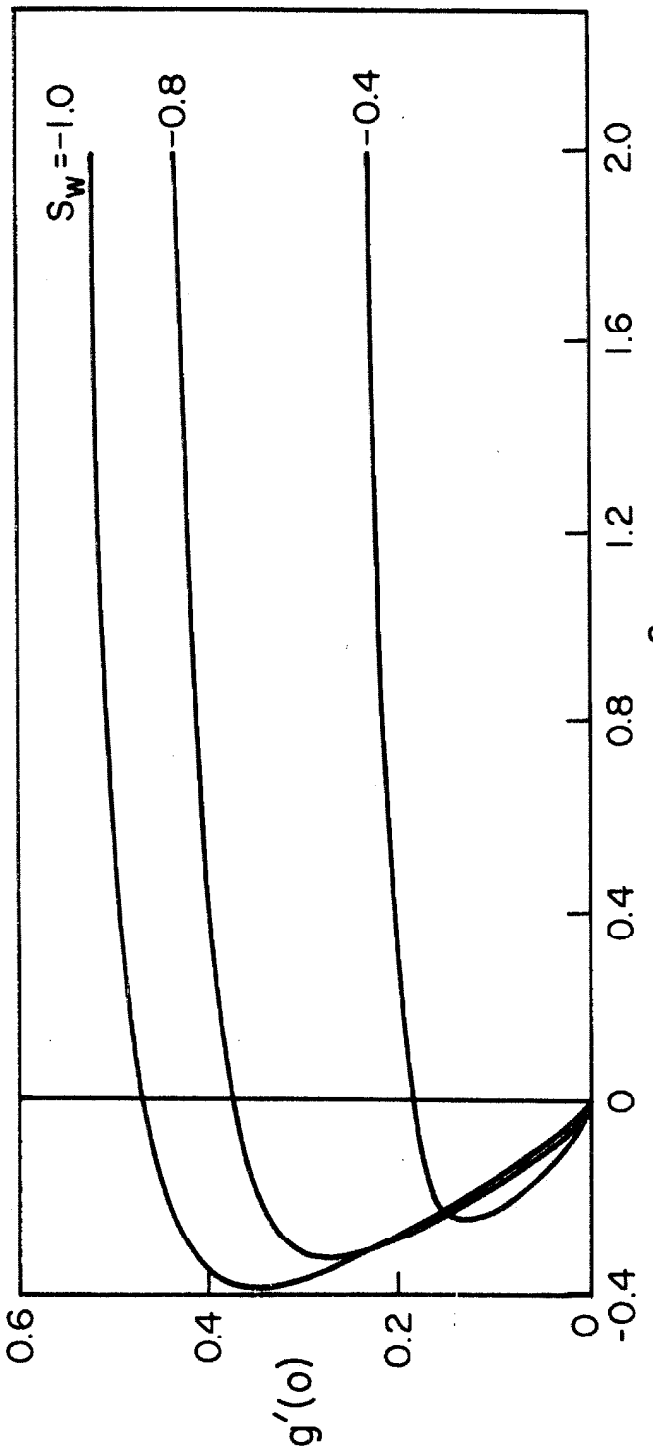

FIG. A2 DISTRIBUTION OF ENTHALPY GRADIENT AT WALL.

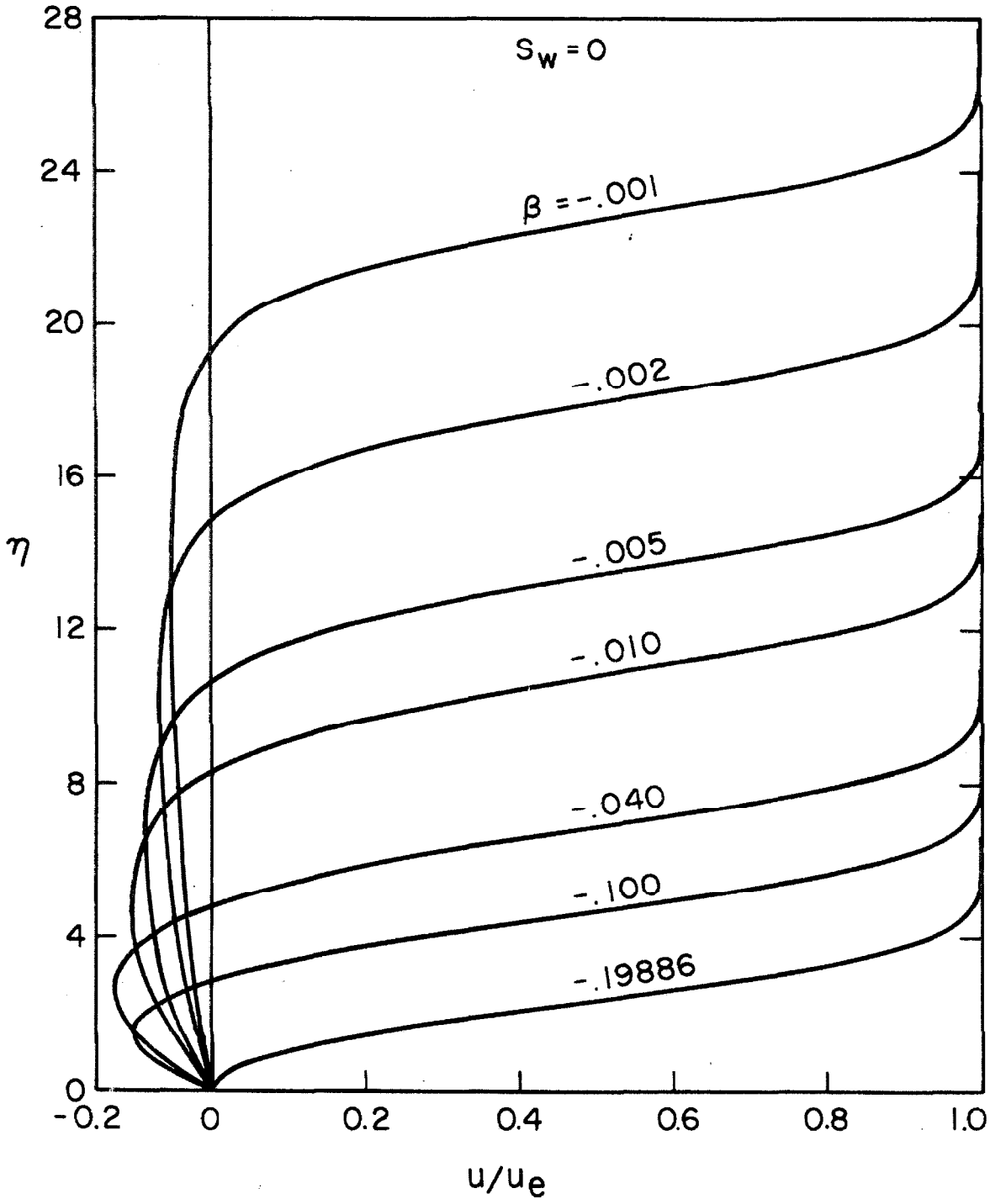

FIG. A3 REVERSED-FLOW VELOCITY PROFILES FOR $S_w = 0$

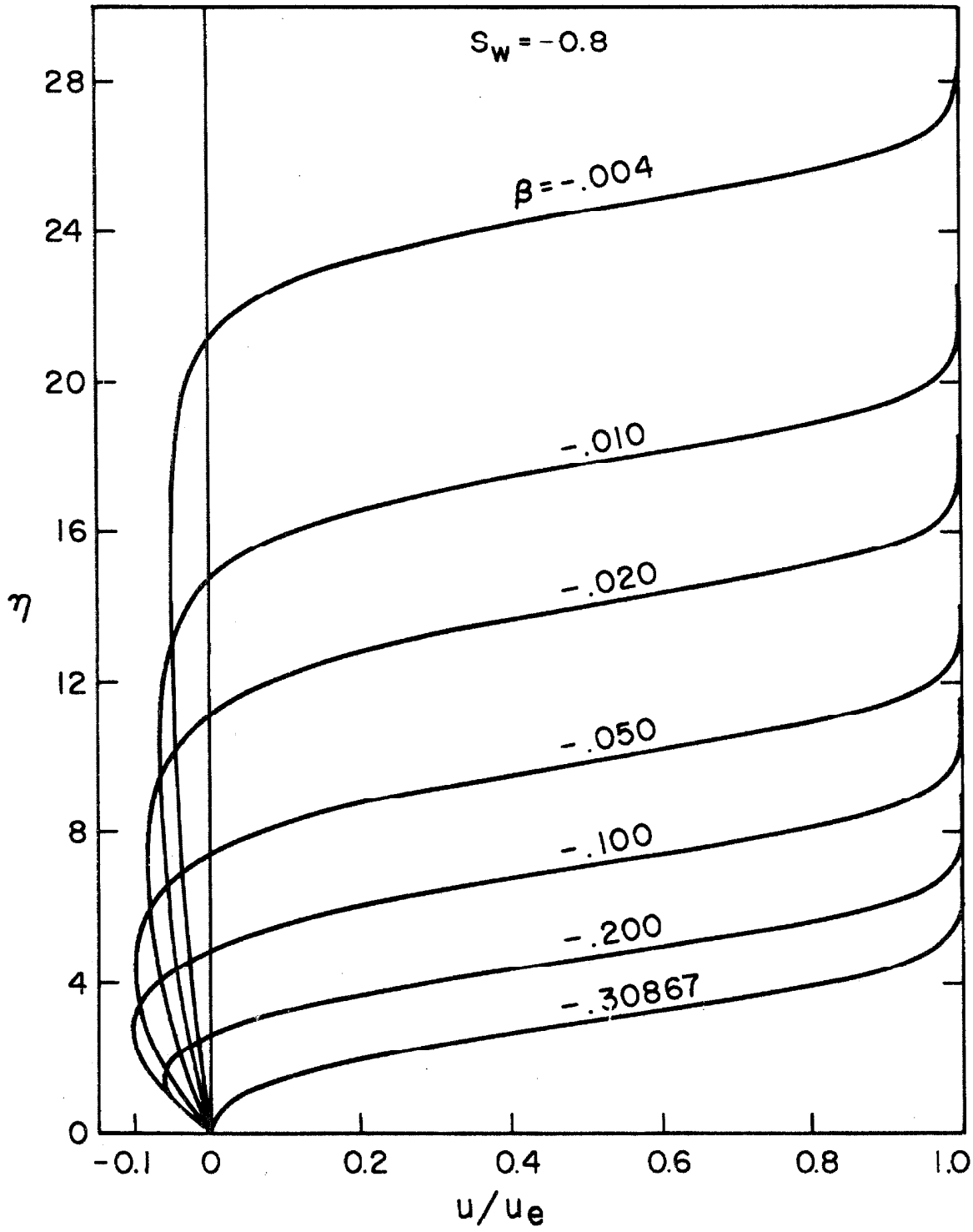

FIG. A4 REVERSED-FLOW VELOCITY PROFILES FOR $S_w = -0.8$

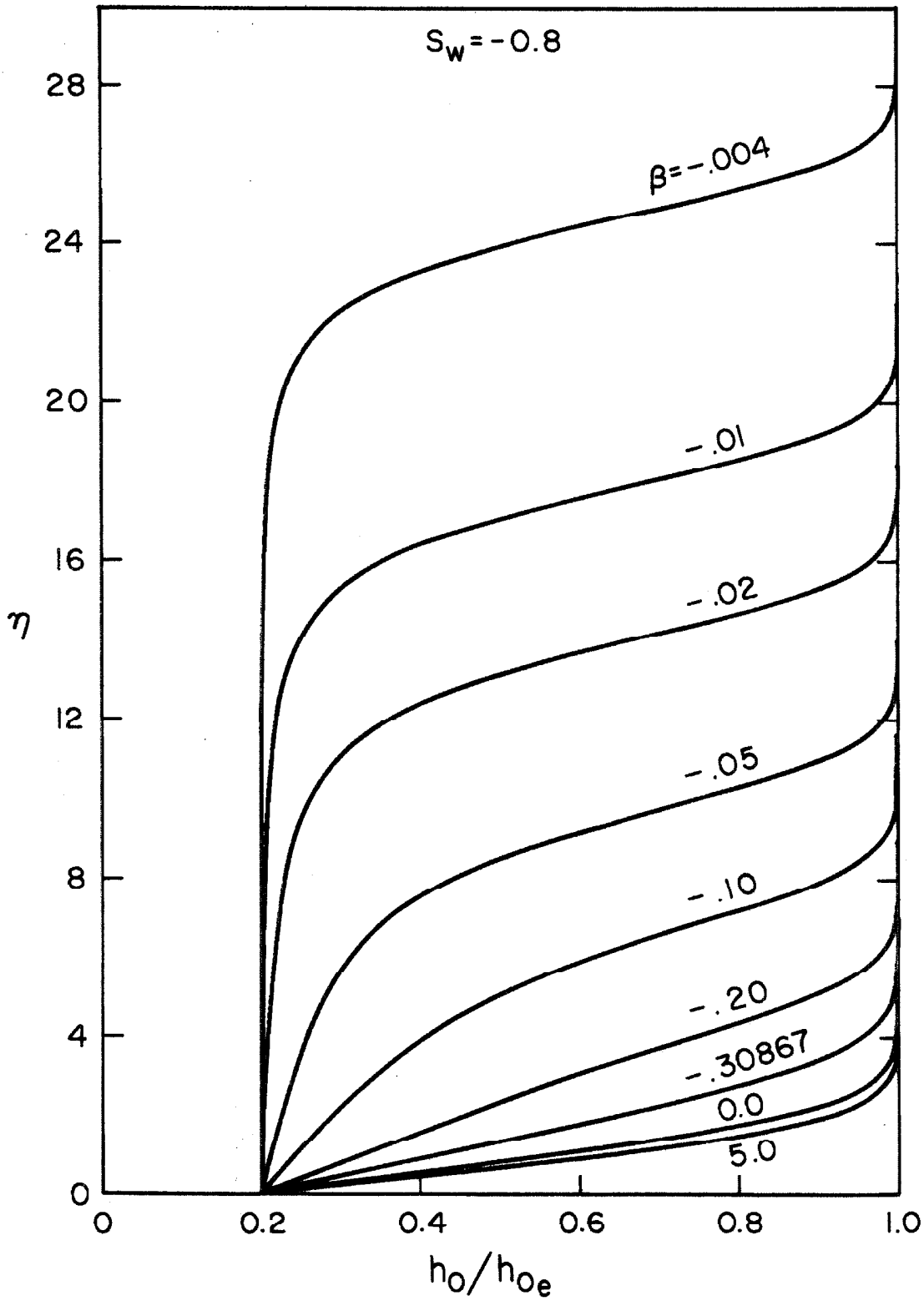

FIG. A5 TOTAL ENTHALPY PROFILES FOR $S_w = -0.8$

APPENDIX B

APPLICATION OF THE MOMENT METHOD TO ADIABATIC FLOW OVER A CIRCULAR CYLINDER*

B. 1. Introduction

An understanding of the flow structure in the near-wake region behind smooth, blunt bodies at supersonic and hypersonic speeds has been possible as a result of the experimental studies of Dewey[35] and McCarthy and Kubota[36], and the theoretical analysis of Reeves and Lees[10]. The key to the solution of this problem is the strong interaction between the viscous flow originating in the boundary layer and free shear layer, and the external inviscid flow (Fig. B1a). Unlike the situation in ordinary boundary-layer theory the pressure distribution along the wake axis is not known a priori, but must be obtained as part of the solution. Viscous-inviscid interaction occurs through the pressure field generated by the induced streamline deflection at the outer edge of the viscous layer. According to this model the compression along the wake axis is a smooth process rather than the sudden compression assumed by Chapman[37] and others.

Because of the complexity of this problem, the integral or moment method discussed in Section III must be used to describe the viscous flow. As originally shown by Crocco and Lees[6], this type of formulation leads to the conclusion that the near-wake flow is subcritical at the rear stagnation point, but passes through a throat into

---

* Published as "Laminar Boundary-Layer Separation and Near-Wake Flow for a Smooth Blunt Body at Supersonic and Hypersonic Speeds," Jean-Marie Grange, John M. Klineberg and Lester Lees, AIAA Journal, Vol. 5, No. 6, June 1967.

the supercritical region somewhere downstream of this location. At a given Mach number and Reynolds number, the base pressure or flow angle is uniquely determined by the requirement for the correct trajectory to pass smoothly through the throat. In this sense the situation is entirely analogous to the interaction caused by a compressive disturbance in highly-cooled flat-plate flow (Fig. B1b).

In order to obtain a complete solution to the base-flow problem for a blunt body, the near-wake interaction region must be joined to the boundary-layer separation-interaction region on the body. Since Reeves and Lees[10] were primarily concerned with the near-wake interaction zone behind a circular cylinder, they assumed that the separation point was held fixed at a location 125° around the body from the forward stagnation point. By using standard methods, the boundary layer growth up to this fixed point was calculated on the basis of a known (experimental) static pressure distribution, and the velocity profile was allowed to jump to the separation-point profile across a discontinuity at this location. Since only a small pressure rise is required to separate a laminar boundary layer, the external Mach number M_e was assumed constant across the jump. By using mass conservation, all quantities just downstream of the jump were determined, and these values provided the initial conditions for the constant-pressure mixing region downstream of separation. No attempt was made to match the shear-layer angle to the induced angle $\Theta(\delta)$ of the boundary layer at separation, and the constant-pressure mixing solution was joined to the near-wake interaction solution by matching M_e [or Θ], U^*, and the mass flow above the zero-velocity line.

Actually the location of the separation point on the body surface is not fixed a priori but moves in response to the pressure rise communicated upstream through the subcritical base flow. To this extent the work of Reeves and Lees is incomplete. In the present study, the separation-interaction region on the body is treated more carefully, and this region is subsequently joined to the constant-pressure mixing and near-wake interaction zones. The numerical example chosen is the identical case of an adiabatic circular cylinder at a free-stream Mach number of 6 treated in Ref. (10).

B.II. Differential Equations: Application to Flow Around an Adiabatic Circular Cylinder

As previously shown, the integral or moment method can be successfully utilized to describe interacting separated and reattaching flows, as well as attached flows, provided the velocity profiles employed as weighting functions have the qualitatively correct behavior. For flows near a solid surface, the Stewartson[4] solutions of the Falkner-Skan equation were shown to be the simplest appropriate family, including the branch corresponding to reversed-flow profiles. For adiabatic wake flows, another set of solutions of the Falkner-Skan equations with zero shear stress on the axis, also found by Stewartson,[4] is the simplest appropriate family. In every case it is essential to unhook the profiles from the pressure gradient parameter β and to describe them in terms of an independent profile parameter, $a(x)$ or $\mathcal{N}(x)$, that is not uniquely related to the local pressure gradient.

For adiabatic flow, the three independent variables of the problem are $M_e(x)$, $a(x)$ or $\mathcal{N}(x)$, and $\delta_i^*(x)$. The history of these

three parameters is determined by three first-order non-linear, ordinary differential equations, which can be written in the form:

$$F \frac{d\delta_i^*}{dx} + \delta_i^* \frac{d\mathcal{N}}{da} \frac{da}{dx} + f \frac{\delta_i^*}{M_e} \frac{dM_e}{dx} = \beta C \frac{M_N}{M_e} \frac{h}{Re_{\delta_i^*}} \tag{B1}$$

$$\mathcal{N} \frac{d\delta_i^*}{dx} + \delta_i^* \frac{d\mathcal{N}}{da} \frac{da}{dx} + (2\mathcal{N}+1) \frac{\delta_i^*}{M_e} \frac{dM_e}{dx} = \beta C \frac{M_N}{M_e} \frac{P}{Re_{\delta_i^*}} \tag{B2}$$

$$J \frac{d\delta_i^*}{dx} + \delta_i^* \frac{dJ}{d\mathcal{N}} \frac{d\mathcal{N}}{da} \frac{da}{dx} + 3J \frac{\delta_i^*}{M_e} \frac{dM_e}{dx} = \beta C \frac{M_N}{M_e} \tag{B3}$$

where all quantities are defined in Section III. For most blunt-body interactions, it is convenient to evaluate the reference conditions in the vicinity of the neck region in the near wake rather than upstream of the bow shock. Thus:

$$h = Re_{\delta_i^*} \frac{M_e}{M_N} \frac{(1+m_e)}{m_e(1+m_N)} \frac{\tan \Theta}{C} \tag{B4}$$

$$Re_{\delta_i^*} = \frac{a_N}{\nu_N} M_N \delta_i^*$$

$$C = (\mu/\mu_N)/(T/T_N) \quad \text{and} \quad \beta = \frac{a_e}{a_N} \frac{p_e}{p_N}$$

For attached and separated flows near a solid surface, the independent parameter a(x) is taken as previously defined, Eq. (31), while in wake flows upstream of the rear stagnation point:

$$a(x) = [f'(\eta)]_{f=0} = \frac{U_{\psi=0}}{U_e} = U^* \tag{B5}$$

and

$$a(x) = f'(0) = \frac{U_{\mathcal{L}}}{U_e}$$

downstream of the rear stagnation point.

For most configurations the Prandtl-Meyer relation connecting Θ with M_e given in Section III can be used, taking the curvature of the surface into account. For the circular cylinder, this relation can be written in the convenient form:

$$\nu(x) - \nu(x_o) = \alpha(x) - [\Theta(x) - \Theta(x_o)] \tag{B6a}$$

where $\nu(x_o)$ is evaluated at some reference station and $\alpha(x)$ is the inclination of the local tangent to the surface measured with respect to the inclination at x_o, i.e.

$$\alpha(x) = x/r - x_o/r \tag{B6b}$$

In this relation and in the differential equations, the independent variable x is measured along the surface of the body, hence:

$$x_{AXIS} = r[1-\cos(x/r)] \tag{B7}$$

To obtain the complete solution, the development of the boundary layer starting at the forward stagnation point should be calculated taking into account the interaction with the external flow. In the supersonic region, for example, such a calculation involves a coupling between the characteristics net and Eqs. (B1)-(B3). Since this problem is a formidable one in itself, and because the main interest in the present study lies in the separation and wake phenomena, it was decided to adopt the procedure of Reeves and Lees[10] and regard $M_e(x)$ as given to the jump location. The pressure distribution on the forward part of the cylinder was taken from McCarthy's[36] measurements, and the variations of M_e and $d(M_e)/d(x/r)$ were

computed assuming isentropic flow around the cylinder. The continuity equation, Eq. (B1), can therefore be dropped and only Eqs. (B2) and (B3) considered, which can be rewritten in terms of the variable

$$\delta_r^* = \frac{1}{C}\left(\frac{a_N}{\nu_N} M_N r\right)\left(\frac{\delta_i^*}{r}\right)^2 \tag{B8}$$

and solved for the unknown first derivatives, yielding:

$$\frac{d\delta_r^*}{d(x/r)} = \frac{\beta M_N\left(P\frac{dJ}{d\nu} - R\right) + \left[3J - (2\nu+1)\frac{dJ}{d\nu}\right]\delta_r^* \frac{dM_e}{d(x/r)}}{\frac{M_e}{2}\left(\nu\frac{dJ}{d\nu} - J\right)} \tag{B9}$$

$$\frac{da}{d(x/r)} = \frac{\beta M_N (R\nu - PJ) + J(1-\nu)\,\delta_r^* \frac{dM_e}{d(x/r)}}{M_e \delta_r^* \frac{d\nu}{da}\left(\nu\frac{dJ}{d\nu} - J\right)} \tag{B10}$$

Initial values for $\delta_r^*(0)$ and $a(0)$ are given by the requirements for boundedness of the derivatives at the forward stagnation point, where $M_e = 0$ and $x/r = 0$. This condition requires that the numerators on the right-hand side of Eqs. (B9) and (B10) vanish, i.e.:

$$3JP = (2\nu+1)R \tag{B11}$$

or

$$a_{stag} = 2.967$$

and

$$(\delta_r^*)_{stag} = \frac{\beta M_N P}{(2\nu+1)\left[dM_e/d(x/r)\right]_{x/r=0}} \tag{B12a}$$

According to McCarthy's data $\left[dM_e/d(x/r)\right]_{x/r=0} \approx 1$ and $M_N = 2.5$ (neck Mach number for a free-stream Mach number of 6.0), hence for this case

$$(\delta_r^*)_{stag} = 26.97 \tag{B12b}$$

One can show by a linearization of Eqs. (B9) and (B10) around a_{stag} and $(\delta_r^*)_{stag}$ that the stagnation point is a saddle point in the $(a-\delta_r^*)$ plane; therefore the integration of the equations must be initiated by perturbing the solution away from the critical point by a small amount. The results of the integration for the distributions of a, δ_r^* and the normalized physical boundary layer thickness are shown in Fig. B2, where:

$$\frac{\delta}{r}\sqrt{\frac{a_N}{\nu_N}M_N r} = \left(\frac{1+m_e}{1+m_N}\right)^{\frac{\gamma+1}{2(\gamma-1)}}\left[m_e(1+\lambda)+1+Z\right]\sqrt{\delta_r^*} \qquad (B13)$$

One can see that at $(x/r) = 1.20$, the parameter a(x) exceeds the maximum value (3.92) obtained from the similar solutions of the Falkner-Skan equation, indicating that the profiles are actually non-similar downstream of that point. In order to continue the solution with this family of velocity profiles, it was assumed that a(x) remained constant and equal to 3.92, and that all integral functions retained their values at a = 3.92, i.e., the profiles were assumed to take a constant shape for $(x/r) > 1.20$. Eq. (B10) was therefore dropped and Eq. (B9) integrated downstream of that location; this equation becomes:

$$\frac{d\delta_r^*}{d(x/r)} = \frac{2\beta M_N}{M_e}\left[\frac{(2\lambda+1)R-3JP}{J(1-\lambda)}\right]_{a=3.92} \qquad (B14)$$

At $x/r = 1.20$, the outer flow is supersonic and the angle of the streamline at the edge of the boundary layer with the wall can be calculated from the continuity equation, Eq. (B1), written in the form:

$$\tan\Theta = \frac{1}{\sqrt{\left(\frac{a_N}{\nu_N}M_N r\right)\delta_r^*}}\left(\frac{1+m_e}{1+m_N}\right)^{\frac{\gamma+1}{2(\gamma-1)}} m_e\left[\frac{F}{2}\frac{d\delta_r^*}{d(x/r)}+\frac{f\delta_r^*}{m_e}\frac{dM_e}{d(x/r)}\right] \qquad (B15)$$

since a(x) is held constant.

It is now possible to calculate the subsequent development of the viscous layer starting from an arbitrary point at which the solution is assumed known from Eqs. (B9)-(B15). Returning to the full set of equations, Eqs. (B1)-(B3), one finds that the viscous flow becomes supercritical at a = 3.92 and M_e = 2.4, corresponding to x/r = 1.69. The wake flow is initially subcritical, however. In order to join these two regions, the flow must experience a sudden jump on the body surface from a supercritical to a subcritical state, followed by a smooth compression and flow separation leading into the near-wake region.

B. III. Adiabatic Supercritical-Subcritical Jump Conditions

The jump conditions for the general case of non-adiabatic flow have been derived in Section V. The relative change in Mach number across an adiabatic supercritical-subcritical jump is extremely small, and in this situation the pressure change can be connected to the velocity difference by the approximate relation

$$p_2 - p_1 \approx -\tfrac{1}{2}\left[(\rho_e u_e)_1 + (\rho_e u_e)_2\right](u_{e_2} - u_{e_1}) \qquad \text{(B16)}$$

Using this expression in the jump relations, Eqs. (82)-(89), Eq. (88) becomes

$$\left[m_{e_2} F_2 \mathcal{Y}_1 - m_{e_1} F_1 \mathcal{Y}_2\right] = \left[1 - \frac{u_{e_2}}{u_{e_1}}\right]\left[Z_2 \mathcal{Y}_2 - \left(\frac{\rho_{e_1} u_{e_1} + \rho_{e_2} u_{e_2}}{2\rho_{e_2} u_{e_2}}\right)\right.$$

$$\left.\left(m_{e_2} F_2 + Z_2\right)\right] m_{e_1} F_1 - \left[\frac{\rho_{e_1} u_{e_1}}{\rho_{e_2} u_{e_2}} - 1\right]\left[m_{e_2} F_2 + Z_2\right] \mathcal{Y}_1 \qquad \text{(B17)}$$

while the combination of Eqs. (88) and (89) for adiabatic flow can be written:

$$[\mathscr{K}_1 J_2 - \mathscr{K}_2 J_1] = \left[1 - \frac{u_{e_2}}{u_{e_1}}\right] \left\{\left[Z_2 - \mathscr{K}_2 - \left(\frac{\rho_{e_1} u_{e_1} + \rho_{e_2} u_{e_2}}{2\rho_{e_2} u_{e_2}}\right)(m_{e_2} F_2 + Z_2)\right] J_1 \right.$$

$$\left. - \left[\left(1 + \frac{u_{e_2}}{u_{e_1}}\right)(Z_2 - J_2) - \frac{2u_{e_2}}{u_{e_1}}\left(\frac{\rho_{e_1} u_{e_1} + \rho_{e_2} u_{e_2}}{2\rho_{e_2} u_{e_2}}\right)(m_{c_2} J_2 + Z_2)\right] \mathscr{K}_1 \right\} \quad \text{(B18)}$$

Since these equations involve the differences between quantities which are nearly equal, it is possible to obtain an expansion of the downstream values $\mathscr{K}_2$ and M_{e_2} in terms of the known upstream conditions. Defining the differences η and μ such that

$$\eta = \mathscr{K}_1 - \mathscr{K}_2$$
$$\mu = \frac{M_{e_1}}{M_{e_2}} - 1 \quad \text{(B19)}$$

the jump relations, Eqs. (B17)-(B18), can be expanded in terms of these functions. For example:

$$1 - \frac{u_{e_2}}{u_{e_1}} = \left(\frac{1}{1+m_{e_1}}\right)\mu - \frac{1}{1+m_{e_1}}\left[1 - \frac{3m_{e_1}}{2(1+m_{e_1})}\right]\mu^2 + \cdots$$

$$J_1 - J_2 = \left(\frac{dJ}{d\mathscr{K}}\right)_1 \eta - \left(\frac{d^2 J}{d\mathscr{K}^2}\right)_1 \frac{\eta^2}{2} + \cdots$$

Retaining terms to second order, Eqs. (B17)-(B18) can be expressed in the form:

$$A_1\eta + A_2\eta^2 + A_3\eta\mu + A_4\mu + A_5\mu^2 = 0$$
$$B_1\eta + B_2\eta^2 + B_3\eta\mu + B_4\mu + B_5\mu^2 = 0 \quad \text{(B20)}$$

where the coefficients, evaluated at the upstream station, are:

$$A_1 = J - \mathscr{V}\frac{dJ}{d\mathscr{V}} \tag{B21}$$

$$A_2 = \frac{1}{2}\mathscr{V}\frac{d^2J}{d\mathscr{V}^2}$$

$$A_3 = 2\mathscr{V}\frac{dJ}{d\mathscr{V}} - J$$

$$A_4 = (1-\mathscr{V})\,J$$

$$A_5 = \mathscr{V}[2m_eJ+J+Z]\left[\frac{1}{(1+m_e)^2}\right] - J(1-\mathscr{V})\left[1+\frac{m_e}{2(1+m_e)}\right]$$
$$+\frac{1}{2}[(2\mathscr{V}-J)Z - (1+m_e-m_e\mathscr{V})J]\left[\frac{M_e^2-1}{(1+m_e)^2}\right]$$

and

$$B_1 = 1 + m_e$$

$$B_2 = 0$$

$$B_3 = \left[1+m_e+m_e\mathscr{V}+\mathscr{V}\frac{dZ}{d\mathscr{V}}\right]\left[\frac{M_e^2-1}{1+m_e}\right] - [1+m_e-m_e\mathscr{V}]$$

$$B_4 = (1+\mathscr{V})[1+m_e-m_e\mathscr{V}) - \mathscr{V}[1+m_e+m_e\mathscr{V}+Z]\left[\frac{M_e^2-1}{1+m_e}\right]$$

$$B_5 = (1+\mathscr{V})\left[3m_e\mathscr{V} - (1+m_e+m_e\mathscr{V})\left(1+\frac{m_e}{2(1+m_e)}\right)\right]$$
$$-\mathscr{V}[1+m_e+m_e\mathscr{V}+Z]\left[1-\frac{3m_e}{2(1+m_e)} + M_e^2\left(\frac{2\gamma-1}{\gamma-1}\frac{m_e}{1+m_e} - \frac{5}{2}\right)\right]$$
$$\left[\frac{1}{1+m_e}\right] + \frac{1}{2}[1+m_e+m_e\mathscr{V}][(1+m_e)(1+\mathscr{V}) - Z+\mathscr{V}]\left[\frac{M_e^2-1}{(1+m_e)^2}\right]$$

Using these relations, solutions of the two algebraic equations, Eqs. (B20), are relatively easy to obtain. Some typical jumps are shown in Fig. B3.

B.IV. Flow Field Downstream of the Jump

Between the critical point on the cylinder at x/r = 1.69 and the pressure minimum at x/r = 2.13, the quantities δ_i^*, a and M_e are known (Fig. (B2)), hence a possible jump to subcritical conditions can be computed at each location x/r. Also, the streamline inclination Θ_1 just upstream of the jump can be obtained from Eq. (B15), and Θ_2 can be calculated from Θ_1 by adding the turning angle across the weak compression. Thus at each location $(x/r)_2 = (x/r)_1$, initial conditions $\delta_{i_2}^*$, a_2, M_{e_2} and Θ_2 required to start the computation of the interaction between the subcritical viscous layer downstream of the jump and the outer flow are known. These subcritical trajectories are calculated by integrating the full set of equations, Eqs. (B1)-(B3), using the Prandtl-Meyer relation including the effect of surface curvature (Eq. (B6)).

In Fig. B4, two subcritical trajectories through separation and into the constant-pressure mixing region are shown for the eigensolutions obtained in Section B. VI. The positive pressure gradient decreases rapidly downstream of separation, partly because the body surface is falling away from the tangent to the local streamline at the outer edge of the boundary layer. For a typical case ($Re_{\infty, d}=4.8\times10^4$), the angular turn measured around the cylinder surface from the jump location to the beginning of the pressure plateau is approximately 13°.

In the constant-pressure mixing region, the basic equations are considerably simplified by dropping both the term containing $\frac{dM_e}{dx}$ and the continuity equation, Eq. (B1). These reduced equations were solved for $\frac{d(\delta_i^*/r)}{da}$ and $\frac{d(x/r)}{da}$ and integrated to a value of a = 0.7,

corresponding to $u^*_{mixing} = 0.56$.

B. V. Near-Wake Interaction Region and Joining Conditions

Since the location of the separation point on the body and the length of the constant-pressure mixing region are not known a priori, it is more convenient to begin the calculation of the near-wake interaction solution at the rear stagnation point, where a = 0. Starting at this point with a given value of $(\delta_i^*/r)_{rsp}$ and a given value of $Re_{N,d}$, Reeves and Lees[10] have shown that there is only one value of M_e at the rear stagnation point which allows the solution to pass through the throat in the wake. The procedure adopted was to integrate the basic equations, Eqs. (B1)-(B3), downstream of the rear stagnation point with various trial values of $(M_e)_{rsp}$ until a solution was obtained which passed as close to the singularity at D = 0 as possible. Here P = 0 in Eq. (B2), the curvature term $\alpha(x)$ in the Prandtl-Meyer relation (Eq. (B6)) is absent, and the curve-fits to the functions $\mathcal{Y}$, R, J, Z for wake flows given in Ref. (10) were utilized in the integration. It is more convenient to take the reference point far downstream, hence $\Theta = \nu(M_{\infty+}) - \nu(M_e)$, where the conditions $M_{free\text{-}stream} = 6.0$, or $(M_{\infty+})_{wake} = 2.5$ were selected. Once the correct value of $(M_e)_{rsp}$ is determined for a given choice of $(\delta_i^*/r)_{rsp}$ and $Re_{\infty,d}$, Eqs. (B1)-(B3) can be integrated in the upstream direction away from the rear stagnation point in order to generate a family of possible wake solutions.

At some point in the near-wake region the constant-pressure mixing solution must be joined to the wake interaction solution. For a given value of $Re_{\infty,d}$ and $M_{free\text{-}stream}$ the boundary-layer growth on the cylinder up to the jump location is determined, but the jump

can be placed at any point on the body downstream of the critical point ($\frac{x}{r} = 1.69$). For a given jump location the flow is determined completely up to the beginning of the pressure plateau, but the length of the constant-pressure mixing region is arbitrary; any point on the mixing solution curve corresponding to a certain U* is a possible joining point to the wake interaction solution. For an assumed value of $(\delta_i^*/r)_{rsp}$ the length of the wake interaction upstream of the rear stagnation point is also arbitrary. Thus, four conditions are required at the matching point in order to determine the complete solution uniquely.

Three conditions can be obtained directly from the requirements for the continuity of M_e, of U*, and of the mass flow above the dividing streamline, which is proportional to $M_e \delta_i^* Z$. The fourth condition is a geometric constraint: the length of the constant-pressure mixing zone and the wake thickness $\frac{h}{r}$ at the joining point must be so determined that the angle Θ of the dividing streamline is compatible with the Prandtl-Meyer turning angle for $(M_e)_{pp}$, i.e. (Fig. B1),

$$\frac{\left(\frac{d_1}{r} - \frac{h}{r}\right)}{(x/r)_{mixing}} = \left[\nu(M_e)_{pp} - \nu(M_{\infty+})\right] \tag{B22}$$

where

$$\frac{d_1}{r} = \left(1 + \frac{\delta_{pp}}{r}\right) \sin\left[\pi - \left(\frac{x}{r}\right)_{pp}\right] \tag{B23}$$

These four joining conditions uniquely determine the complete solution for a given pair of values of $Re_{N,d}$ and $M_{\infty+}$.

B. VI. Complete Solutions

In order to illustrate the method of solution previously described, a typical computation is shown for the adiabatic circular

cylinder at $M_{\infty+} = 2.5$ and $Re_{N,d} = 8,000$, corresponding to free-stream conditions $M_\infty = 6$ and $Re_{\infty,d} = 4.8 \times 10^4$. A useful diagram employed in matching the wake interaction and constant-pressure mixing regions is given in Fig. B5. For every assumed value of $(\delta_i^*/r)_{rsp}$, the wake interaction eigensolution is integrated in the upstream direction away from the rear stagnation point to produce a locus of pairs of values of M_e and U^*; these curves are labelled "wake solution" in Fig. B5. Every point on each of these curves also corresponds to known local values of (δ_i^*/r) and Z. For a given trial jump location on the body surface, the separating flow is determined to the beginning of the pressure plateau; hence $M_e = (M_e)_{pp}$ is known in the constant-pressure mixing region. The horizontal dashed lines in Fig. B5 represent the constant-pressure mixing solutions for U^* as a function of (δ_i^*/r), for each assumed jump location. At the intersection of these dashed lines and the solid curves calculated from the wake interaction solution, M_e and U^* are automatically matched. The correct choice of the remaining two unknowns $(x/r)_{jump}$ and $(\delta_i^*/r)_{rsp}$ is determined by matching the mass flow above the dividing streamline and by satisfying the geometric constraint embodied in Eqs. (B22) and (B23).

Fig. B6 shows a comparison between the predicted static pressure distribution on the circular cylinder at $Re_{\infty,d} = 4.8 \times 10^4$ and McCarthy's[36, 38] experimental measurements at the Reynolds number of 4.7×10^4. Evidently the computed base pressure $[p(180°)]$ is somewhat low, but the location of separation on the cylinder is predicted quite accurately. Of course in practice the jump occurs over

a distance of one or two boundary-layer thicknesses.

The predicted effect of free-stream Reynolds number is shown in Fig. B7. As expected, the jump and the separation points both move forward on the cylinder with increasing Reynolds number, and this behavior agrees qualitatively with experimental observations.[36]

The constant-pressure and near-wake interaction regions between the pressure plateau and a point near the neck are shown in Fig. B8. As observed by Reeves and Lees[10] the predicted rear stagnation point is located somewhat aft of Dewey's[35] measured location. Presumably the accuracy of the wake interaction solution can be improved, especially at low Reynolds numbers, by utilizing the two-parameter velocity profiles of Ref. (39), rather than the one-parameter profiles employed here.

As suggested by A. Roshko[40] it is often useful to examine the limiting case of infinite Reynolds number in order to clarify one's ideas. In the present problem, the near wake flow consists mainly of the constant-pressure mixing region in this limit, and U* approaches the Chapman value. As shown in Ref. (10), the recompression pressure ratio $\frac{p_{\infty+}}{p_b}$ also approaches a limiting value, which differs from the value obtained from Chapman's sudden isentropic compression model. As a result, the angle of inclination of the free shear layer also approaches a limiting value. Since the pressure rise required to separate the laminar boundary layer on the cylinder $\to 0$ as $Re_\infty \to \infty$, the subcritical viscous interaction region downstream of the jump shrinks to zero. The jump and separation-point locations coincide, and this point on the body is determined by the jump conditions and

the limiting value of $\frac{p_{\infty+}}{p_b}$. Once this point is known, the location of the rear stagnation point is determined by the simple geometric relation, Eq. (B22) and (B23),

$$\frac{d_1}{x} = \nu(M_e)_{pp} - \nu(M_{\infty+}),$$

where $\frac{\delta_{pp}}{r}$ and $\frac{h}{r} \to 0$

while $M_{e_{pp}}$ coincides with the value of the Mach number just downstream of the jump. Of course the length of the near-wake interaction region in the vicinity of this point also shrinks to zero in this limit. (As observed by Roshko[40] the axisymmetric case is still something of a mystery.)

This illustrative example demonstrates that the theoretical approach employing an integral or moment method is fully capable of predicting the location of separation and the entire near-wake interaction region for laminar flow without the introduction of additional ad hoc assumptions. The extension of the calculations to show the effect of a highly-cooled surface on the location of separation is presently under investigation at this laboratory. The general method described here is applicable not only to blunt bodies, but also to slender bodies with smooth bases, provided the radius of curvature at the base is large compared to the boundary-layer thickness.

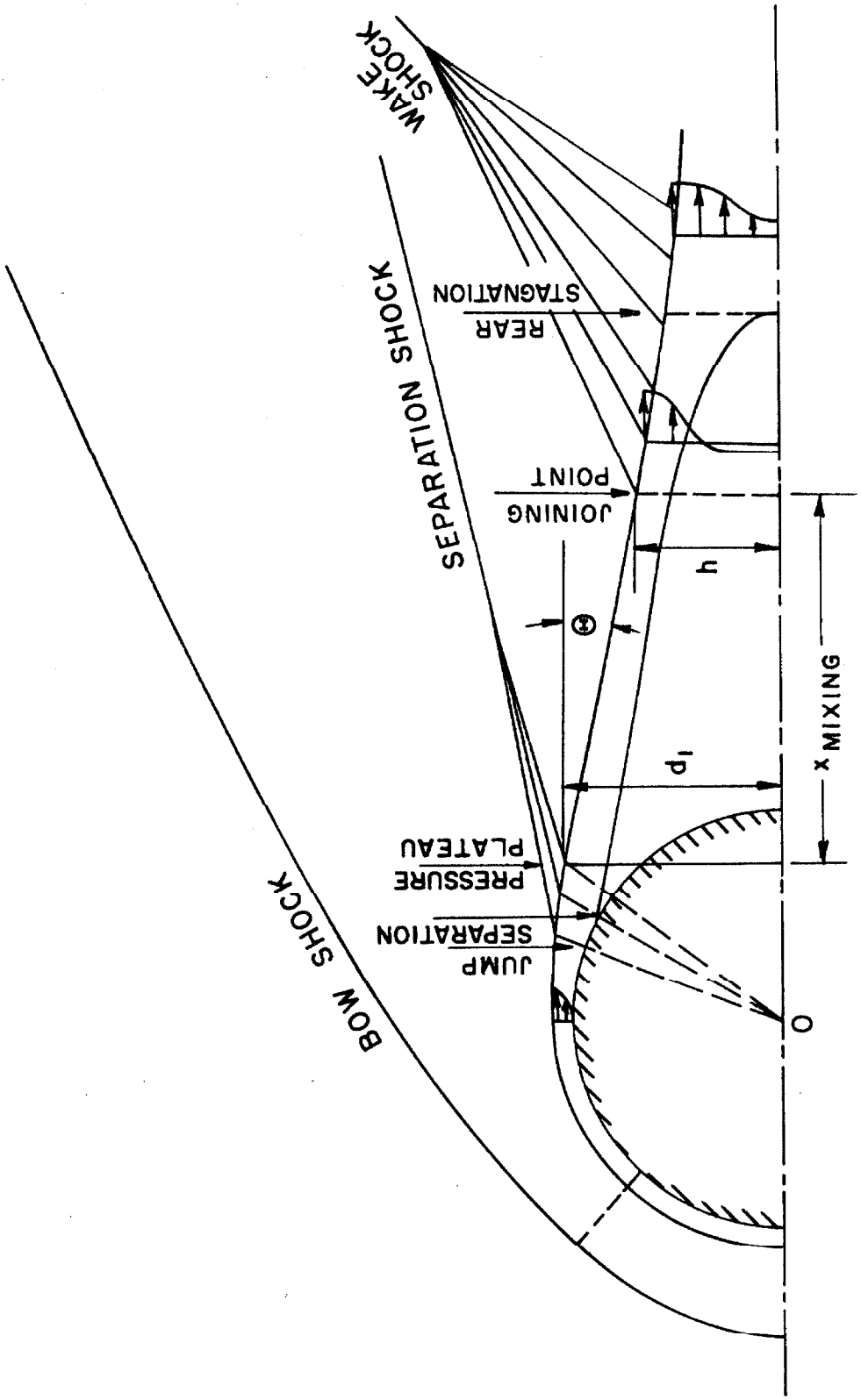

FIG. B1a SEPARATION AND NEAR-WAKE INTERACTION REGIONS FOR A BLUNT BODY AT HYPERSONIC SPEEDS (SCHEMATIC)

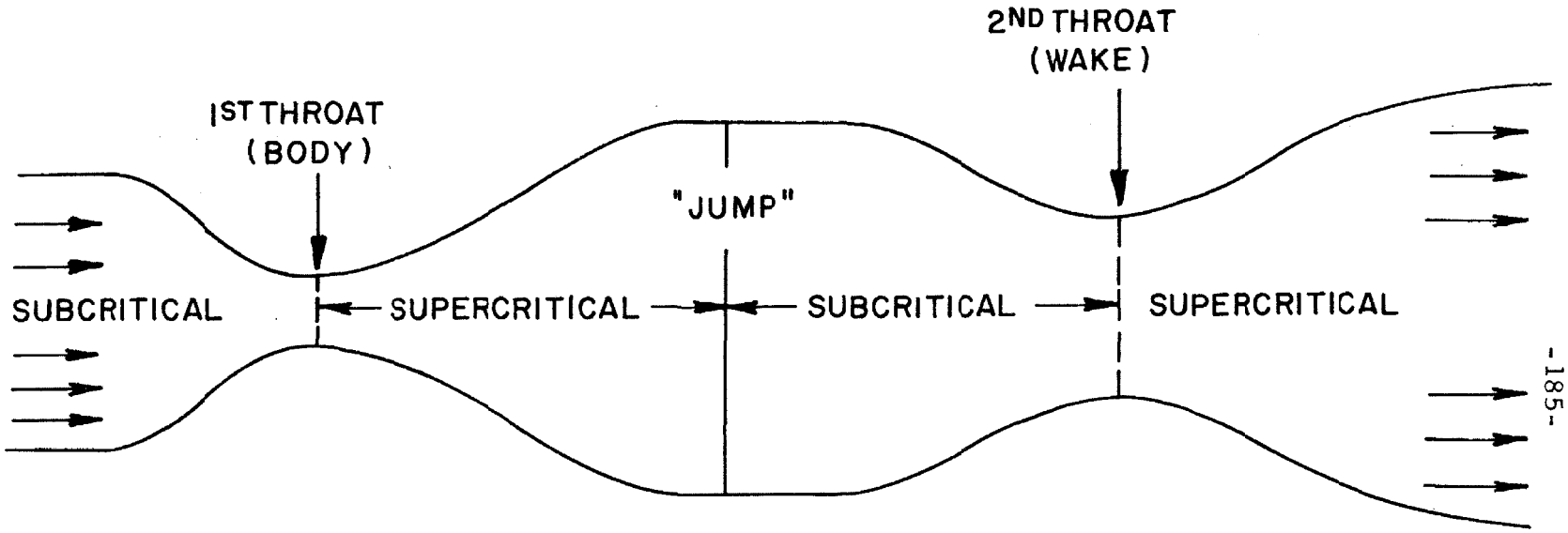

FIG. B1b SCHEMATIC REPRESENTATION OF INTERACTING VISCOUS FLOW OVER BLUNT BODY

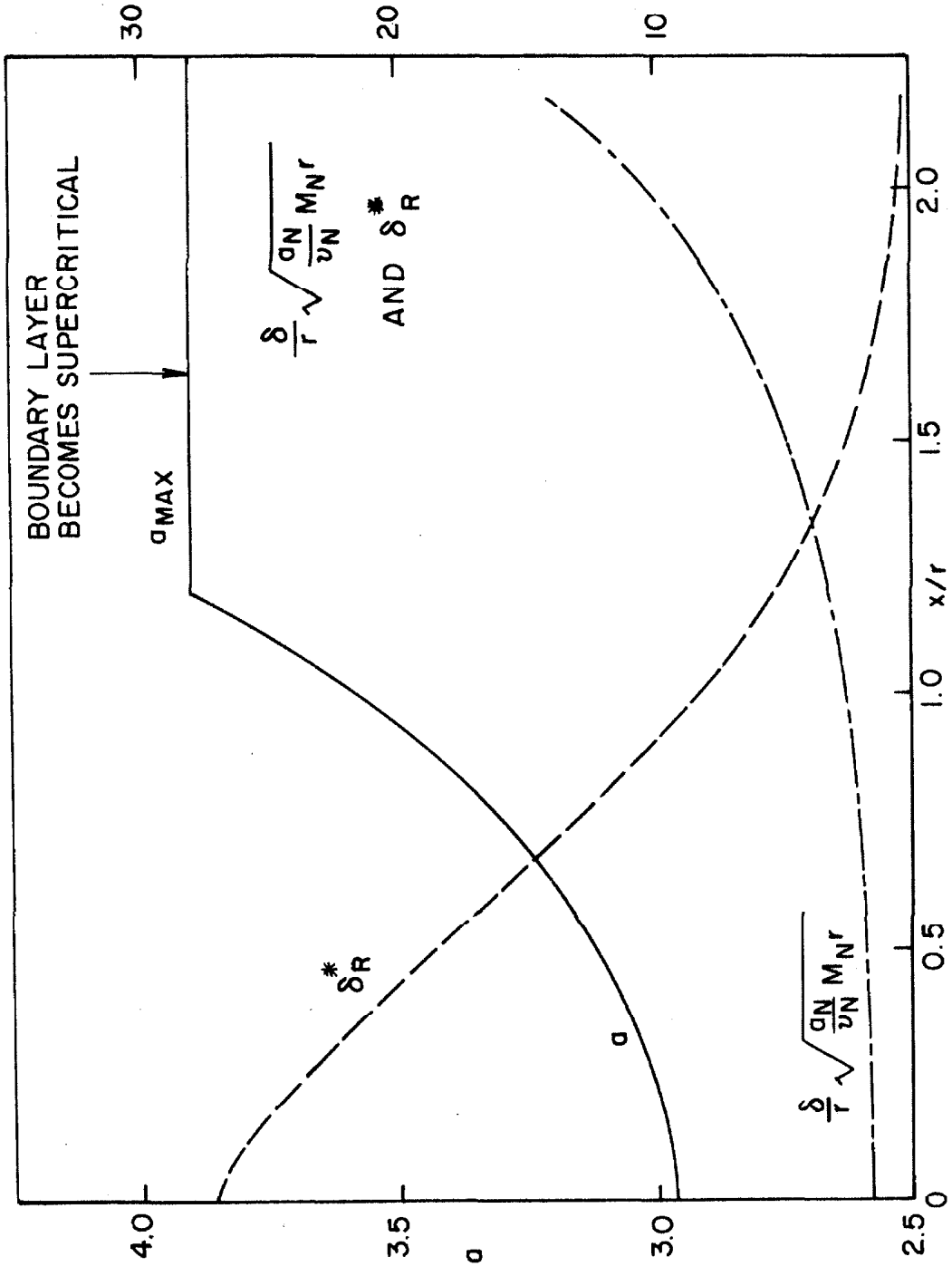

FIG. B2 DISTRIBUTION OF δ_r^*, $\frac{\delta}{r}$ AND a(x) OVER ADIABATIC CYLINDER

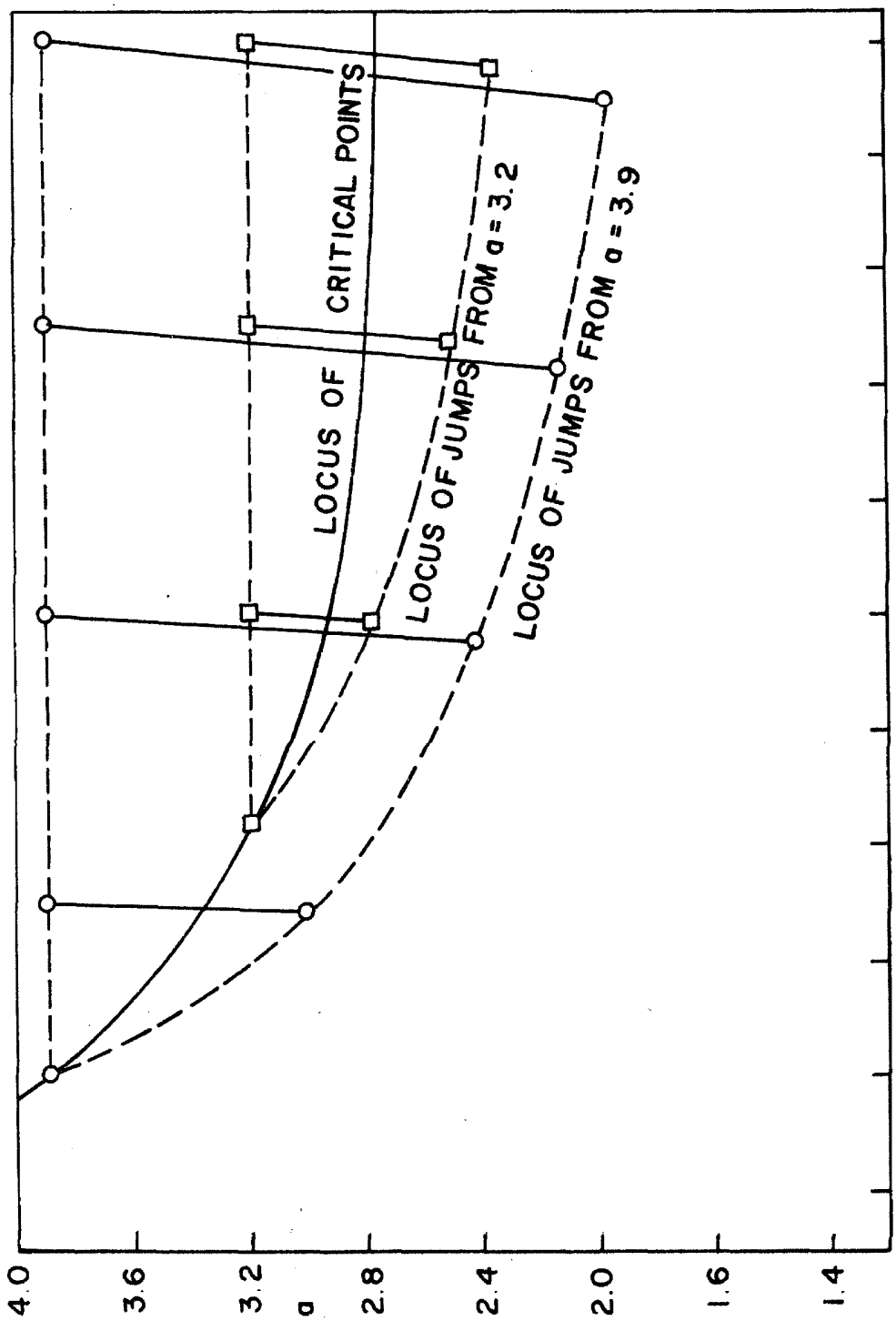

FIG. B3 TYPICAL LAMINAR ADIABATIC SUPERCRITICAL-SUBCRITICAL JUMPS

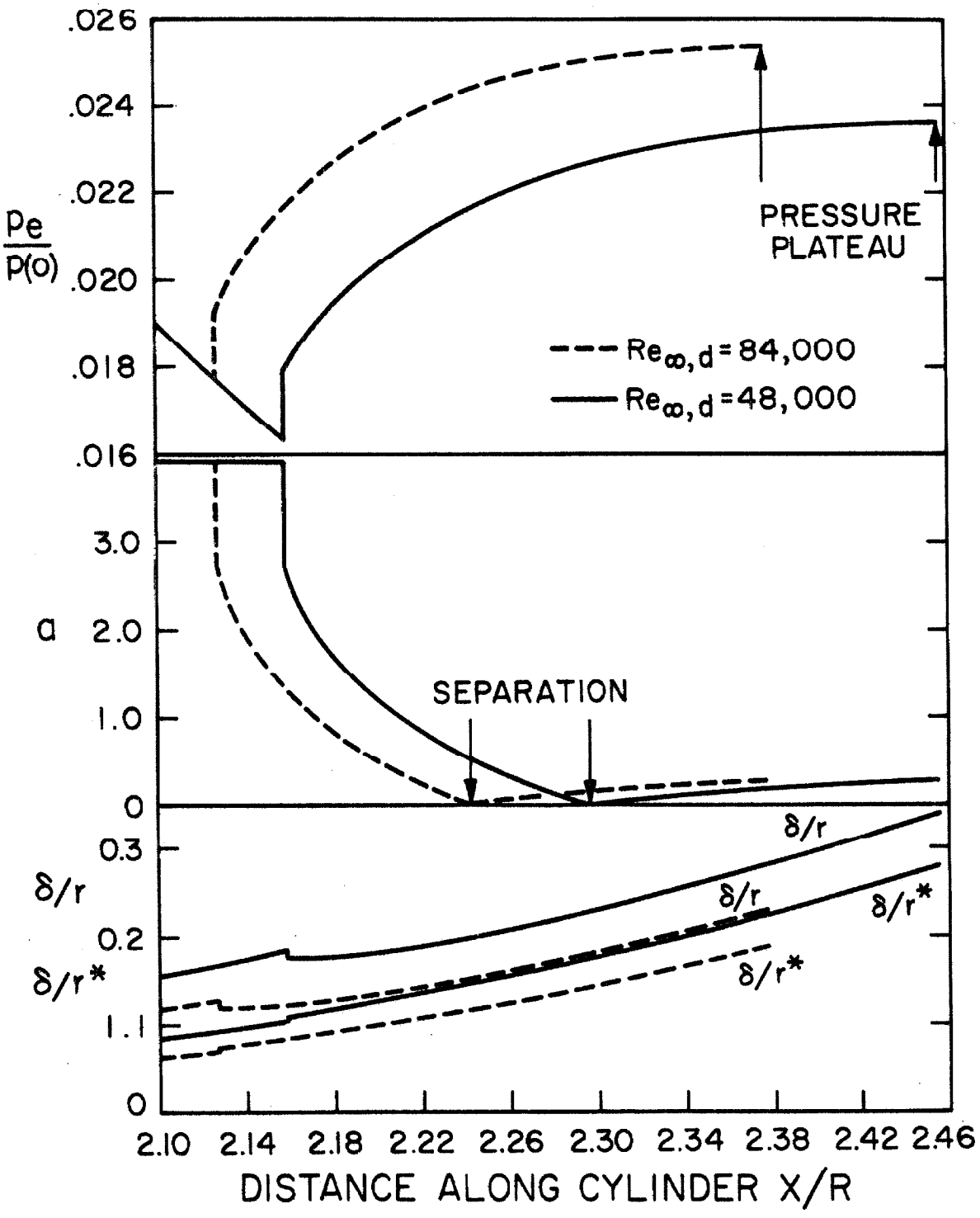

FIG. B4 INTERACTIONS IN VICINITY OF JUMP.

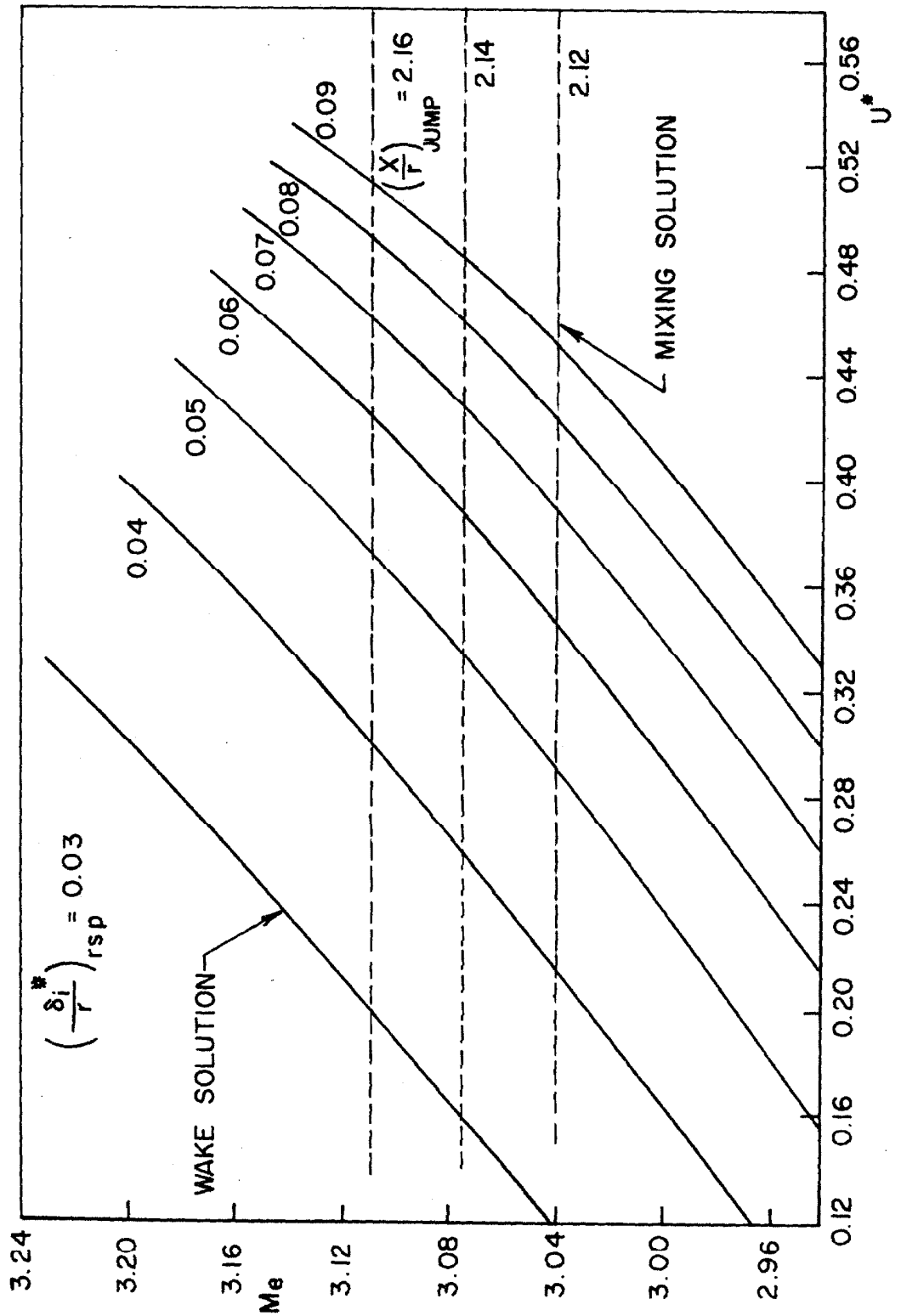

FIG. B5 MATCHING OF MIXING AND WAKE SOLUTIONS

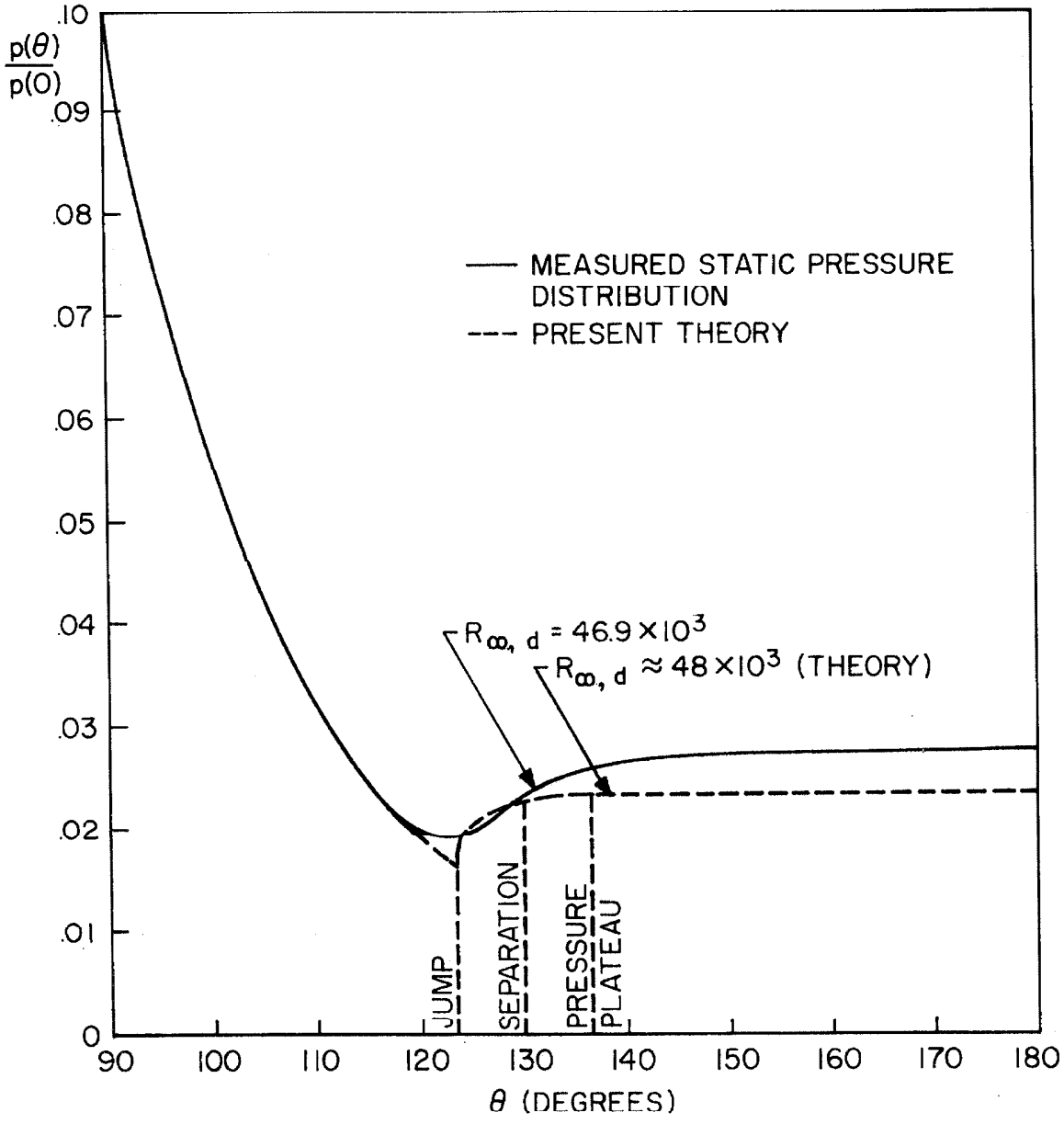

FIG. B 6 COMPARISON OF THEORY WITH Mc CARTHY'S EXPERIMENTS

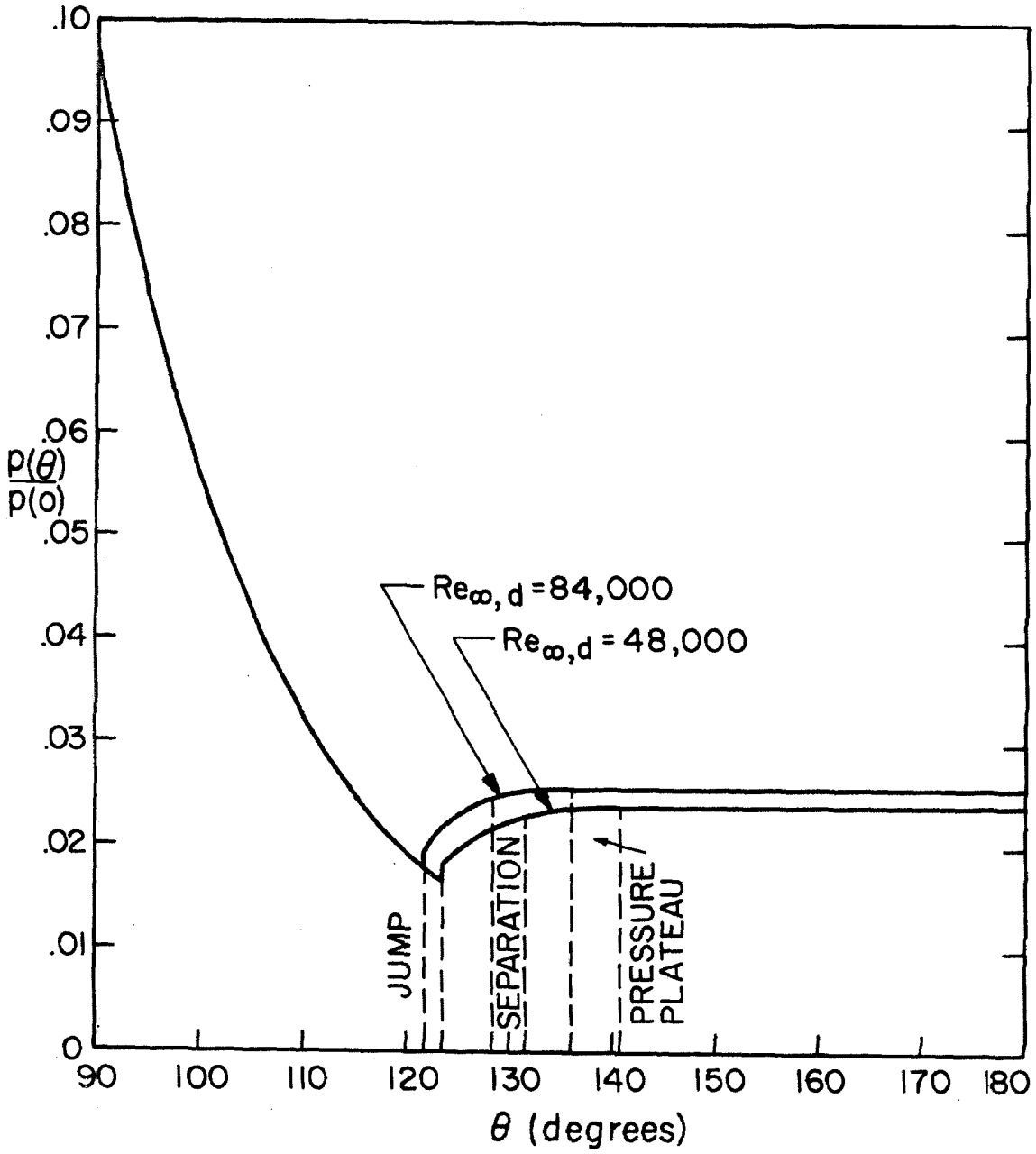

FIG. B7 EFFECT OF REYNOLDS NUMBER ON BASE REGION.

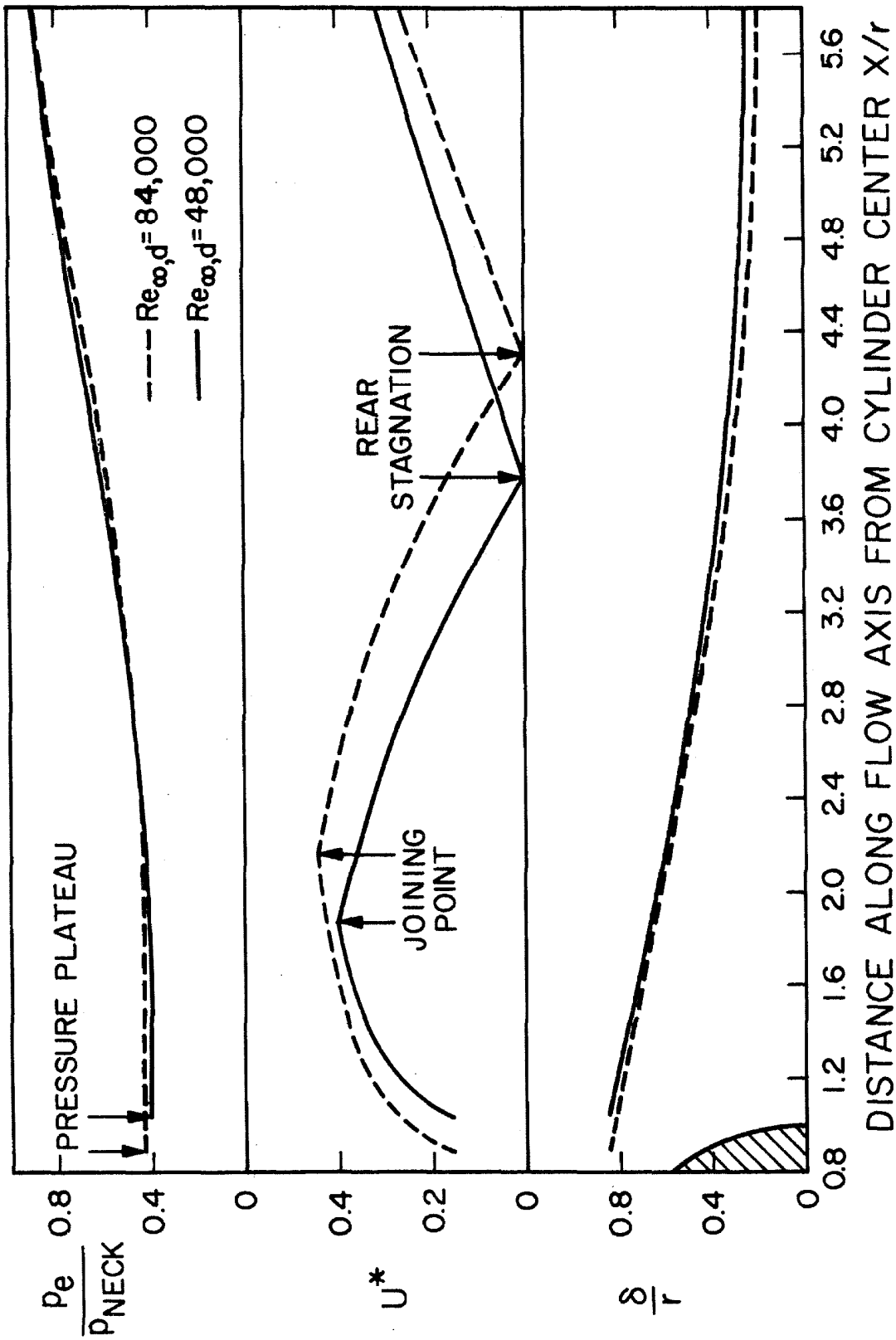

FIG. B8 NEAR-WAKE INTERACTION REGIONS.

REFERENCES

1. Prandtl, L.: "The Mechanics of Viscous Fluids," Aerodynamic Theory, W. F. Durand Ed., Vol. III, Dover Publications, Inc., New York, pp. 34-208 (1963).

2. Lees, L. and Reeves, B. L.: "Supersonic Separated and Reattaching Laminar Flows: I. General Theory and Application to Adiabatic Boundary-Layer/Shock-Wave Interactions," AIAA J. 2, 1907-1920 (1964).

3. Falkner, V. M. and Skan, S. N.: "Some Approximate Solutions of the Boundary Layer Equations," R & M. No. 1314, British A.R.C. (1930).

4. Stewartson, K.: "Further Solutions of the Falkner-Skan Equation," Proc. Cambridge Phil. Soc. 50, 454-465 (1954).

5. Cohen, C. B. and Reshotko, E.: "Similar Solutions for the Compressible Laminar Boundary Layer with Heat Transfer and Pressure Gradient," NACA Rept. 1293 (1956).

6. Crocco, L. and Lees, L.: "A Mixing Theory for the Interaction Between Dissipative Flows and Nearly Isentropic Streams," J. Aerospace Sci. 19, 649-676 (1952).

7. Sutton, W.G.L.: "An Approximate Solution of the Boundary Layer Equations for a Flat Plate," Phil. Mag. 23, 1146-1152 (1937).

8. Walz, A.: "Anwendung des Energresatzes von Wieghardt auf einparametrige Geschwindingkeits profile in lammaren Grenzschichten," Ing.-Arch. 16, 243-248 (1948).

9. Tani, I.: "On the Approximate Solution of the Laminar Boundary Equations," J. Aeronaut. Sci. 21, 487-504 (1954).

10. Reeves, B. L. and Lees, L.: "Theory of the Laminar Near Wake of Blunt Bodies in Hypersonic Flow," AIAA J. 3, 2061-2074 (1965).

11. Chapman, D. R. and Rubesin, M. W.: "Temperature and Velocity Profiles in the Compressible Laminar Boundary Layer with Arbitrary Distribution of Surface Temperature," J. Aeronaut. Sci. 16:9, 547-565 (1949).

12. Stewartson, K.: "Correlated Incompressible and Compressible Boundary Layers," Proc. Roy. Soc. (London), Ser. A, Vol. 200, No. A1060, 84-100 (1949).

REFERENCES (Cont'd)

13. Coles, D.: "The Laminar Boundary Layer Near a Sonic Throat," 1957 Heat Transfer and Fluid Mechanics Institute, Preprints of Papers, Stanford University Press, Stanford, Calif., pp. 119-137.

14. Lees, L.: "Viscous-Inviscid Flow Interactions at Supersonic Speeds," First Annual Dean's Lecture, University of Notre Dams, April 10-11, 1967.

15. Lighthill, M. J.: "Reflection at a Laminar Boundary Layer of a Weak Steady Disturbance to a Supersonic Stream Neglecting Viscosity and Heat Conduction," Quart. J. Mech. Appl. Math. 3, 303-325 (1950).

16. Crocco, L.: "Considerations on the Shock-Boundary Layer Interaction," Proceedings of the Conference on High-Speed Aeronautics, Polytechnic Inst. of Brooklyn, 75-112 (Jan. 20-22, 1955).

17. Tyson, T. J.: "Laminar Boundary Layers in the Neighborhood of Abrupt Spatial Disturbances," Calif. Inst. of Technology, Pasadena, Calif., Ph. D. Thesis (1967).

18. Kubota, T." "Singular Point at Downstream Infinity on Flat Plate," GALCIT Notes, pp. 1-4, no date.

19. Lewis, J. E., Kubota, T. and Lees, L.: "Experimental Investigation of Supersonic Laminar, Two-Dimensional Boundary-Layer Separation on a Compression Corner With and Without Cooling," AIAA J., 6:1, 7-14 (1968).

20. Kubota, T.: "A Note on Hypersonic Laminar Boundary Layer with 'Strong' Local Interaction," GALCIT Notes, pp. 1-4, (March 15, 1966).

21. Ko, D.R.S. and Kubota, T.: "Supersonic Laminar Boundary Layer Along a Two-Dimensional Adiabatic Curved Ramp," Preprint No. 68-109, AIAA 6th Aerospace Sciences Meeting, New York, N. Y., Jan. 22-24, 1968.

22. Lees, L.: "Influence of the Leading-Edge Shock Wave on the Laminar Boundary Layer at Hypersonic Speeds," J. Aero. Sciences, 23:6, 594-612 (1956).

23. Stewartson, K.: "On the Motion of a Flat Plate at High Speeds in a Viscous Compressible Fluid-II. Steady Motion," J. Aero. Sciences, 22:5, 303 (1955).

REFERENCES (Cont'd)

24. Mirels, H.: "Approximate Analytical Solutions for Hypersonic Flow Over Slender Power Law Bodies," NASA TR R-15 (1959).

25. Lees, L.: "On the Boundary Layer Equations in Hypersonic Flow and Their Approximate Solutions," J. Aero. Sciences, 20, 143-145 (1953).

26. Lees, L.: "Hypersonic Flow," *Preprint No. 554, Fifth International Aeronautical Conf.* (IAS-R. Ae. S), Los Angeles, Calif. (June 20-24, 1955).

27. Reeves, B. L.: "The Compressible Boundary Layer in Separated Flow Past a Compression Corner," Space General Corporation Report, May 3, 1963.

28. Miller, D. S., Hijman, R. and Childs, M. E.: "Mach 8 to 22 Studies of Flow Separations Due to Deflected Control Surfaces," AIAA J. 2:2, 312-321 (1964)

29. Savage, S. B.: "The Effect of Heat Transfer on Separation of Laminar Compressible Boundary Layers," Graduate Aeronautical Laboratories, Calif. Inst. of Tech., Separated Flows Research Project, Technical Report No. 2, June 1, 1962.

30. Rae, W. J.; "A Method for Estimating Separated-Flow Profiles Over an Axisymmetric Afterbody," Cornell Aero. Lab., Inc. Technical Report CAL No. AI-2187-A-7 (1967).

31. Kubota, T. and Fernandez, F. L.: "Boundary-Layer Flows with Large Injection and Heat Transfer," AIAA J. 6:1, 22-28 (1967).

32. Strahle, W. C.: "Theoretical Studies on the Effects of Blowing and Suction in Laminar Separated Regions," Preprint No. 67-192, AIAA 5th Aerospace Sciences Meeting, New York, N. Y., Jan. 23-26, 1967.

33. Green, J. E.: "Two-Dimensional Turbulent Reattachment as a Boundary Layer Problem," Proc. Royal Soc., London, A 237, pp. 543-559 (1956).

34. Alber, I. E.: "Integral Theory for Turbulent Base Flows at Subsonic and Supersonic Speeds," Calif. Inst. of Technology, Pasadena, Calif., Ph.D. Thesis (1967).

35. Dewey, C. F., Jr.: "Measurements in Highly Dissipative Regions of Hypersonic Flows. Part II. The Near Wake of a Blunt Body at Hypersonic Speeds," Ph.D. Thesis, Calif. Inst. of Tech. (1963), also AIAA J. 3, 1001-1010 (1965).

REFERENCES (Cont'd)

36. McCarthy, J. F., Jr. and Kubota, T.: "A Study of Wakes Behind a Circular Cylinder at M = 5.7," AIAA J. 2, 629-636 (1964).

37. Chapman, D. R., Kuehn, D. M. and Larson, H. K.: "Investigation of Separated Flows in Supersonic and Subsonic Streams with Emphasis on the Effect of Transition," NACA Rept. 1356 (1958).

38. McCarthy, J. F. Jr.: "Hypersonic Wakes," GALCIT Hypersonic Research Project, Memorandum No. 67 (1962).

39. Webb, W. H., Golik, R. J., Vogenitz, F. W. and Lees, L.: "A Multimoment Integral Theory for the Laminar Supersonic Near Wake," Proceedings of the 1965 Heat Transfer and Fluid Mechanics Institute, Stanford University Press, Stanford, California, pp. 168-189.

40. Roshko, A.: "A Look at our Present Understanding of Separated Flow," Paper presented at AGARD Symposium on Separated Flow, Brussels, Belgium, May 10-13, 1966.